UNIVERSITY OF OKLAHOMA

GRADUATE COLLEGE

# STRUCTURAL AND STRATIGRAPHIC EVALUATION OF THE SOUTHERN BELGIAN ANTICLINE AREA, NORTH MIDWAY-SUNSET FIELD, SAN JOAQUIN BASIN, CALIFORNIA

A THESIS

SUBMITTED TO THE GRADUATE FACULTY

In partial fulfillment of the requirement for the

Degree of

MASTER OF SCIENCE

By

W. SEBASTIAN BAYER PRINCE

Norman, Oklahoma

2007

# STRUCTURAL AND STRATIGRAPHIC EVALUATION OF THE SOUTHERN BELGIAN ANTICLINE AREA, NORTH MIDWAY-SUNSET FIELD, SAN JOAQUIN BASIN, CALIFORNIA.

A THESIS APPROVED FOR THE
SCHOOL OF GEOLOGY AND GEOPHYSICS

By

[redacted]

Dr. Roger M. Slatt, Chair

[redacted]

Dr. Shankar Mitra

[redacted]

Dr. James Forgotson Jr.

## ACKNOWLEDGEMENTS

**I am immensely thankful to God, for the things that have happened in my life.**

I am very grateful to my parents Kurt Bayer and Fabiola Prince for their love, and their example that I follow; "rewards only come with honest hard work and personal effort". For that I owe them all my present and future success.

Veronica is my soul mate and was my constant support through the completion of the Master degree and this thesis. I consider her my partner and a guide that God put in my life to help me find the right path. Without her, her unconditional love, and invaluable advice I would not be the person I am today.

Confidence and trust are values that are not for granted among people; I found these with Dr Slatt and Dr Mitra. They saw something I couldn't see at the time and believed in me in crucial moments in my life; I consider them my mentors and friends.

I remember when I came to this country as an exchange student, I planned to come for one year and go back to my country. Yes, that was 5 years ago, that was until I enrolled in one of Dr Mitra's classes, where the idea for my undergraduate thesis arose extending my stay for one more semester. Presenting my thesis I was offered an internship that was extended for a year doing what I learned in OU as an undergrad geologist. At this decisive moment Dr Slatt opened one of the most important doors in my life and gave me the opportunity to work with him and pursue a Master in Geology. This takes me to this very moment; "the completion of my master and a new stage in my life".
I would like to thank my professors at OU for giving me the tools I have today to start my professional life.

I also want to thank Dr Forgotson for his help when I was a teaching assistant and in the review of this thesis. I really appreciate the help provided by Subho as he trained me and taught me the things I know in GIS, and LithoTect.

This Thesis would not have been possible without the support of Bob Davis who is one of my best friends who stepped-up, helped, and guided me (when he barely knew me) through the initial stages of this work and introduced me to Steve Boleng and Joel Pomerane in BERRY Petroleum Company in Bakersfield, California. I really appreciated all the help provided by Steve and Harry during my visit to the company and during our short trip to the field were I learned a lot. I am very grateful to Joel who helped me with advise and in the process to obtain all the financial support and the well-logs for this thesis.
I would really like to thank Mark Gamache with the State of California Conservation Commission for providing valuable information for wells in the work area and who helped me obtain the data: Sincerely, thank you very much.

There have been amazing people that I have met in the course of my up-to-now short career. I want to thank them for their invaluable advice and for unconditionally sharing the vast knowledge they have built during their careers in the petroleum industry; they are Bill Schoellhorn, Rob Merrit (my first boss in America), Randy Ponder, Jaques-Anoine Dal, Gwuen Gerin, Jan Philippe, Dona Evans, David Dunbar, Mike Hoi, Jhon Hu, and Angela Goodarzi. Thank you for providing me with priceless experience and the kind of knowledge that is only learned working.

I could not finish these acknowledgements without thanking Donna Mullins in the eight floor for solving all my problems (yes! I mean all). To Niki for being always there for me, Nancy and Therese for helping me with all the money stuff, Jan Dodson for her support, Heidi Correa for "The Gocad day with Heidi" and to the Department of Geography for allowing me to work on my thesis in their labs for a full semester.

I want to thank my professors from the National University of Colombia and specially to Dr Fernando Etayo who gave me the foundation to become a Geologist, my friends in "the Colombian Mafia"; Javier Perez, Rodrigo Bastidas, Carlos Bahammon, David Ramirez, and Heidi Correa. I want to thank my host family; Lyndal and Susan who were always there for me, and finally, my friends in Norman: Juan (el cuñado), Marco Vignali, Isel, Anuar, Edwin, Johanna, Andres, Franz, Camilo, Yoscel, and Roderik.

**I wanted to put these words in my thesis to thank God for placing these incredible people in my path and for rewarding me with so many special and favorable situations.**

TABLE OF CONTENTS

## LIST OF FIGURES

## LIST OF APPENDIXES

## ABSTRACT

The Midway-Sunset field is located in the West Side fold belt in the San Joaquin Basin of California. The structures in the area, including the Midway-Sunset, Buena Vista, and Elk Hills anticlines, were formed during multiple episodes of compressive deformation, separated by periods of extension, between the Upper Miocene and present. A regional study of a 250 square mile area was conducted to understand the structure and stratigraphy within the fields on these structures. The study utilized existing geologic maps and data from over 400 wells to construct three regional structural and seven stratigraphic cross sections. One of the structural sections was kinematically reconstructed through time to understand the tectonic history. The Midway-Sunset and Buena Vista structures are interpreted as a series of parallel, fault-bounded structures, cored by deeper fault-bend folds. Many of the larger structures display overturned or steep flanks. Some of the reservoir units, such as the Stevens and Potter deep water turbidite sandstones, were deposited in an active tectonic environment, so that the depositional history is closely related to the structural events.

A more detailed structural-stratigraphic study was conducted to evaluate an approximately 15 square mile area within the Southern Belgian anticline. A three-dimensional structural model was constructed using five closely-spaced balanced structural cross sections constrained by dipmeter logs and surface structural data. This structural model will provide a tool to evaluate potential bypassed reservoirs in the Potter Sandstone, and new targets in deeper reservoirs.

# 1. INTRODUCTION

## 1.1 General

This thesis is focused on the Upper Miocene units of the Monterey and Etchegoin Formations, represented in The Southern Belgian anticline area by deep-water deposits (Quinn, 1990). All the data and economic support for this thesis was provided by Berry Petroleum, an independent oil company located in Bakersfield, CA.

## 1.2 Location

This thesis covers two scales of detail; the sub-regional scale (general study area, figure1, B) which includes three cross sections covering the entire north portion of the Midway-Sunset structure, and a detailed scale covering the Belgian Anticline area, located in the northeast quarter of (Sections 1- 3, 10-12, and 13-15) Township 31 South, Range 22 East in Kern County California (figure1, A).

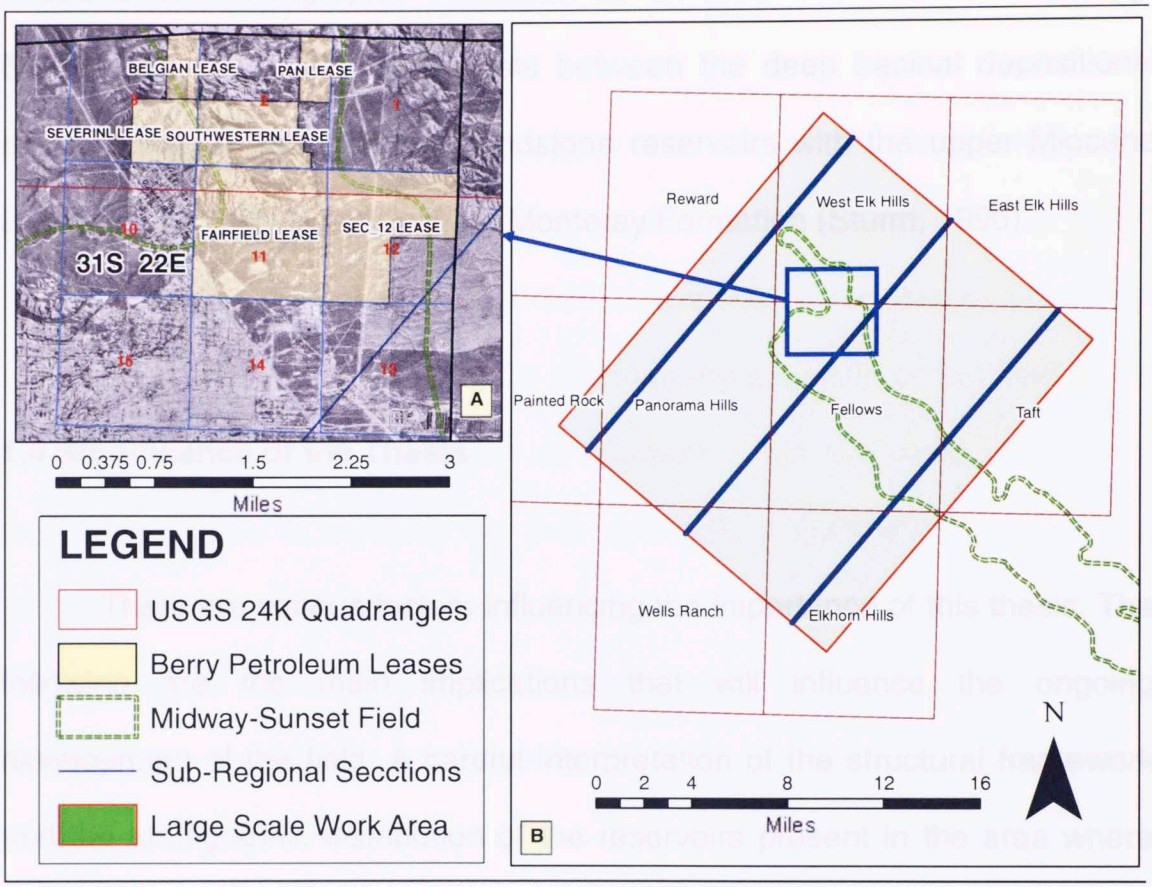


**Figure 1.** Location and scales of detail A. South Belgian Anticline area (detailed). B. Large scale study area, note the sub-regional cross sections in dark blue (Midway sunset extension digitized from R. L. Gardiner, A. S. Wylie, Jr., M. J. Gagner., 1996, Pg. 176, Figure 1).

## 1.3 Purpose of This Thesis

The main purpose of this thesis is to construct a detailed geologic model to plan future drilling in the South Belgian Anticline area (north Midway-Sunset) and to present a case study that can be used as an analog for similar areas of exploration. In more detail, this study is intended to address the

structural and stratigraphic evaluation for an area to the north of Midway-Sunset and the relation that exists between the deep basinal depositional environments of the Miocene sandstone reservoirs with the upper Miocene Belridge Diatomite Member of the Monterey Formation (Sturm, 1996).

### 1.4 Significance of the Thesis

There are various factors influencing the importance of this thesis. The following are the main implications that will influence the ongoing development of the field. A careful interpretation of the structural framework and the stratigraphic distribution of the reservoirs present in the area where Berry Petroleum holds leases will ultimately translate into a more efficient drilling effort and in a better design for the secondary-recovery-steam-flooding program that is currently being conducted. The high resolution geologic model, focused on a strong analysis of the structures, will allow the location of bypassed areas with new potential. Finally a possible impact of the project is to evaluate the prospectivity of deeper zones based on the structural interpretation and the relationship that exists with the "continuous turbidite sand deposition throughout the upper Miocene" (Gregory, 1996) in the Midway-Sunset field.

## 1.5 Previous studies

A complete description and interpretation regarding the geology, and specific information on the Midway-Sunset field can be found in Nilsen, Wylie, Jr., and Gregory (1996). Here, a well documented compilation of papers concentrate on the different aspects affecting the evolution of this field. This vast understanding and availability of information has motivated the present work that intends to evaluate the data and build a complete structural and stratigraphic representation for the South Belgian Anticline area, north Midway-Sunset. Excellent descriptions on the stratigraphy of the southeastern San Joaquin Valley that are used in the present work are found in Taff, (1933).

As a starting point, a cross section presented by Namson and Davis (2004, cross section 16-16', figure 83 in this thesis) was revised and used in combination with wells, surface structural data, and formation tops from the literature (various authors in Nilsen, 1996) to produce the structural interpretation here proposed.

## 1.6 Existing Data

The data used for this thesis includes good outcrop exposure of the formations of interest, more than 1200 surface structural data points (strike and dip), geologic maps from which geologic contacts for all Pre-Pleistocene formations were digitized and corrected, a digital elevation model (30m resolution) for the area of interest, digital orthophotos (1m resolution DOQQ) covering the entire Midway-Sunset field extension, 19 wells for the sub-regional area of study (see figure 1), and 17 wells provided by Berry Petroleum Company for the South Belgian Anticline area. The log suite for the majority of the wells include GR, SP, resistivity, conductivity and sonic in addition to other curves.

## 2. REGIONAL GEOLOGY

### 2.1 San Joaquin Basin

The San Joaquin Basin Province (figure 2) occupies the southern half of the Great Valley of California and is an asymmetrical structural depression filled with more than 36,000 ft of Upper Cretaceous and Cenozoic, predominantly marine clastic sediments (Callaway and Rennie, 1991 in Beyer, 1988).

The province is bordered on the east by the Sierra Nevada Mountains, on the south by the northern Transverse Ranges, on the west by the San Andreas Fault Zone and southern Diablo Range, and arbitrarily on the north by the Stanislaus-San Joaquin County line (Beyer, 1988). It extends for about 200 mi, averages 65 mi in width, occupies an area of 14,423 square miles and contains about 30,000 cubic miles of sedimentary rocks (Callaway, 1971; Varnes and Dolton, 1982, in Beyer, 1988).

The San Joaquin Basin Province is divided into nine confirmed plays and one hypothetical play (Beyer, 1988). The area of this study corresponds to the West Side Fold Belt sourced by post-Lower Miocene Rocks and a portion of the lower section sourced by pre-Middle Miocene Rocks (figure 3).

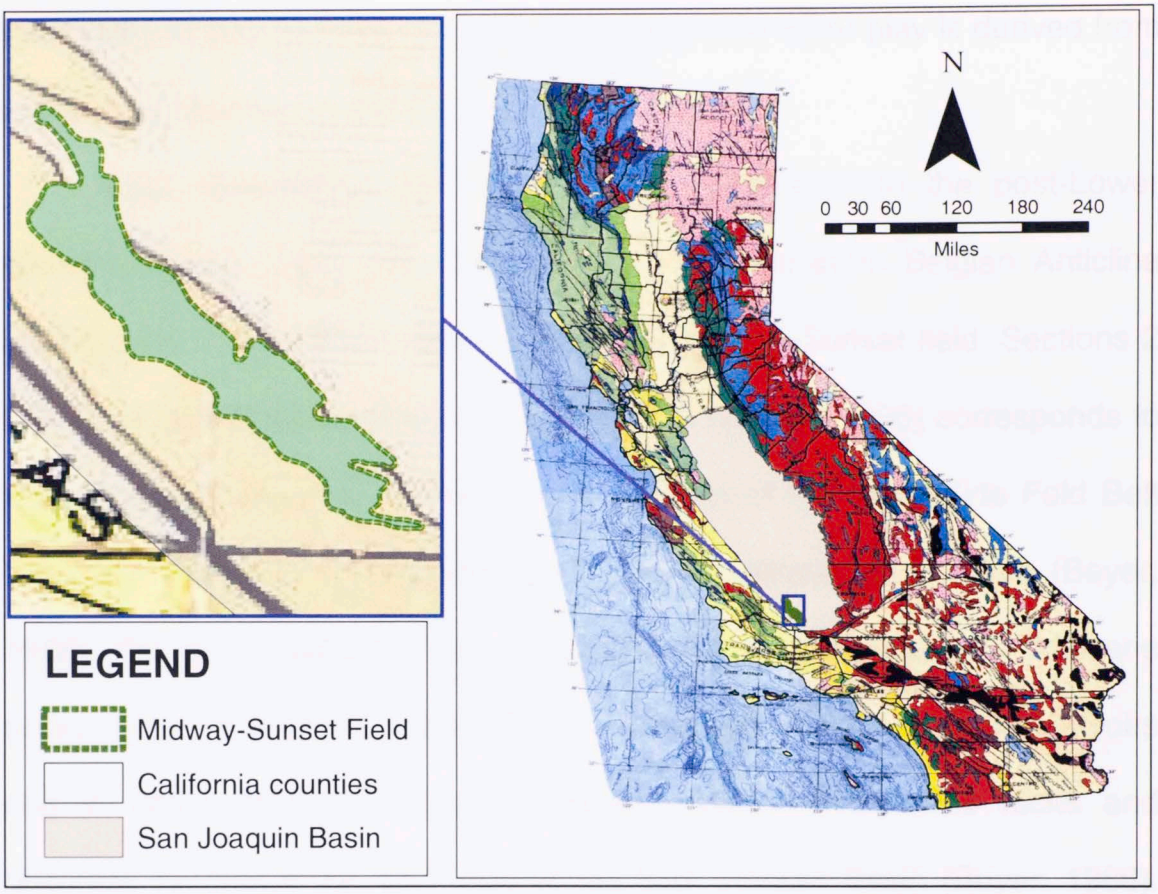


**Figure 2.** Location of the San Joaquin Basin Province (Midway sunset extension digitized from R. L. Gardiner, A. S. Wylie, Jr., M. J. Gagner., 1996. Pg. 175-181, Figure 1., San Joaquin boundary from the USGS NOGA).

## 2.2 West Side Fold Belt Area

The Midway-Sunset field is located in the West Side Fold Belt. This area includes two separate plays (figure 3). The aspect that differentiates the two plays is the origin of the oil. In one play the oil originated from middle

Miocene and younger source rocks; the oil from the other play is derived from pre-middle Miocene source rocks (Beyer, 1988).

Most reserves in the field primarily correspond to the post-Lower Miocene source rocks play. The portion of the Southern Belgian Anticline area (figure 1, A) at the northern limit of the Midway-Sunset field, Sections 2 and 11, T31S, R22E (Gardiner, Wylie, Jr., and Gagner, 1996) corresponds to the pre-middle Miocene source play. Both parts of the West Side Fold Belt Area are confirmed stratigraphic and structural-stratigraphic plays (Beyer, 1988). Oil and associated gas accumulations of the post-lower Miocene source play are found in upper Miocene to Pleistocene sandstone reservoirs and in upper Miocene to lower Pliocene fractured siliceous rocks and diatomite located in the west side of the San Joaquin Basin (Beyer, 1988). Reservoirs are associated with stratigraphic and combination traps attributed to structural deformation, marine transgressive cycles, or both throughout and since late Miocene time (Harding, 1976 in Beyer, 1988). A considerable amount of oil has already been found in fields like Midway-Sunset in this level of the play, restricting the remaining potential for undiscovered accumulations probably to new pool or new area discoveries in existing fields (Beyer, 1988). Most future new field discoveries will be subtle stratigraphic traps of moderate to small size and will be found at greater depth than discovered accumulations (Beyer, 1988).

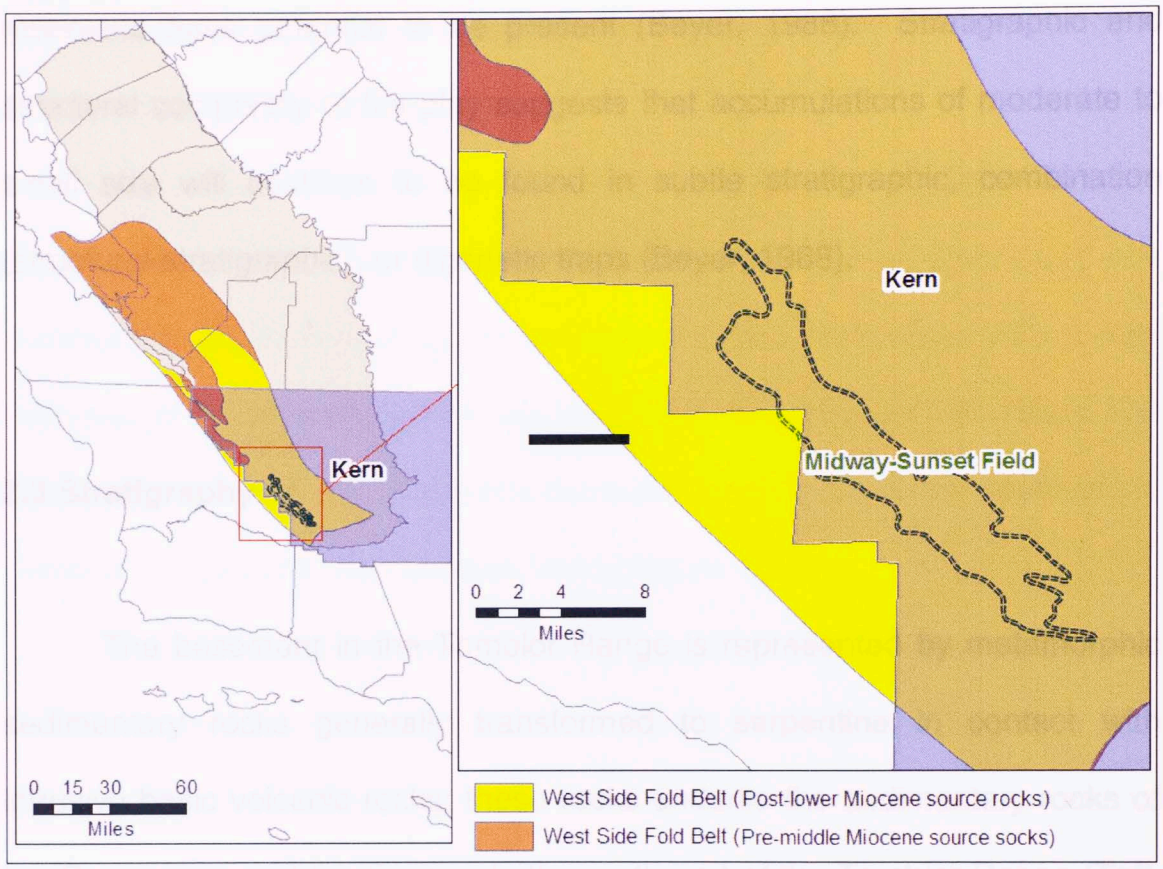


**Figure 3.** Location of the two play areas in the petroleum system of the Midway-Sunset field in the San Joaquin Basin province (Midway sunset extension digitized from R. L. Gardiner, A. S. Wylie, Jr., M. J. Gagner., 1996. Pg. 175-181, Figure 1., Play boundaries from the USGS NOGA).

For the pre-middle Miocene source rocks play, where the Southern Belgian Anticline structure is located, oil accumulations and associated gas have been discovered in Eocene to middle Miocene sandstone reservoirs and Eocene fractured siliceous rocks (Beyer, 1988). Many areas of the play have not been thoroughly tested because pre-middle Miocene rocks are at great depth or traps are not evident. Even though diagenesis reduces expectations for discovery of good quality reservoirs at greater depth, fractured rock

reservoirs have potential to be present (Beyer, 1988). Stratigraphic and structural complexity of the play suggests that accumulations of moderate to small size will continue to be found in subtle stratigraphic, combination (structural-stratigraphic), or digenetic traps (Beyer, 1988).

## 2.3 Stratigraphy

The basement in the Temblor Range is represented by metamorphic sedimentary rocks generally transformed to serpentine in contact with intrusive basic volcanic rocks; these rocks underlie the sedimentary rocks of the Cretaceous and the Eocene in the north part of the Temblor Range (Taff, 1933). To the south the basement is in sharp contact with Cenozoic rocks and corresponds to granitic rocks with schist and crystalline limestone inclusions (Taff, 1933).

*Cretaceous - Paleogene*

There are no outcrops of the Cretaceous or the Paleocene in the Midway-Sunset area (Nilsen, 1996); the closest evidence to corroborate the existence of Cretaceous and Eocene rocks in the subsurface is the deep Elk Hills 934-29R well in the Naval Petroleum Reserve. This well is the deepest

well ever drilled in the San Joaquin Valley, reaching Upper Cretaceous rocks at 24,442 feet (Nigrini, 1996).

The Cretaceous of the 934-29R well is undifferentiated (figure 7B), but to the north in the Diablo Range area it is represented by dark shale and monotonous sandstone of the Knoxville and Chico Formations with a total thickness of approximately 5000 and 4000 feet, respectively (Taff, 1933). The Cretaceous and Eocene formations decrease in thickness to the south of the Temblor Range in the San Joaquin Valley (figure 4).

Unconformably on the Cretaceous (figure 7 B), the fine sandstones and siltstones of the Canoas sandstone underlie the Kreyenhagen Shale (E.R Atwill, 1935). The Kreyenhagen Shale is an organic shale with occasional lenses of fine-grained sandstone and limestone (Von Estorff, 1930). The Tumey Formation unconformably overlies the Kreyenhagen shale (figure 7 B) represented by a lower sandstone section and a thick section of shales 800 and 885 feet thick, respectively, in an area north of Arroyo Ciervo (Atwill, 1935).

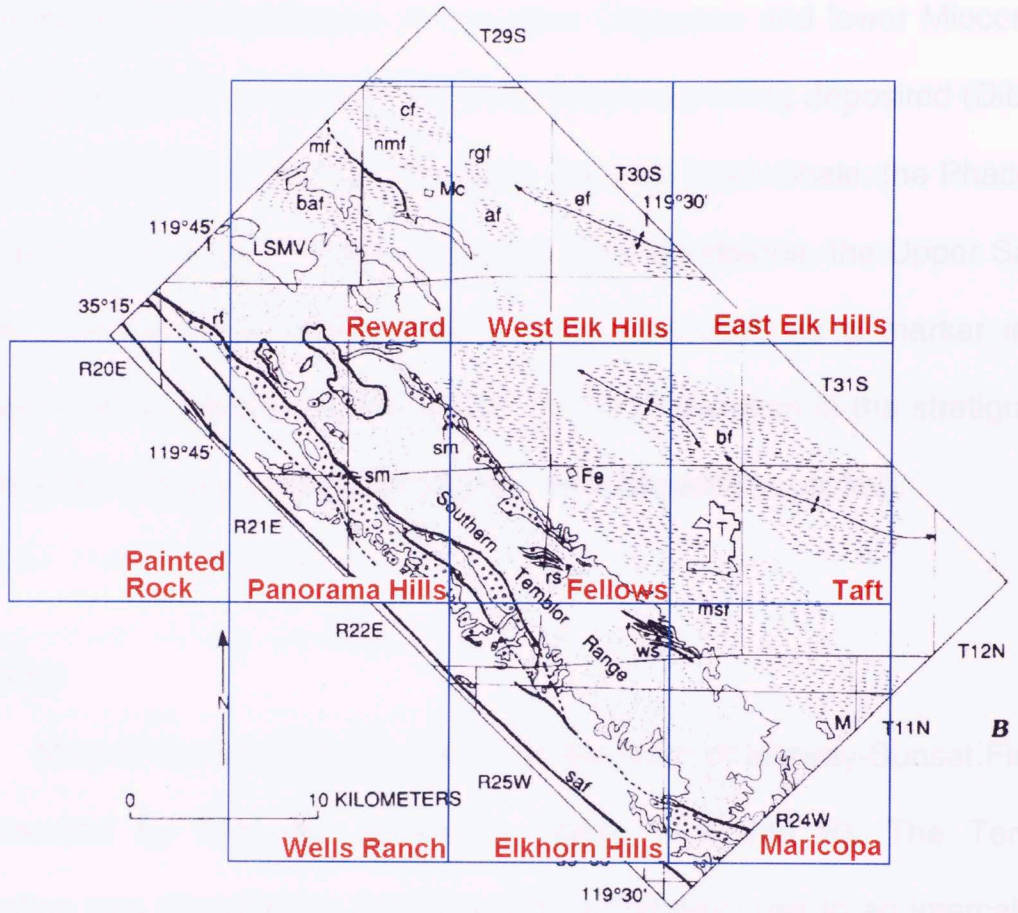


**Figure 4.** Location of the Southern Temblor Range area (from Ryder and Thomson, 1989, Fig. 1 in Nilsen, 1996, Fig. 2, Pg 12) Geologic symbols sm, Santa Margarita Formation; rs, Republic sandstone; ws, Williams sandstone. Geographic symbols saf, San Andreas fault; rf, Recruit Pass fault. Mc, McKittrick; Fe, Fellows; T, Taft; M, Maricopa (Nilsen). Blue boxes identify the USGS 24k quadrangles covering the southern temblor range.

*Oligocene – Lower-Miocene*

The Temblor Formation is unconformable to the Lower-Cenozoic marine sedimentary sequence represented by the equivalent Tumey Shale and Oceanic Sandstone of the Wagonwheel Formation, the Kreyenhagen Shale, and the Point of Rocks Sandstone (Dibblee, 1973). The beginning of

diatomite deposition occurred in the upper Oligocene and lower Miocene as the shale members of the Temblor Formation were being deposited (Dibblee, 1973b). These are in stratigraphic order: the Salt Creek Shale, the Phacoides Sandstone, the Lower Santos Shale, the Agua Sandstone, the Upper Santos Shale, and the Media Shale; this last unit was used as a marker in the present work to identify the top of the Temblor Formation in the stratigraphic interpretation (figure 7 and stratigraphic cross sections in pocket).

*Miocene*

Most of the stratigraphic column to the north of Midway-Sunset Field is represented by Cenozoic sediments (figure 7 A and B). The Temblor formation was deposited in a marine setting that gave rise to an intercalation of conglomerates, sandstones, and shales with abundant foraminifers (Taff, 1933). These sediments accumulated in water depths of 1200 feet to the north of the area now occupied by the Temblor range, and in water depths of 3000 ft to the south, resulting in sedimentary deposits that range from 200 to 3000 feet thick in the vicinity of the McKittrick oil field (Taff, 1933).

*The Monterey Formation*

The name Monterey Formation or Monterey Shale (figure 6 and 7) is used for marine sediments of middle to upper Miocene age which are characterized by high percentages of biogenic silica (Mercer, 1996). In the Maricopa area (figure 4) it is represented by organic shales that accumulated to a thickness of 4000 to 5000 feet (Taff, 1933). The basal part of the formation consists of brown foraminiferal shales and bentonitic clays that are followed conformably by fine laminated siliceous diatomaceous shale, with sparse bands of limestone and calcareous concretions (Taff, 1933). At about 1000 feet below the top of the Monterey Shale there is evidence of an emergence of the land to the south of the Temblor Range (figure 4) that interrupted the deposition of diatomite; this generated an alternating deposition of granitic to arkosic sands with diatomaceous shale. The sand strata range from thin layers to lenses that can be up to 100 feet in thickness (Taff, 1933). Diatom blooms from marine upwellings that settled on the ocean floor deposited thousands of feet of organic-rich diatomaceous mudstones, which represent the Monterey Formation (figure 5) In the Midway-Sunset area (Gregory, 1996). The siliceous shale members of the Monterey (figure 6) are, from oldest to youngest, the Devilwater/Gould, McDonald, Antelope, Belridge, and Reef Ridge (Gregory, 1996) with the entire section being over 5000 feet thick and interbedded from oldest to youngest (figure 6) with the Williams,

Republic, Spellacy, and Potter sandstones (Mercer, 1996). The Monterey siliceous shale members are important source beds, particularly along the west side of the San Joaquin Valley from the Lost Hills Field (approximately 2.5 miles north of the study area) to the Midway-Sunset Field (Mercer, 1996). All the members of the Monterey Shale are present in outcrops along the western edge of the field (Mercer, 1996).

The Devilwater/Gould Shale (figure 6) is separated from the underlying Temblor Formation by an unconformity (Harding, 1976 in Fortier, 1996). The age of this unconformity has been dated as at least 16.5 Ma (Bartow, 1991 in Fortier, 1996). This places the base of the Devilwater/Gould Shale (figure 7) in the Relizian (early Miocene) stage (Fortier, 1996). The lower part of the McDonald Shale is assigned to the early Mohnian (late Miocene) stage (Foss and Blaisdell, 1968 in Fortier, 1996), for this reason the top of the Devilwater/Gould Shale in this area is placed at the Luisian/Mohnian boundary at about 13.9 million years in the middle Miocene (Fortier, 1996).

The McDonald Shale (figure 6) conformably overlies the Devilwater/Gould Shale and is assigned to the beginning of the upper Miocene by Foss and Blaisdell (1968); their work with foraminifers places the top of the McDonald Shale at 8.6 million years in the late Miocene (Fortier, 1996).

The contact between the Antelope Shale (figure 6) and the McDonald Shale is conformable (Fortier, 1996). Dumont (1993) found that core and local outcrop samples from the middle and upper Antelope Shale at Midway-Sunset Field contain diatoms dating from 8.4 to 7.6 million years; indicating that the age of the Antelope Shale and the enclosed producing sands is approximately late Miocene and the age of the top of the unit is 7.6 Ma (Fortier, 1996).

Even though it is believed that the contact at the base of the Reef Ridge is conformable, the reconstruction of the structural cross-sections and the stratigraphic interpretation in this thesis suggests there is an unconformity between the two members; this observation is also suggested by other authors (figure 6., Campbell 1996). Pieces of whole core and local outcrop samples from this unit contain diatoms from the late Miocene suggesting that the age of the Belridge Diatomite and the enclosed Marvic, Spellacy, and Monarch Sands is 7.6 Ma to the base and 7.0 Ma to the top of the unit (Fortier, 1996).

The Reef Ridge Shale conformably overlies the Belridge Diatomite in the Midway-Sunset area. Kleinpell (1938) assigned the Reef Ridge Shale to the latest Miocene age based on studies of foraminiferal assemblages that Indicate an age of 7.0 million years for the basal part of the unit and 5.3 million years for the top of the shale member, placing the enclosed producing

Potter, Lakeview, Sub-Lakeview, and Gibson Sands in the late Miocene (Fortier, 1996).

*Upper Pliocene-Pleistocene*

Even though the Etchegoin Formation (figures 6, 7) is considered to be Pliocene in age, radiometric dating indicates that the lower part of the formation may be of late Miocene age (Wylie, and Huntoon, 1996). The Etchegoin Formation has produced most of the first billion barrels of Midway-Sunset's cumulative oil production (Wylie, and Huntoon, 1996). Production from the San Joaquin Formation, at the Midway-Sunset field, is minor; the oil is 12° to 28° API gravity and is found in both stratigraphic and structural traps (Walter, 1996). The Tulare Formation is divided based on log character into upper, middle and lower members (figure 6), the lower member being the one that has provided the bulk of production (Campbell, 1996). The oil produced from Tulare reservoirs is heavy with wide ranges of gravity and viscosity (Campbell, 1996).

*The Etchegoin Formation*

The Etchegoin Formation unconformably overlies the Reef Ridge Shale (figure 6) reaching a thickness of approximately 4000 feet in the vicinity of the McKittrick field (Taff, 1933). Molluscan fauna and foraminiferal assemblages indicate that it was deposited in nearshore-marine to intertidal and estuarine environments (Wylie, and Huntoon, 1996). During the early Pliocene, tectonic influences fluctuated and a major structural uplift of the Temblor Range occurred, producing rapid changes in the depositional setting (Wylie, and Huntoon, 1996). As a result, the sandstone bodies of the Etchegoin Formation are generally small, but numerous and generated in several depositional environments (Wylie, and Huntoon, 1996). The rise of the Coastal Ranges separated the great valley embayment from the Pacific Ocean and brought to a close the deposition of marine sediments of the Pliocene, ending the deposition of the Etchegoin Formation (Taff, 1933).

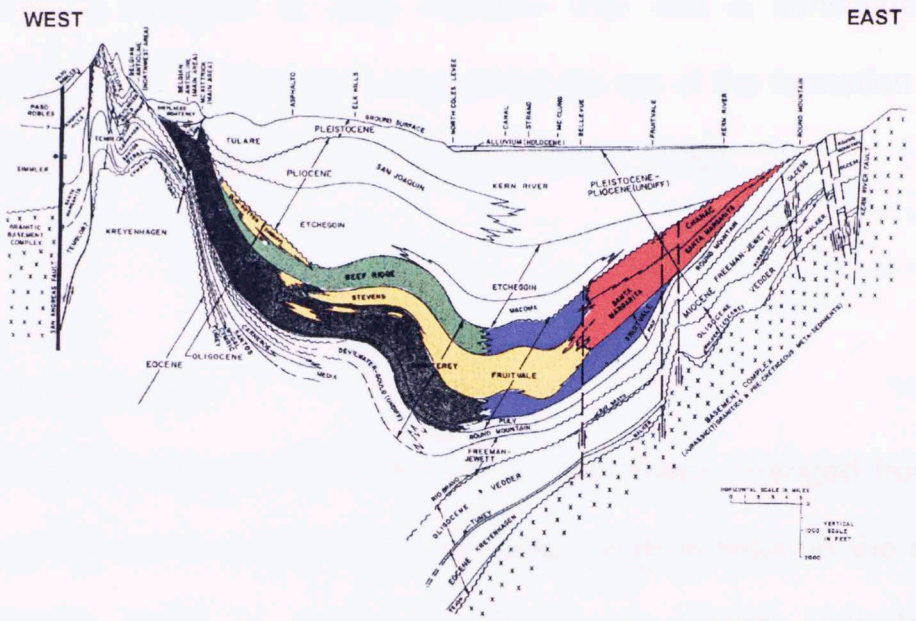


**Figure 5.** Cross section of the San Joaquin Basin across the north section of the Midway-Sunset field (extracted from M. F. Mercer in Nilsen, T.H., Wylie, Jr., A.S., and Gregory, G.J., 1996 fig 2 Pg. 97-110).

*The San Joaquin Formation*

The name "San Joaquin Clays" was first used by F. M. Anderson (1905) to designate a sequence of banded clays, about 1500 ft thick, in the Diablo Range (Walter, 1996). At Midway-Sunset (figure 5) The San Joaquin Formation unconformably overlies the Etchegoin Formation (figure 6). The section ranges in thickness from 150 ft in the north to 1100 ft in the south (Walter, 1996). Reservoir deposits in this unit are represented by clay-rich, very fine to fine grained sandstones alternating with siltstone and claystone (Walter, 1996). Fossil assemblages indicate shallow water deposition with alternating brackish and freshwater conditions (Walter, 1996). The basal part

of this unit is assigned to early Pliocene time and is considered to be approximately 4.0 Ma. The age assigned for the top of the formation is better constrained and is believed to be 2.35 Ma (Fortier, 1996).

*The Tulare Formation*

During Pliocene to Pleistocene times the waters changed from saline to fresh giving rise to a period of fresh water sedimentation in the southern San Joaquin basin, a region dominated by alluvial and lacustrine environments when the Tulare Formation was deposited (Taff, 1933). The resulting deposits are the conglomerates, sandstones and shales of the lower, middle, and upper informal members (figure 6) of the Tulare Formation (Campbell, 1996). The lower member seating unconformably on the San Joaquin Formation is dominated by debris flow-rich alluvial fan deposits, the middle member is predominately represented by lacustrine mudstones with minor sandstones and siltstones, and finally the upper member consists of several commonly air-saturated sands (Campbell, 1996).

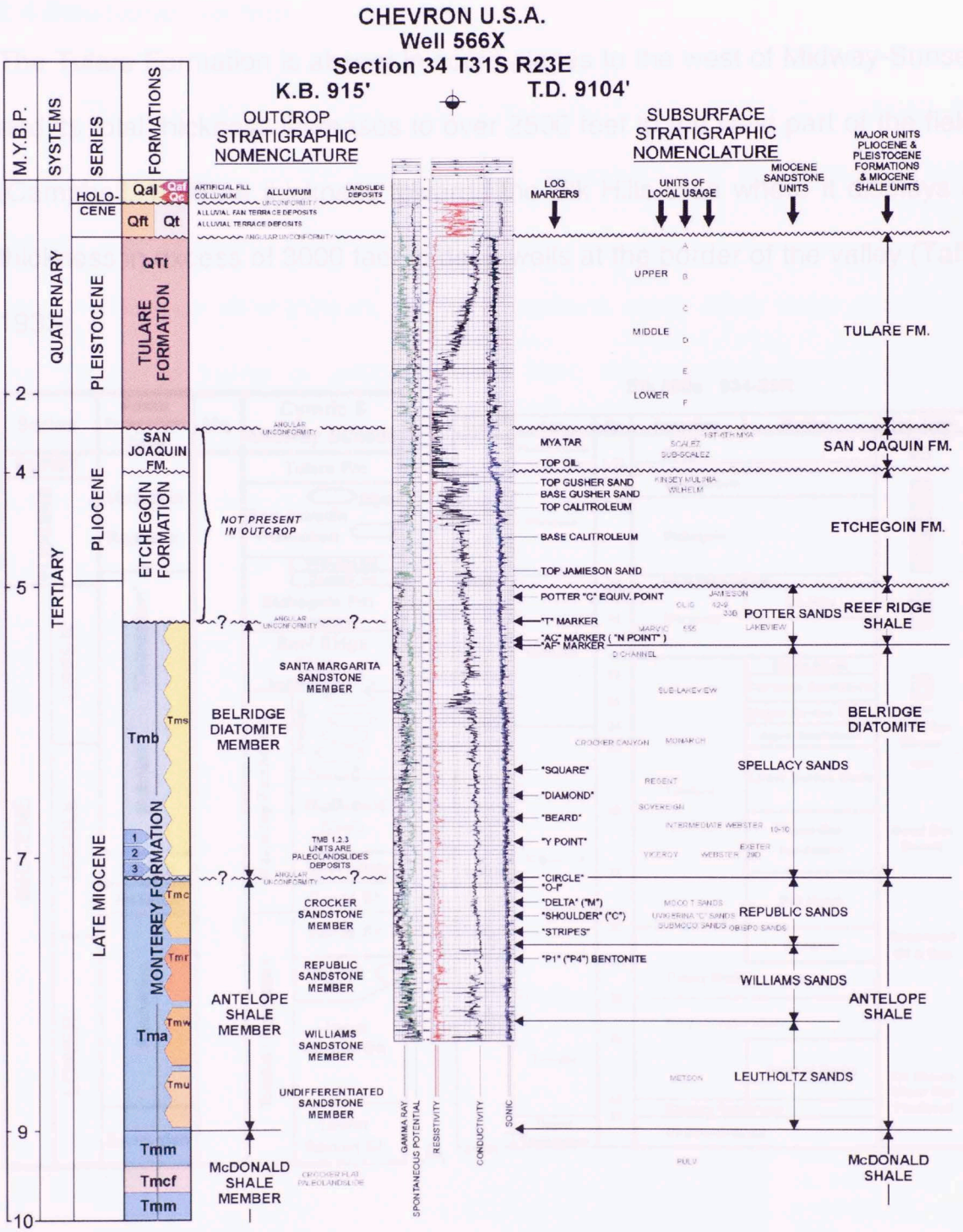


**Figure 6.** Type well and stratigraphic column of the Neogene formations (extracted from M. J. Campbell in Nilsen, T.H., Wylie, Jr., A.S., and Gregory, G.J., 1996 fig 1 Pg. 214-224).

The Tulare Formation is absent in some places to the west of Midway-Sunset and its total thickness increases to over 2500 feet to the west part of the field (Campbell, 1996); it thickness towards the Elk Hills area where it displays a thickness in excess of 3000 feet in deep wells at the border of the valley (Taff, 1933).

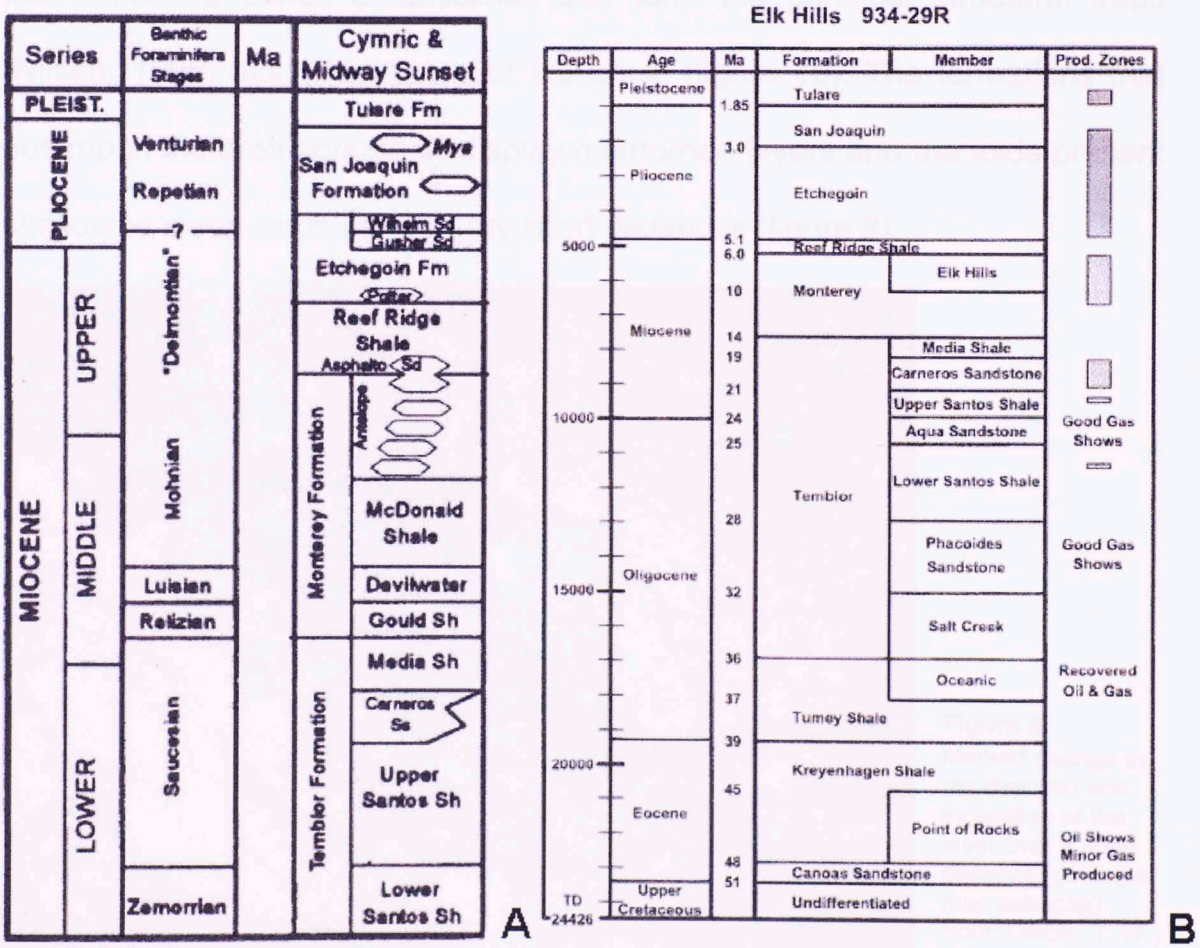


**Figure 7.** A. Stratigraphic units from the Temblor Formation to the Tulare Formation in the vicinity of the Midway-Sunset filed (modified from Nilsen in Nilsen, T.H., Wylie, Jr., A.S., and Gregory, G.J., 1996 fig 10 Pg. 19.). B. Stratigraphic column from the Elk Hills 934-29R deep well (A. Nigrini in Pioneer project, 1996, Michigan Technological University, current research).

## 2.4 Structural Geology

The San Joaquin Valley has been structurally active throughout its history, accounting for the very complex structures that are present. Even though the southern San Joaquin basin has the overall aspect of an asymmetrical syncline (Nilsen, 1996), it contains many other large structures that include a series of anticlines that form the principal structural traps (Nilsen, 1996) along the flanks of the basin (figure 10). The formations that outcrop in the area commonly display overturned layers and the folds present shallow to steep limbs across very short distances (figure 8).

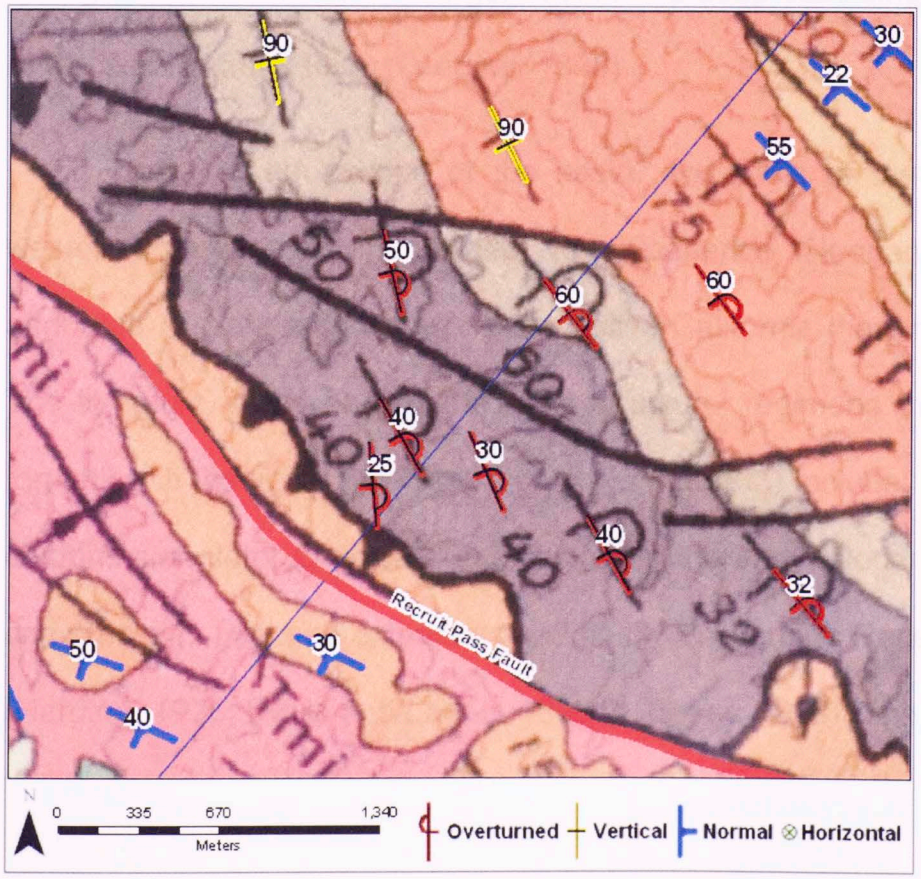


**Figure 8.** Marked change in dip direction and inclination of the layer over a short distance (geologic map extracted from; Dibble, T. W., Jr., 1973, USGS investigation – 757).

Folding, faulting and erosion were active between the Cretaceous and the Eocene periods of deposition (Taff, 1933), which is part of the evidence that suggests multiple tectonic events occurred during the evolution of the basin. The northern portion of the basin was developed as part of a fore-arc basin from the Cretaceous to the Paleogene (Beyer, 1988). During the Miocene, the Mendocino triple junction (figure 9) was migrating in a northwest direction past the San Joaquin basin, changing the tectonic framework from a convergent margin to a transform margin (Bent, 1988 in Gregory, 1996) along the San Andreas right-lateral fault (Gregory, 1996). The San Joaquin basin changed from a forearc convergent basin to a deep subsiding basin northeast of the San Andreas Fault (Gregory, 1996).

The southern portion of the basin, and parts of the transform-rifted western margin, also subsided to experience Neogene compression attributed to plate motions along the active California margin (Beyer, 1988). The literature suggests that the main structural regimens that affected trap formation in the West Side Fold Belt plays (figure 3) include: Early Oligocene compression, later Oligocene extension into the early Miocene, late Miocene compression, Pliocene extension, and finally Pliocene to Recent compression (Harding, 1976; Davis and Lagoe, 1988 in, Beyer, 1988). The work presented

here also suggests that there were four main events prior to the late Miocene (see petroleum system analysis appendix).

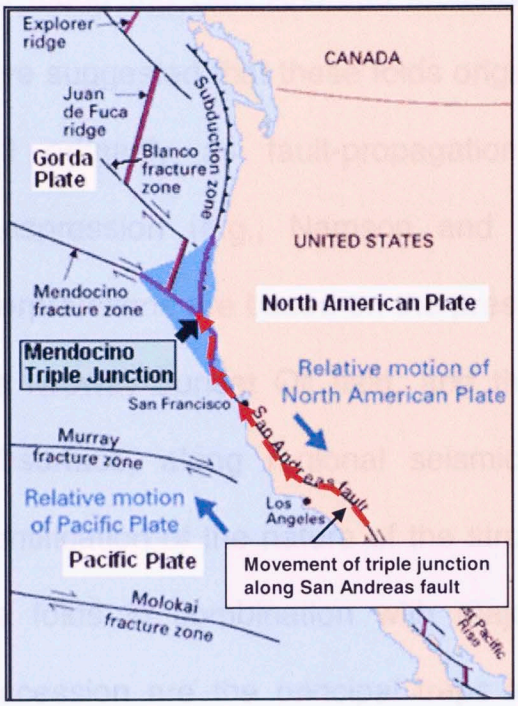


**Figure 9.** Approximate present Location of the Mendocino triple junction (modified from the Department of Geological sciences web page of The University of Colorado at Boulder. Migration path of the Mendocino triple junction from G. J. Gregory., 1996 fig 18 pg. 74)

The structure of the Midway-Sunset field is dominated by many small synclines and anticlines (figure 10) which generally display a northwest trend (Nilsen, 1996). The Midway syncline separates the Midway-Sunset field (figure 10) from the Buena Vista field (Nilsen, 1996).

Many workers have attributed different origins for the folds in the area. Early workers suggested a right-lateral transpression along the San Andreas Fault (e.g., Harding, 1976 in Nilsen, 1996). They based their interpretation on the observation that the axis of the folds are en-echelon with a more easterly

trend than the strike of the San Andreas fault (figure 10), the fold terminations commonly to the right, and the well-documented large amount of right-lateral-slip along the San Andreas fault (Dibblee,1973b in Nilsen). Other workers have suggested that these folds originated in a compressional fold-and-thrust belt primarily as fault-propagation folds, rather than as a result of transpression (e.g., Namson and Davis, 1988 in Nilsen, 1996). These interpretations are based on the presence of prominent faults in the vicinity of the Midway-Sunset Oil field, and the observation of their geometry in the subsurface, along regional seismic lines (in Nilsen, 1996). The proper identification of the nature of the structures is crucial in this thesis given that the folds in combination with major unconformities of the post-Miocene succession are the principal traps for hydrocarbon accumulation (Gregory, 1996) in the area of study. Here all available raw data (surface structural data and dipmeter-logs) were analyzed to understand the evolution of the folds, and based on this understanding closely spaced balanced cross-sections were constructed to develop the structural framework for the north part of Midway-Sunset.

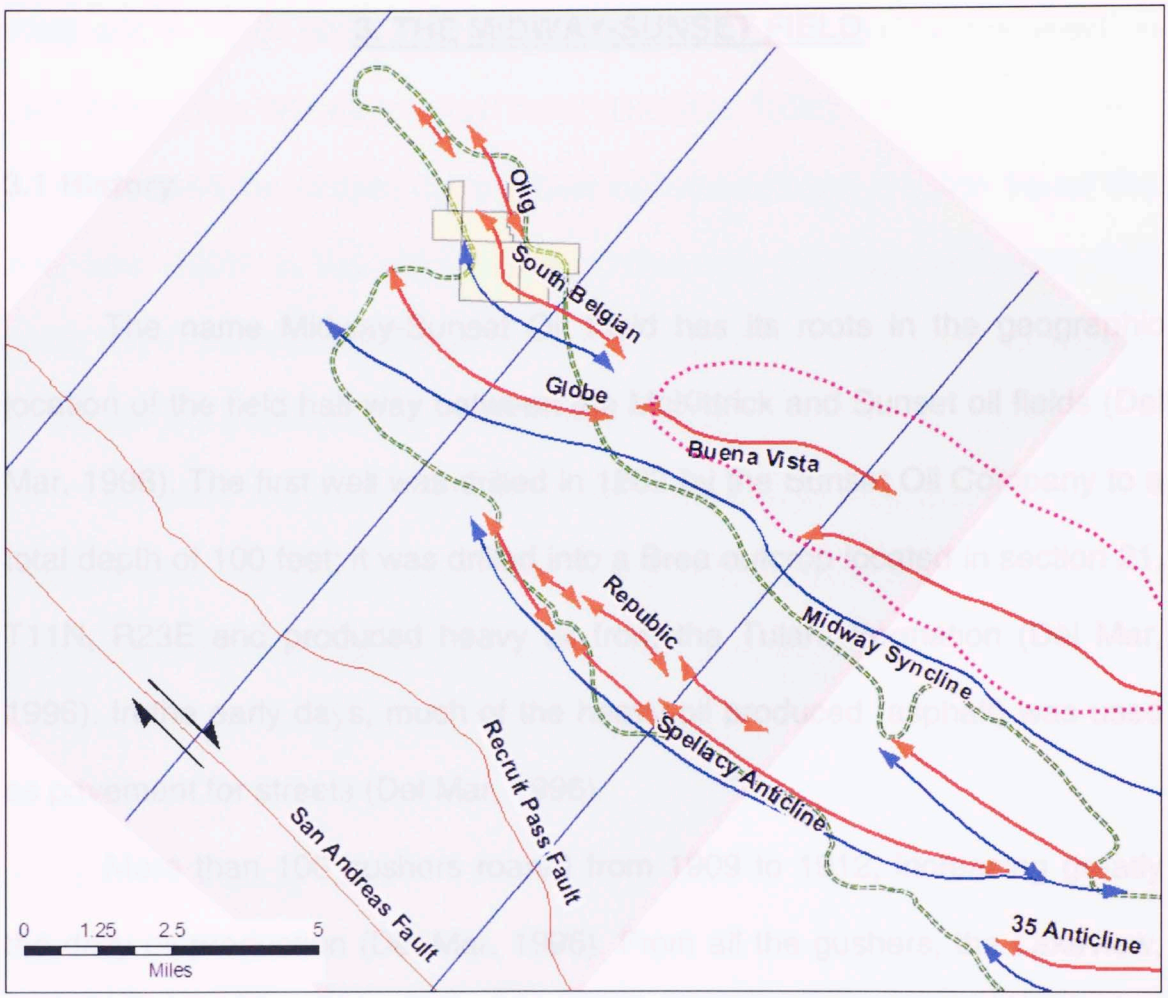


**Figure 10.** Main folds and faults in the work area (fold axes and Midway-Sunset field extension extracted from G. J. Gregory., 1996, figure 9, pg 18).

# 3. THE MIDWAY-SUNSET FIELD

## 3.1 History

The name Midway-Sunset Oil Field has its roots in the geographic location of the field half-way between the McKittrick and Sunset oil fields (Del Mar, 1996). The first well was drilled in 1887 by the Sunset Oil Company to a total depth of 100 feet; it was drilled into a Brea outcrop located in section 21, T11N, R23E and produced heavy oil from the Tulare Formation (Del Mar, 1996). In the early days, much of the heavy oil produced (asphalt) was used as pavement for streets (Del Mar, 1996).

More than 100 gushers roared from 1909 to 1912, increasing greatly the daily oil production (Del Mar, 1996). From all the gushers, the Lakeview, in section 25, T12N, R24W, is the most famous, blowing wild for 18 months and producing approximately 9 million barrels of oil (Rintoul, 1990 in Sturm, 1996).

In 1910, the newly discovered reserves in the Buena Vista area were included as part of the "Midway Field". By 1920 the area was known as the Sunset-Midway Field (Del Mar, 1996). In 1934 the California Division of Oil and Gas separated the Midway Field, the Buena Vista field, and the Sunset

Field and in 1942, recognized the "Midway Field" and the "Sunset Field" as part of the same "Midway-Sunset Field" (Del Mar, 1996).

In 1968 the Midway-Sunset field became officially a billion barrel field (Del Mar, 1996) in the giant category. Currently the Midway-Sunset Field holds the 4$^{th}$ position among the largest oil fields in the U.S. (internet source*) ranking in this position since 1953 (Lennon, 1990).

Between the years 1990 and 1995 the average daily oil production of the field was 163,400 barrels, reaching a cumulative production of 2.3 billion barrels of oil and 563 billion cubic feet of gas (Gregory, 1996).

### 3.2 Drilling activity

Up to 1995, there were 700 steam injector wells, 4100 shut-in wells and 9600 producing wells, accounting for more than 14,400 active wells in the Midway-Sunset field (Gregory, 1996). In the past years, more than a thousand wells have been plugged and abandoned (Gregory, 1996). The northern one-third of the field, includes more than 6,000 producing wells (1996) from the thermally enhanced oil recovery projects in the Potter Sandstone with 95,000 barrels of 10 to 17 API gravity oil produced daily (Gardiner, Wylie Jr., and Gagner, 1996). The development of the Belridge

Diatomite member of the Monterey Formation began in 1984 and continues to date with more than 150 wells drilled (Mercer, 1996). Lighter oil (20°- 36° API) is produced from deeper sand bodies (e.g. Potter Sand) and fractured diatomaceous shales (Gregory, 1996); with depths ranging from 300 to 5000 feet (Mercer, 1996).

Thermal history studies conducted in the Elk Hills 934-29R deep well by the Michigan Technological University and Digital Petrophysics Inc., suggests that reservoirs shallower than approximately 17,000 feet are prospective (Nigrini, 1996). This indicates that there is good potential for new prospects in the Midway-Sunset area were most of the production currently comes from shallower reservoirs.

### 3.3 The Potter Sandstone

The name "Stevens" has been widely used by many writers (e.g. MacPherson 1978, Webb 1981, Quinn, 1990) when referring to "deep-water turbidites found in the central San Joaquin basin" (Sturm, 1996). In a more general way, the name Stevens is used for all upper Miocene turbidite sandstones found in the southern San Joaquin basin (Quinn, 1990). Therefore, upper Miocene clastic sediment gravity flows referred to as

Spellacy and Potter in the subsurface producing area of Midway-Sunset field, are referred to as Stevens in the central basin where they may have had continued deposition through the intra-slope environment during the time of deposition (Ryder and Thomson, 1989 in Sturm, 1996). This suggests that they can be considered equivalent stratigraphic units.

The Potter Sandstone reservoirs are believed to be deep water sediments (Gregory, 1996). These deposits are encased in the diatomaceous mudstones of the Belridge Diatomite, which acts as a source rock and a seal (Gregory, 1996) in the system. When the Diatomite is fractured, and depending upon the depth of burial, it is also considered a reservoir (Gregory, 1996).

Based on well-log correlations it is apparent that the Potter pinches-out into the Reef Ridge Shale down structural dip to the south and along strike to the north (Gardiner, Wylie Jr., and Gagner, 1996) this is also apparent in the stratigraphic interpretation conducted in this thesis. The unit is represented by conglomerates and arkosic sandstones[1] ([1]personal preliminary observation on samples taken during visit to Bakersfield) filling apparent submarine canyons cut into the older Belridge Diatomite[1] (Gardiner, Wylie Jr., and Gagner, 1996). The Potter sandstone is one of the younger members of the Santa Margarita (Gregory, 1996); a name by which it is recognized in outcrop.

Outcrop mapping of the Santa Margarita by Nilsen in 1995 (Gardiner, Wylie Jr., and Gagner, 1996) indicates that conglomeratic sandstones "clearly fill deeply incised submarine canyons cut into the Belridge Diatomite" in contrast to the stratigraphically higher medium and fine grained sandstones which have a sheetlike geometry and are interbedded with laterally continuous diatomite units (Gardiner, Wylie Jr., and Gagner, 1996). Sandstone and conglomeratic deposits of the Potter interval correspond to the upper Miocene, Pliocene and Pleistocene. Dipmeter analysis of this section suggests that there was a prevailing northeast depositional direction for the early sandstone reservoirs followed by a rotation of the axis of deposition to a southeast direction for the upper Potter sandstone (G. J. Gregory, 1996). The transport of debris and turbidity flows in a northeast direction toward the San Joaquin basin caused "time-transgressive" deposition of northwest-stepping submarine fans (Gregory, 1996).

The Potter producing area is roughly limited to the north part of the Midway-Sunset field, (Gardiner, Wylie Jr., and Gagner, 1996) particularly to townships 30 and 31 south range 22 east (figure 11).

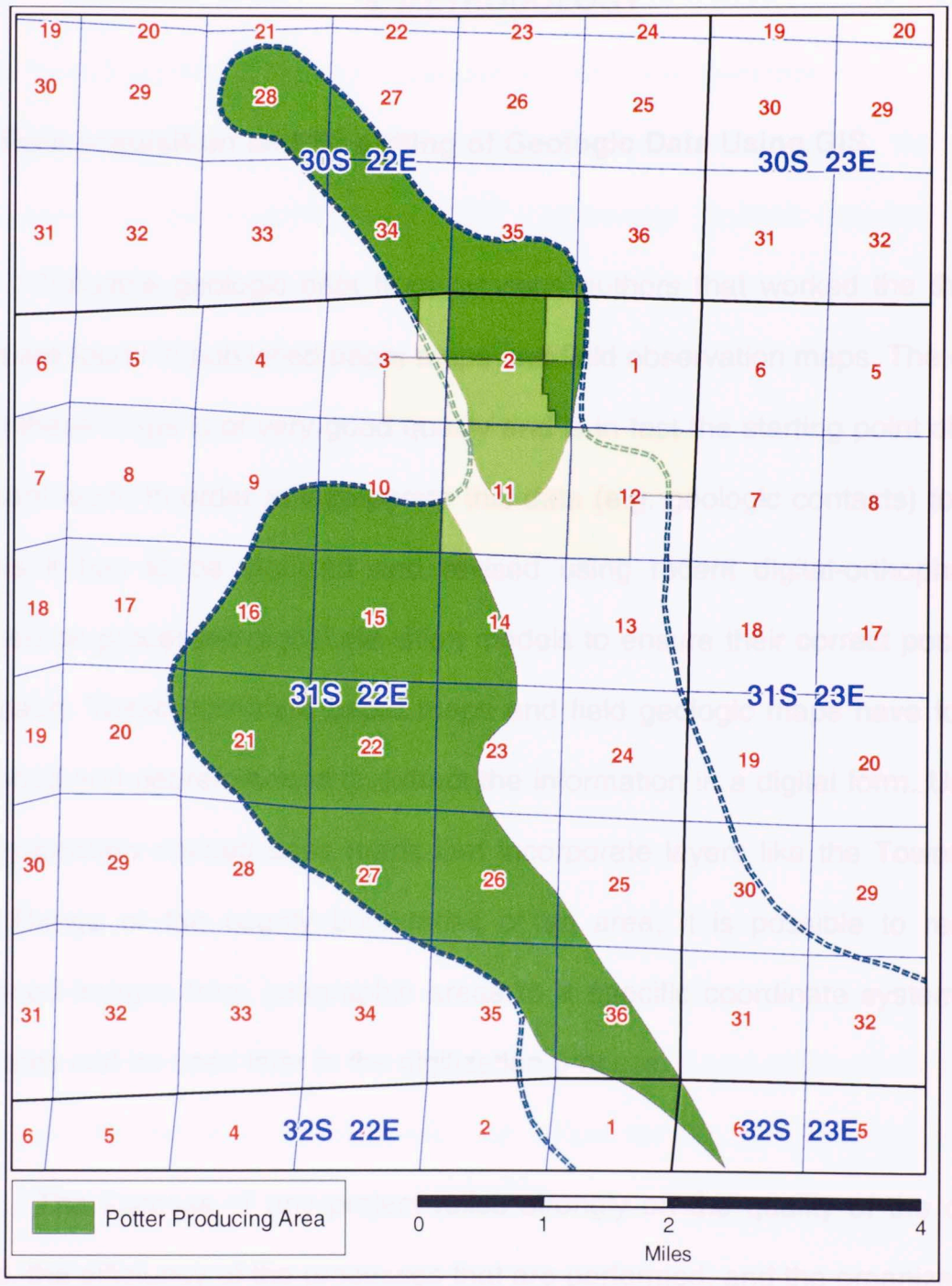


**Figure 11.** Potter producing area, note that almost all the area is distributed in townships 31 and 32 south range 22 east (Midway sunset extension and potter producing area digitized from R. L. Gardiner, A. S. Wylie, Jr., M. J. Gagner., 1996, Pg. 176, Figure 1).

# 4. METHODOLOGY

## 4.1 Data acquisition and 3D editing of Geologic Data Using GIS

Valuable geologic data from previous authors that worked the thesis area are found in published paper maps and field observation maps. The data from these maps is of very good quality and is in fact the starting point of the present work. In order to incorporate this data (e.g. geologic contacts) to the thesis it has to be digitized and revised using recent digital-orthophotos draped on processed digital elevation models to ensure their correct position in space. These published paper maps and field geologic maps have to be scanned and georeferenced to extract the information in a digital form. Using geographically revised base maps that incorporate layers like the Township and Range or the county boundaries of an area, it is possible to rectify scanned images from geographic areas to a specific coordinate system so that they can be used later in the digitization process.

The success of any project relies strongly on the quality of the data used, the efficiency of the processes that are performed, and the organization of the data obtained from external sources or the data created in the project. The quality of geographic data is most sensitive in terms of accuracy; a good

coordinate system suitable for the specific work area ensures no distortion of shapes, and minimizes the error associated with measurements.

It is important to obtain data from reliable sources, where the data accuracy can be trusted (e.g. USGS, University Spatial libraries, and Government agencies). Even though the data obtained may be reliable, it has to be tested and revised using known spatial data points to check for errors before base maps are created for the georeferencing process.

Once all geographic data layers were obtained for this thesis, digital orthophotos and pre-rectified topographic maps (DRG's digital raster graphics) were gathered. These maps and photos are high resolution images that aid in the rectification process of the geologic maps.

The geologic maps for this work are those of Dibblee (1972, 1973) and cropped images from Nilsen, (1995). For more information on these maps see bibliography. Two maps (Dibblee 1972, 1973) and 22 images (Nilsen, 1995) were scanned at 300 dpi (dots per inch) and rectified to preserve their resolution. The maps were then loaded into the project and digitized. In order to check the match of the data with the actual terrain, 10 digital elevation models (DEM's) were obtained from the USGS (30 meter resolution); these were then merged and clipped (figure 25) to match the exact area of interest and used to display maps and high resolution orthophotos in 3D.

After revising the quality of the data and editing (3D) all errors and mismatches; it was possible to extract more then 700 geologic contacts, 1266 surface strike & dip structural data, 172 fold axes, and 292 polygons for the areas covered by geologic formations in the work area. Using spreadsheets from vendors and state agencies, a database with the location of more than 20000 wells in the area of interest was created.

## 4.2 Data gathering, GIS, and process

### *4.2.1 General*

The purpose of this thesis is to produce a structural and stratigraphic interpretation of an area in the San Joaquin valley in southern California. An important part of this thesis is to organize a reliable and complete geodatabase; that includes data for location, physical geology, geographic data, well-log data, and topographic data from digital elevation models (DEM) for terrain modeling. The ability to obtain and maintain position accuracy is a priority. To minimize error, all the data acquired and all new data produced or edited are projected using the same coordinate system. The Universal Transverse Mercator projection; specifically the North American Datum (NAD)1983 UTM Zone 11N coordinate system, with meters as the linear unit,

was used. This coordinate system ensures low distortion of shapes and measurement accuracy for the geographic location of the thesis.

*4.2.2 Universal transverse Mercator*

The Mercator projection is a conformal projection; this means that angles and shapes in small areas on the terrain are projected as the same angles or shapes on a map (UWGB *website*, 2006). The Transverse Mercator projection is very accurate in laterally narrow zones (east to west direction). For this reason the Universal Transverse Mercator System or UTM System was created (UWGB *website*, 2006). The UTM System has a cylindrical transverse projection; this means that a cylinder is situated crossways to the earth intersecting it at a line, following a North to South direction (figure 12).

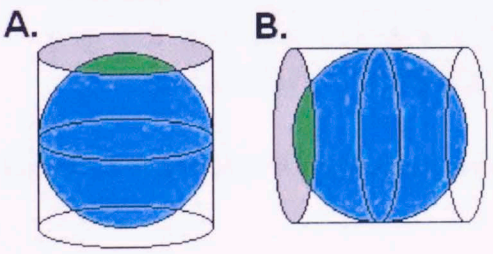


**Figure 12.**
A) Normal Mercator projection.
B) Transverse Mercator projection (extracted from the University of Wisconsin webpage, 2006).

The UTM system is subdivided into 60 zones (figure 13), each covering 6 decimal degrees in width (longitude). Each one of these 6 decimal degree bands has a separate projected coordinate system which is very accurate and useful for geographic areas restricted laterally to a single zone. These zones

are numbered in consecutive order to the East from Zone 1 (between 180° and 174° West) to Zone 60 (between 174° and 180° East), with meters as lineal unit. Based on the characteristics mentioned above and the fact that the work area lies completely within Zone 11, the NAD_1983 UTM Zone 11N coordinate system was selected for the present work (figure 14).

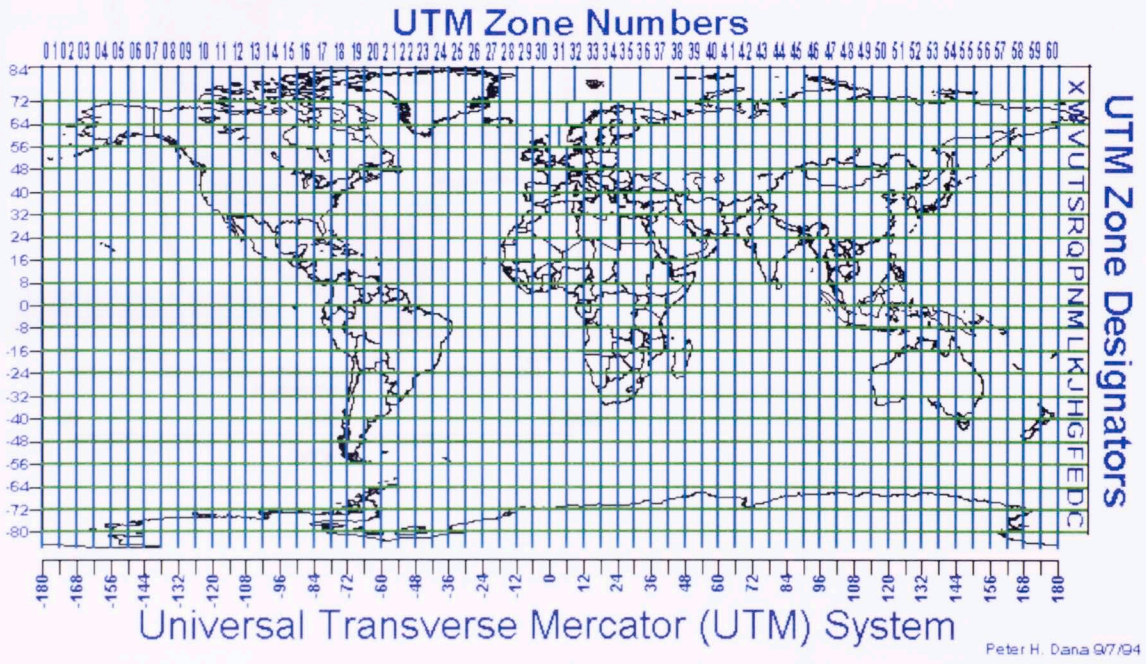


**Figure 13.** The UTM Zones (extracted from the University of Colorado at Boulder web page, 2006).

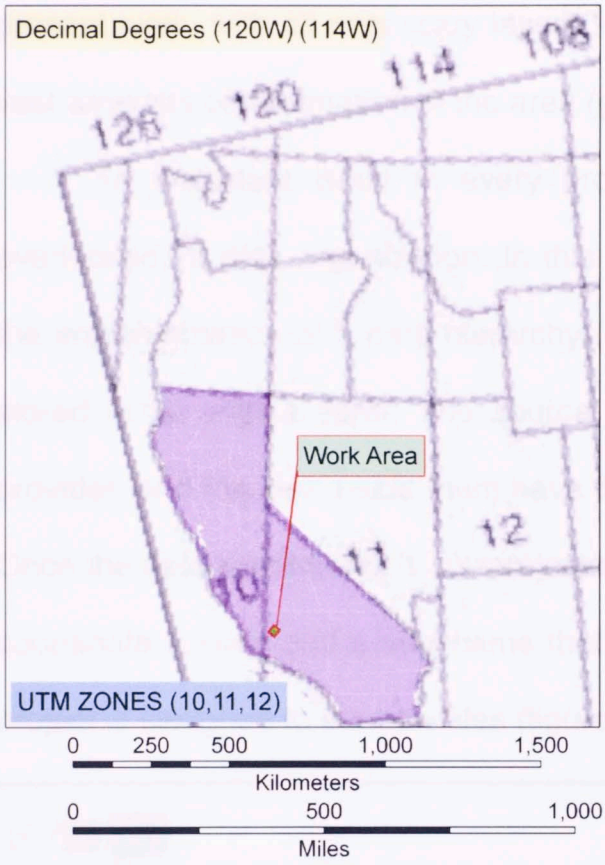


**Figure 14.**
Location of work area in zone 11N (modified from the Spatial Analysis Laboratory webpage, 2006).

## 4.3 Work flow

### *4.3.1 Location-Maps and Layers*

Various layers were obtained from 3 different spatial information databases (see references), these are the California Spatial Information Library, ESRI's Census 2000 Data, and the USGS (GEODE, GIS-Data Depot, and NOGA). This intense search of data resulted in a robust database for the

present work, with all necessary layers for location (digital vector layers) and vast amounts of information of the area (geographic data).

An important issue in every project in Geosciences, that is often overlooked, is data organization. In this thesis, this issue was addressed by the implementation of a data hierarchy (A, B, and F in figure 15). All data is stored in its original form. The source folders have the name of the data provider, and the files inside them have the original names from the raw data. Once the data is obtained, it is reprojected into the NAD_1983-UTM-Zone11N coordinate system and a new name that is meaningful for the purpose of the project is assigned to the new files (figure 16).

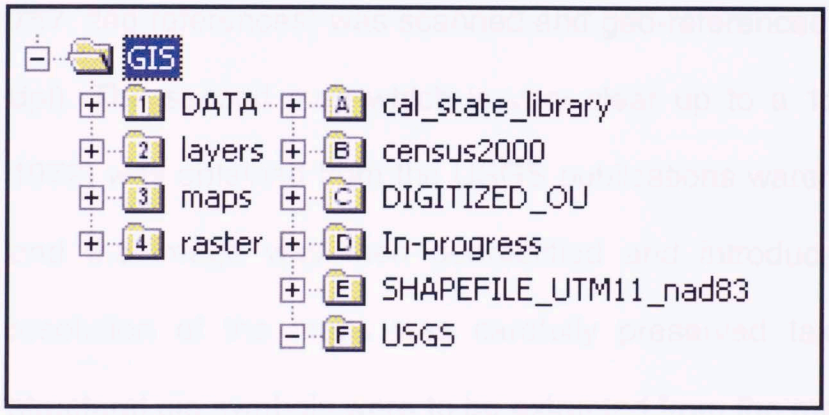


**Figure 15.**
Data hierarchy implemented for this thesis; data is organized by source, type of data, and status of the data (completed or in progress).

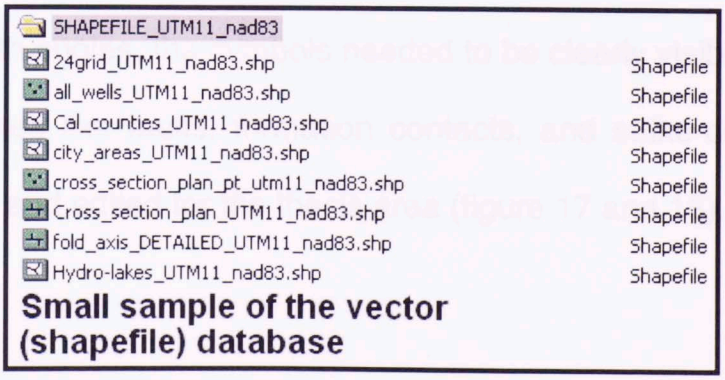


**Figure 16.**
Example of the reprojected data in the SAHPEFILE_UTM11_nad83 folder.

Other types of data (raster), like digital orthophoto quarter quadrangles (DOQQ's), digital raster graphics (DRG's, these are rectified topographic maps), digital elevation models (DEM's), and coverage files (vector line or polygon data), with more information are stored in the USGS folder (figure 15, folder F) organized by data type. A broader explanation on these data types is found further in the text.

*4.3.2 Data from Surface Physical Geology*

The best quality geologic maps available were acquired. The first map at a scale of 1:125000 (Dibblee, 1973, USGS geologic investigation MAP I-757, see references) was scanned and geo-referenced in high resolution (300 dpi). The second map which is very clear up to a 1:25000 scale (Dibblee, 1972) was obtained from the USGS publications warehouse (see references) and the image was then georectified and introduced in the project; the resolution of the maps was carefully preserved taking into account that structural dip symbols were to be extracted from the maps and that in order to be able to obtain the azimuth angles, the symbols needed to be clearly visible (figure 17). Geologic features like faults, formation contacts, and strike-dip data were digitized, revised and edited for the thesis area (figure 17 and 18).

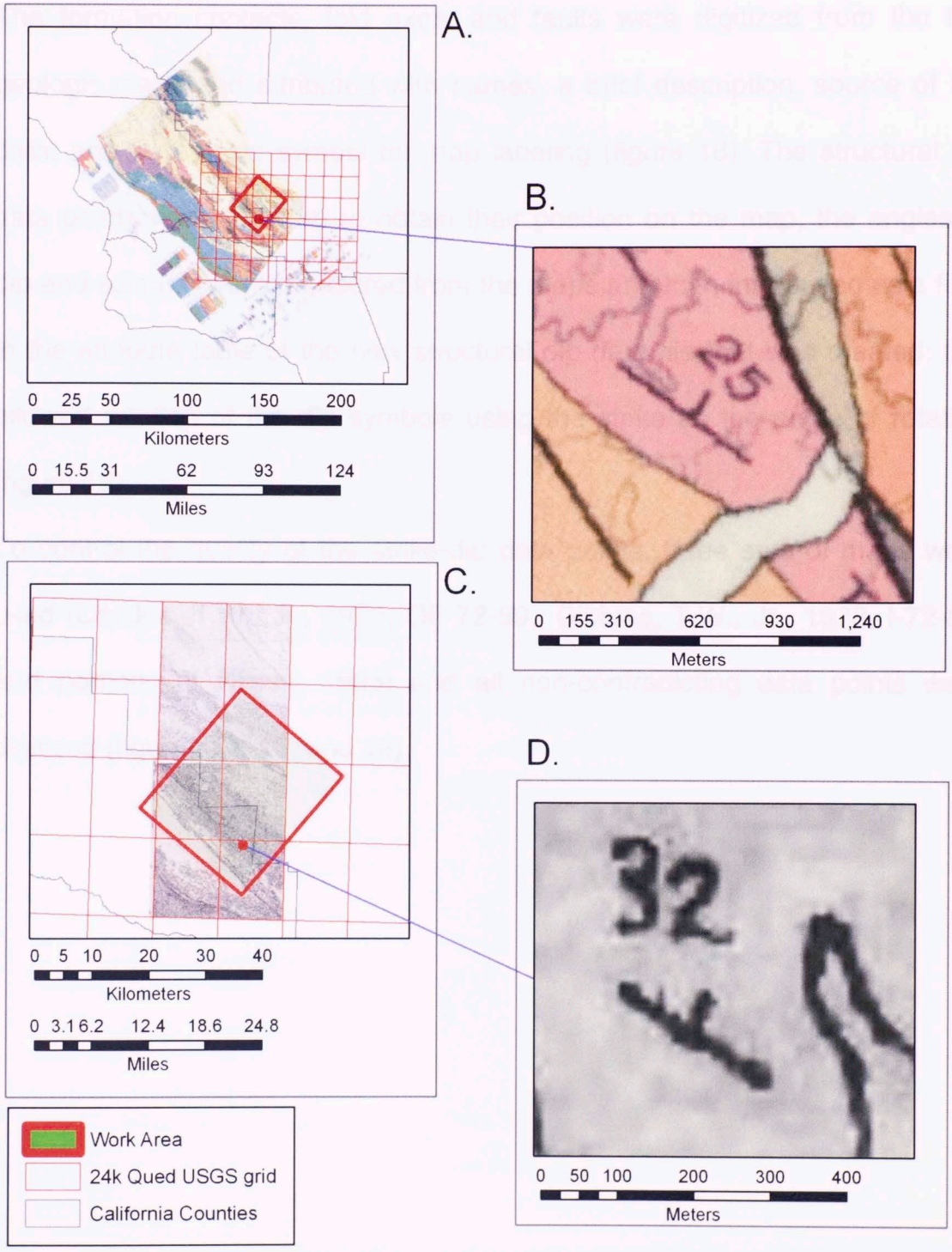


**Figure 17.** A) Georectified version of Geologic map 1 (Dibblee, 1973). B) level of resolution preserved; note the structural dip symbol (aprox. 0.5 cm in printed copy). C) Georectified version of Geologic map 2 (Dibblee, 1972). D) Level of resolution preserved; all structural dip symbols were preserved in the georeferenced map to this level of detail.

The formation contacts, fold axes, and faults were digitized from the two geologic maps and attributed with names, a brief description, source of the data, and a geologic symbol for map labeling (figure 18). The structural dip data points were digitized to obtain their position on the map, the angles of dip and azimuth were measured from the maps and then introduced as a field in the attribute table of the new structural dip data file that was created; this allowed rotation of the dip symbols using the strike as the angle of rotation (figure 19).

To control the quality of the strike-dip data points, three sets of maps were used (Dibblee, T.W., Jr., 1972, OF 72-89., Dibblee, T.W., Jr., 1973, I-72-89, and portions of Nilsen, 1995) and all non-contradicting data points were digitized (figures 17, 18, and 19).

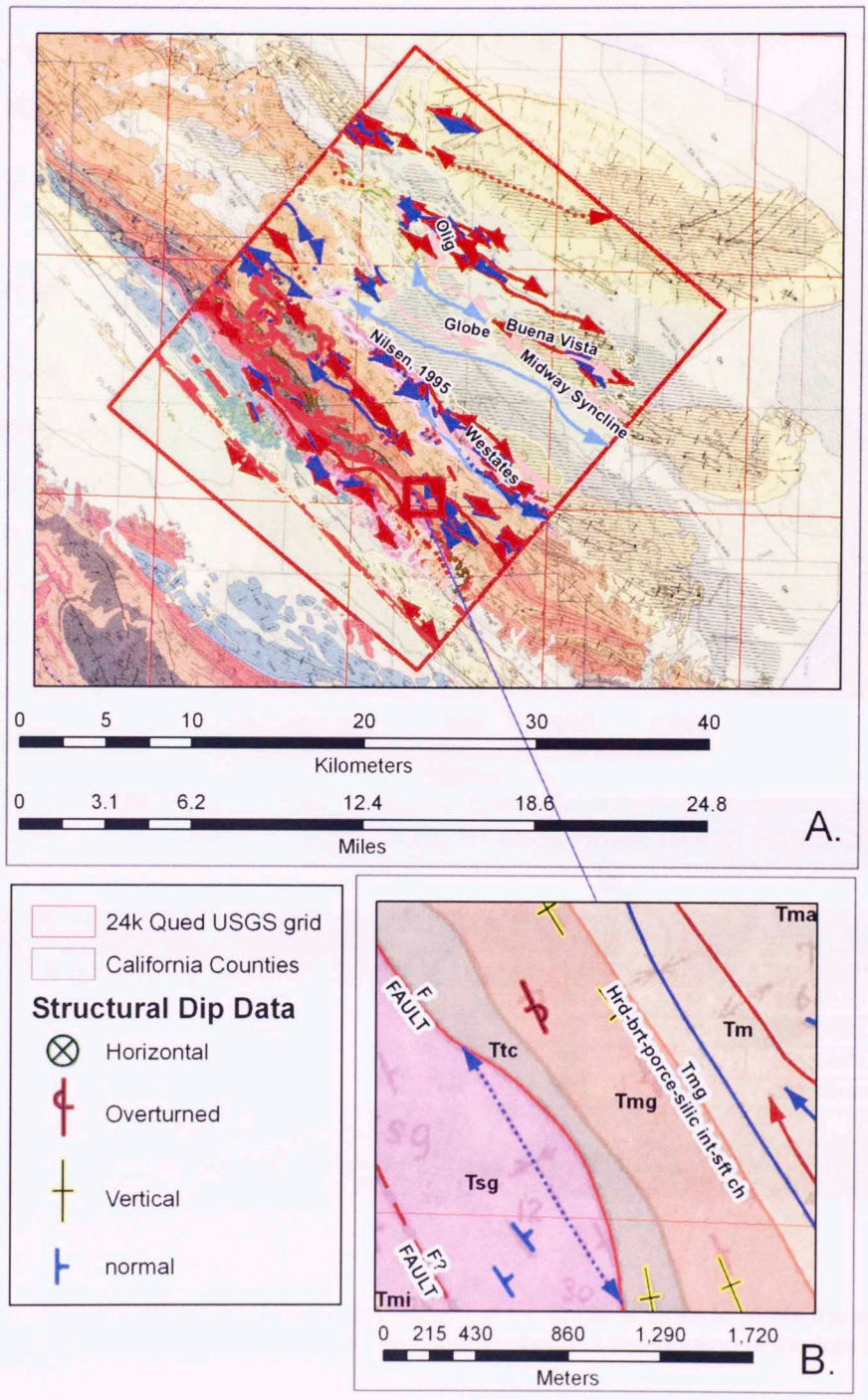


**Figure 18.** A) Complete digitization of all formation contacts, fold axes, faults, and structural dip data obtained from maps. B) Attributed data used for labeling and symbolization, notice labeling of geologic contacts and different symbols for structural dip data.

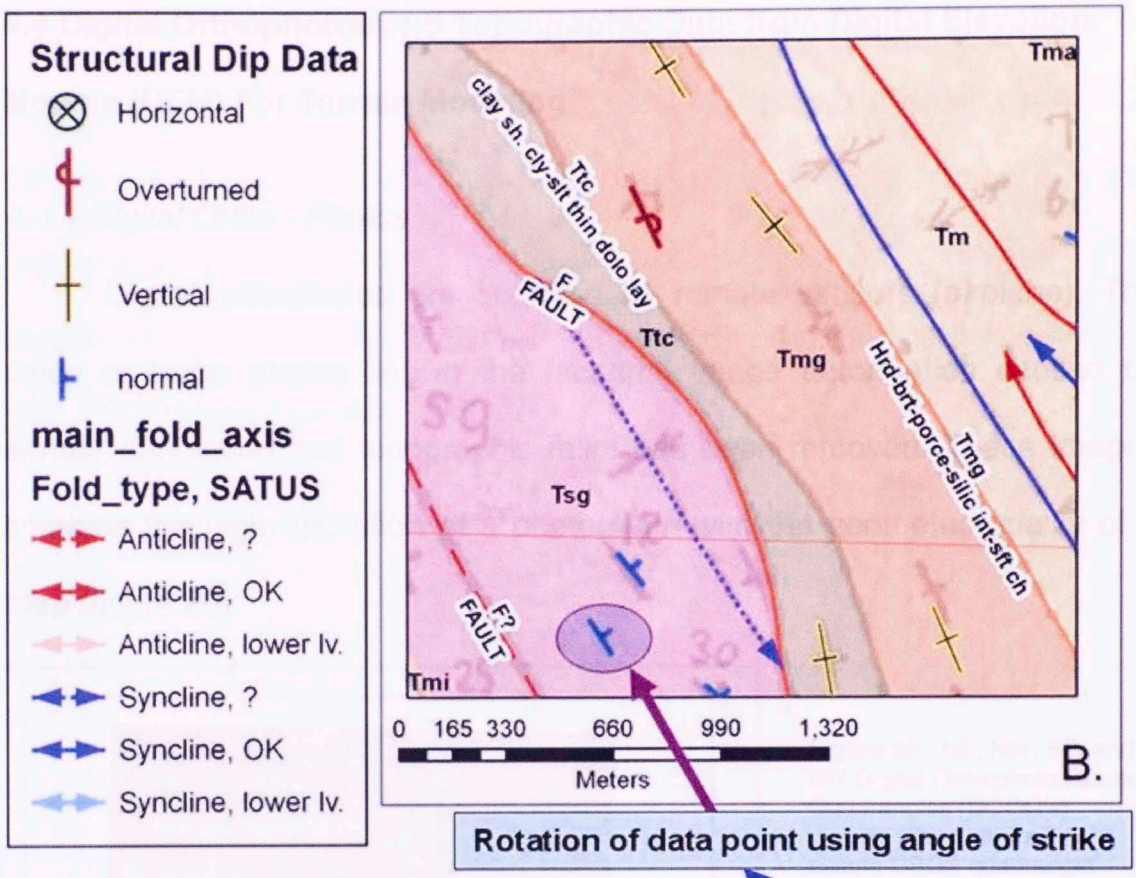


Attributes of dip_data_revised_UTM11_nad83

| FID | Shape* | Id | STATUS | status_num | INCL | DIP_DIREC | STRIKE_ | SOURCE |
|---|---|---|---|---|---|---|---|---|
| 1115 | Point ZM | 0 | normal | 1 | 25 | 55 | 325 | Dib72 OF_72-89 |
| 1237 | Point ZM | 0 | normal | 1 | 23 | 55 | 325 | Dib72 OF_72-89 |
| 57 | Point ZM | 0 | normal | 1 | 30 | 56 | 326 | Dib73 Inv - 757 |
| 412 | Point ZM | 0 | normal | 1 | 10 | 56 | 326 | Nilsen, 1995 |

Record: 0 Show: All Selected Records (0 out of 1266 Selected.) Options

**Figure 19.** Display of the structural dip data and the use of the angle of strike to rotate the symbols. Note also the number of data points in the attribute table (1266) and the labeling of the fold axes.

## 4.4 Digital Orthophotos and Topographic Data from Digital Elevation Models (DEM) For Terrain Modeling

### *4.4.1 Digital Ortho - Photos*

Digital orthophotos are acquired by remote sensors (airplane). The value of these photos lies in the fact that image deformation caused by sensor orientation and topographic relief has been removed. These images combine the high resolution of a photograph with the geometric quality of a map (figure 20).

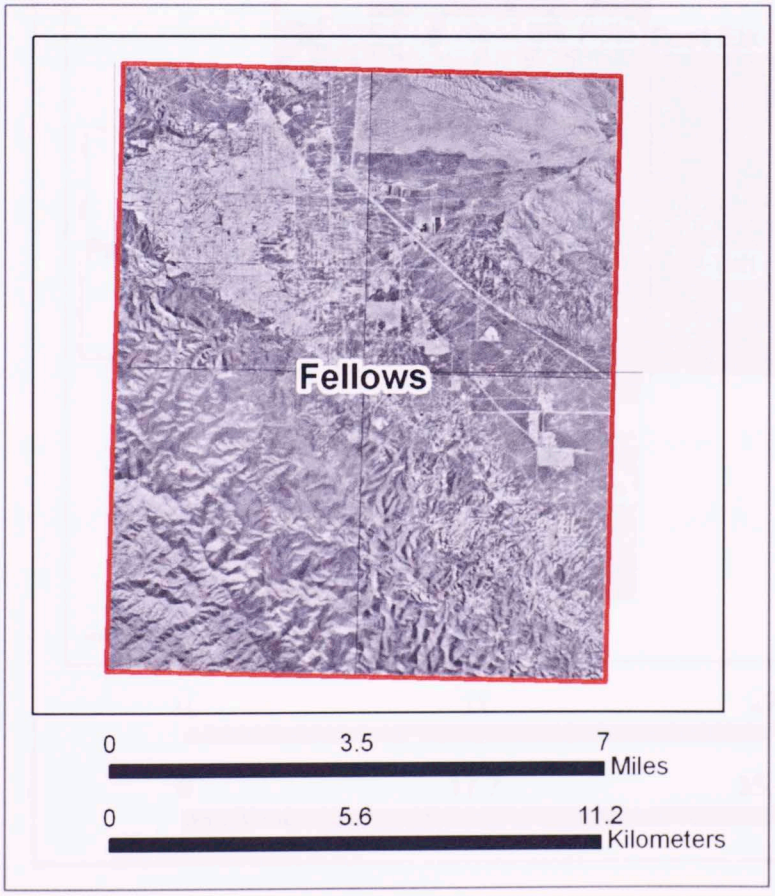


**Figure 20.** NE, NW, SE, and SW Digital Orthophoto Quarter Quadrangles (DOQQ's) covering the Fellows 7.5 minute USGS quadrangle (boundary marked by the red line).

The photographs used for this project have a cell size of 1 meter, (1 m. resolution) and cover a quarter of a 7.5 minute USGS quadrangle (figure 20). To cover larger areas, mosaics are created using multiple photos. For this reason orthophotos come with additional overlapping bands (minimum of 50 meters and maximum of 300 meters) to the edges of the photographs (USGS, National Mapping Division, 2006).

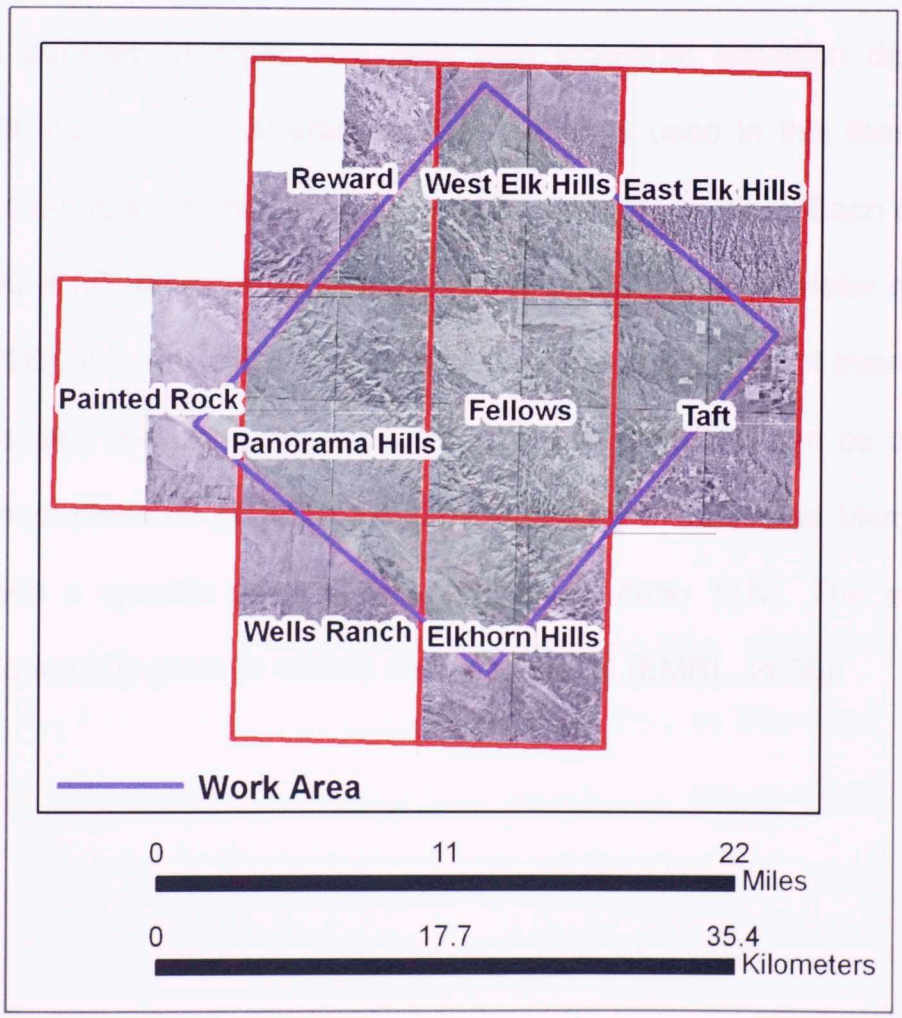


**Figure21.** Display of the 29 DOQQ's and 9 USGS quadrangles covered by the work area.

In order to obtain a complete coverage of the entire area, 29 DOQQ's had to be acquired; they cover completely or in some cases partial areas of 9 USGS 7.5 minute quadrangles (figure 21). The orthophotos come already projected to the UTM coordinate system used for the present work.

*4.4.2 Digital Elevation Model (DEM)*

A DEM is a type of DTM (Digital Terrain Model) in raster format, meaning that it consists of equal size cells with individual elevation data (figure 22A). DEM's come in different scales; the ones used in this thesis are 1:24.000 covering a 7.5 minute USGS quadrangle (figure 22C). Each cell represents a 30 X 30 meter block of terrain, thus producing a 30 meter resolution (figure 22B). If a single DEM does not cover the entire area of interest, a new DEM mosaic compiling the necessary number of DEM's can be constructed. The most common projection is UTM (Universal Transverse Mercator), in meters with a specific point of reference (e.g. Zone 11N). The elevation is also commonly given in meters above sea level (EMRL, 2006)

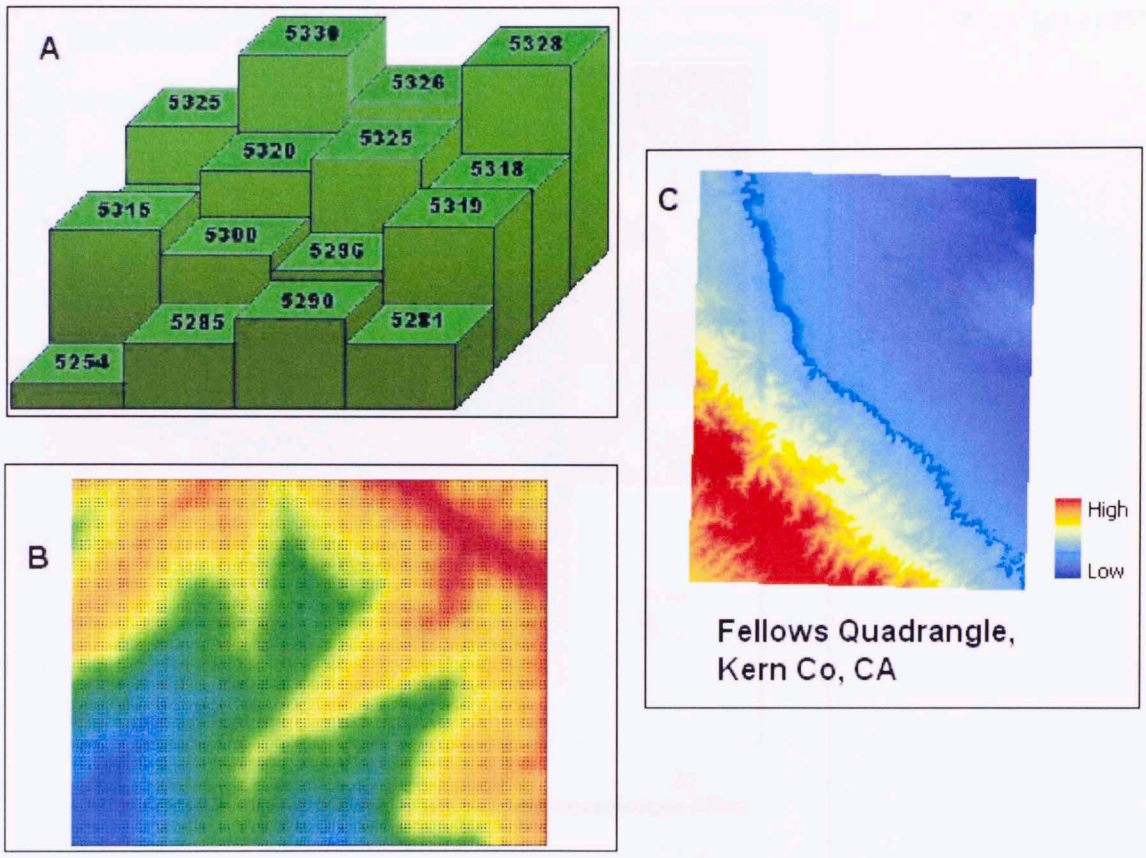


**Figure 22.** A) Representation of DEM data, each cell corresponds to a unique elevation. B) DEM portion at scale of 1:2400 (7.5 minutes quadrangle) each black dot represents a cell on the DEM. C) Example of one DEM used in the present work (Modified from; EMRL. April, 2006).

Similar to the situation with the DOQQ's, multiple DEM's had to be obtained to cover the entire area of interst; in this case 10 DEM's were required, covering the following USGS 7.5 minute Quarter Quadrangles: Reward, West Elk Hills, East Elk Hills, Painted Rock, Panorama Hills, Fellows, Taft, Wells Ranch, Elkhorn Hills, and a small portion of Maricopa to the southeast (figure 23 and 24).

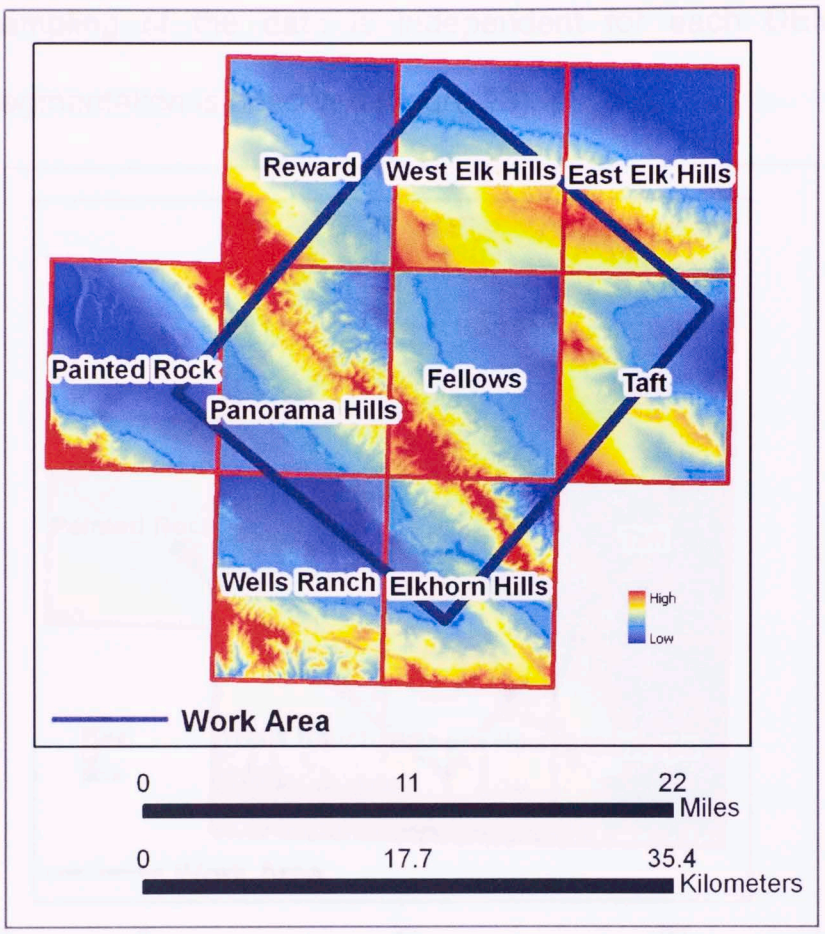


**Figure 23.**
Main set of DEM's covering the work area, 9 in total. Notice that the sampling of the data is restricted to each DEM creating the impression of discontinuity between each digital elevation model. Also notice Maricopa is not included in the figure to illustrate the small size of the work area that lies in this quadrangle.

When all the DEM's are displayed at the same time the impression of discontinuity between data boundaries is observed. This is due to the fact that the program assigns an extreme tone of blue to the minimum value and extreme tone of red to the maximum value of each DEM separately. Since the

sampling of the data is independent for each DEM file, this apparent segmentation is observed (figure 23).

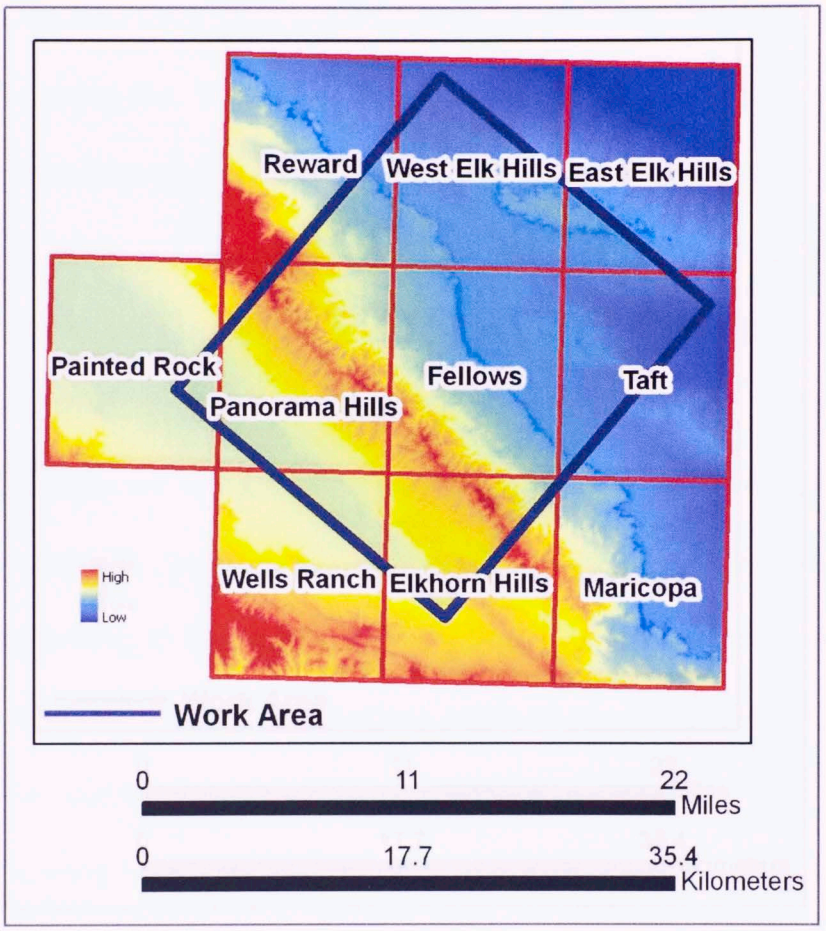


**Figure 24.**
Display of the DEM constructed for the entire area covered by the 10 USGS 7.5 minute quadrangles. Notice that the DEM for Maricopa is also added, as a small portion of the study area falls inside this quadrangle.

This apparent data discontinuity can be removed by merging all DEM's into a new single file for the entire area covered by the previous DEM's (figure 24). This file is very convenient for the continuous display of DEM data, but due to its large size, it considerably diminishes computer performance and uses a considerable amount of disk space. In order to solve this problem, this DEM was cropped to exactly match the thesis area, downsizing the DEM file

approximately 50%, maintaining the original resolution (30 meters), and considerably enhancing the performance of the computer (figure 25).

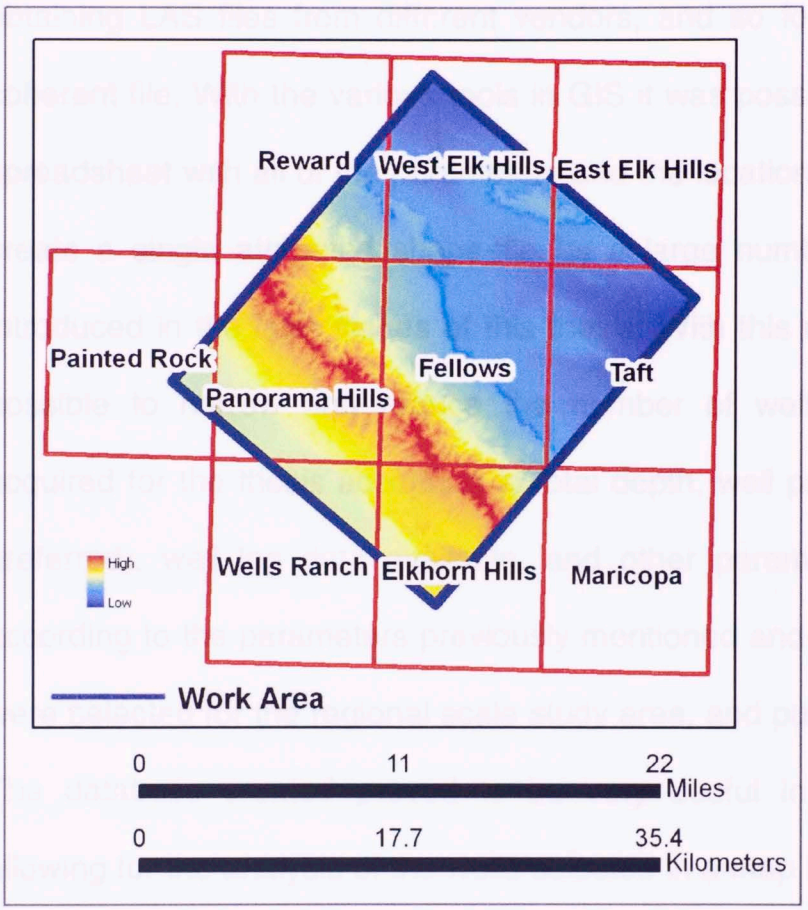


**Figure 25.**
Cropped DEM; this DEM matches the work area perfectly, enhancing computer performance and minimizing storage requirements, keeping the same resolution of the original DEM's.

## 4.5 Location of Wells in the Thesis Area

Many wells have been drilled in the work area and in order to construct the structural cross sections, a high level of well coverage is necessary. The data for these wells was spread among various vendors and databases

making it necessary to merge these small pieces of information from each well (well location, well logs available, maximum depth drilled, cost of obtaining LAS files from different vendors, and so forth), into a single and coherent file. With the various tools in GIS it was possible to create a master spreadsheet with all of the parameters and the location for each well to finally create a single attributed shape-file for a large number of wells that were introduced in the later stages of this thesis. With this new file created it was possible to narrow and reduce the number of wells that needed to be acquired for the thesis according to total depth, well path (vertical well being preferred), well log data available, and other parameters. The best wells according to the parameters previously mentioned and their strategic location were selected for the regional scale study area, and purchased from vendors. The database created proved to be very useful in the budget planning allowing for the analysis of the wells selected in a map interface observing the immediate economic implications of the purchase of each particular well, saving time and enabling a more efficient well selection (figure 26)

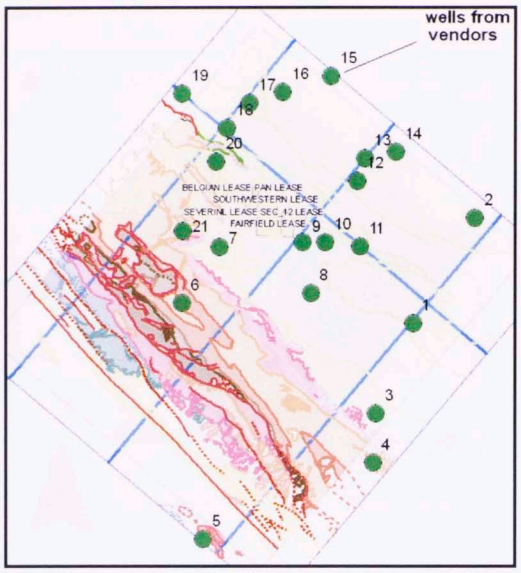


**Figure 26.**
Wells purchased from vendors after inspection and ranking of available wells according to specific parameters (TD, verticality, well-logs available, cost of LAS files and position with respect to the location of the cross-sections).

## 4.6 Terrain Modeling and 3D Geologic Data Editing

Initially all geologic data was digitized accurately following the geologic maps (figure 27) and evaluating the three geologic maps available for the best representation in the different zones of the work area.

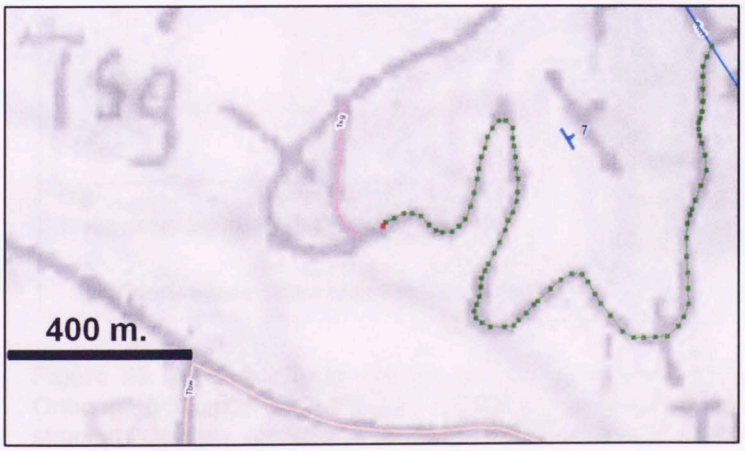


**Figure 27.** Density of points included in the editing process of the geologic maps. The original accuracy of the maps was preserved through the digitization process.

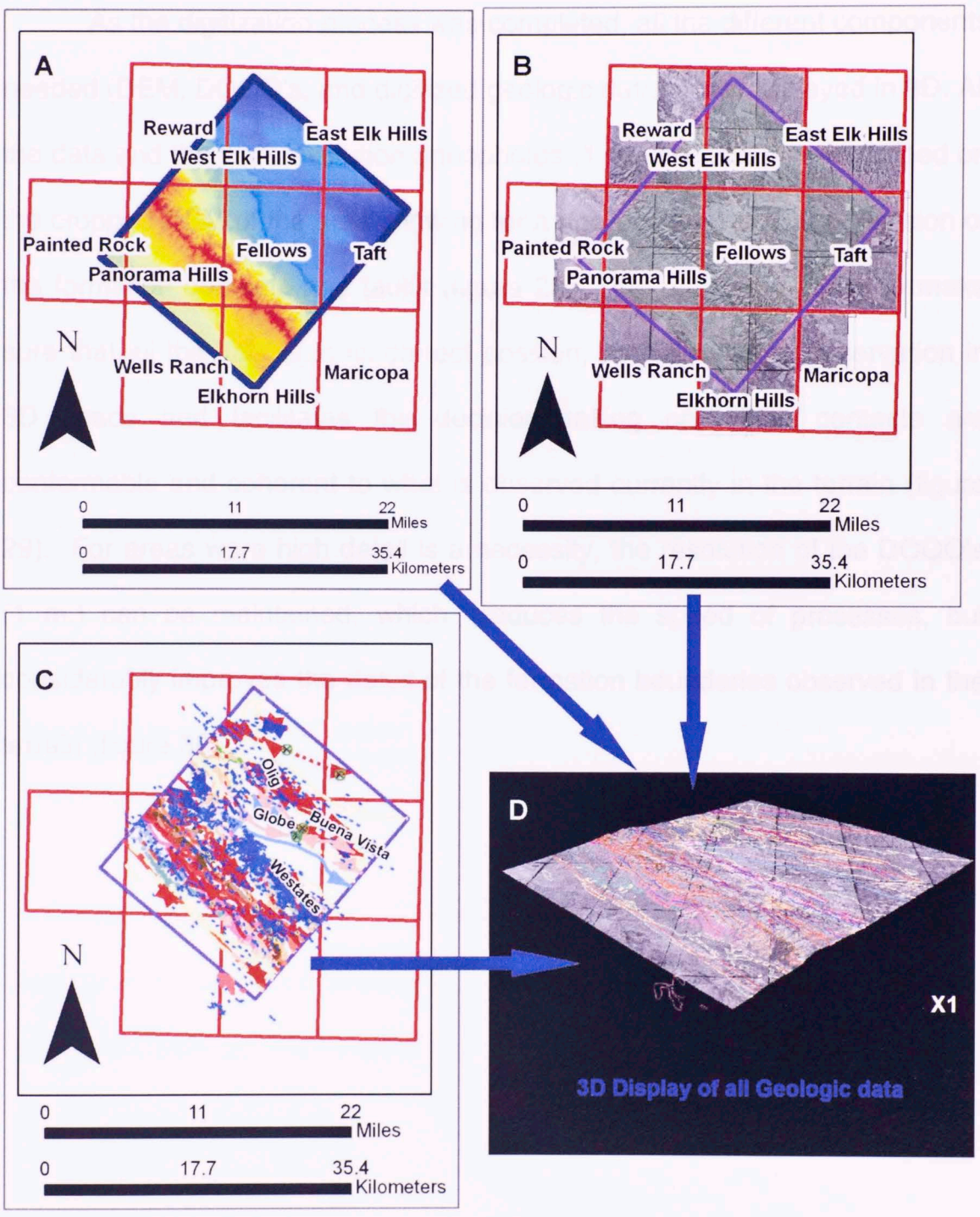


**Figure 28.** All components needed for the 3D display. A) Digital Elevation Model DEM. B) Digital Orthophoto Quarter Quadrangles DOQQ's. C) Digitized data: formation tops and faults, surface structural dip data, and fold axes. D) 3D display of the geologic data draped on the 3D DOQQ surface.

As the digitization process was completed, all the different components needed (DEM, DOQQ's, and digitized geologic data) were displayed in 3D. All the data and the high resolution orthophotos (1 m. resolution) were draped on the cropped DEM of the area allowing for a rigorous quality control revision of the formation contacts and faults (figure 28). This process is done to make sure that all the data is in its correct position, as it allows the observation in 3D space and facilitates the decision-making on which contacts are conformable and coherent to what is observed currently in the terrain (figure 29). For areas were high detail is a necessity, the resolution of the DOQQ's (1 m.) can be maintained, which reduces the speed of processes, but considerably improves the detail of the formation boundaries observed in the terrain (figure 30).

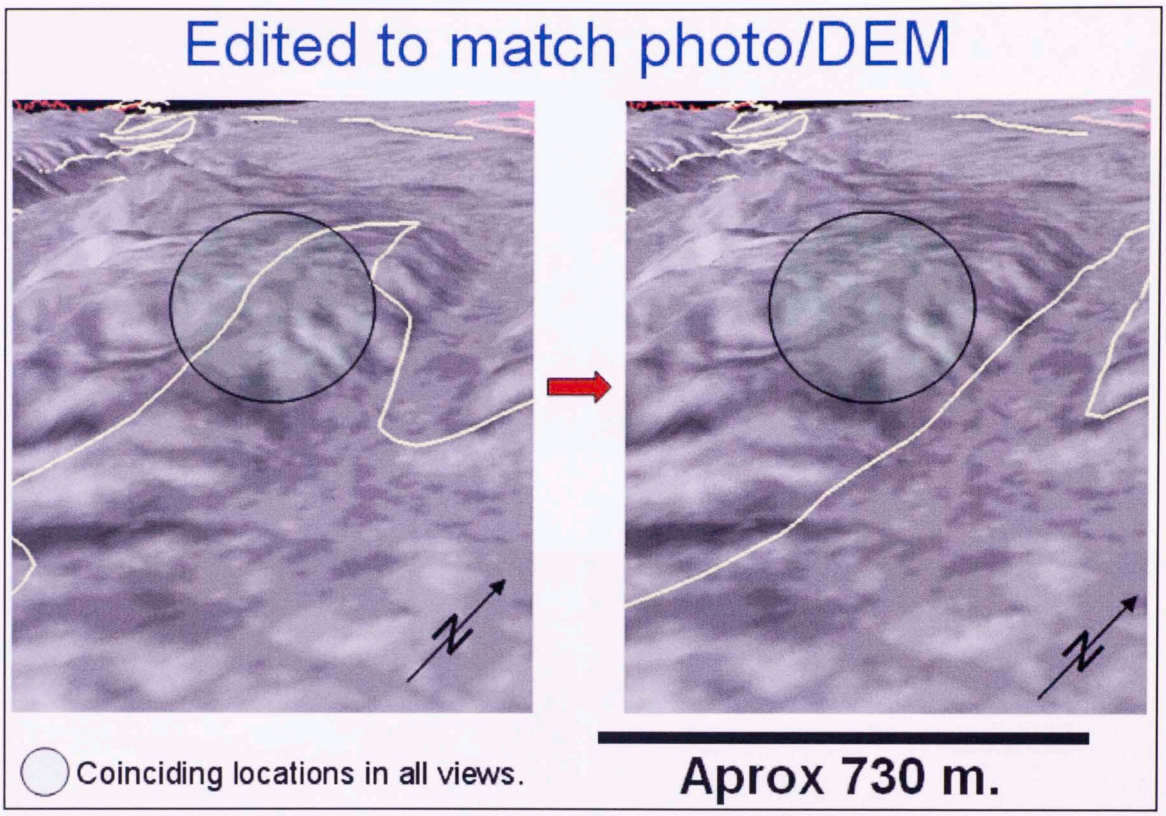


**Figure 29.** Adjustment of geologic contact, Pleistocene Paso Robles Formation. The contact was not conformable with the terrain. To the left contact prior to 3D edition, 3D edited contact to the right.

High resolution 3D models of the surface permit the use of rivers, drainage, and outcrops in the editing process to validate changes to data from the original geologic maps (figure 30).

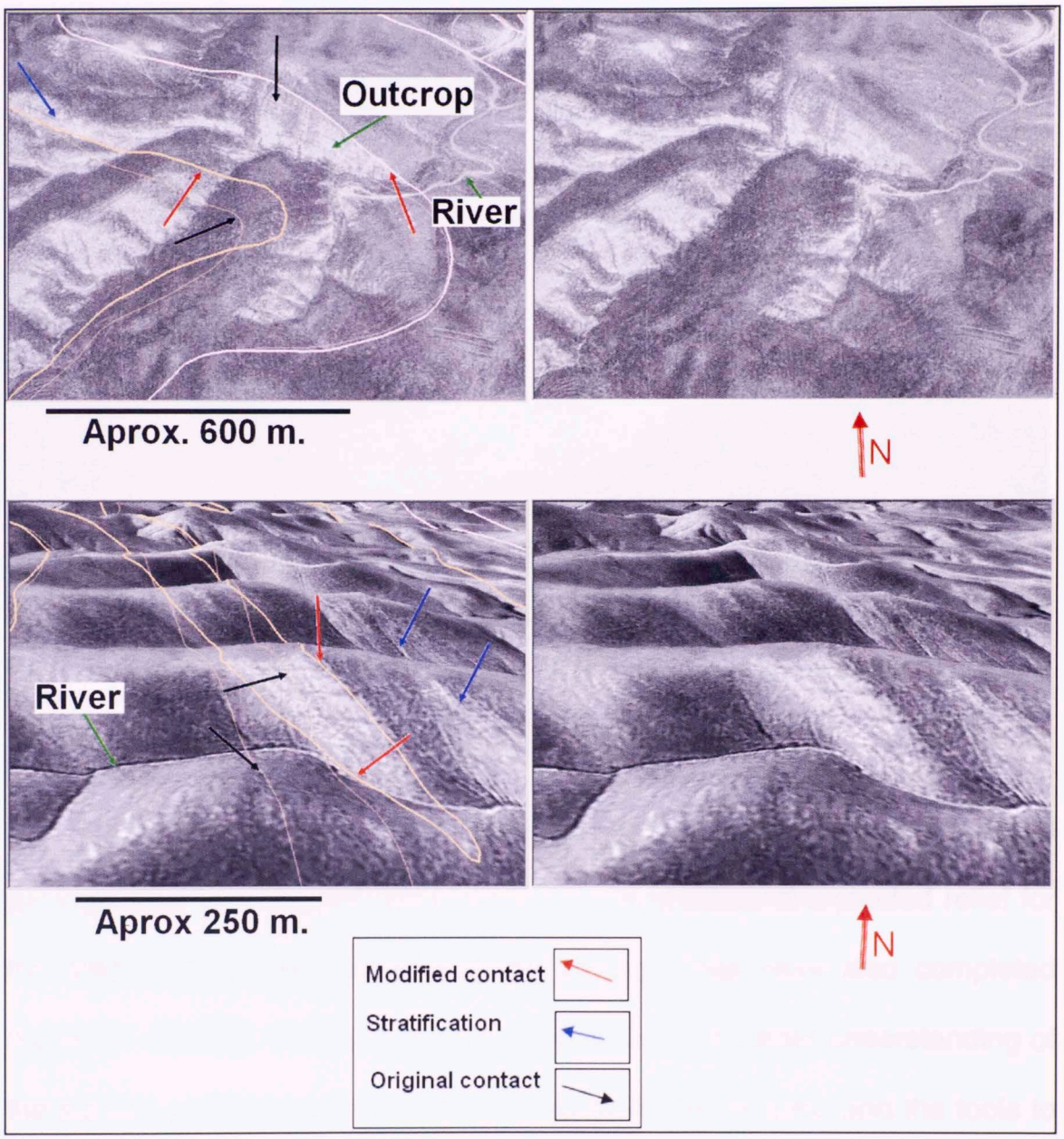


**Figure 30.** The resolution of the DOQQ's (1 m.) can be maintained; this reduces computer performance but considerably enhances the quality of the display. Note formation boundaries and bedding planes. Compare to uninterpreted image to the right.

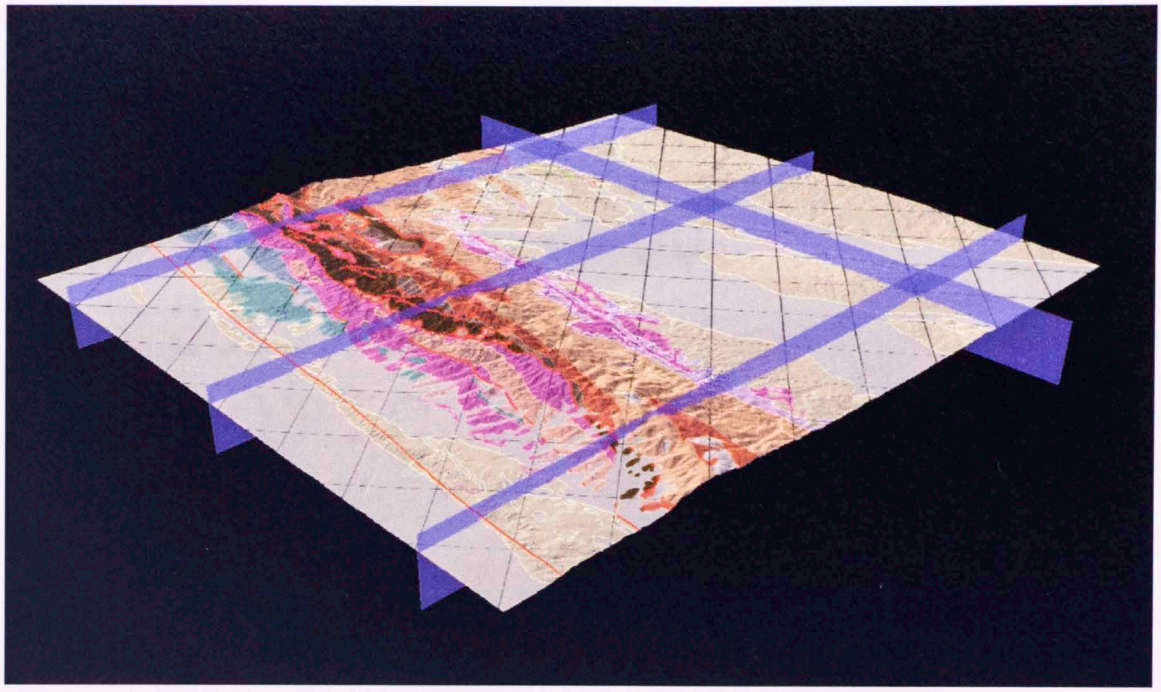

**Figure 31.** 3D model of the surface geology in the work area. Note the benefits of using a raster image to display the geologic formations.

With all previously mentioned tasks completed, a corrected digital geologic map was created; other tasks like the creation of a shaded relief for the area, and a raster version of the geologic map were also completed (figure 31 and 32). These new layers provide a much better understanding of the surface geologic setting of this structurally complex area, and the tools to better interpret the subsurface structural geology in the thesis area.

All the geologic data that was obtained (surface structural dips, the 3D edited geologic contacts and faults) were imported into structural interpretation software for the construction of structural cross-sections. All of

this was preformed to obtain a better understanding of the structural geometry and the fold-fault relationships in the area. The construction of the digital geologic map is explained in greater detail later in the text along with the construction of the closely spaced cross-sections.

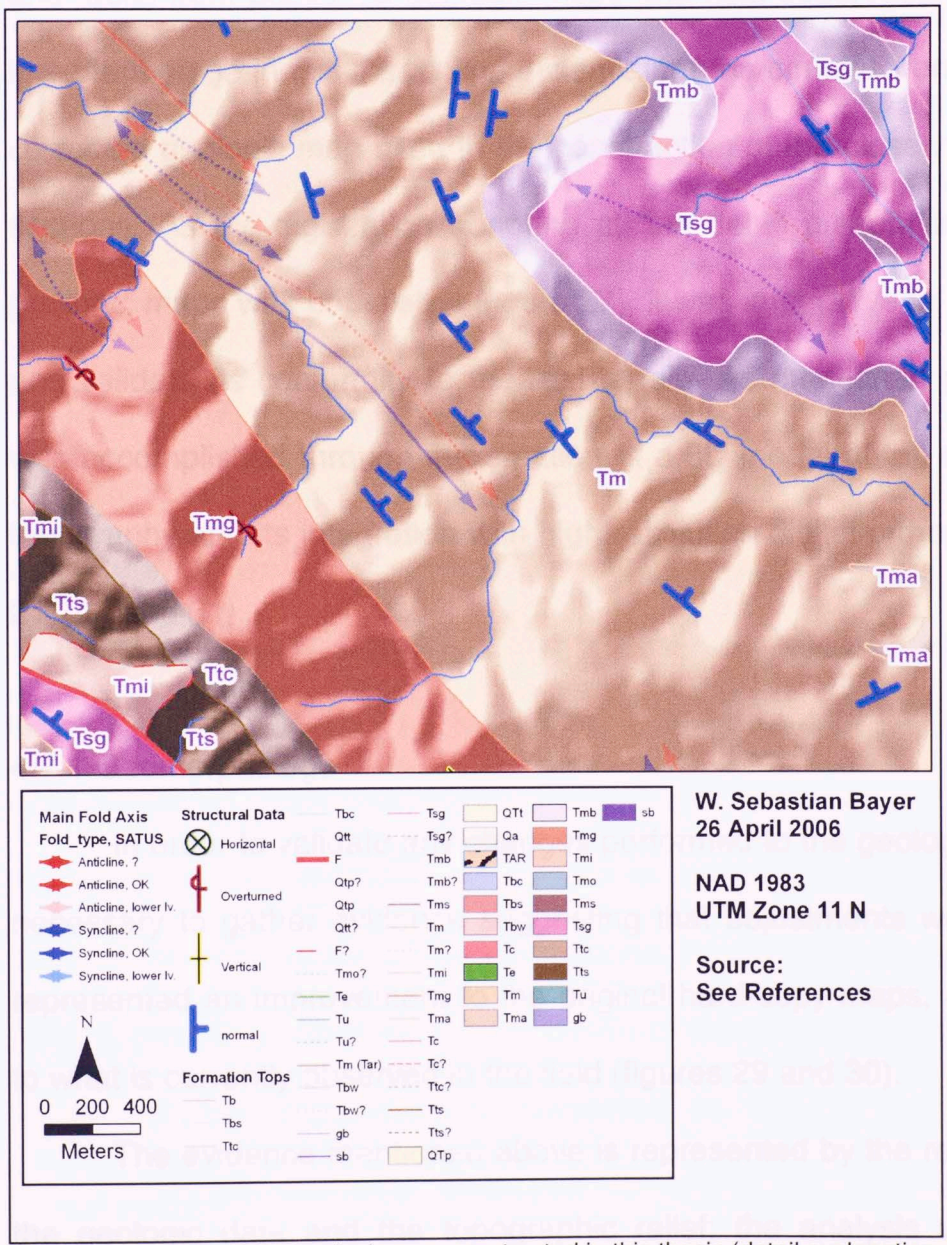


**Figure 32.** Portion of the geologic map constructed in this thesis (detail explanation on the construction found further in the text; see annexed full version of the geologic map).

## 4.7 Construction of the Geologic Map of the Study area

The revision and careful modification of the formation tops, fold axes and faults from published geologic maps and field observation maps was an important stage in this thesis and essential for the construction of the digitally corrected geologic map used in the construction of the closely spaced cross-sections. As the digitization honoring all the detail present in the available geologic maps was completed (figure 27), it was imperative to check the data and validate its conformity to the real terrain. As mentioned previously, this was accomplished through the creation of a 3D model of the current surface topography and its integration with high resolution digital orthophotos (figures 21, 28, and 31).

### 4.7.1 Geomorphology

In order to validate any changes performed to the geologic maps it was necessary to gather evidence suggesting that adjustments were necessary, represented an improvement to the original hard-copy-maps, and conformed to what is currently observed in the field (figures 29 and 30).

The evidence mentioned above is represented by the relation between the geologic data and the topographic relief; the analysis was conducted

during the photo-geologic phase of this thesis. It was accomplished using the digital elevation model and the high resolution orthophotos to produce a realistic view of the terrain similar to that obtained with a stereographic pair of aerial photos; with the advantage that in this case any distortion away from the center of the paper photos is removed. Here the occurrence of softer lithologies associated with smooth landscapes and resistant lithologies related to sharp slopes and more prominent buildups was observed. Other pieces of evidence that validate the changes that were performed are the relation of Quaternary fluvial deposits with river paths and the presence of resistant pre-Pleistocene formations as a control for streams present in the field and observed in the aerial photos (DOQQ's). The presence of flatirons in places where structural dip data points were extracted from the literature served as verification of the dip direction and the approximate slope of the bedding planes allowing the revision and validation of the surface structural data extracted from the maps. Finally, the verification of sand bodies mentioned in the literature and present in the geologic maps was possible through the observation of intra-formational lens-shaped bodies in the aerial photos, providing confidence in the quality of the geologic maps used and the validity of the improvements presented in this thesis. The different geomorphologic elements employed to validate the modifications here proposed are listed and explained extensively below.

*4.7.1.1 Lithologic Character of Geologic Formations*

The relative competence of the rocks is a very useful indication of changes in the lithology. Changes in relief associated with the competence variations of lithologic units were successfully used in this thesis to identify the accurate position of formation tops. Competent formations like the Tbw (Bitterwater formation) produce prominent mounds, while softer, friable lithologies like Tu (unnamed marine sediments) form soft slopes and smooth profiles (figure 33, B and D). Sandstone and conglomerate formations like the Tsg (Santa Margarita Formation) are represented by resistant morphologies that stand out in the terrain when observed in contact with non-competent units. Figure 33 illustrates this case; the interpretative sketch (D) shows the differences in the topographic profile as the lithology changes. The original contacts from the literature were edited and moved to conform to the slope changes observed and to fit the morphologies characteristic of each geologic unit. The corrected formation tops (figure 33, C) clearly match the topography and display natural conformity to the terrain.

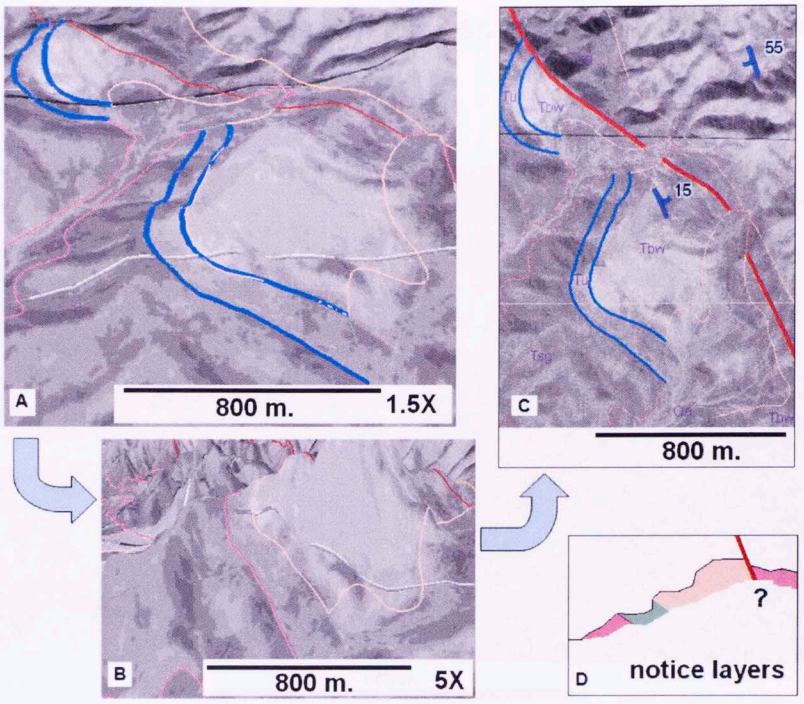


**Figure 33.** A) Geologic contacts observed in the terrain; the vertical exaggeration is 1.5. B) Geologic units observed in the terrain; exaggerated 5 times. C) Representation of the corrected formation tops in map view. D) Sketch of the topographic profile produced by the different lithologies.

Different lithologies produce different topographic profiles; these subtle differences are noticeable in the terrain model. Figure 34 shows the differences between the original maps (Dibblee, 1972) and the contacts obtained after revision of the DOQQ's. In the orthophotos it is possible to identify the presence of the Belridge Diatomite as it displays a distinctive white color when exposed and weathered (figure 34). These observations are not conclusive on their own and to validate these changes, topographic cross-

sections were constructed. Marked changes produced by different lithologies where observed in the profile (figure 35, B).

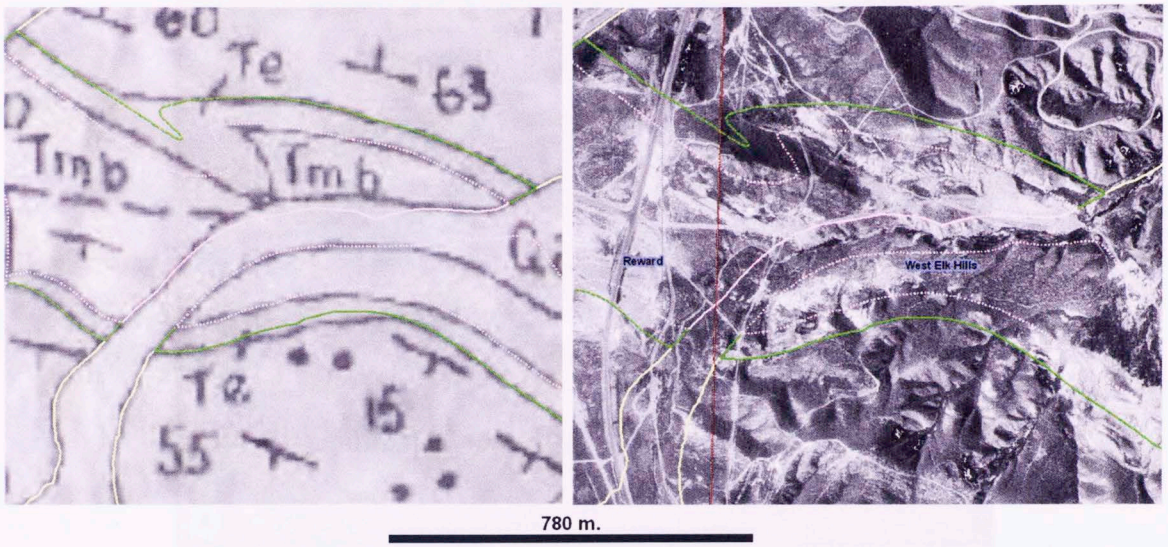


**Figure 34.** The figure to the left shows the original maps (Dibblee, 1972) with the edited geologic contacts (Fm. Tops) superimposed. The figure to the right displays the edited geologic contacts overlying the orthophotos; notice the difference in color to the center of the photo (white); here the Belridge diatomite is exposed.

The Belridge Diatomite (Tmb); a white porous, fissile diatomaceous shale (Dibblee, 1973) produces a soft morphology that is observed as a concave slope on a topographic profile (figure 35 B). The Etchegoin Formation (Te) composed of marine arkosic sandstone is brown when weathered (Dibblee, 1973). This lithology produces a sharp edge, resistant to erosion that can be observed in the schematic cross-section of figure 35; notice the sharp relief present in the contact between Tmb and Te (Te is younger).

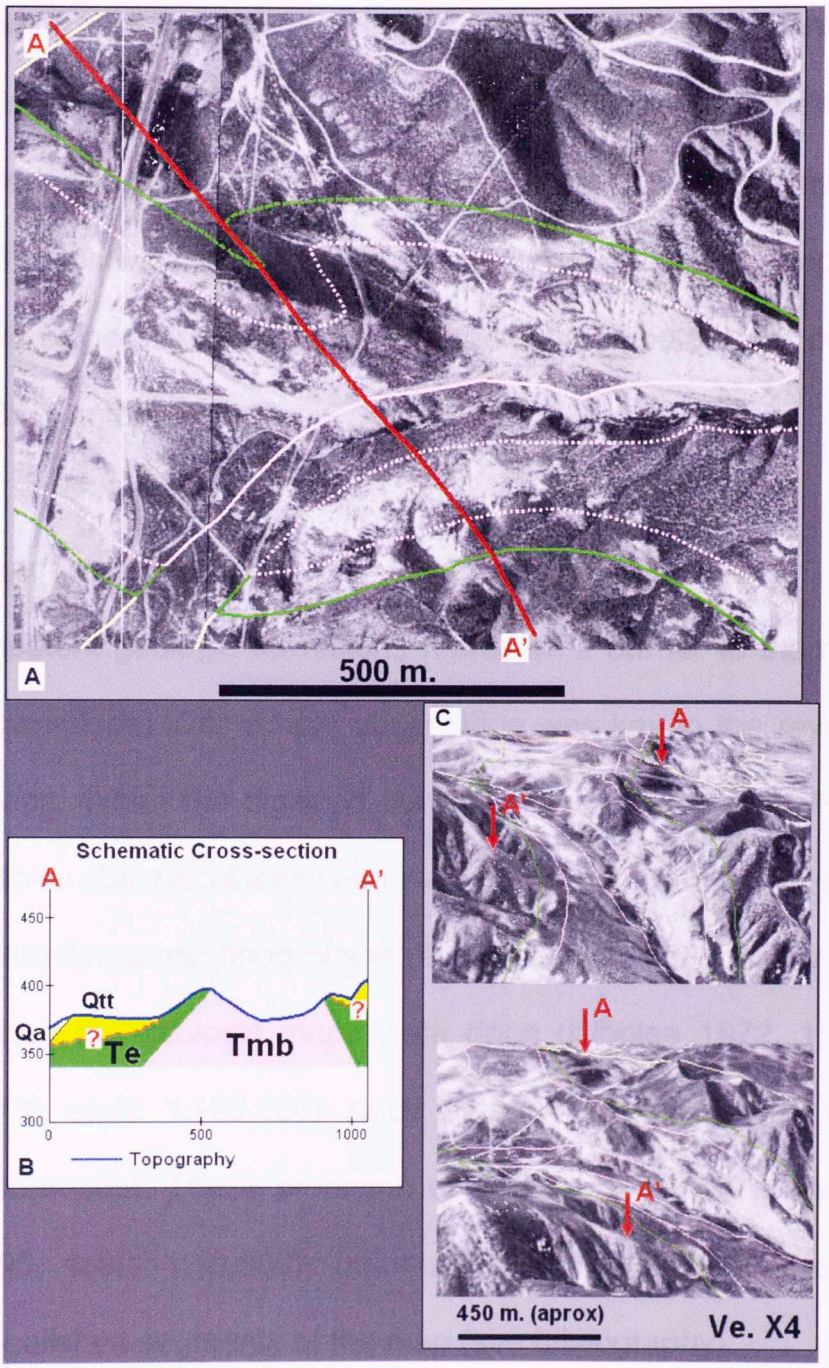


**Figure 35.** Geomorphologic differences of lithologies. A) Edited Formation tops overlying the orthophotos, also location of the schematic cross-section. B) Schematic cross-section; notice the sharp profile that is produced at the contact between Tmb and Te. C) Formation tops draped on the terrain model (3D view) notice how the river valley is preferably craved in the soft diatomite, opposed to the resistant morphology presented by more competent lithologies (Te).

The morphologic differences mentioned above are better observed in the terrain model; notice in figure 35 C how the river valley is preferentially carved following the soft diatomite; this river path is actually located in the core of an anticline. The contact between Tmb and Te is marked by the beginning of a soft concave slope or the termination of a small competent cliff produced by Te (figure 35 B and C).

*4.7.1.2 Response of Streams*

Competent geologic formations represent a barrier to the normal flow of rivers down-slope. This simple observation was key in the revision of the geologic maps. When the digitized contacts were draped onto the terrain it was possible to observe places were river paths were omitted by mapping or passed arbitrarily across flood plains (figure 36). This is possibly due to the scale at which the geologic maps were done (Dibblee 1972, 1:25000 and Dibblee 1973 scale 1:125.000) since at such scales smaller details are difficult to represent. These problems where not observed in the maps by Nilsen (1995, scale 1:10.000), unfortunately for this thesis we only had access to published segments of the map (see bibliography).

Streams in the area are controlled by the exposure of competent formations. For instance, the river shown in figure 36 is controlled by the outcropping

conglomeratic (pebbles to granules) sandstones of the Santa Margarita Formation (Tsg, see figure 37). In the figure, the formation tops were modified to fit the limit observed between the steeper slope of Tsg and the smoother Quaternary sediments deposited by the river. The numbers in red and black indicate the approximate location from where the original contacts where moved to the current interpreted position (figure 36).

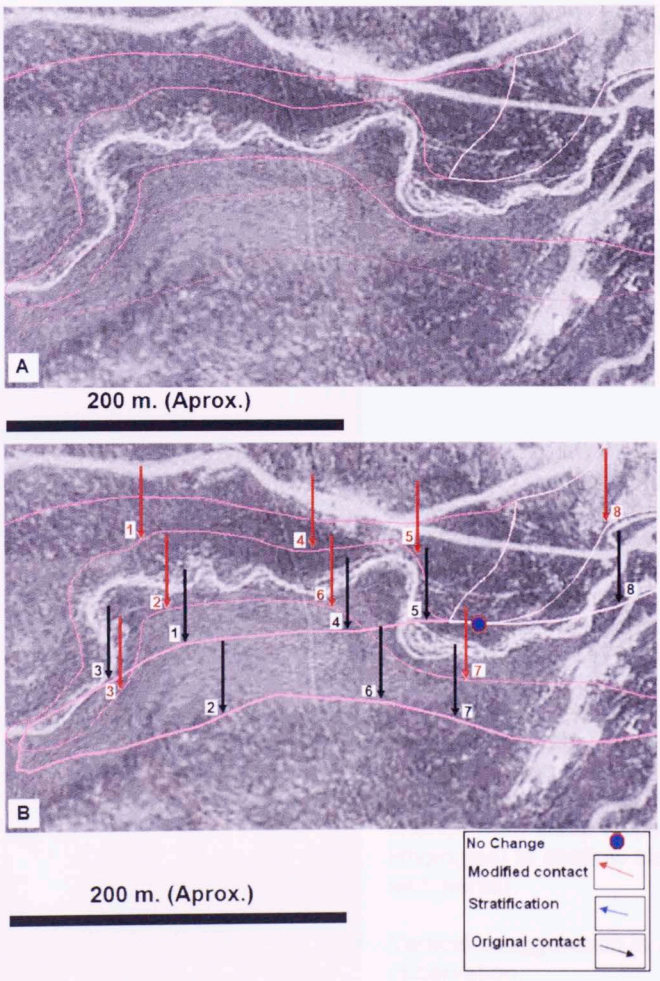


**Figure 36.** Geologic contacts (formation tops) modified to honor the river path and recent quaternary fluvial deposits. Black arrows indicate the original position of the contact, red arrows indicate the new position proposed in the present work, and numbers are intended to illustrate the approximate location from were the contacts were moved.

Detailed observation of the shallow topography produced by recent sedimentary (Qa) deposits from rivers, the alluvial deposits of the Tulare (Qtt) and Paso Robles (Qtp) formations and comparing it to the more competent and prominent geomorphology of the pre-Pleistocene formations permitted accurate identification of the boundary that exists between them (figure 37). This sharp edge is also apparent at the limit between the flood plain and resistant lithologies (figure 38). Careful search to find these characteristics was performed at all principal rivers and streams present in the sub regional work area. This allowed for the precise identification of this limit, marked by a break in the slope of the topography from steep to shallow (figures 37 and 38).

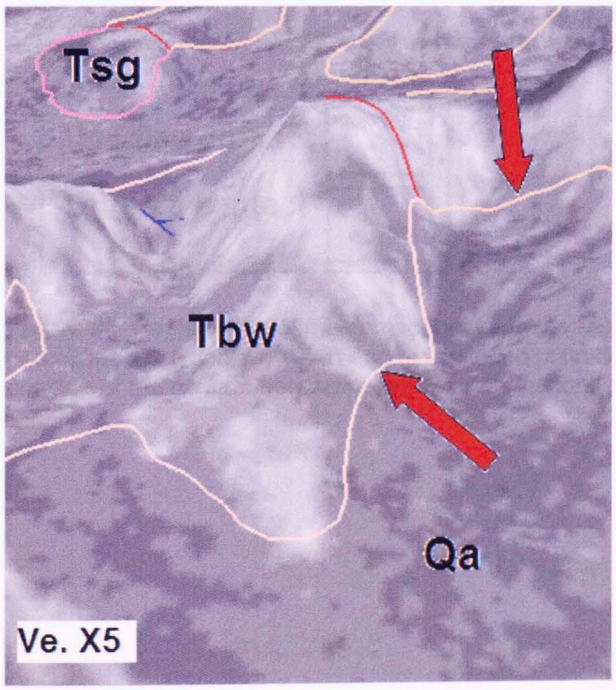


**Figure 37.** Competent formations produce prominent morphologies. Bitterwater shale (Tbw); hard brittle shale interstratified with sandstone. Santa Margarita Formation (Tsg); conglomerate of granitic and metamorphic clasts (boulder to pebble) in a sandstone matrix (Dibblee, 1973). Surficial Quaternary sediments (Qa).

Red arrows indicate interpreted position of the contact between competent formations and recent sedimentary Qa deposits. Notice the change from steep slope (competent lithologies) to shallow slope (recent sediments).

Vertical exaggeration is X5 for easier observation.

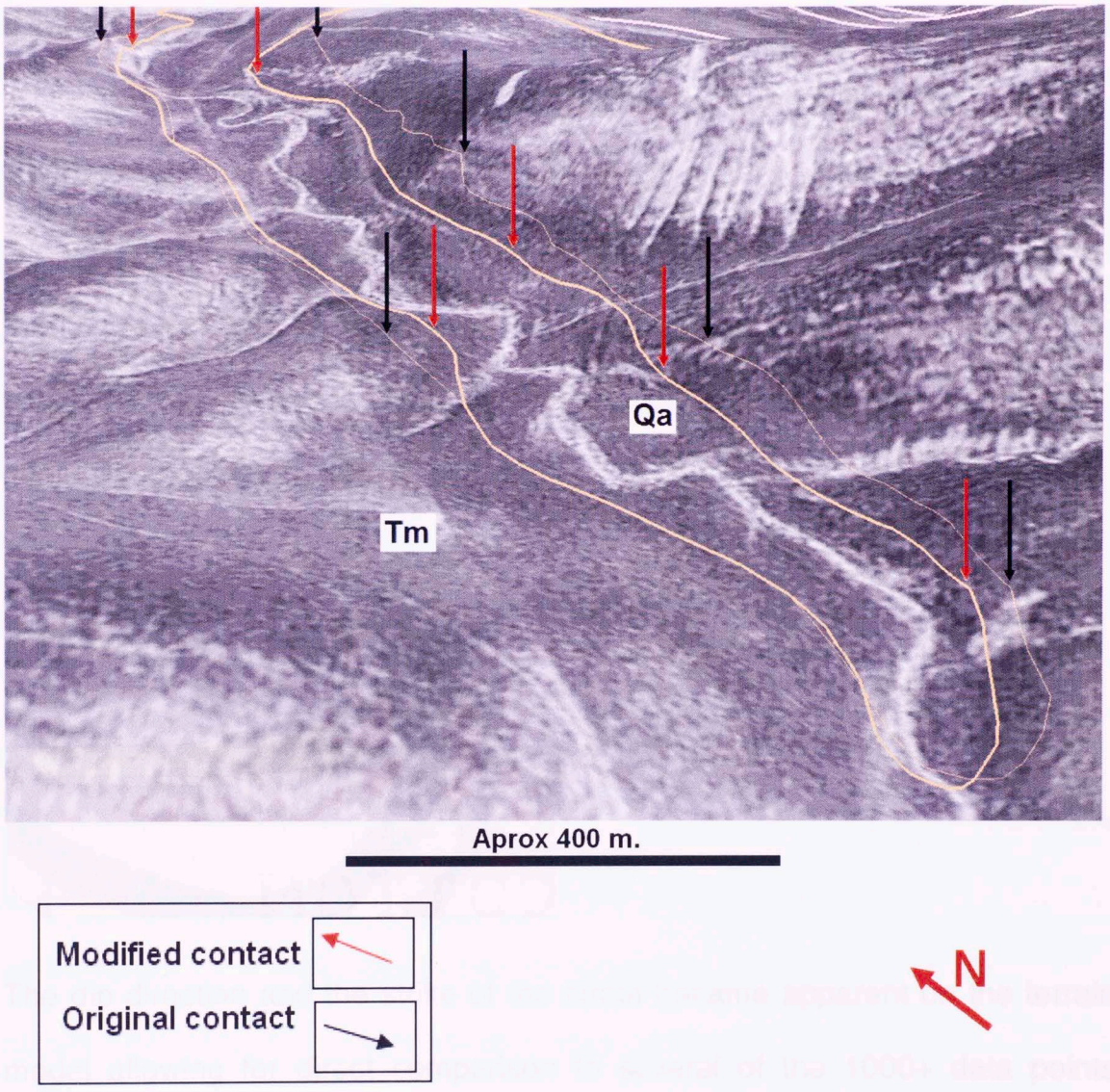


**Figure 38.** Rectification of the contact between the Monterrey McLure shale member (Tm); hard brittle porcelaineous (Dibblee, 1973) and recent flood plain deposits (Qa). Red arrows indicate interpreted position of the contact between competent formations and recent sediments. No vertical exaggeration.

*4.7.1.3 Use of flat-irons*

When bedding planes outcrop exposing the stratigraphic top of the layers as a flat surface, the true dip of the strata can be obtained. If the exposed plane is large enough it can be observed with remote sensors (aerial-photos); this exposure is known as a "flat-iron" (figure 39). In this thesis flat irons were used to verify structural dip data obtained from the geologic maps (figure 40).

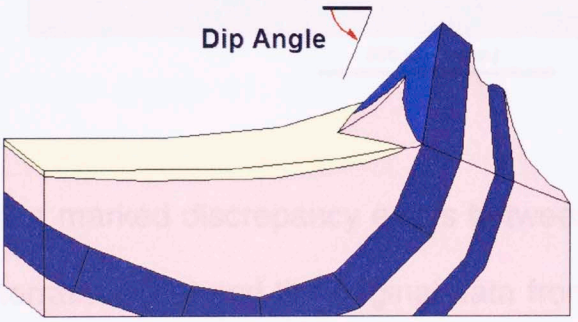


**Figure 39.** Schematic representation of a flat-iron. Blue layers are competent lithologies like sandstones and conglomerates. Pink layers represent soft formations like diatomite.

The dip direction and the strike of the strata became apparent on the terrain model allowing for direct comparison to several of the 1000+ data points obtained from the literature. The inclination of the bedding is observable for features larger than approximately 100 meters. For this reason the data obtained provide a general value from the multiple elevation points of each 30x30 meter cell. The slope of the plane observed is useful to determine and verify the dip direction of data points. The flat irons indicate the general dip

direction which data points (obtained from the actual bedding plane surface) should approximately follow (figure 40).

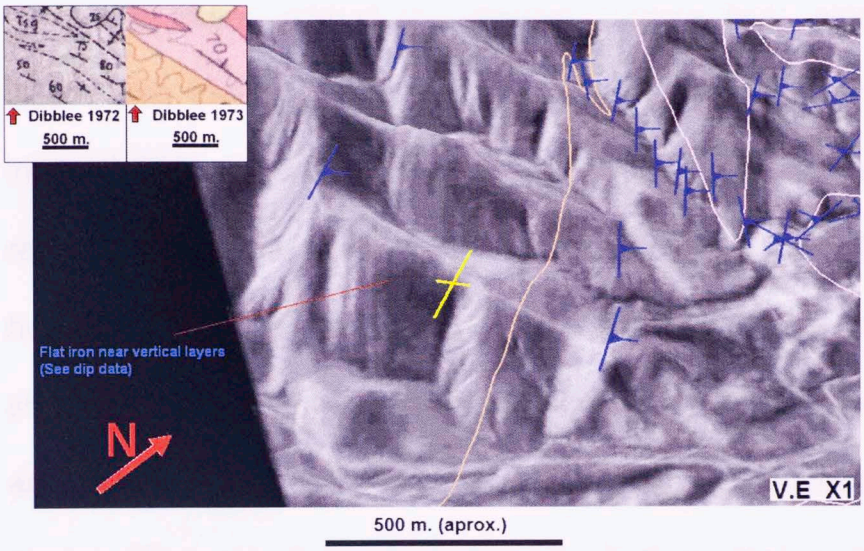


**Figure 40.** Use of flat-irons in this thesis. The data-points follow the general trend of the layers. The layers here are steeply dipping to the northeast (60-90°).

The insert to the top left corner shows the area as it is in the original geologic maps.
Dip-data is extruded from its actual surface location for better observation.

If a marked discrepancy exists between the general trend of the layers in the terrain model and the original data from the geologic maps, it is necessary to either remove the data points from the project or go to the field to revise and obtain new data. A cautious revision was performed to the data points that offered the opportunity for revision and comparison to the strata in the terrain model. From this revision it was concluded that good correlation exists between what is observed in the field and features observed in the 3D model (figure 40).

*4.7.1.4 Rule of V's*

When streams cut through stratigraphic units, a distinctive "V" shape pattern is observable in topographic contour lines along the stream. The layers also display a "V" shape that is controlled by the dip direction, the inclination of the strata and the topographic relief (gradient of the stream) represented by the contours along the river (figure 41). When the strata are horizontal, the contact between two lithologic units precisely resembles the shape of the topographic contours (figure 41, A). If the strata are dipping with angles around 30° to the opposite direction of the topographic slope along the stream (figure 41, B) the beds form a "V" shape that is wider than that shown by the topographic contours with the apex of the "V" pointing in the same direction as the "V" produced by the contour lines. When the layers are vertical they will produce a straight line (band) that cuts across the "V's displayed by the contours (figure 41, C). Layers dipping downstream with a steeper angle than that of the topographic slope along the stream will produce a "V" shape with an apex pointing downstream; this is opposite to the direction of the "V's" formed by the contour-lines (figure 40, D). When beds are dipping at angles slightly higher than the gradient of the stream they form two bands that broaden upstream until they reach the point where the top and the base of the layer is exposed (figure 41, E).

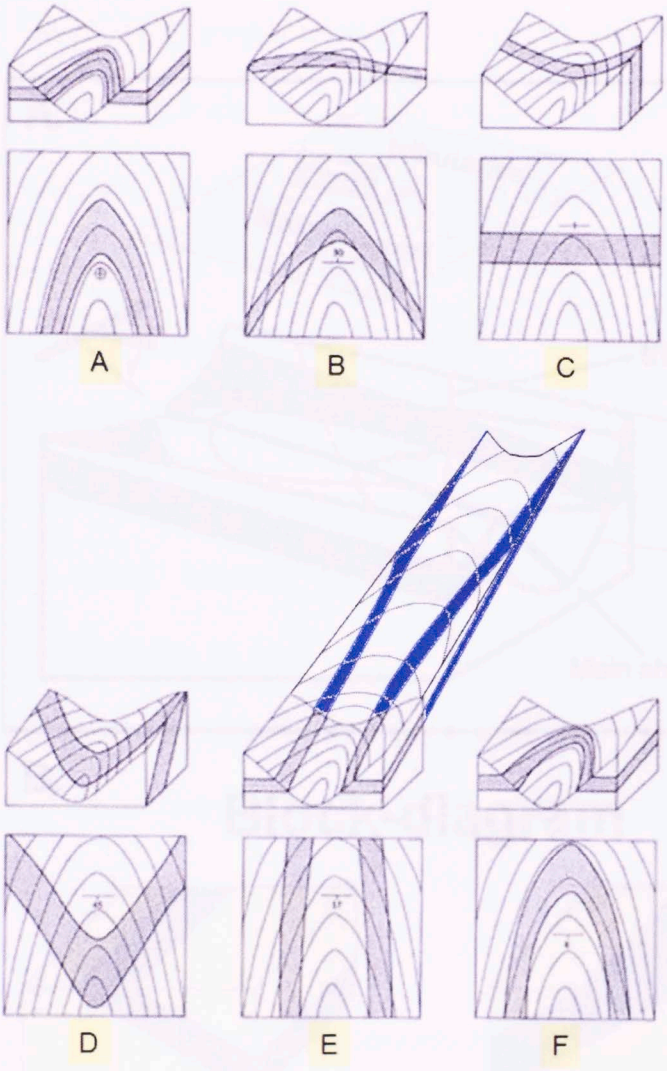


**Figure 41.** Rule of "V's"
A.) Horizontal beds; bedding follows the contours. B) Bedding dipping to the opposite direction of the gradient, the bedding crosscuts across the contours forming a broad "V". C.) Vertical strata. D.) Bedding dipping in the same direction of the gradient, "V" of the contours and "V" of the bedding pint in opposite directions E.) The beds are dipping with a slightly higher inclination, in the same direction of the gradient. F.) Layers dipping with the same inclination as that of the gradient.

**Modified from:**
http://www.geology.cwu.edu/dept/courses/g360/topo1.jpg

For the case where layers dip in the same direction and with the same inclination as the gradient of the stream, the "V" formed by the strata is similar to the one displayed by the contours, with the exception that they cut through the contours indicating the strata are not horizontal (Figure 41, F).

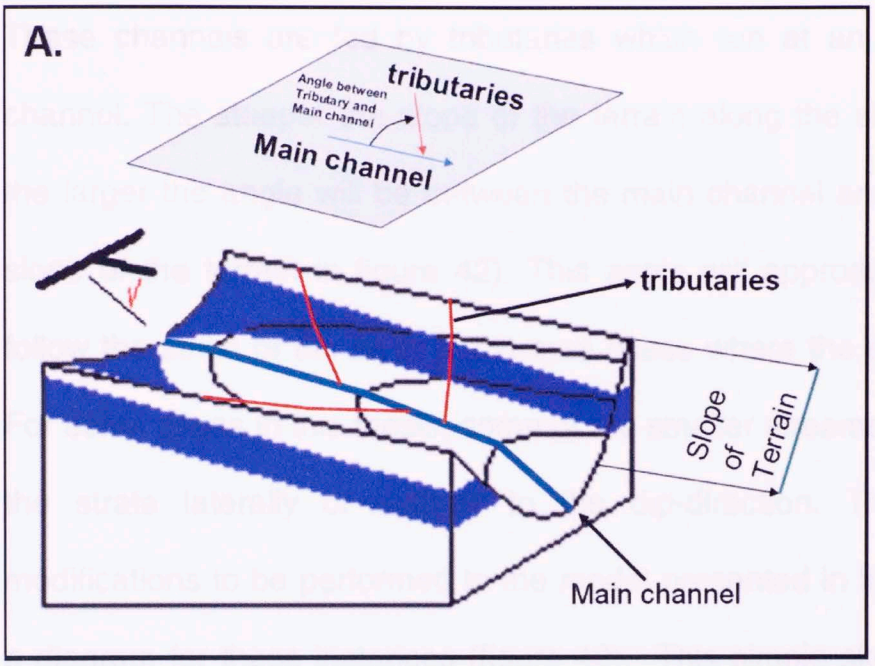


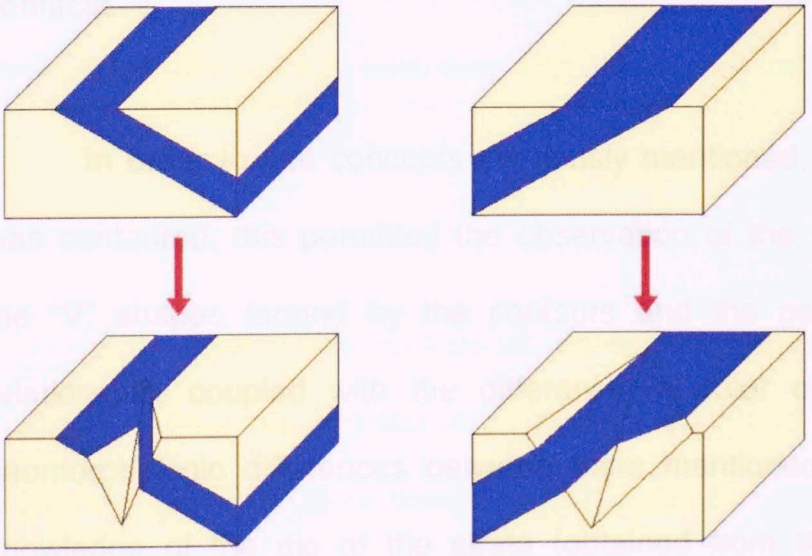


**Figure 42.**

A.) Case where tributaries feed the master channel of streams.

The tributaries will run at an angle to the dip direction; while the main channel will run parallel to the dip direction.

The steeper the slope of the terrain the larger the angle will be between the main channel and the tributary (approaching the strike of the layer when he slope is high).

B.) Block-diagram showing the case mentioned above (tributaries cross-cutting bedding planes perpendicular to the dip-direction).

The tributaries will form V's similar to those in the block diagram.

The main channels of streams in the study area cut strata in the dip direction. These channels are fed by tributaries which run at an angle to the main channel. The steeper the slope of the terrain along the sides of the channel the larger the angle will be between the main channel and the tributary (see slope of the terrain in figure 42). This angle will approach 90 degrees and follow the strike of the layer in extreme cases where the slope is very steep. For some cases in this thesis, some of the smaller streams and tributaries cut the strata laterally or oblique to the dip-direction. This required some modifications to be performed to the model presented in figure 40 and create a diagram for these instances (figure 42). This simple sketch was useful for the case mentioned above, in the prediction of the path followed by the contacts.

In order to use concepts previously mentioned, the 3D terrain model was contoured; this permitted the observation of the relationships between the "V" shapes formed by the contours and the geologic contacts. This relationship, coupled with the difference in color of the lithologies, the geomorphologic differences between them mentioned previously, and the knowledge of the dip of the strata (obtained from the dip data from the geologic maps) allowed for a more accurate interpretation of the position of the formation tops (figure 43).

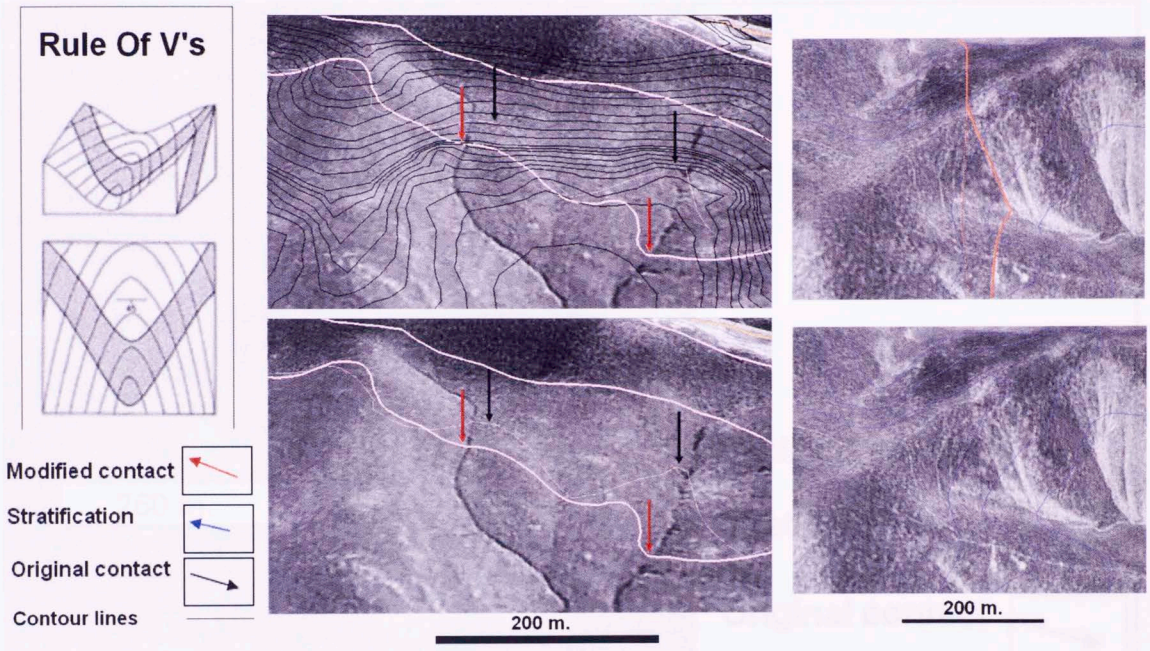


**Figure 43.** Contouring of the 3D terrain model for observation of the relation between contour-lines and formation tops across streams.

Even though the position of the geologic contacts is correct to the scale they were constructed (e.g Dibblee, 1973 1:125000), they had to be edited for the purpose of constructing a geologic model for the detail study area. The contacts were edited to conform to the "V's" expected as the units are being cut by the streams (figure 44).

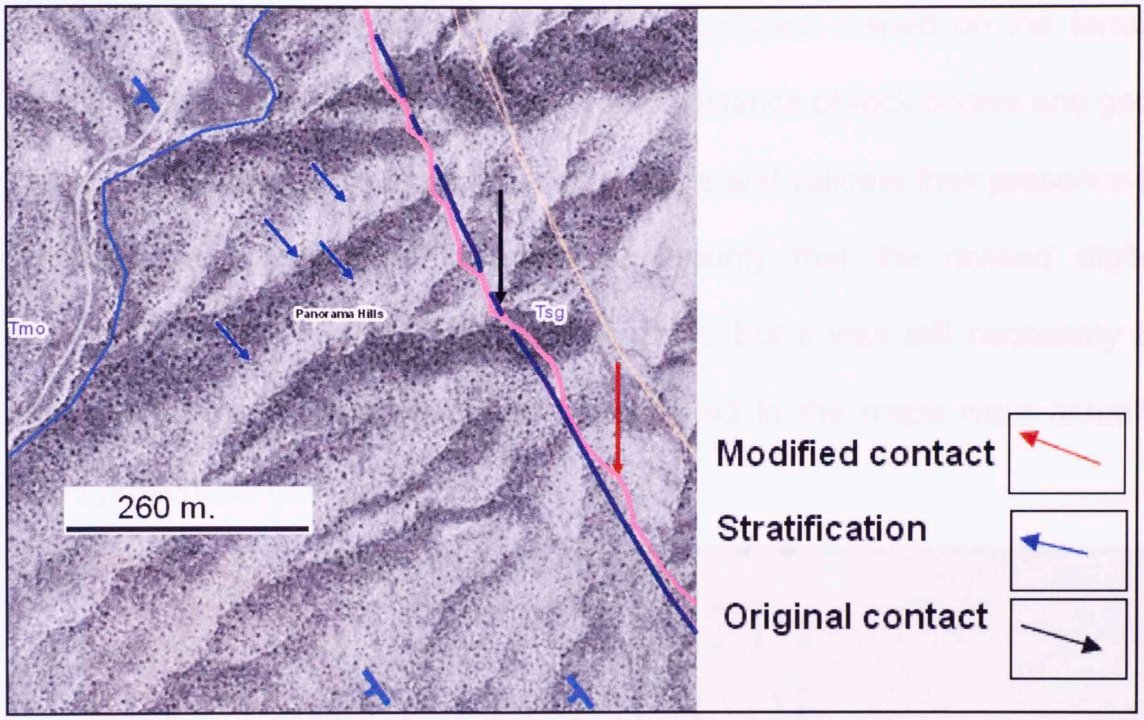


**Figure 44.** Top view of the original contacts showing a general straight path across streams and the edited formation tops honoring each one and displaying the expected "V: shape across the streams.

Figure 44 shows the original contact in blue following a roughly straight path and the modified contact in pink showing a more curvilinear path honoring all streams cutting across the bedding.

*4.7.1.5 Verification and Validation of the Geologic Map*

The geologic map presented in this thesis was revised by checking the conformity of digitized contacts with the orthophotos draped on the terrain model. This method allowed us to verify the existence of rock bodies and geo-forms extracted from the original geologic maps and validate their presence in the field. Accomplishing this provided certainty that the revised digital geologic map was geomorphologically correct. But it was still necessary to confirm that the geologic formations mentioned in the maps were actually those present on the terrain.

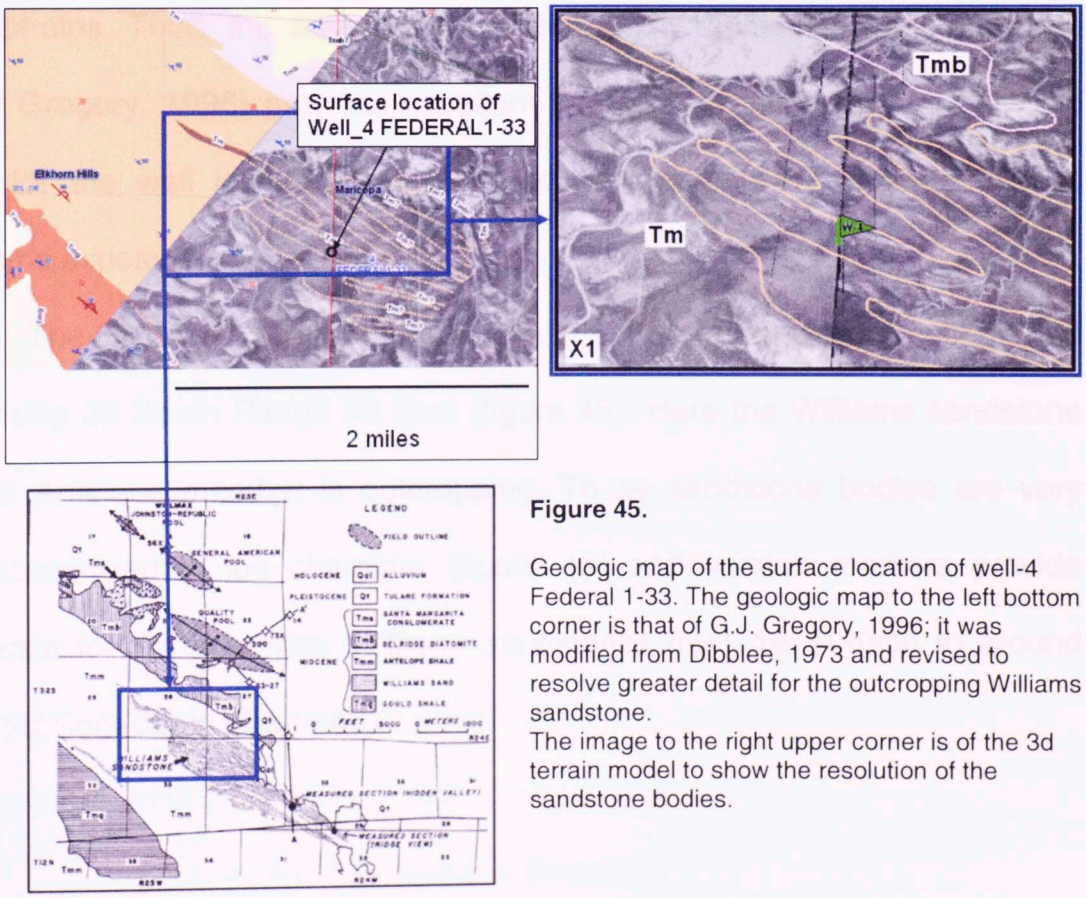


**Figure 45.**

Geologic map of the surface location of well-4 Federal 1-33. The geologic map to the left bottom corner is that of G.J. Gregory, 1996; it was modified from Dibblee, 1973 and revised to resolve greater detail for the outcropping Williams sandstone.
The image to the right upper corner is of the 3d terrain model to show the resolution of the sandstone bodies.

In order to confirm the presence of the formations presented in the original geologic-maps at the correct stratigraphic level, one well was selected; taking its surface location into account. This well occurs on the lenticular sandstone bodies of the Antelope member of the Monterey Formation (according to the geologic maps by Dibblee 1972, 1973 and G. J. Gregory 1996). This well was particularly useful for verifying and validating the geologic map for various reasons; one is that the Tulare Formation is absent in the area, thus preventing it from covering the Monterey Formation. The second reason is that the lenses mentioned are very-well visualized in the high-resolution orthophotos. Third, the area has been thoroughly studied and the literature (G. J Gregory, 1996) provides excellent information and a revised geologic map for the well location and surroundings that is very detailed for the Williams exposure (Figure 45).

The Federal 1-33 well is located in the NE-quadrangle of Section 33 of Township 32 South Range 23 East (figure 45). Here the Williams sandstone of the Antelope member is outcropping. These sandstone bodies are very well-recognized in log character (figure 46) and various markers provide evidence for the presence of these sandstones from the surface to around 800 ft-drillers-depth (figure 46).

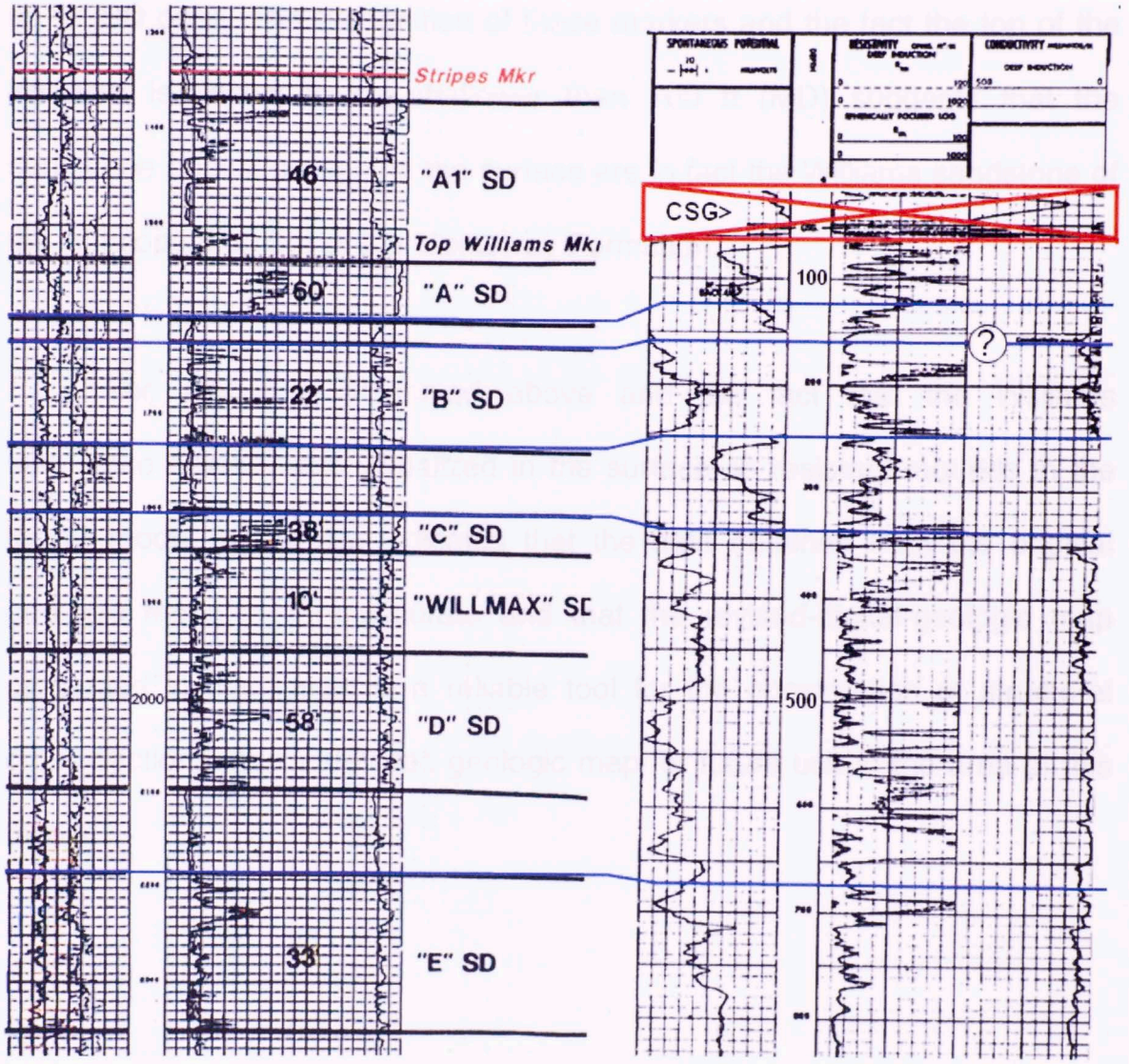


**Figure 46.**
Log-markers of the Williams sandstone, note that the top of the Williams falls somewhere above 100 ft (MD). The top Williams marker is not interpreted due to its proximity to the casing limit.

The markers that indicate the presence of the Williams sandstone are in stratigraphic order: “E” SD, “D” SD, “Willmax” SD, “C” SD, “B” SD, “A” SD – Top Williams marker, “A1” SD, and the Stripes Marker (figure 46, Markers up

to "B" SD only). The recognition of these markers and the fact the top of the Williams is shown to be shallower than 100 ft (MD) suggests that the sandstone bodies present in the surface are in fact the Williams sandstone of the Antelope member of the Monterrey Formation.

The evidence presented above and the fact that the Williams sandstone bodies were visualized in the surface as resistant mounds in the terrain-model (figure 45) indicates that the data obtained from the original geologic maps is very accurate and that the revised-digital-geologic map presented in this thesis is a reliable tool for the construction of structural cross-sections, and a detailed geologic map for future use in the area of this thesis.

## 4.8 Construction elements for the Structural cross-sections

To understand the regional structural framework of the study area, three sub-regional cross sections and one strike line were constructed. These provided large scale understanding of the structures and a regional tie for the five closely-spaced cross sections built in the detailed area (figure 1). Nineteen wells distributed in the sub-regional area and 17 in the detailed area were used to build the cross sections (figure 47) which are located in the southern Belgian anticline area to the north of the main Midway-Sunset structure. The smaller-scale cross sections provided the frame to build the structural geologic model (figure 48).

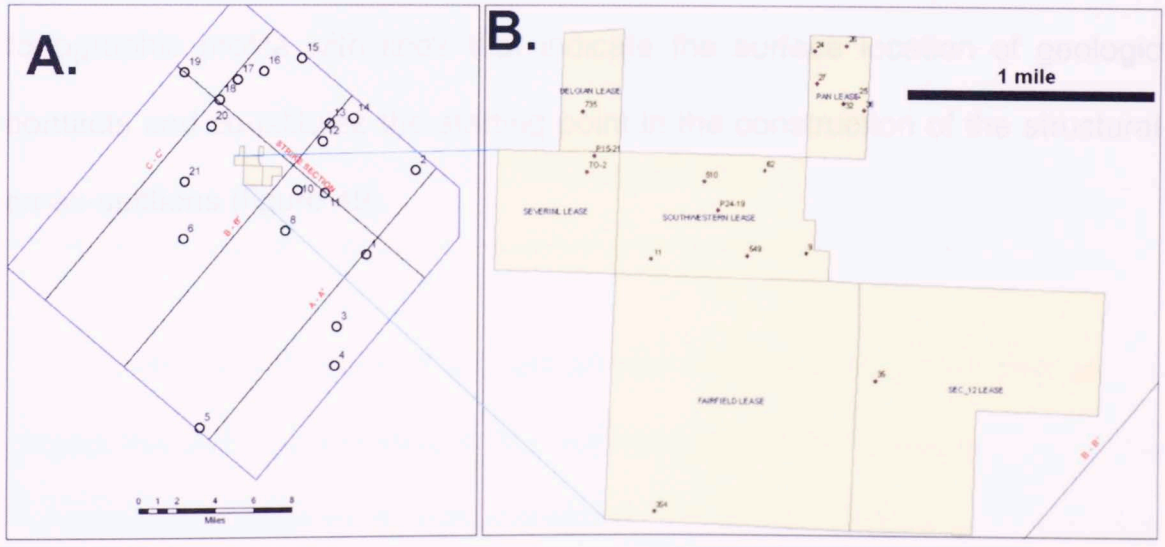


**Figure 47.**
A) Location of the wells used for the sub regional cross-sections. The dark blue lines indicate the location of cross sections AA', BB', CC' (from south to north), and the strike section.
B) Location of the wells with dipmeter-logs used for the localized cross sections.

The log suite used for the interpretation of the formation tops at the selected wells includes resistivity, conductivity, SP, and gamma-ray. Additional parameters taken in account for the well selection were that drilling depths had to be at least 3000ft, the wells had to be vertical or close to vertical, and computed tadpoles from dipmeter logs had to be available for all wells.

Once all the wells were selected, topographic profiles were obtained for all the sections. Data points including X, Y (NAD83-UTM-Z11 coordinates), and Z values (elevation-meters) were extracted from the DEM every 30 meters and projected to the cross sections. Subsequently corrected geologic contacts obtained from the 3D edited geologic map were extracted at the intersection of the cross sections and the surface. This produced a topographic profile with lines that indicate the surface location of geologic contacts and constitutes the starting point in the construction of the structural cross-sections (figure 49).

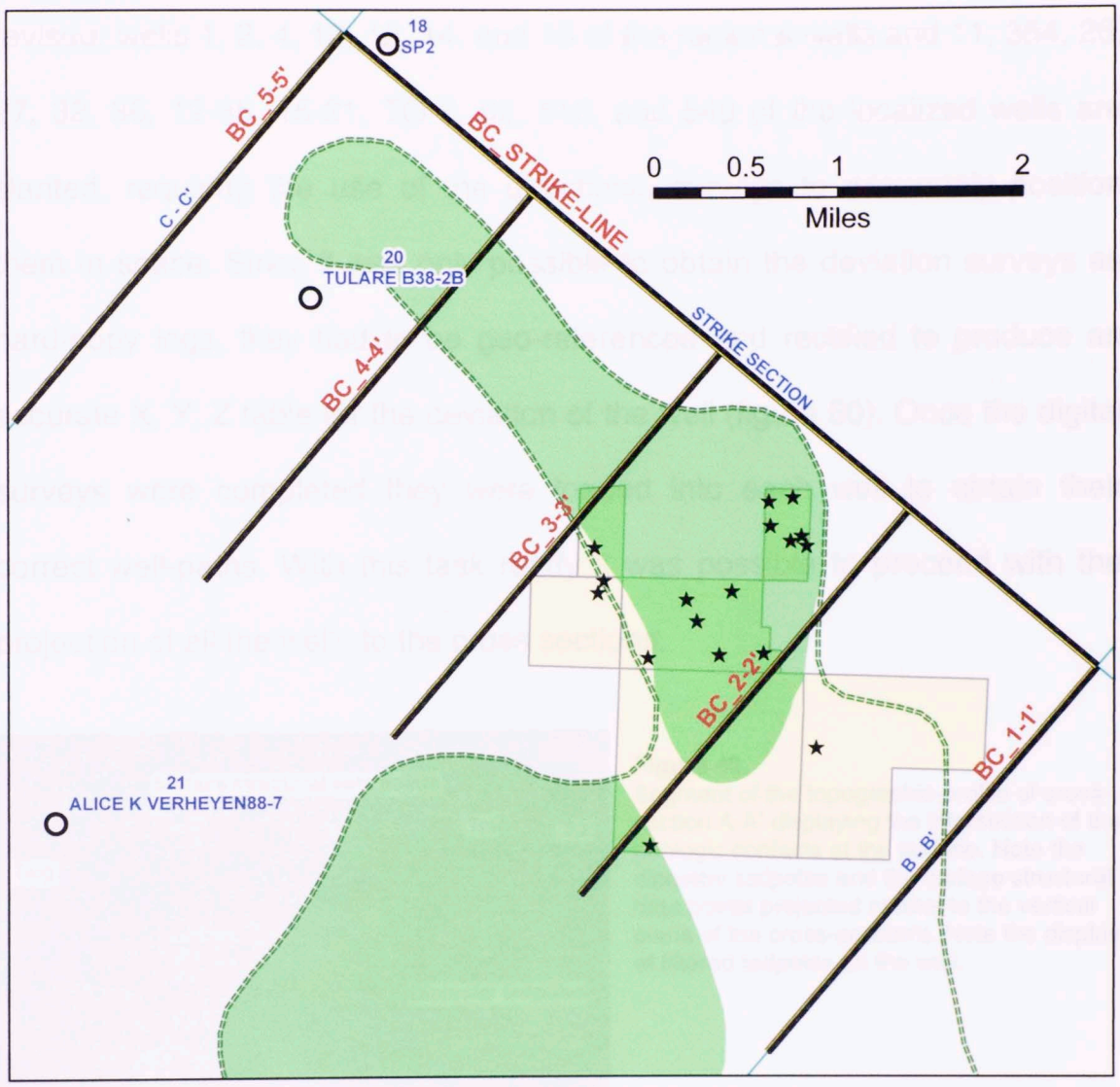


**Figure 48.** Distribution of the localized cross-sections in the Southern Belgian anticline area.

With the extraction of the topography completed, the next step was to project the well paths normal to the vertical plane of the cross sections. This is somewhat simple for straight boreholes but more demanding for deviated wells. For this reason before deviated wells could be projected they had to be

revised; wells 1, 2, 4, 10, 12, 14, and 15 of the regional wells and 11, 354, 26, 27, 32, 36, 12-35, 15-21, TO-2, 62, 510, and 549 of the localized wells are slanted, requiring the use of the directional surveys to accurately position them in space. Since it was only possible to obtain the deviation surveys as hard-copy logs, they had to be geo-referenced and rectified to produce an accurate X, Y, Z table for the deviation of the well (figure 50). Once the digital surveys were completed they were loaded into each well to obtain their correct well-paths. With this task ready it was possible to proceed with the projection of all the wells to the cross sections.

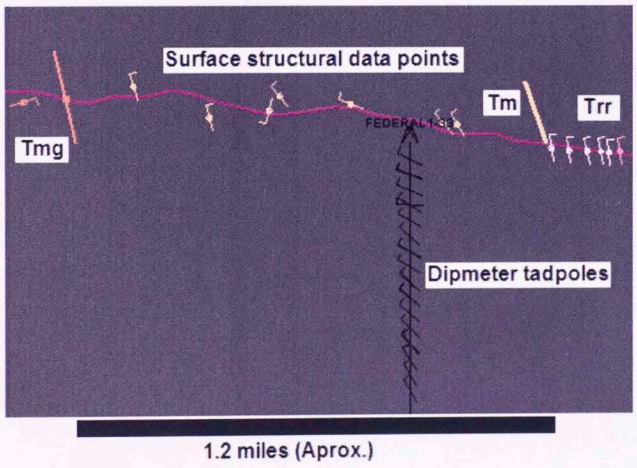


**Figure 49.**
Segment of the topographic-profile of cross-section A-A' displaying the intersection of the geologic contacts at the surface. Note the dipmeter tadpoles and the surface structural data points projected normal to the vertical plane of the cross-section's. Note the display of filtered tadpoles on the well.

Once all deviated wells were loaded into the structural interpretation software, the computed tadpoles were tied to the well paths; for quality control a selective scrutiny was performed to the dipmeter data and only tadpole calculations reaching a confidence of 60% or more were loaded into the project (figure 51).

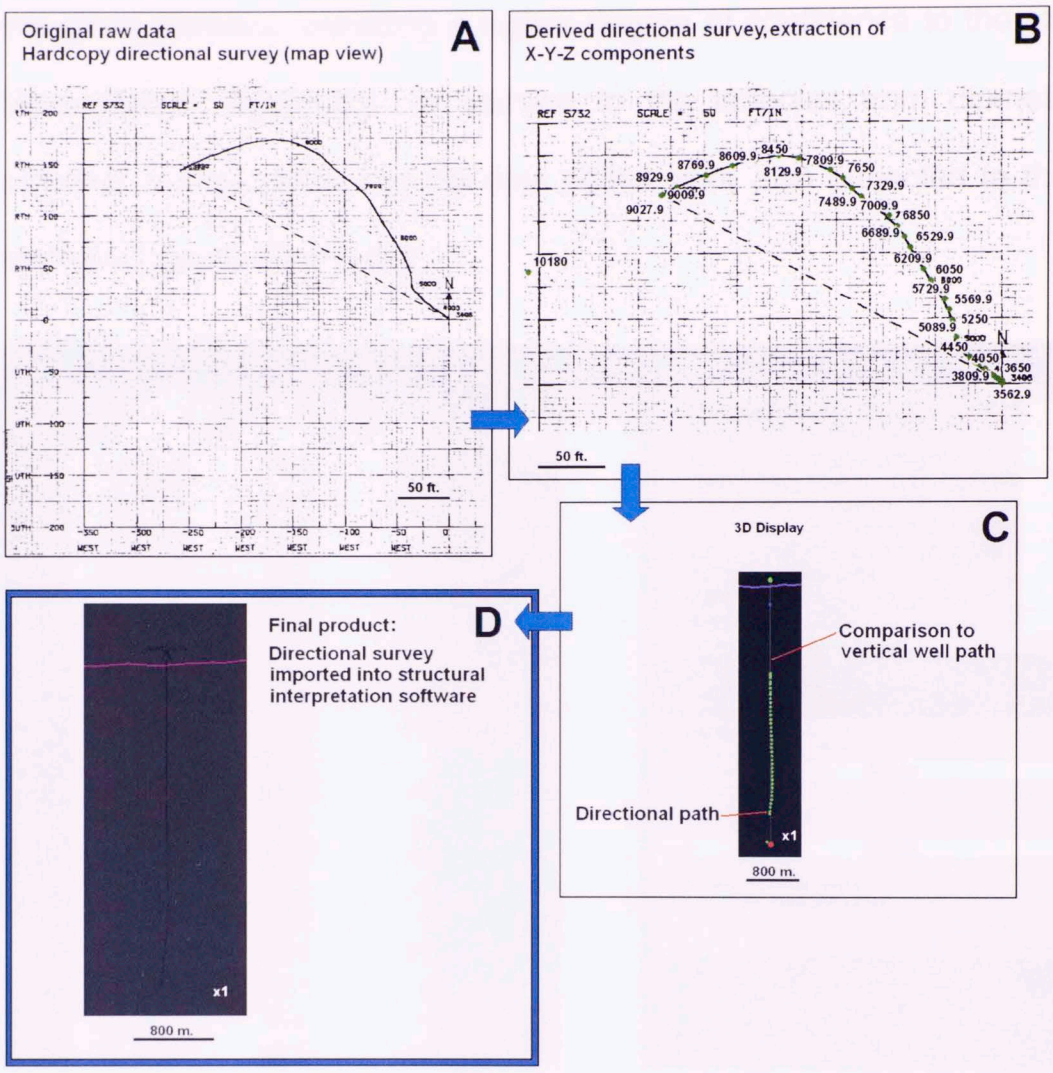


**Figure 50.**
Sample directional survey. A) hard-copy. B) Digitized and geo-referenced deviation survey. C) 3D revision of the directional path. D) deviated well projected to cross-section A-A'.

Active structural controls and shifting of sand sources throughout the depositional history caused stratigraphic thickness to vary significantly within short distances in the study area. To prevent errors due to stratigraphic thickness changes associated with this phenomenon, the wells were projected from a maximum lineal distance of 5 km (3.125 miles). away from

the cross sections, providing a higher degree of confidence to the structural interpretation (figure 52). In addition to the tadpoles from dipmeter-logs, selected surface strike and dip data points were also projected to the cross sections (figures 49 and 52).

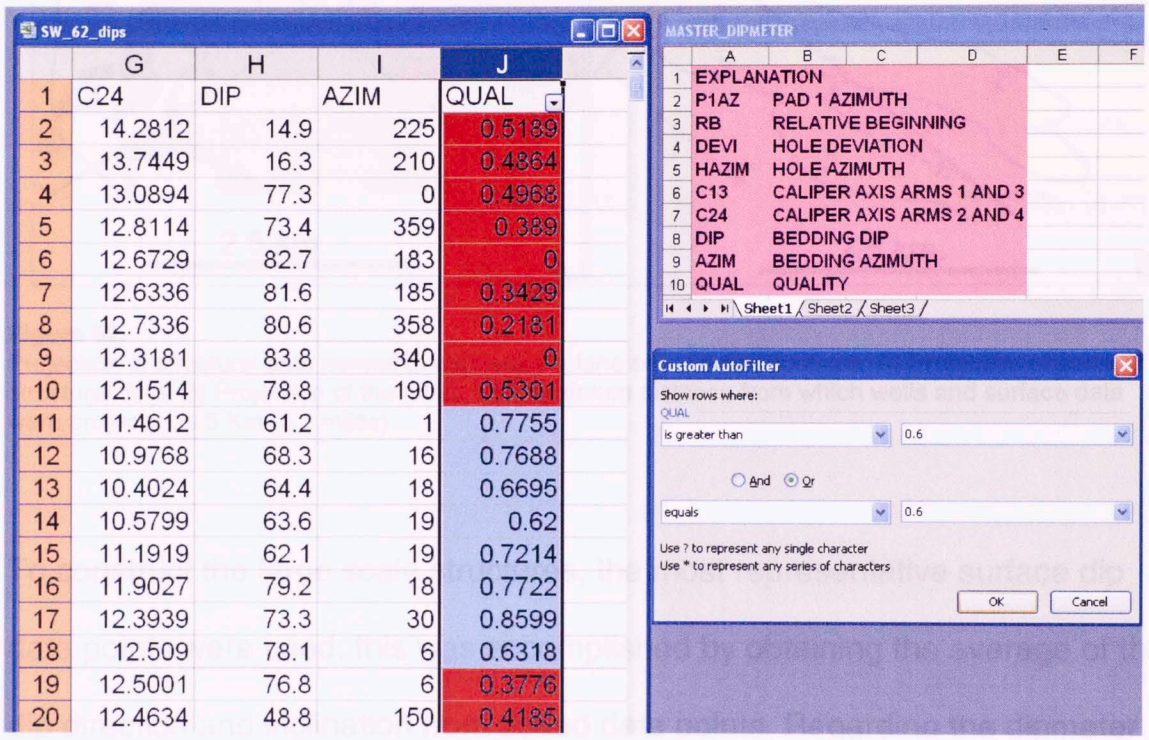

SW_62_dips

| | G | H | I | J |
|---|---|---|---|---|
| 1 | C24 | DIP | AZIM | QUAL |
| 2 | 14.2812 | 14.9 | 225 | 0.5189 |
| 3 | 13.7449 | 16.3 | 210 | 0.4864 |
| 4 | 13.0894 | 77.3 | 0 | 0.4968 |
| 5 | 12.8114 | 73.4 | 359 | 0.389 |
| 6 | 12.6729 | 82.7 | 183 | 0 |
| 7 | 12.6336 | 81.6 | 185 | 0.3429 |
| 8 | 12.7336 | 80.6 | 358 | 0.2181 |
| 9 | 12.3181 | 83.8 | 340 | 0 |
| 10 | 12.1514 | 78.8 | 190 | 0.5301 |
| 11 | 11.4612 | 61.2 | 1 | 0.7755 |
| 12 | 10.9768 | 68.3 | 16 | 0.7688 |
| 13 | 10.4024 | 64.4 | 18 | 0.6695 |
| 14 | 10.5799 | 63.6 | 19 | 0.62 |
| 15 | 11.1919 | 62.1 | 19 | 0.7214 |
| 16 | 11.9027 | 79.2 | 18 | 0.7722 |
| 17 | 12.3939 | 73.3 | 30 | 0.8599 |
| 18 | 12.509 | 78.1 | 6 | 0.6318 |
| 19 | 12.5001 | 76.8 | 6 | 0.3776 |
| 20 | 12.4634 | 48.8 | 150 | 0.4185 |

MASTER_DIPMETER

| | A | B | C | D | E | F |
|---|---|---|---|---|---|---|
| 1 | EXPLANATION | | | | | |
| 2 | P1AZ | PAD 1 AZIMUTH | | | | |
| 3 | RB | RELATIVE BEGINNING | | | | |
| 4 | DEVI | HOLE DEVIATION | | | | |
| 5 | HAZIM | HOLE AZIMUTH | | | | |
| 6 | C13 | CALIPER AXIS ARMS 1 AND 3 | | | | |
| 7 | C24 | CALIPER AXIS ARMS 2 AND 4 | | | | |
| 8 | DIP | BEDDING DIP | | | | |
| 9 | AZIM | BEDDING AZIMUTH | | | | |
| 10 | QUAL | QUALITY | | | | |

Sheet1 / Sheet2 / Sheet3 /

Custom AutoFilter

Show rows where:
QUAL
is greater than
0.6
And Or
equals
0.6
Use ? to represent any single character
Use * to represent any series of characters
OK
Cancel

**Figure 51.**
Selection of dipmeter computation data with a reliability of 60% or more. Values highlighted in red are data points that were removed. Values with quality control higher than 60% were retained and projected to the cross-sections.

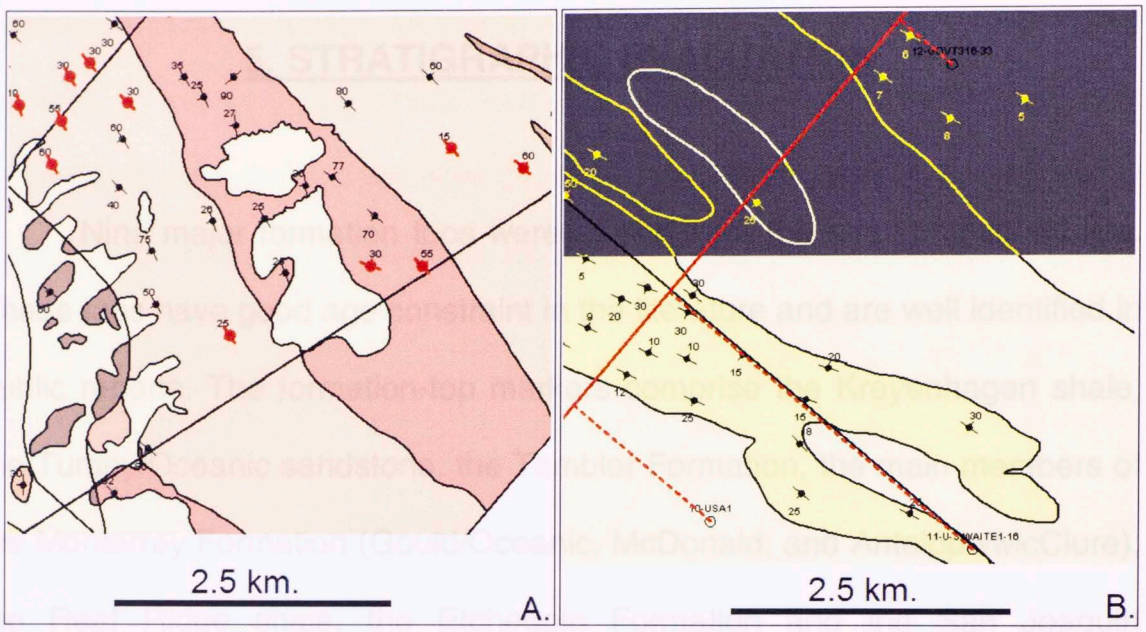


**Figure 52.**
Projection of structural data normal to the vertical plane of the cross sections. A) Projection of surface structural data. B) Projection of the wells. The maximum distance from which wells and surface data were projected is 5 Km (3.1 miles).

To construct the large scale structures, the most representative surface dip data points were used, this was accomplished by obtaining the average of the dip direction and inclination from zoned data points. Regarding the dipmeter logs, 2 tadpoles were available each 10 feet. This was good since all the data was available but the data density was too much for the purpose of display and practical use of the data. This was solved by filtering the data at 1 tadpole every 20, 30, 40 and 100 feet. This procedure was very useful and considerably improved the data cluttering observed when using the raw dipmeter-logs at regional scales (figure 49).

# 5. STRATIGRAPHIC EVALUATION

Nine major formation tops were selected for the stratigraphic studies. These tops have good age constraint in the literature and are well identified in public reports. The formation-top markers comprise the Kreyenhagen shale, the Tumey/Oceanic sandstone, the Temblor Formation, the main members of the Monterrey Formation (Gould/Oceanic, McDonald, and Antelope/McClure), the Reef Ridge shale, the Etchegoin Formation and the San Joaquin Formation. A tenth marker was interpreted in this study for the Basement (TJo). These represent the surfaces that were later used to build the structural framework; other secondary-markers were used for stratigraphic position identification. More than 37 secondary-markers identified in 4 type wells were selected and used to expand the interpretation (figure 53). These wells were used to identify the 9 main tops for 17 regional wells (figure 47 and 53). Once all recognizable secondary markers were identified and the interpretation of the 9 major formation tops was completed, 7 stratigraphic cross-sections were constructed to cover the regional area of study and get a comprehensive idea of the stratigraphy. The stratigraphic interpretation includes the identification of main turbidite sandstone bodies, from the lower Phacoides sandstone in the Temblor formation to the Potter and Olig

sandstone in the Belridge Diatomite (figures 74-81, and stratigraphic cross sections in pocket). The nine formation tops were additionally used to construct three balanced regional cross sections that provided the frame for the detailed structural model of the Southern-Belgian Anticline area.

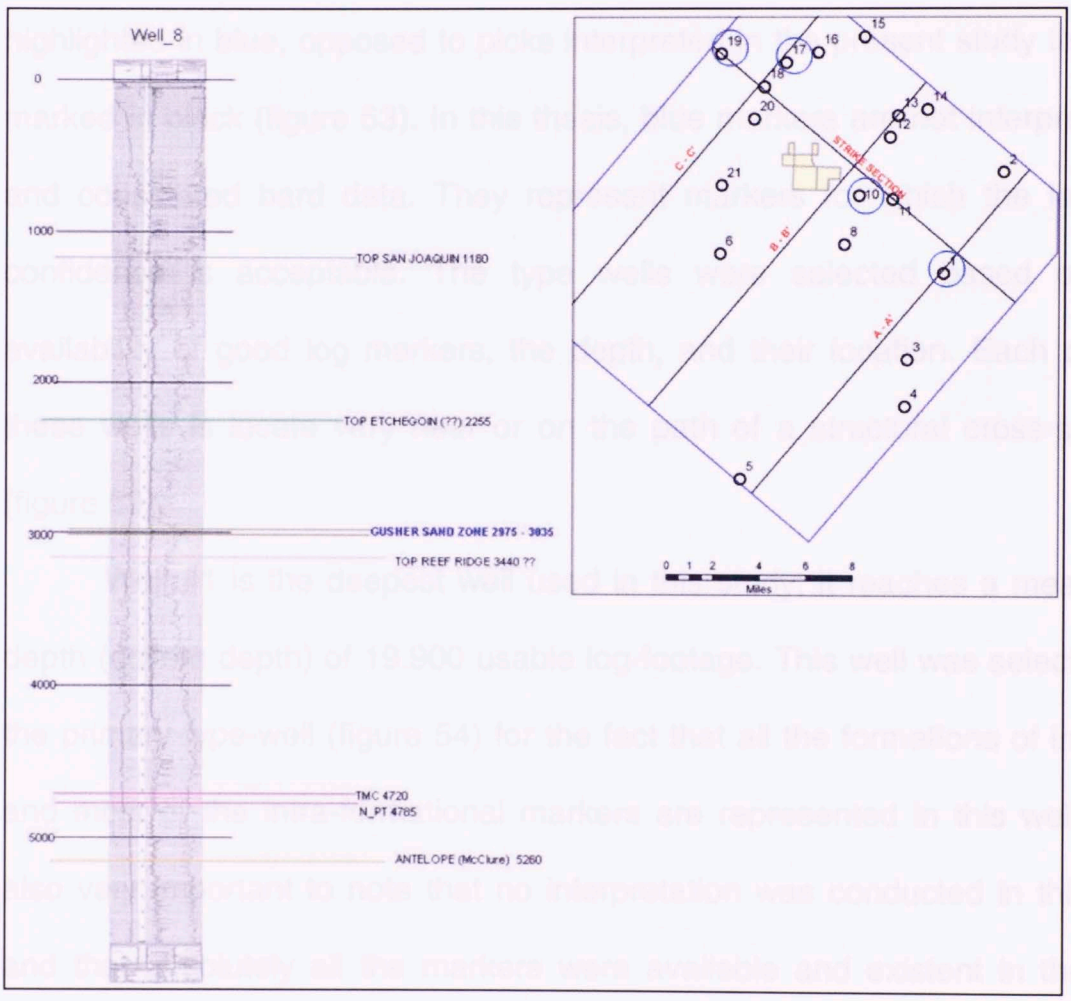


**Figure 53.** Example of log-picks used; markers in blue were extracted from the drilling report of well 8, markers in black were interpreted in the present work using log character (left side). Location of the 4 type wells selected for the interpretation, the wells are highlighted with blue circles (right side).

Each type well is located on the path of a structural cross-section.

Well 1 – cross section AA' Well 10 – cross section BB'
Well 17 – cross section CC' Well 19 – strike section

## 5.1 Type wells

The log picks present at each one of the type wells and in various interpretation wells were obtained from public well drilling reports consigned in the State of California Conservation Commission. These markers are highlighted in blue, opposed to picks interpreted in the present study that are marked in black (figure 53). In this thesis, blue markers are not interpretative and considered hard data. They represent markers for which the level of confidence is acceptable. The type wells were selected based on the availability of good log markers, the depth, and their location. Each one of these wells is locate very near or on the path of a structural cross-section (figure 53).

Well #1 is the deepest well used in this study; it reaches a measured depth (drillers depth) of 19.900 usable log-footage. This well was selected as the primary-type-well (figure 54) for the fact that all the formations of interest and most of the intra-formational markers are represented in this well. It is also very important to note that no interpretation was conducted in this well and that absolutely all the markers were available and existent in the well report.

Well #10 was very useful to obtain constrained-markers in the shallow formations since it displays all the formations of interest (blue markers) from the San Joaquin Formation to the Antelope member of the Monterey

Formation. The Williams sandstone marker was interpreted for this well (see stratigraphic cross sections in pocket) to populate missing data and to expand the interpretation (figure 55).

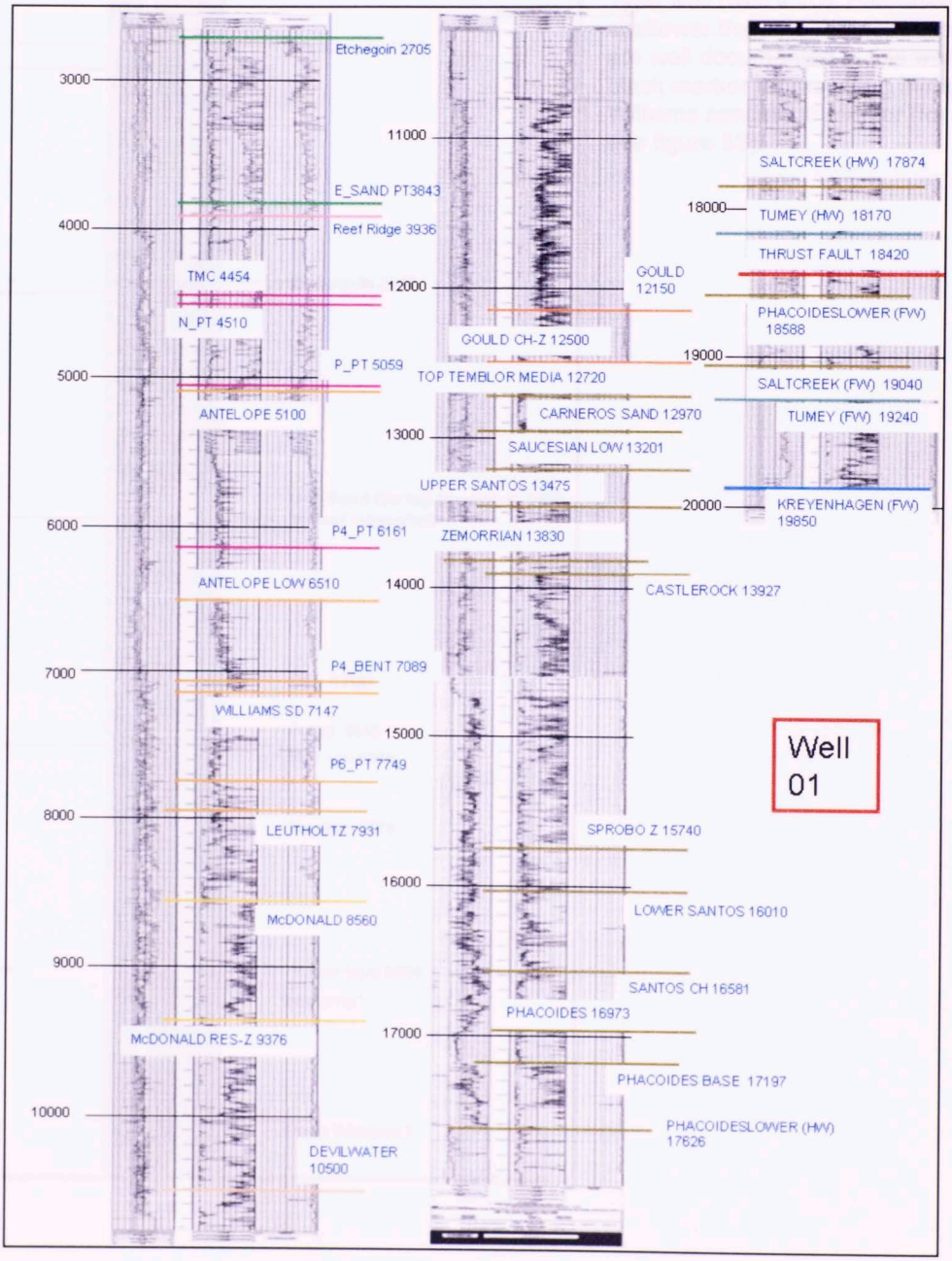


**Figure 54.** Main type-well (well # 1). Note the depth of the well; usable measured depth of the log is 19.900 ft. Data markers in blue obtained from well-report (for location see figure 53).

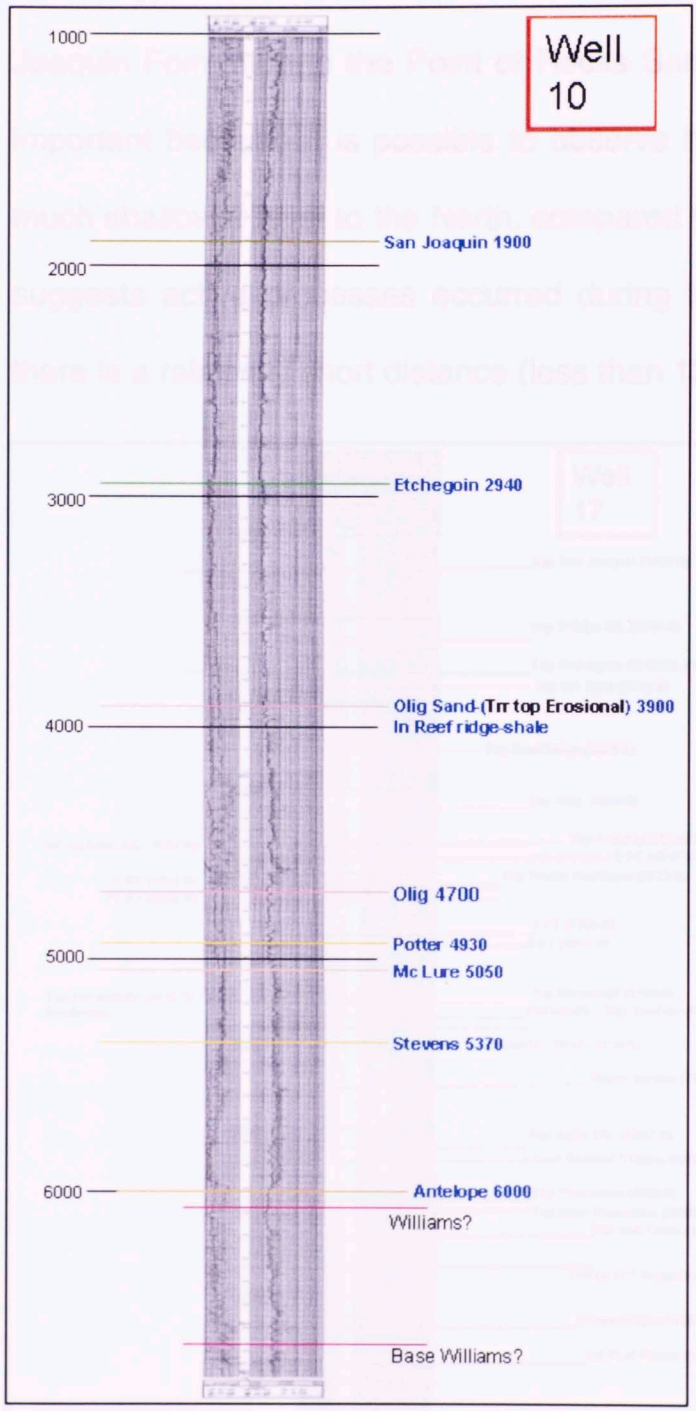


**Figure 55.**
Type well (well # 10), Formations shallower than the Antelope member are well documented in this well. Note black marker representing interpretative Williams sandstone marker (for location see figure 53).

Type well #17 has excellent marker representation from the San Joaquin Formation to the Point of Rocks Sandstone. This well is particularly important because it is possible to observe how the formation tops are at a much shallower level to the North, compared to that observed in well # 1; this suggests active processes occurred during the deposition, considering that there is a relatively short distance (less than 13 mi.) between wells 1 and 17.

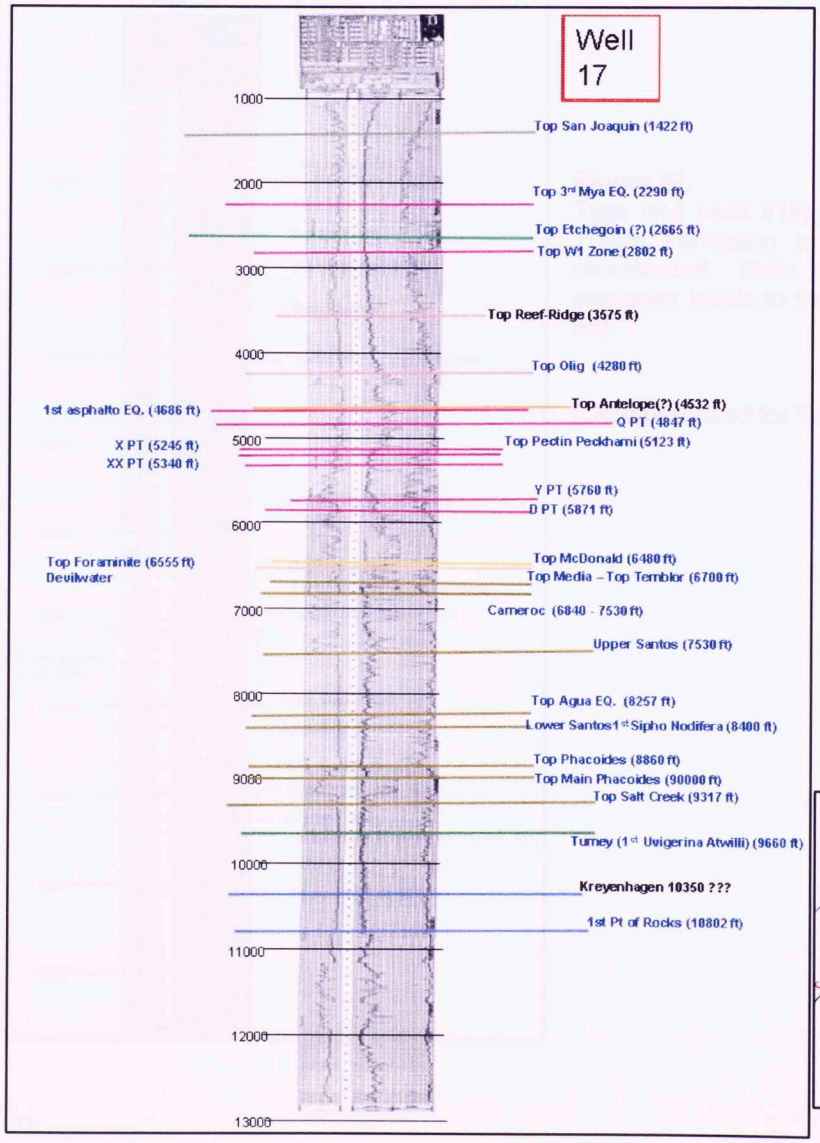


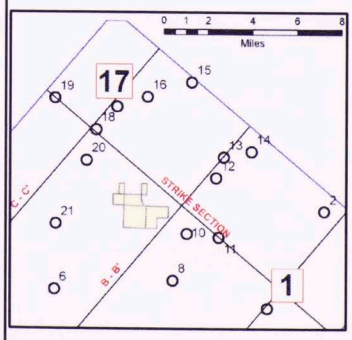


**Figure 56.**
Type well (well #17), Main tops and secondary markers are very well defined from the San Joaquin Formation to the Point of Rocks sandstone. Secondary markers are highlighted in pink; they were used to locate adjacent main markers (for location see figure 53).

(Light pink used for Trr and Top Olig, these are not secondary markers).

Well # 17 also has the most intra-formational secondary data markers available; these markers are represented with pink lines indicating that they are not a formation top or the top of a main sandstone body. These pink-markers were very convenient to locate well log-signature levels adjacent to formation tops and contributed in the interpretation of these main markers in other wells (figure 56).

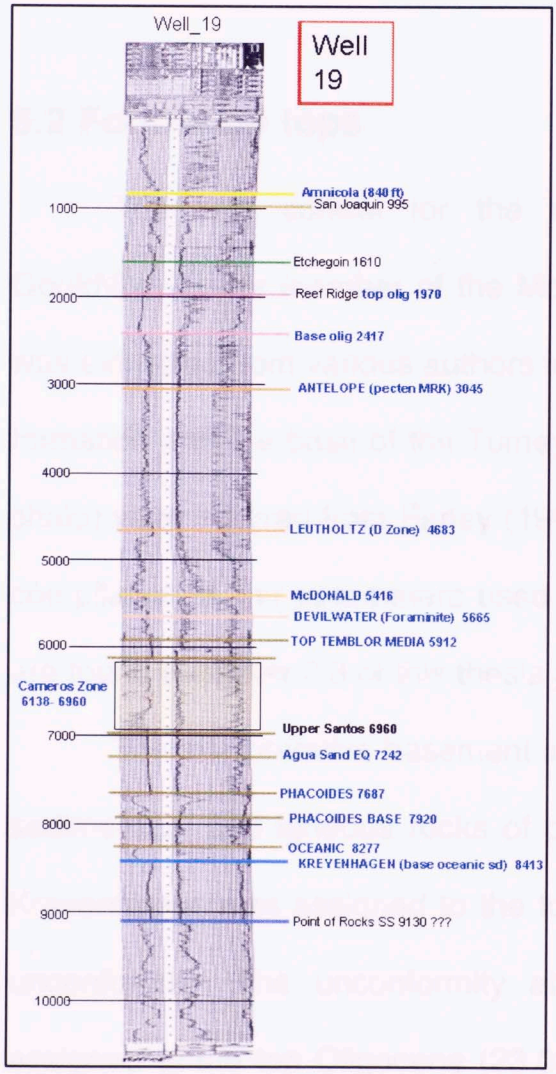


**Figure 57.**
Type well (well #19), All formations from the basal Tulare Formation to the Kreyenhagen shale are represented. Note the trend of formations at shallower levels to the North (for location see figure 53).

(Light pink used for Trr and Olig sandstone.)

All formation tops from the Tulare (Amnicola marker) to the Kreyenhagen shale are represented in type well #19. The general trend mentioned before of shallower depths for correlative formation tops to the north is also observed in this well. Note the top of the Kreyenhagen shale at around 9100 ft. compared to 10350 ft. in well #17, and 19850 ft. in well #1 to the South (figures 57, 56, and 54).

## 5.2 Formation tops

The age control for the main markers from the base of the Gould\Devilwater member of the Monterey formation to the Tulare formation was extracted from various authors in Fortier (1996). The base of the Temblor formation and the base of the Tumey/Oceanic (contact with top Kreyenhagen shale) were inferred from Farley (1990), Dibblee (1973), and Beyer (1988). A compilation of the parameters used to assign the ages of the main markers are found (Chapter 2.3 of this thesis Stratigraphy).

The interpretative basement in this study refers to the undifferentiated-sedimentary and igneous rocks of pre-Cretaceous to Jurassic age. The top Kreyenhagen was assigned to the top of the Eocene (33.9 Ma.) marking the unconformity. The unconformity at the top Tumey/Oceanic marker was assigned to the top Oligocene (23.03 Ma.) The marker corresponding to the top Temblor was assigned an age of 16.4 million years. Three major

subdivisions were established for the members of the Monterey Formation; these are the Gould\Devilwater, the McDonald, and the Antelope Markers; the ages assigned were 13.9, 8.9, and 7.0 million years, respectively. The 7.0 million year mark is very important as it is proposed in this study as an unconformity between the Antelope and the Reef Ridge shale. Three main unconformities that are widely recognized in the area were used as time constrained markers in this thesis; these are the Reef Ridge (5.3 Ma.), the Etchegoin (4.0 Ma.), and the San Joaquin (2.35 Ma.) markers (figure 58). The lower-Tulare formation is included in the present study, but no marker was identified as this study is focused on the deeper levels of the stratigraphic section.

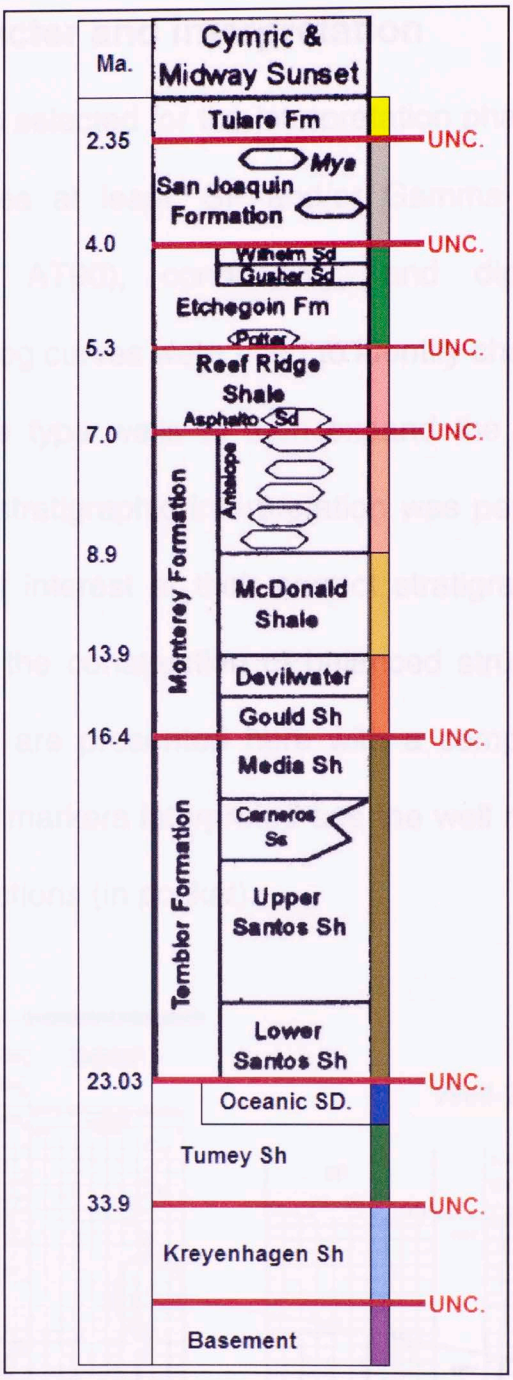


**Figure 58.**
Generalized stratigraphic column proposed in this thesis. Red lines indicate unconformities. Ages were assigned in accordance with the literature and observation of published geologic maps and stratigraphic columns. (Portion from base-temblor to Tulare Formation extracted and modified from: T. H. Nilsen in Nilsen, T.H., Wylie, Jr., A.S., and Gregory, G.J., 1996 fig 10 Pg. 19., Ages added according to J. D. Fortier)

## 5.3 Well-log character and interpretation

The suit of logs selected for the interpretation phase at each one of the regional wells includes at least, SP and/or Gamma-Ray (GR), resistivity (AT10, AT30, and AT90), conductivity, and dipmeter-logs (tadpole computation). These log curves were used to identify characteristic signatures of the markers at the type wells to then expand the interpretation into all available wells. This stratigraphic interpretation was performed to accurately locate the markers of interest at their correct stratigraphic position to then provide constrain for the construction of balanced structural cross-sections. Selected log-markers are presented here with a comparison to one of the type wells; For all the markers interpreted see the well markers portion of the stratigraphic cross-sections (in pocket).

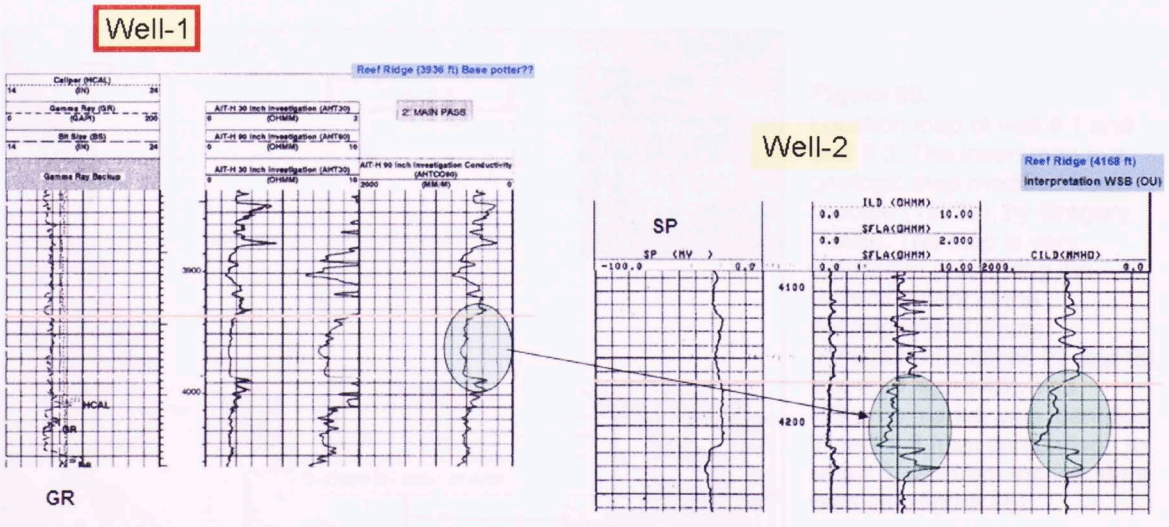


**Figure 59.** Correlation between Well # 1 (type well and well # 2 at the Reef Ridge level. Representation of the SP-log (right) and GR-log in diatomite rich lithologies; note that the GR curve shows a similar response compared to the clear changes observed in the resistivity and conductivity curves. A better response is obtained with the SP-log (well #2).

As was mentioned earlier, the west-side of the San Joaquin Basin was characterized by active deposition of diatomite during the late Paleogene and throughout the Neogene. This produced thick diatomite-shale deposits intercalated with sandstone bodies. Diatomite-shales are made of silica and are poorly detected with the GR-log. This is possibly due to the lack of radioactive elements found in these clean, clay-size sedimentary deposits; causing diatomite packets to appear very similar to sandstone lithologies when observed using solely the GR-log (figure 59). Since diatomite distribution is widely encountered in most of the stratigraphic section, it was important to use the full suite of logs available for the correlation. The conductivity log along with the SP log proved to be the best logs to differentiate lithologies in the study area (figure 59).

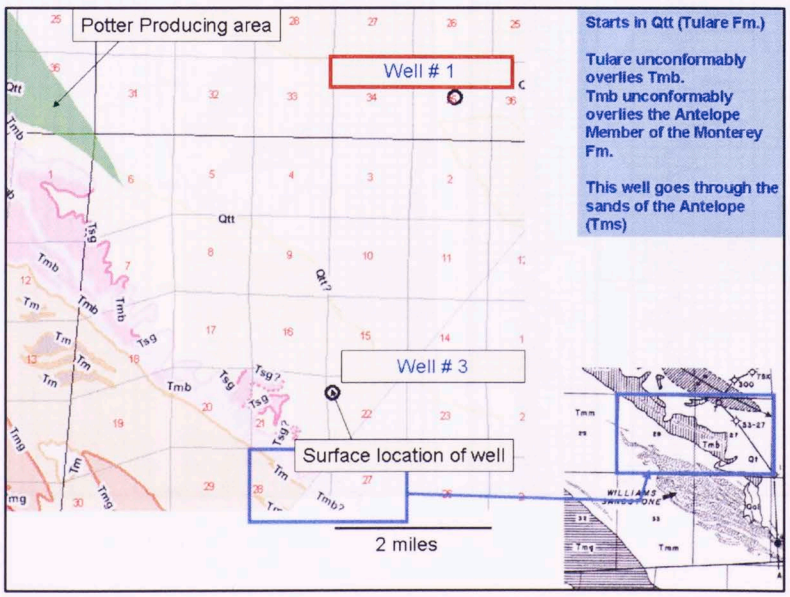


**Figure 60.**
Location map of well # 1 and well # 3. The insert map is a geologic map modified from Dibblee (1973b), by Gregory (1996). The map is very detailed in presenting the surface extent of the outcropping Williams sandstone (sections 27 and 28, see also figure 45). The Williams marker was identified in well # 3 from comparison to well # 1 and from the literature (see also figure 46).

The outcropping turbidite sandstone bodies of the Antelope Shale are excellent examples of the relation between sandstone and diatomite in the area (figure 60). These Upper Miocene sandstones are present in type well # 1 and were interpreted in well # 3, from the Leutholtz Sandstone near the base to the Williams Sandstone in the upper-Antelope Shale member. The resistivity log was used to identify similar patterns in the signature at detailed scales, while the conductivity log was used to validate the correlation to a larger scale (figure 61).

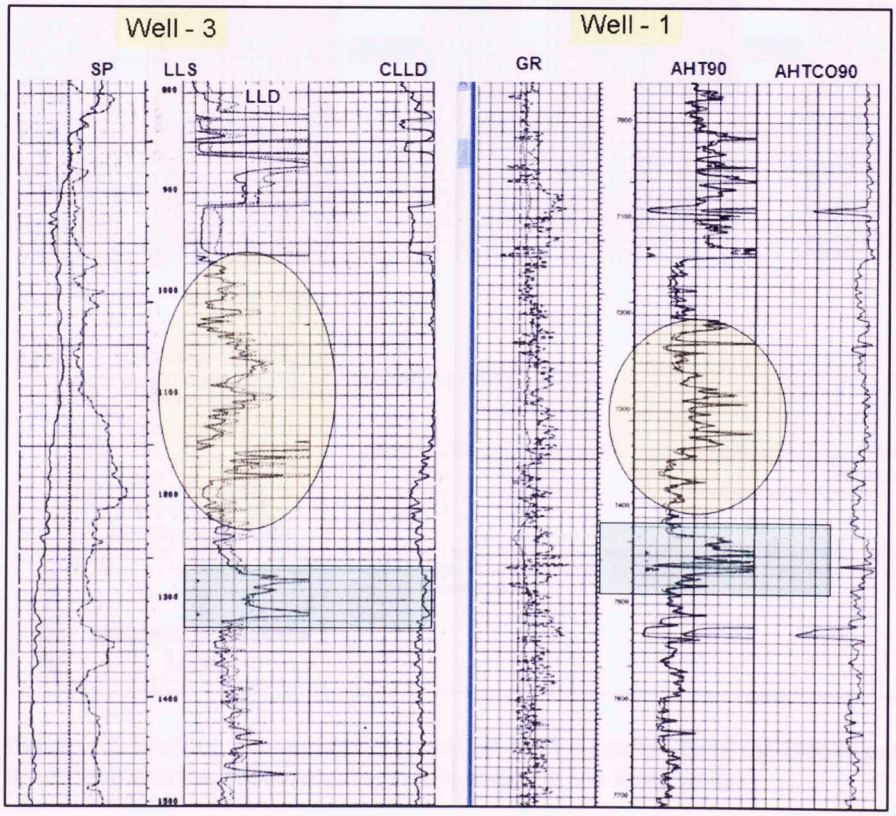


**Figure 61.** Correlation of well # 3 with Type well # 1. Note the similarity of the well-log response at the Williams Sandstone level in the Antelope member of the Monterrey Formation.

### *5.3.1 Point of Rocks Sandstone and Kreyenhagen Shale*

The Point of Rocks Sandstone was penetrated by wells 19, 17, and 20 of the regional wells. It is represented by a series of blocky sandstone packages beneath a clear shale line in the SP-log, that are identified as the first sandstone bodies (top to bottom) beneath the Kreyenhagen shale (figure 62).

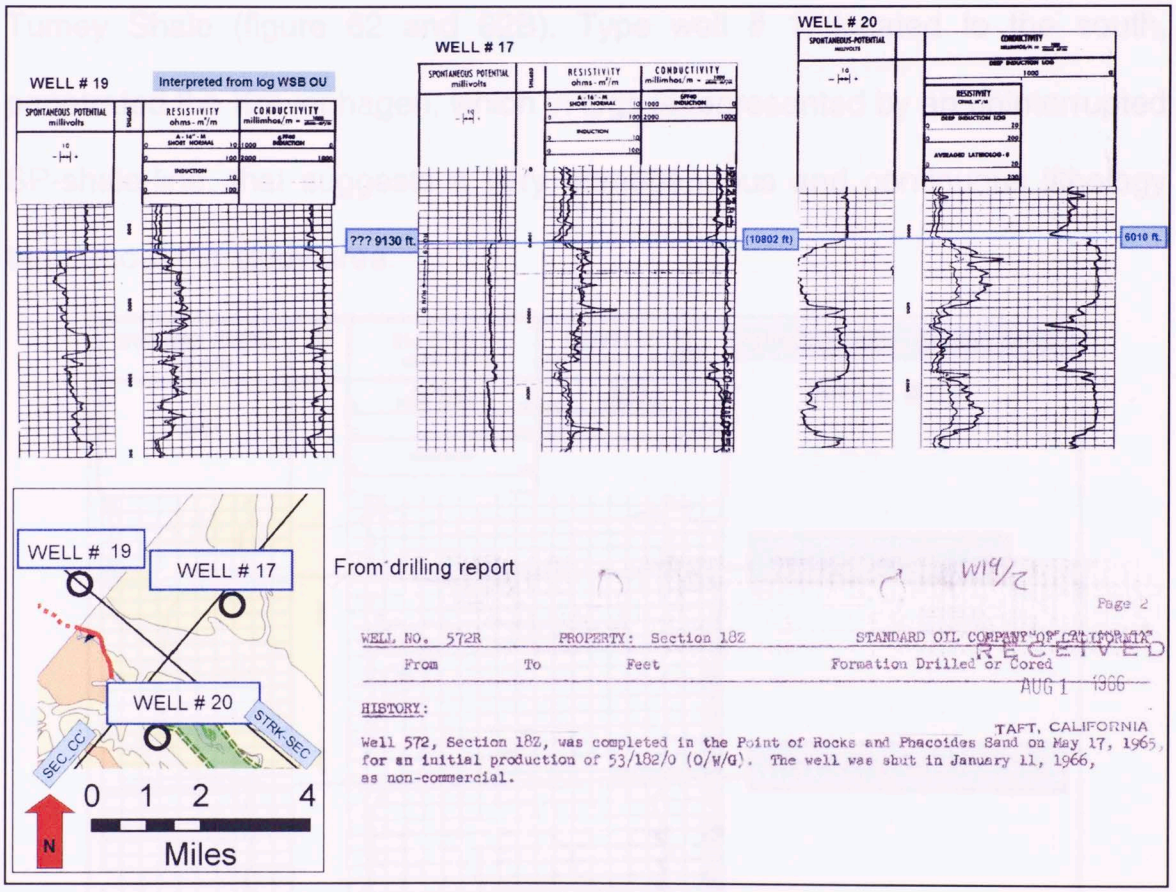


**Figure 62.** Well-log character of the Point of Rocks marker. Note the blocky pattern of the sandstone in the SP-log and the intercalation with thin shales at the three wells.

The marker for the Point of Rocks Sandstone was available in the well-reports of well # 17 and well # 20 (figure 62). This data and the log character

provided the confidence to interpret the marker in well # 19. Also, the marker for the top-Kreyenhagen was available in well # 19 (see stratigraphic cross sections) and the drilling report mentions that the well was completed in the Point of Rocks Sandstone (figure 62).

The Kreyenhagen is a thick continuous shale packet above the Point of Rocks Sandstone and is directly beneath the Oceanic Sandstone of the Tumey Shale (figure 62 and 62B). Type well # 1, located to the south, penetrated the Kreyenhagen, which in logs is represented by an uninterrupted SP-shale-line, that suggests a very homogeneous and continuous lithology throughout the study area.

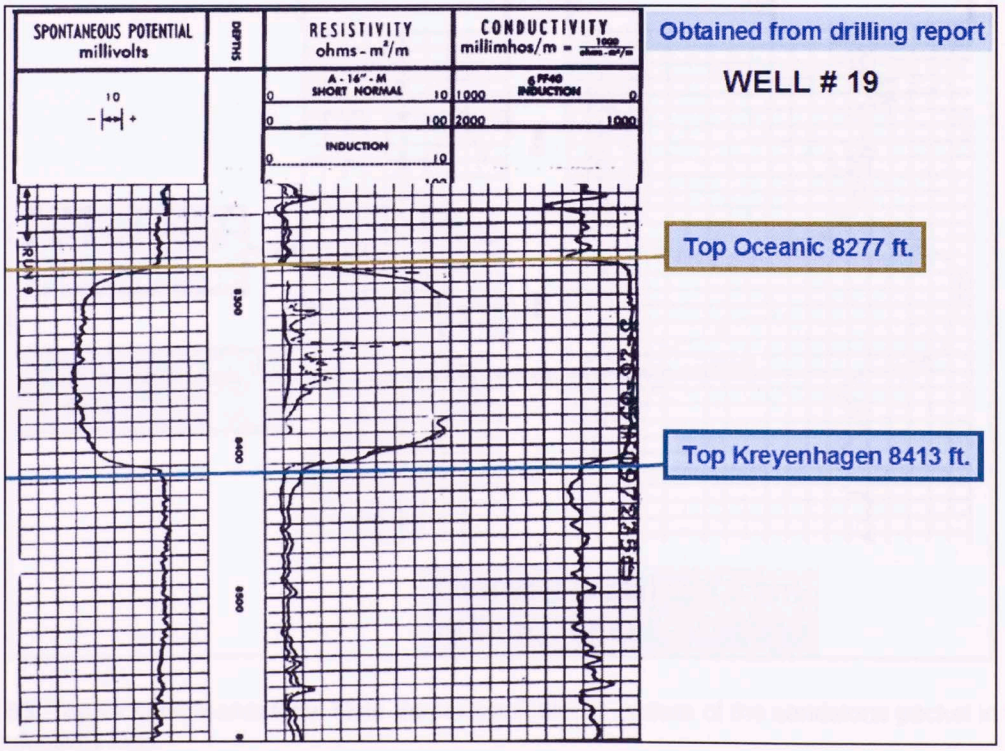


**Figure 62B.** Top Kreyenhagen (marker). Note the continuous SP-shale-line directly below the Oceanic Sandstone. Note the blocky pattern of the Oceanic sandstone.

The Oceanic Sandstone is time equivalent to the Tumey Shale marker and when present, the Oceanic Sandstone is a very good marker to obtain stratigraphic position as it is the top of a very well defined sandstone packet characterized by its blocky appearance. In well # 20 the sandstone is observed going out of scale in the SP-log conserving its basic blocky pattern (figure 62B and 63).

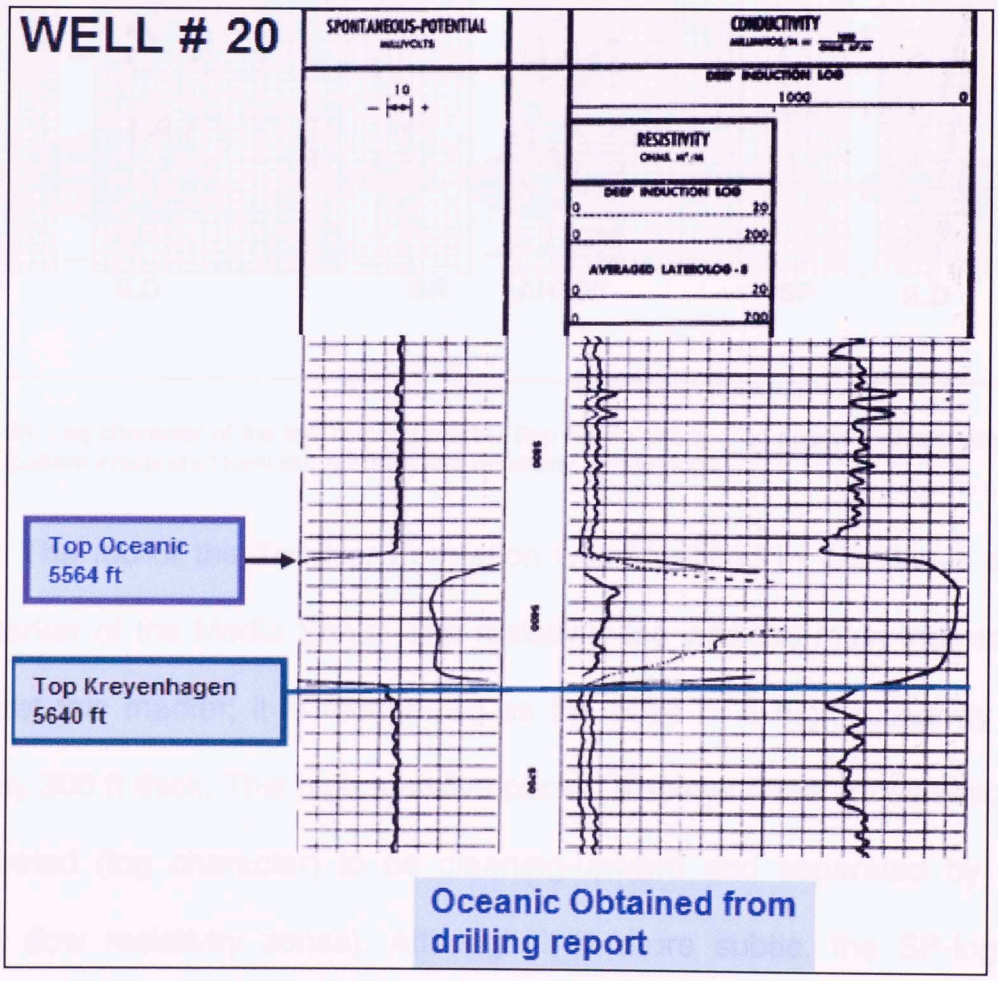


**Figure 63.** Top Oceanic Sandstone. Note the textbook blocky pattern of the sandstone packet in the SP and conductivity logs.

### 5.3.2 Top Temblor-Media Shale

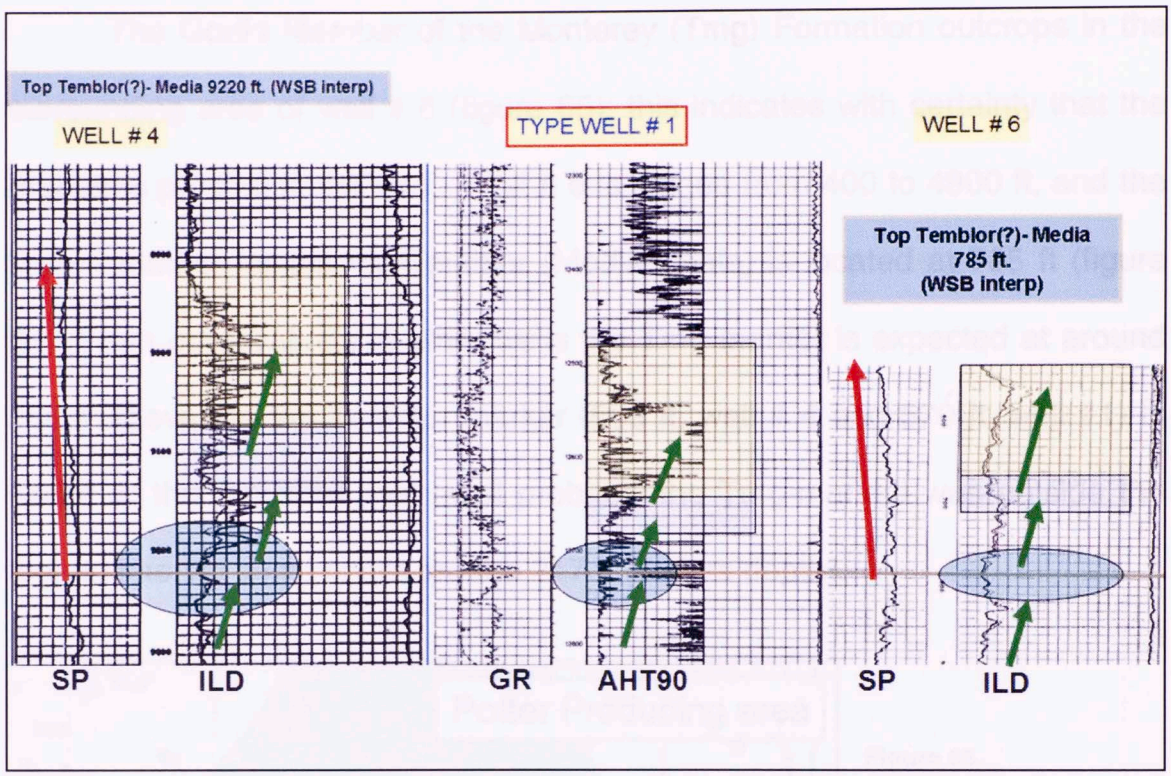


**Figure 64.** Log character of the top-Temblor marker (top Media shale). The arrows indicate coarsening upward pattern interpreted form the SP (red) and resistivity (green) logs.

The top of the Temblor Formation was identified in this thesis as the top-marker of the Media Shale. The resistivity log was the main tool used to interpret this marker; it is recognized as the base of a high resistivity zone roughly 300 ft thick. This high resistive packet displays three zones which are interpreted (log character) to be cleaning-upward and separated by shale layers (low resistivity zones). Although it is more subtle, the SP-log also shows a cleaning upward trend as displayed in wells 4 and 6 (figure 64).

*5.3.3 Shale Members of the Monterey Formation*

The Gould Member of the Monterey (Tmg) Formation outcrops in the surrounding area of well # 6 (figure 65); this indicates with certainty that the marker is present in the well. Well # 6 is logged from 400 to 4900 ft, and the known marker for the top-Temblor (Media Shale) is located at 785 ft (figure 64). From observations in other wells the Tmg marker is expected at around 568 ft above the top Temblor marker (565 ft, well # 4 and 570 ft, well #1) in well # 6; this indicates that most probably the Tmg-marked was outside the logged interval somewhere around 217 ft (drillers depth).

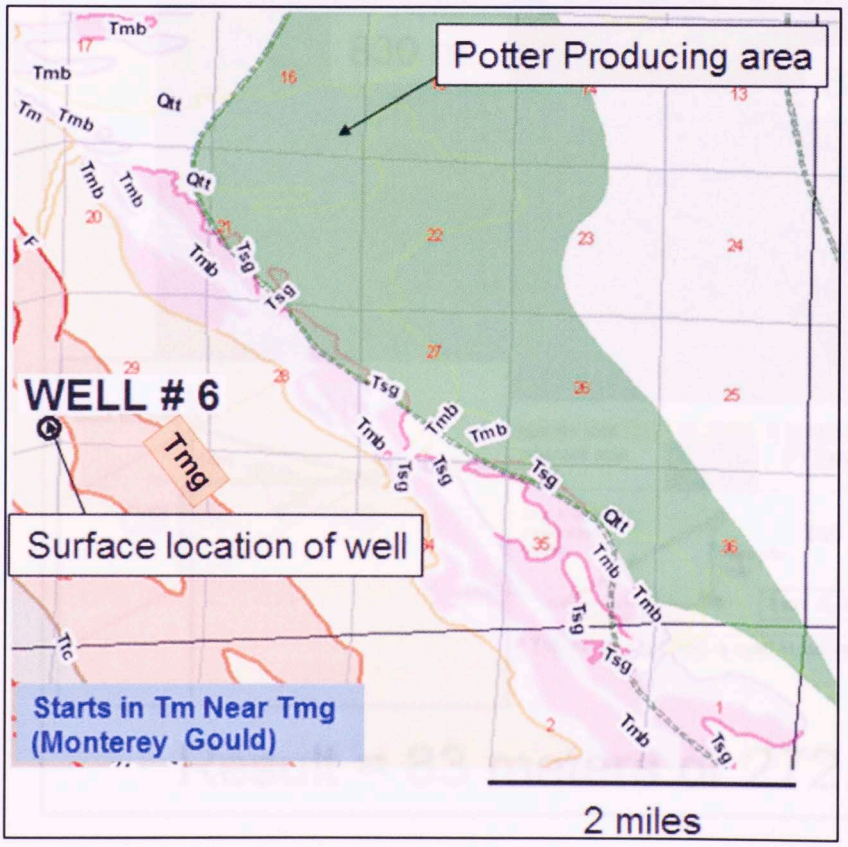


**Figure 65.**
Outcrop of the Top-Gould/Devilwater Marker (Tmg) near Well # 6. The well sits on the upper members of the Monterey Formation.

Midway sunset extension and potter producing area digitized from R. L. Gardiner, A. S. Wylie, Jr., M. J. Gagner., 1996, Pg. 176, Figure 1.

To calculate the expected location of the marker in the well, the known position of the surface marker was projected to the well path taking into account the elevation of the Kelly bushing (from DEM), the surface elevation of the contact (using DEM & DOQQ) and the linear distance from the well to the contact at approximately the dip direction of the beds. With these parameters, the location of the marker was interpreted using the tangent of the dip angle to match the wells. The result was then transformed to feet (figure 66).

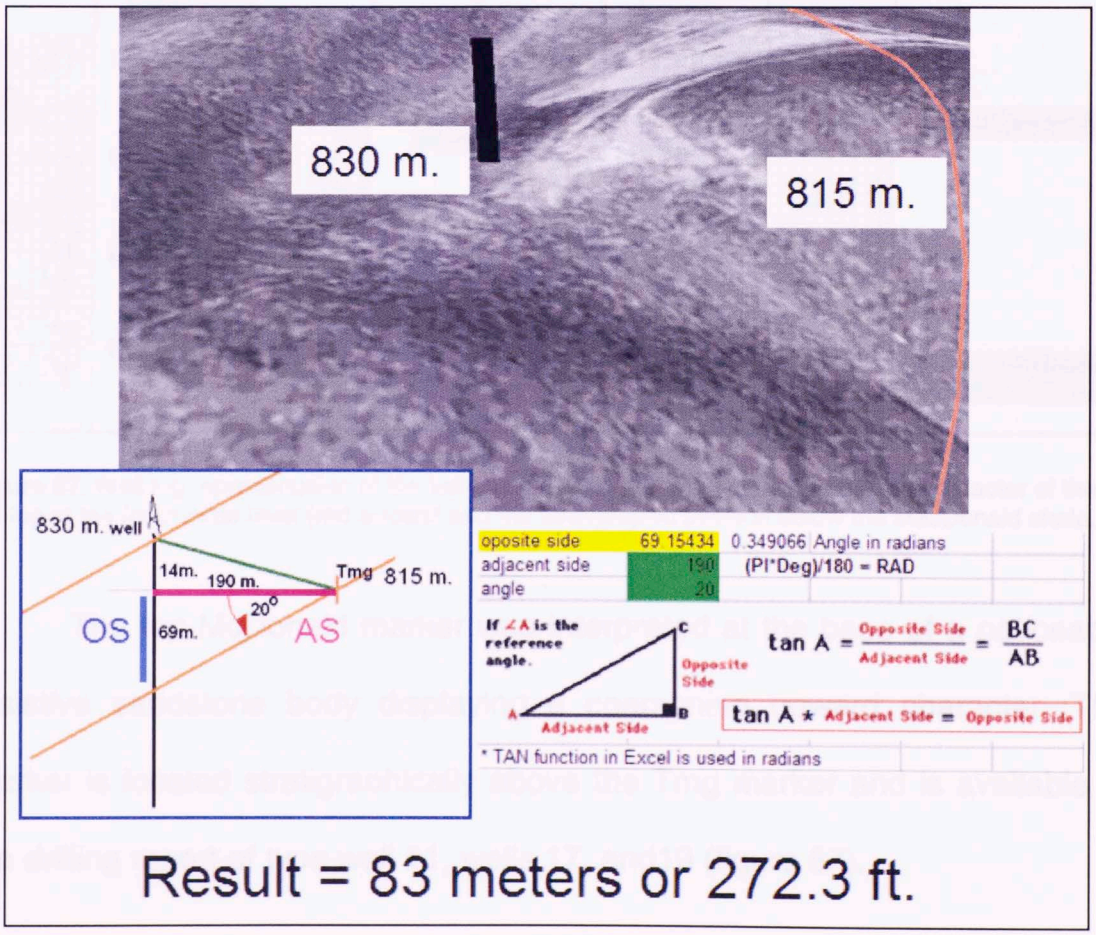


**Figure 66.** Estimation of the approximate location of Tmg in the borehole.

The Gould/Devilwater marker was interpreted at the Foraminite level. The Foraminite is defined paleontologically by the appearance of *Siphogenerina branneri* (Relizian-Luisian age); its stratigraphic position lies between the McDonald and Media Shales (Campbell, 2001). In the present work it was identified by comparative correlation to wells were the Foraminite-marker was available (figure 67).

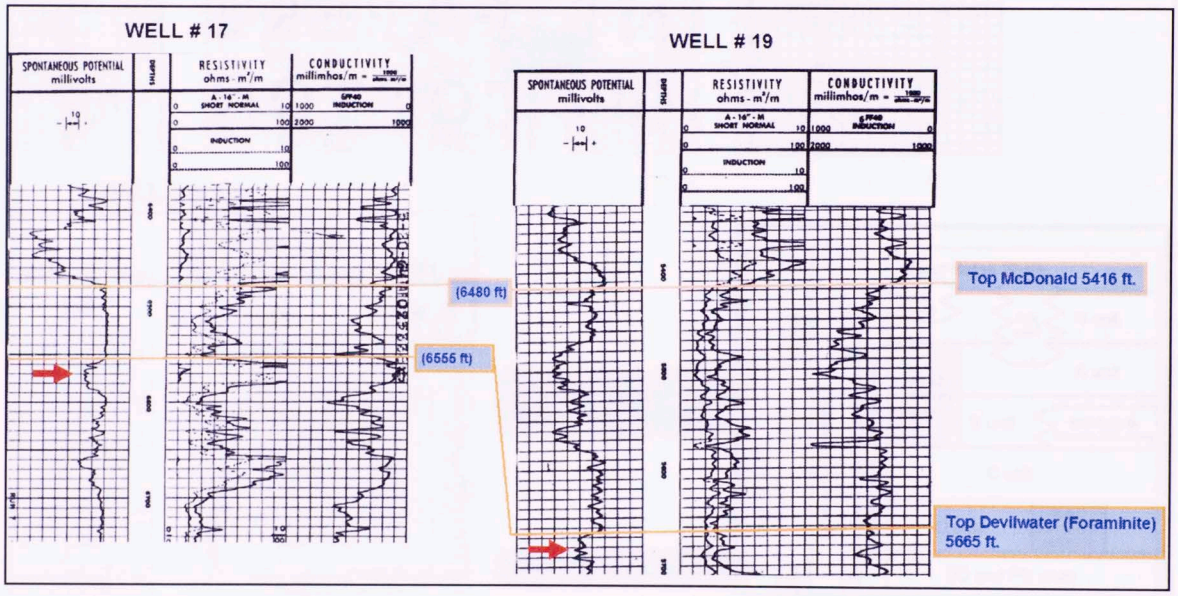


**Figure 67.** Well log representation of the top-Gould/Devilwater marker; notice the log character of the SP-log at the foraminate level (red arrows) and the stratigraphic position below the MacDonald shale.

The top McDonald marker was interpreted at the base of a noticeably resistive sandstone body displaying a coarsening upward character. The marker is located stratigraphically above the Tmg marker and is available in the drilling report of type well #1, wells 17, and19 (figure 67).

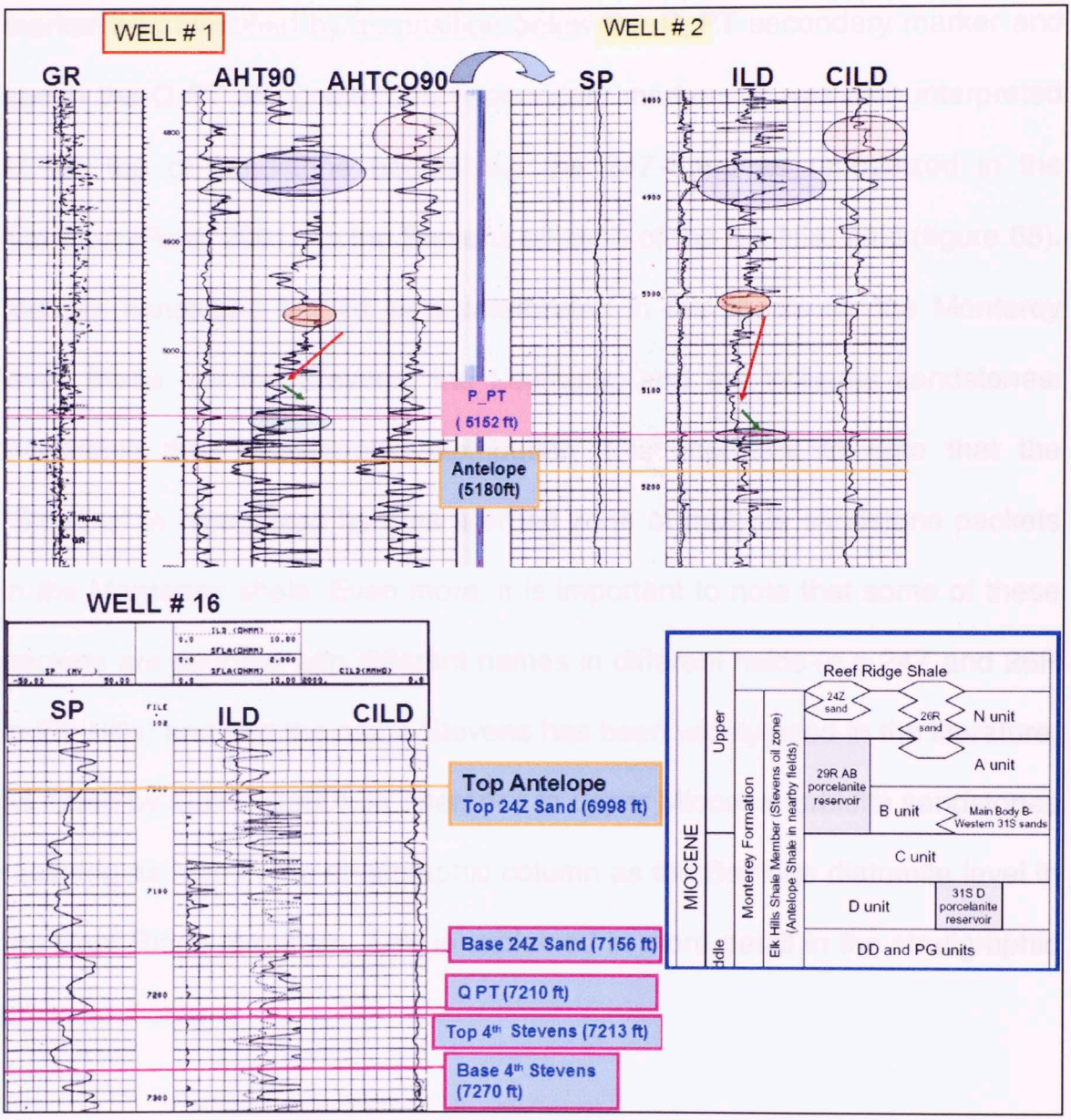


**Figure 68.** Top Antelope-marker; recognized by log character and its stratigraphic position with respect to secondary markers (obtained in well-reports). This marker was also interpreted at the top of known sandstone packets from the literature (insert stratigraphic column from: Reid, 2001., figure 2, pg 171.)

Various secondary markers from the type wells were used to locate the position of main markers; these display characteristic log signatures recognizable in other wells (see log markers in pocket). The top Antelope

marker was identified by its position below the P_PT secondary marker and above the Q-PT along with other secondary markers; it was also interpreted at the top of sandstone bodies like the 24Z-Sand as recognized in the literature (Reid, 2001), in the Stevens oil-zone of the Elk-Hills field (figure 68). Multiple sandstone bodies were interpreted in this thesis for the Monterey level; these are the Stevens, the Leutholtz, and the Williams sandstones. Regarding their stratigraphic distribution it is important to note that the "Stevens" is recognized here as a broad zone of multiple sandstone packets in the Monterrey shale. Even more, it is important to note that some of these packets are denoted with different names in different fields (e.g 24Z and 26R in Elk-Hills) and that the name Stevens has been widely used in the literature, as noted by Quinn (1990), in reference to upper Miocene turbidite sandstones reaching as high in the stratigraphic column as the Belridge diatomite level in the Reef Ridge formation. This is explained in more detail in the stratigraphic cross sections.

*5.3.4 Top Reef Ridge Marker*

The Reef Ridge Marker comprises the Belridge Diatomite and the Bitterwater Shale. It defines the limit between a log section characterized by a serrated and sandier pattern in the SP-log and resistivity logs (Olig sandstone) and the more constant log pattern of the lower Etchegoin

Formation (sub-Gusher Sandstone level). This marker also represents the Upper-Miocene Unconformity, broadly recognized in the literature (figure 69). Sandstone bodies in the Reef Ridge terminate against this unconformity, which is responsible for the absence of the Reef Ridge shale to the north of the study area (see model, figure 117). The Potter Sandstone and the Olig Sandstone were interpreted and are identified as extensive continuous sandstone bodies beneath the Reef Ridge marker (see stratigraphic cross sections).

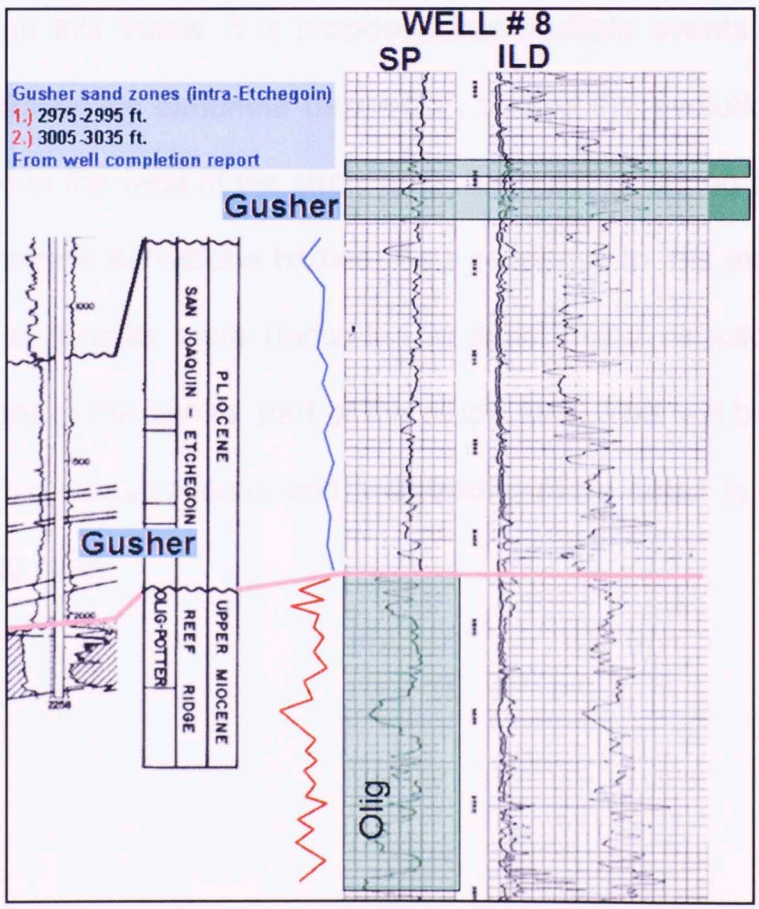


**Figure 69.** Reef Ridge marker; serrated (red) more constant pattern (blue). Insert, modified from: Ingram, 1964 plate IV.

The Olig-Potter level, known as the Santa Margarita Formation in outcrop, is characterized by large lens-shaped sandstone bodies embedded in diatomite. This is the Belridge Diatomite level (Tmb) located stratigraphically beneath the Reef Ridge marker. In the field[1] these lens extend for approximately 100 feet laterally and they are observed encased into the diatomite, cutting into the substrate to the base and overlain by diatomite to the top.

From actual observations in the field (personal field observation during visit to Bakersfield[1]) and the analysis of the stratigraphic and structural interpretation in this thesis, it is proposed that multiple events of sandstone deposition followed by diatomite deposition, tied to the evolution of a major fault-bend-fold to the west of the study area, were active during the deposition of the later Stevens sandstone bodies. As a response to this major structural event, these sediments were deposited in a northeast direction, becoming more prominent to the central part of the study area. This will be observed in the stratigraphic cross-sections and analyzed in more detail in the structural analysis of this study.

### *5.3.5 Top Etchegoin and San Joaquin Markers*

The limit between the Etchegoin and the San Joaquin Formations is not easily interpreted in well-logs. Furthermore, to accurately locate this marker it is necessary to obtain a proper biostratigraphic analysis to identify the unconformity that lies between these two formations. In this study the limit was interpreted by carefully observing the log character of the type wells which had the limit available, studying published well-logs in the literature, and identifying these observations in the interpretation wells.

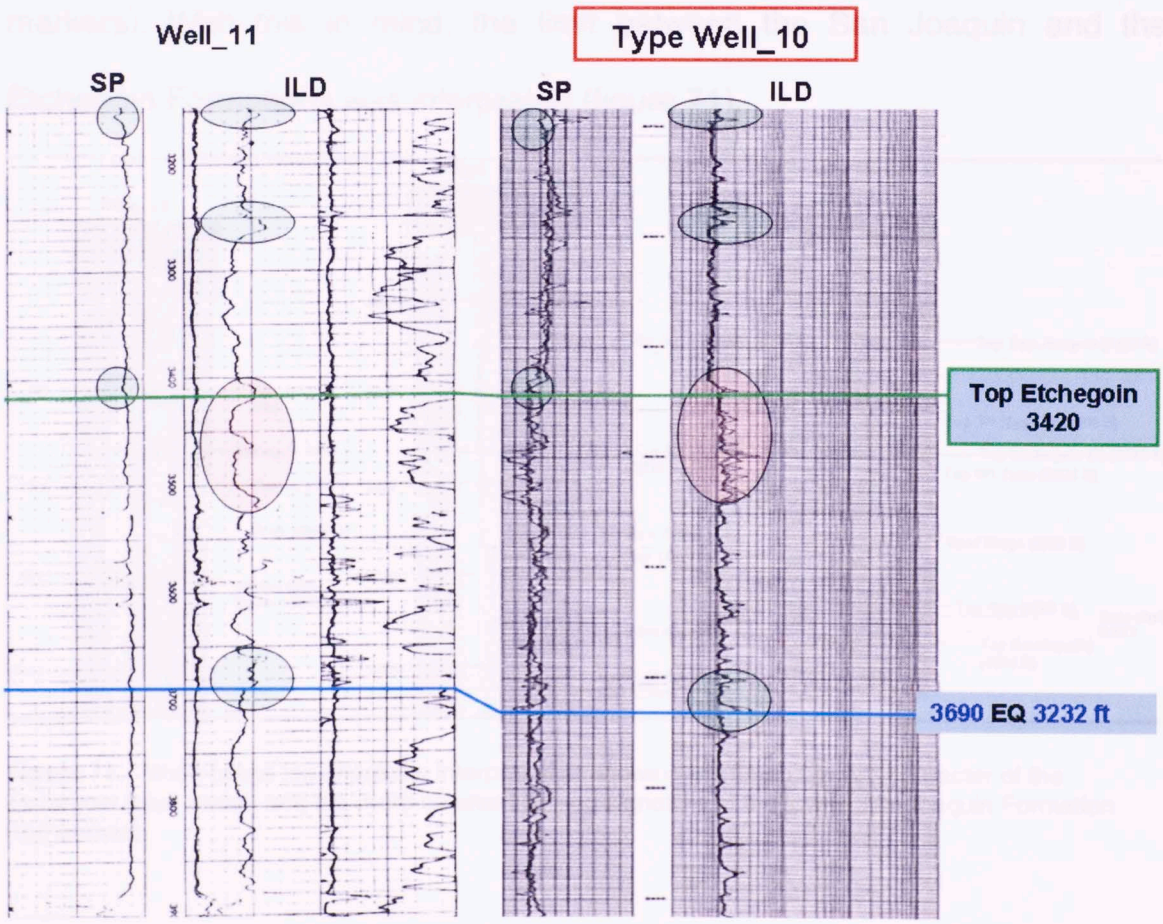


**Figure 70.** Log character of the Etchegoin marker (note resistivity change above the Etchegoin).

A complete large scale (600 ft) comparative correlation analysis was conducted to identify correlative log signatures. This provided an acceptable level of confidence to then observe detailed features in the well logs to locate the top-Etchegoin marker representing the unconformity that separates the Etchegoin and the San Joaquin Formations (figure 70). At a larger scale it was a subtle fining-upward trend above the Reef-Ridge marker, noticeably terminating where a more constant SP-log is characteristic. This was observed in the type wells were the top-Etchegoin was available (blue-markers). With this in mind, the limit between the San Joaquin and the Etchegoin Formations was interpreted (figure 71).

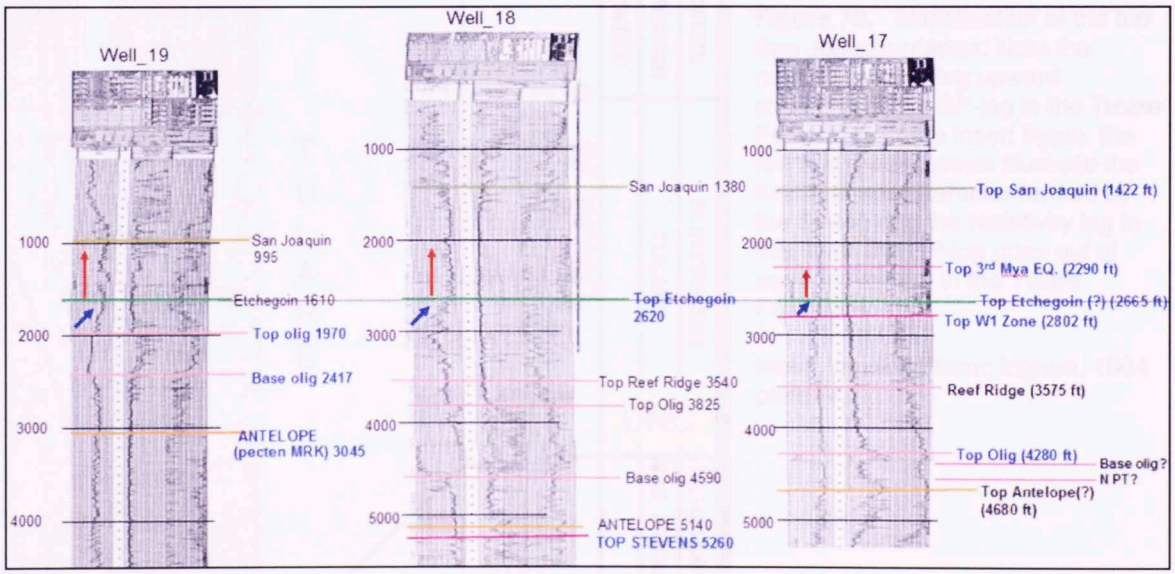


**Figure 71.** Wide-range log-character interpretation showing the fining upward character of the Etchegoin (blue arrow) and the more constant SP-log signature of the lower San Joaquin Formation (red arrows).

The top San-Joaquin-marker was interpreted at the point where a general trend resembling a funnel (SP-Resistivity) terminates into a more constant SP-log character in the San Joaquin Formation. This prominent coarsening upward characteristic in the SP-log of the lower Tulare Formation has been extensively illustrated in the literature, marking the unconformable contact between the Tulare and the San Joaquin Formations. This renowned aspect was used to identify the Top San Joaquin-marker in this thesis (figure 71).

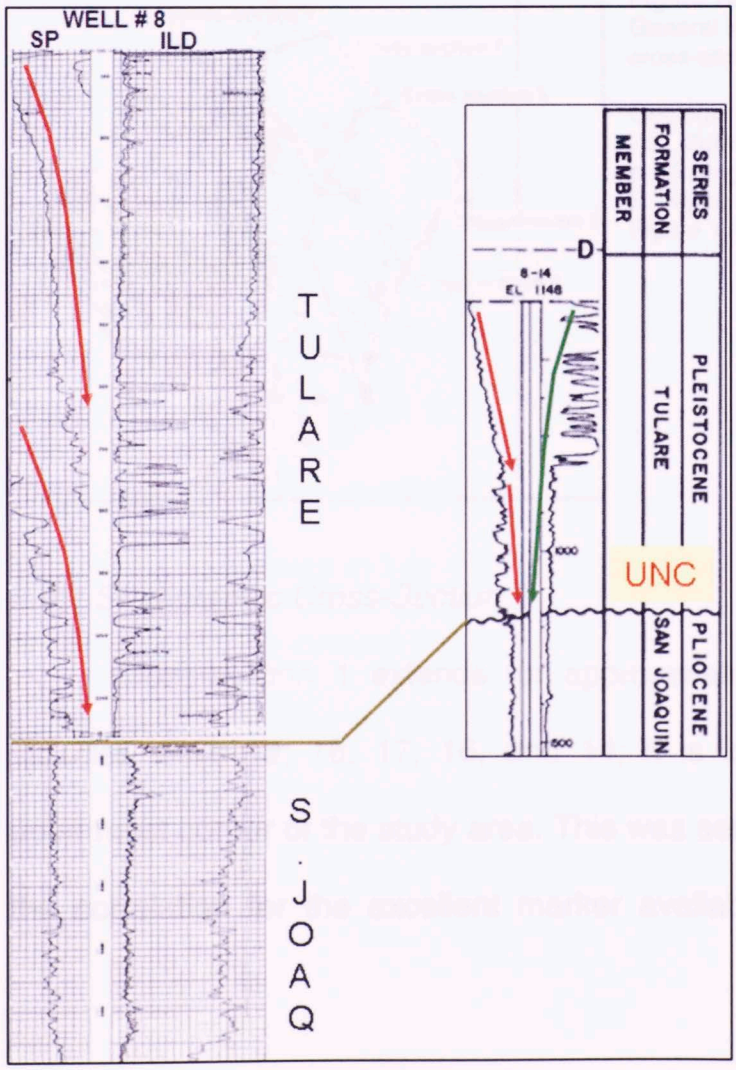


**Figure 72.** Identification of the top San Joaquin marker. Note the marked coarsening upward character of the SP-log in the Tulare Formation. In the insert figure, the red and green arrows illustrate the funnel shape character formed by the Sp-log and the resistivity log in this level; the SP-log goes out of scale in well # 8 in the Tulare Formation.

Insert, modified from: Ingram, 1964 plate IV.

## 5.4 Stratigraphic Cross-Sections

The stratigraphic datum selected for the seven cross-sections is the top-Etchegoin marker. The datum and the location of the sections were selected to understand more clearly the depositional direction and the distribution of the upper-Miocene sandstones in the study area.

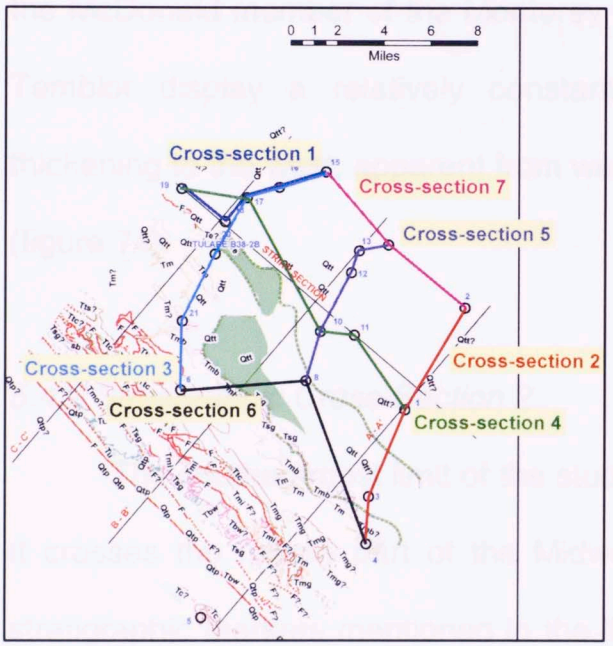


**Figure 73.**
General location map of the seven stratigraphic cross-sections.

Geologic contacts rectified from Dibblee, 1972-73., Midway sunset extension and potter producing area digitized from R. L. Gardiner, A. S. Wylie, Jr., M. J. Gagner., 1996, Pg. 176, Figure 1.

### *5.4.1 Stratigraphic Cross-Section 1*

Cross-section 1 extends for approximately 11.6 km (7.25 mi.) and includes wells 19, 18, 17, 16, and 14; it is located to the North, at the uppermost corner of the study area. This was selected as the starting point of the correlation for the excellent marker availability and the short distance

between the wells. Having numerous data-markers (blue) in a reduced area ensured a less interpretative starting point with less log-signature variability.

Wells 19 and 17 are type wells and include data markers for all the formations from the San Joaquin to the Kreyenhagen marker. The remaining wells include some data markers and TD within the Antelope member. This section shows a general thickening to the Northeast for the formations above the McDonald member of the Monterey Formation. Earlier formations like the Temblor display a relatively constant thickness, with a subtle general thickening to the west, apparent from well 15 to 17 in the Carneros Sandstone (figure 74).

*5.4.2 Stratigraphic Cross-Section 2*

The southernmost limit of the study area is covered by cross-section 2. It crosses the middle part of the Midway-Sunset structure where the main stratigraphic markers mentioned in the literature are present and available in type well # 1, present in this cross-section. This well is the deepest well used in this study. Two reverse faults are presented in this cross-section; the one at the base of the Tumey Shale in type well # 1 was obtained from the report, and the one in well # 3 was interpreted in the present study (see well markers in pocket).

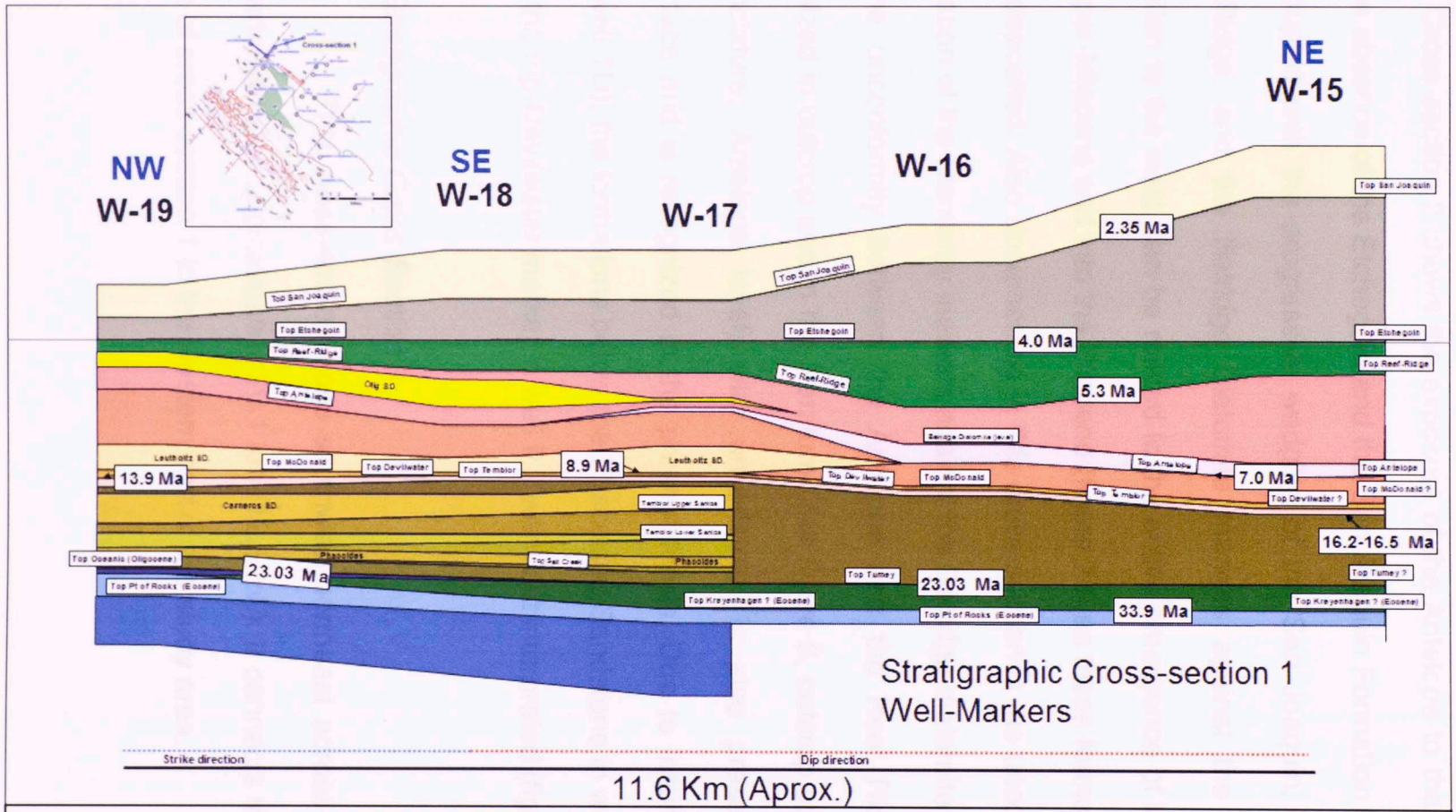


**Figure 74.** Cross-section 1; formations above the top-McDonald marker are thickening to the northeast. The Temblor formation is slightly thickening to the west. (for more detail and well-log markers see the full scale stratigraphic cross-sections in pocket)

Cross-section 2 shows the exposure of the Antelope to the southwest and the absence of the Etchegoin and the San Joaquin Formation in well # 3; this coupled with the progressive wedging of the San Joaquin, Etchegoin, Reef Ridge, and the Belridge Diatomite markers against the Monterrey Formation to the west, can be related to the active emergence of land during the upper-Miocene and into the Pliocene (figure 78) as these formations were being deposited. Also documented in this cross section is the unconformable termination of the Monterey markers against the Belridge-diatomite, indicating that the unconformity between the Antelope and the Reef Ridge Shale recognized in outcrop and in the literature (see figure 6, outcrop stratigraphic nomenclature, Antelope level) with uncertainty, is also present in the subsurface and is recognized in the present thesis. Due to insufficiency of data (well TD), the formations below the Phacoides Sandstone in well # 4 and below the top-Devilwater marker in well # 2 were not interpreted (figure 75).

*5.4.3 Stratigraphic Cross-Section 3*

This cross-section goes southwest-northeast across the study area, extending for approximately 20.1 km (12.5 mi.). It connects the eastern portion of cross-section 1 to the western part of the study area.

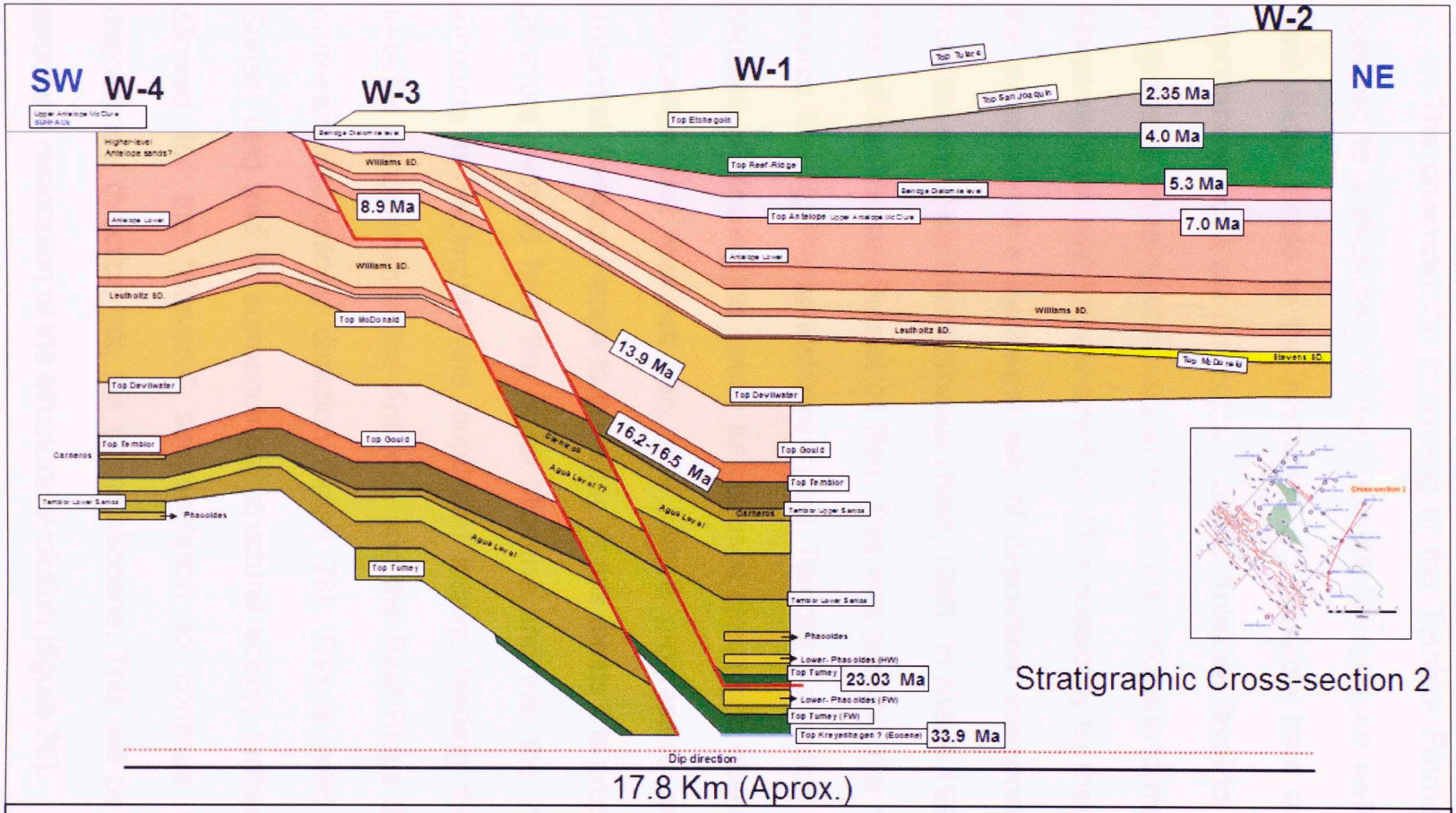


**Figure 75**. Stratigraphic cross-section 2; the San Joaquin , Etchegoin, and Reef Ridge formations are pinching out to the southwest against the outcropping Monterrey Formation. Note also the unconformity between the Antelope shale and the reef Ridge shale (see full-scale stratigraphic cross-sections in pocket).

The characteristic thickening of the Temblor Formation to the west, opposed to a thickening of the upper-Monterrey (see wells 6 and 21) and Reef Ridge Shale to the northeast is noticeable here as well. It is also important to point out the outcrop of the Antelope level to the west and the progressive wedging of the upper-Miocene to Pliocene formations against the Monterey in an east to west direction. One possibility for these observations is the existence of a southwest axis of deposition, transporting the sediment from the ancestral Sierra Nevada (Reid, 1988., in Nilsen 1996), located to the east of the Midway-Sunset oil filed. This was possibly the main sedimentary source feeding the sandstones in the Temblor Formation during the early-Miocene. Following this event, an opposite direction is observed for sediment deposition that matches very well with a progressive emergence of the ancestral Temblor Range to the west. In this thesis it is proposed that as this structure evolved from the upper-Miocene and into the Pliocene, massive amounts of sediment were deposited locally, feeding the upper-Miocene turbidite sandstones in the Antelope and the Reef Ridge Shale, following a northeast depositional direction (figure 78). This is valid for the Midway-Sunset field and its surroundings; structural activity further west may have allowed for the "Stevens" sedimentation to continue its southwestern depositional direction into the upper Miocene. This will be explained in the structural restoration of the structural evolution (figure 76).

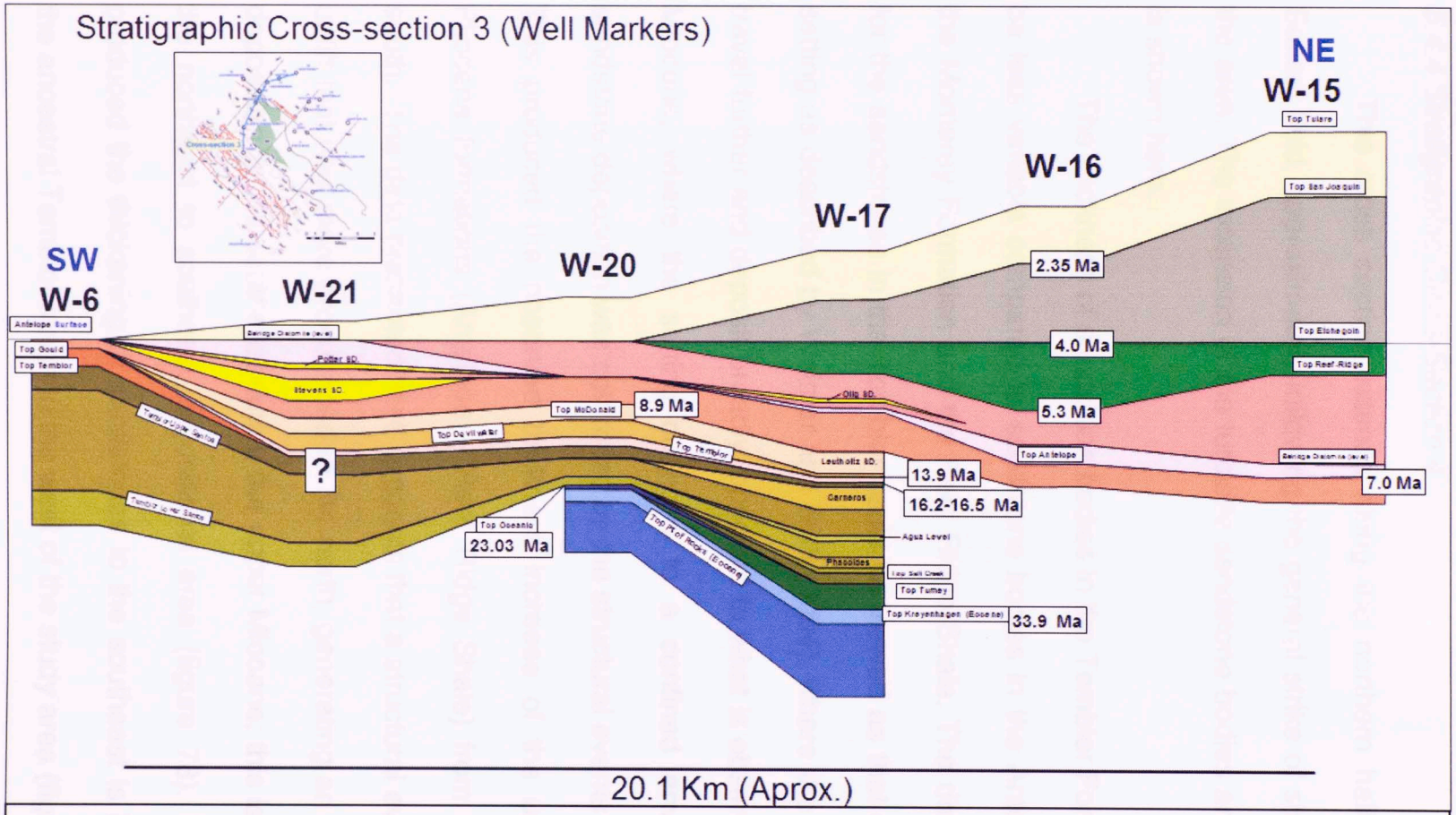


**Figure 76.** Stratigraphic cross-section 3; The thickening of the Temblor formation to the southwest indicates a sedimentary source to the east (ancestral Sierra Nevada). The thickening of the sandstone bodies in the Antelope member and the thickening of the Reef Ridge shale indicate a sedimentary source to the west (Temblor Range). See full-scale stratigraphic cross-sections in pocket.

*5.4.4 Stratigraphic Cross-Section 4*

This cross section extends along the northern half of the Midway-Sunset field, approximately following the general strike of structural heighs in the area. The extension of the turbidite sandstone bodies and their continuity is shown here.

The thickness of sandstone bodies in the Temblor Formation appear to be less variable compared to sandstone bodies in the Antelope member of the Monterey Formation and the Reef Ridge Shale. The depositional setting for the sandstones in the Temblor could be viewed as that of an unconfined setting as described by Weimer and Slatt (2004), where the sediments could travel further and deposit broadly; opposed to what is observed In the Upper Miocene, where the setting changed to a confined environment where sandstone deposition was controlled by the structural events that were active. This produced the observed thickness increase of the upper-Miocene to Pliocene formations (Antelope – Reef Ridge Shale) from the north to the south. The data presented here suggests that a structural event produced an uplift that was more pronounced to the north, generating an axis of sediment deposition to the southeast during the upper Miocene; this is a component of the northeast to southeast depositional area (figure 78). The source that produced the thickening of sandstones to the southeast is interpreted to be the ancestral Temblor range to the west of the study area (figure 77).

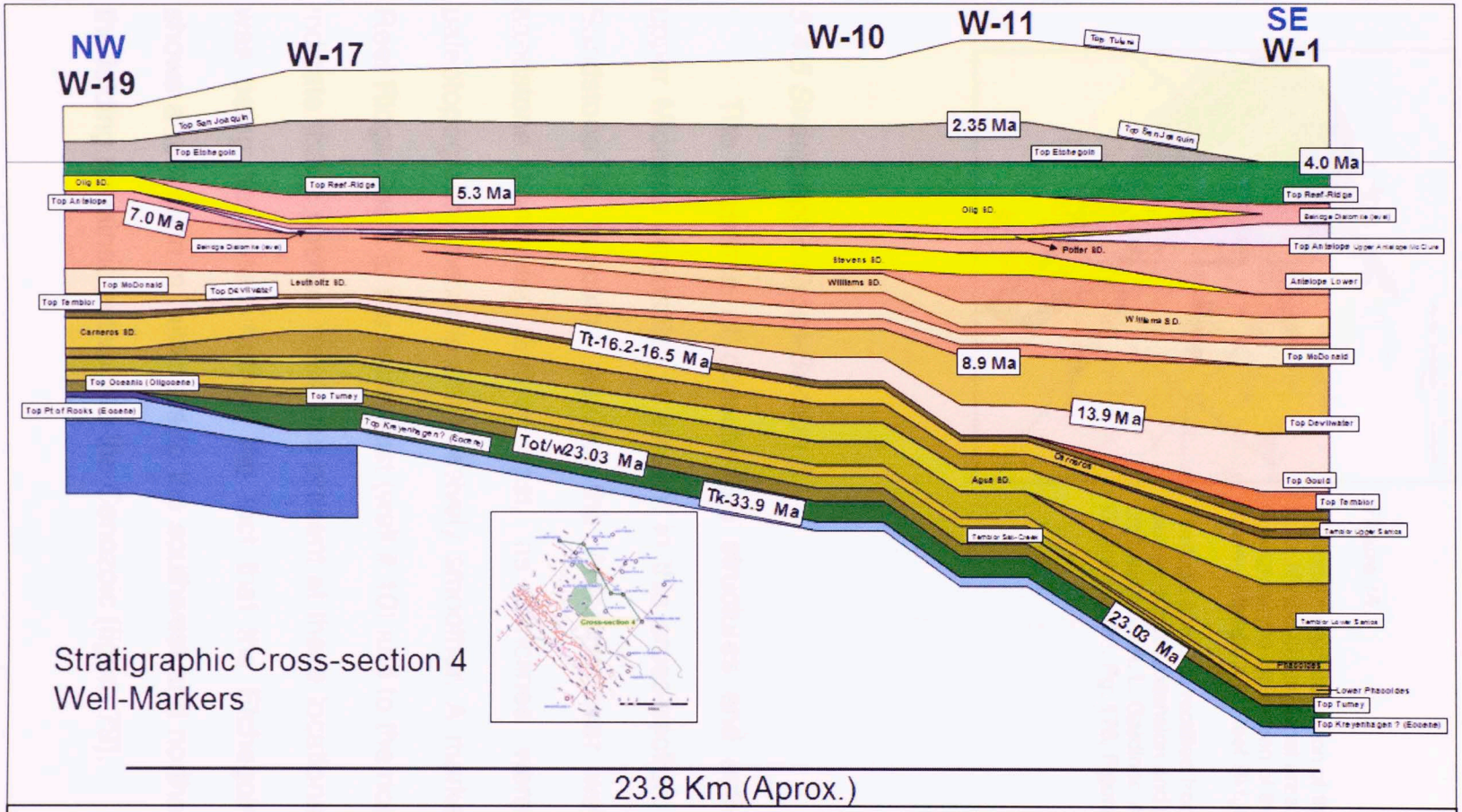


**Figure 77.** Stratigraphic cross-section 4; extension of the northern half of the Midway-Sunset field. Notice the marked thickening of the upper-Miocene and Cenozoic formations to the southeast. Sandstones in the Temblor Formation show a more constant thickness and are more extensive (see full-scale stratigraphic cross-sections in pocket).

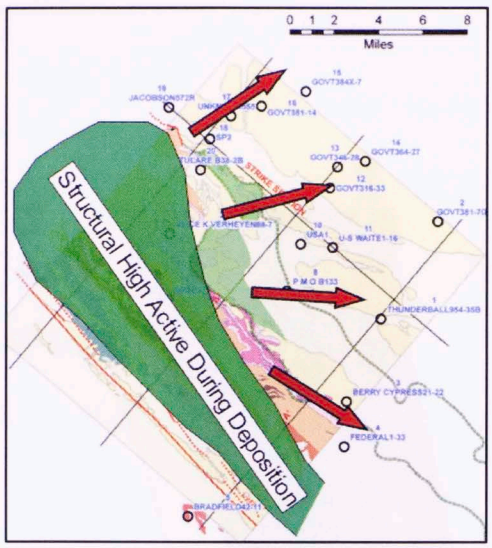


**Figure 78.**

Schematic representation of the interpreted northeast to southeast depositional area that was active throughout the deposition of the turbidite sandstones of the Antelope and Reef Ridge shales.

Geologic contacts rectified from Dibblee, 1972-73., Midway sunset extension and potter producing area digitized from R. L. Gardiner, A. S. Wylie, Jr., M. J. Gagner., 1996, Pg. 176, Figure 1.

### *5.4.5 Stratigraphic Cross-Section 5*

The presence of considerable structures and active folding during upper Miocene deposition is evident in this cross-section. Here, the Potter Sandstone is truncated against the Antelope near well #10, the Olig sandstone continuing further east, as synclines were filled and the paleotopography became progressively smoother. A marked thinning of the Reef Ridge Shale to the southwest (well # 10) and to the northeast (well # 14) indicate that a positive relief was present at these locations as the formation was being deposited; further, the fact that the Etchegoin Formation also shows a reduction in thickness to the southwest and northeast suggests that the folding remained active into the Cenozoic (figure 79).

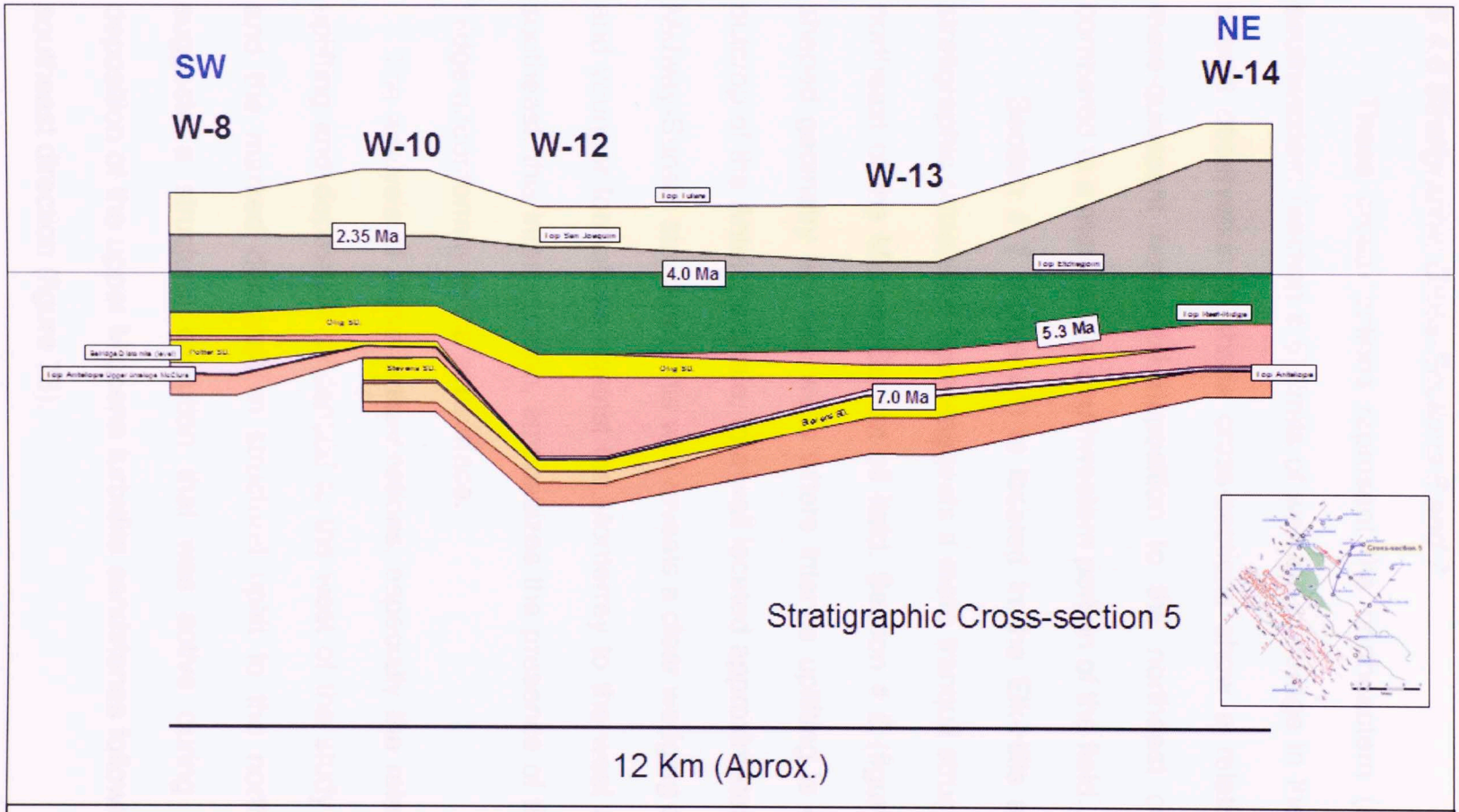


**Figure 79.** Cross-section 5; the decreased thickness of the Reef Ridge shale to the southwest and the northeast could be attributed to the presence of positive relief at these locations. The coincident thinning of the Etchegoin Formation at the same locations indicates that the activity remained active into the Cenozoic (see full-scale stratigraphic cross-sections in pocket).

*5.4.6 Stratigraphic Cross-Sections 6 and 7*

These cross-sections represent the northeastern (section # 7) and southwestern (section # 6) limits of well log coverage in the study area. The overall observation of these cross-sections show a relatively simpler and more-quiescent horizontal deposition to the northeast of Midway-Sunset compared to a more active southwestern portion of the field.

Section # 7 (figure 81) is located in the Elk-Hills area. A smoother stratigraphic correlation here suggests a more tranquil structural realm to the northeast of the Midway-Sunset oil field. Section # 6 (figure 80) with an "L" shaped geometry ties two wells where intense uplifting is evidenced by the outcrop of the Antelope shale, to a well located approximately at the center of Midway-Sunset structure. This well reveals a clear wedging of the Reef Ridge and younger formations against the Monterrey to the west and to the south-southeast; this interpretation, emphasizes the presence of the Antelope-Reef Ridge unconformity in the subsurface.

The analysis of these cross-sections, especially the relationship between uplifting and deposition evidenced to the west of the study area (figure 80), and the marked decrease in structural uplift to the northeast (figure 81) suggests a structural evolution that was active during the sedimentary deposition of the upper Miocene turbidite sandstones following a northeast to southeast direction (figure 78).

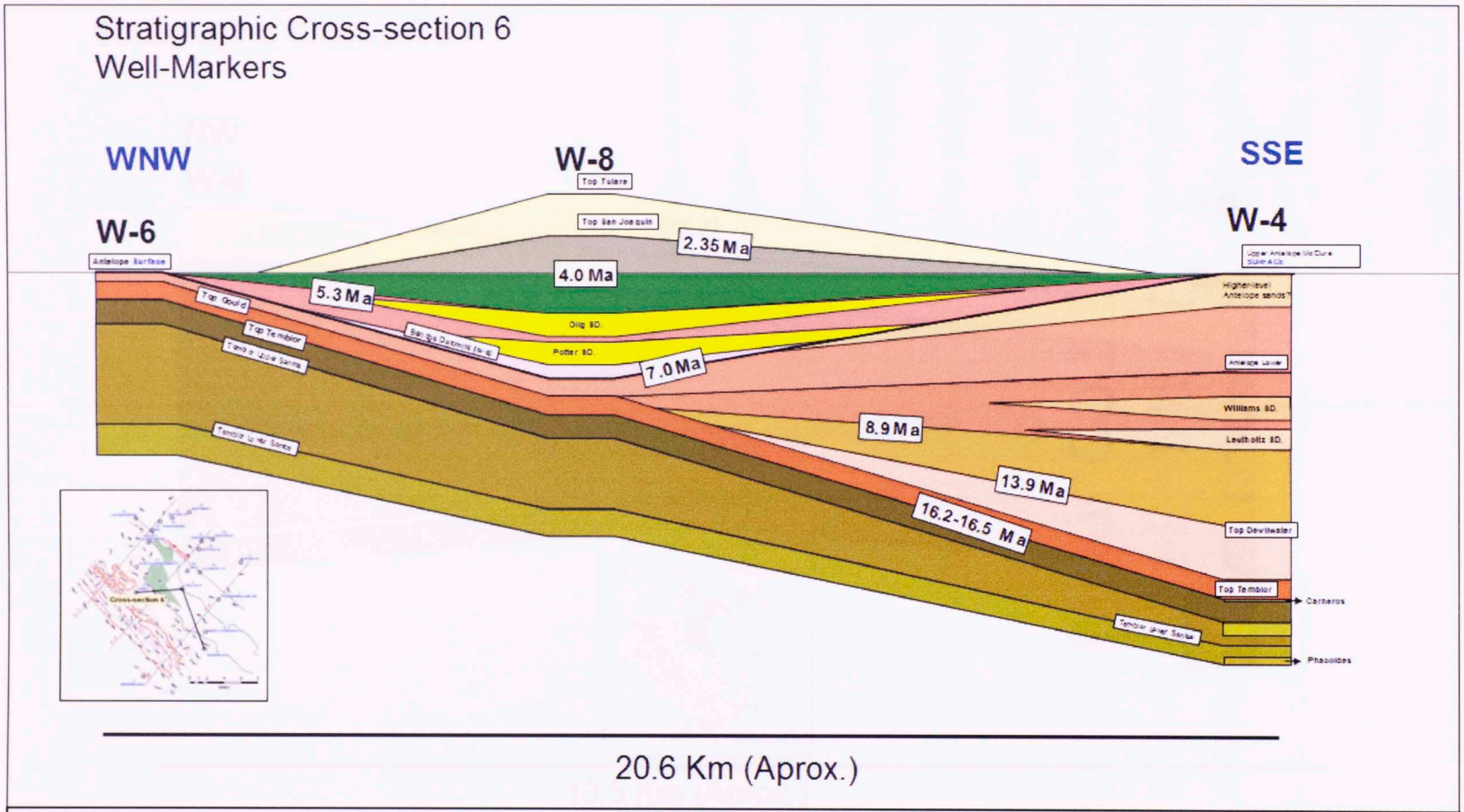


**Figure 80.** Cross-section 6; "L" shaped, ties two wells to the east of the Midway-Sunset structure to one in the middle of the oil field. Notice the wedging of the Reef Ridge and younger formations against the Monterrey Formation, and the presence of the unconformity between the Antelope and the Reef Ridge shales (see full-scale stratigraphic cross-sections in pocket).

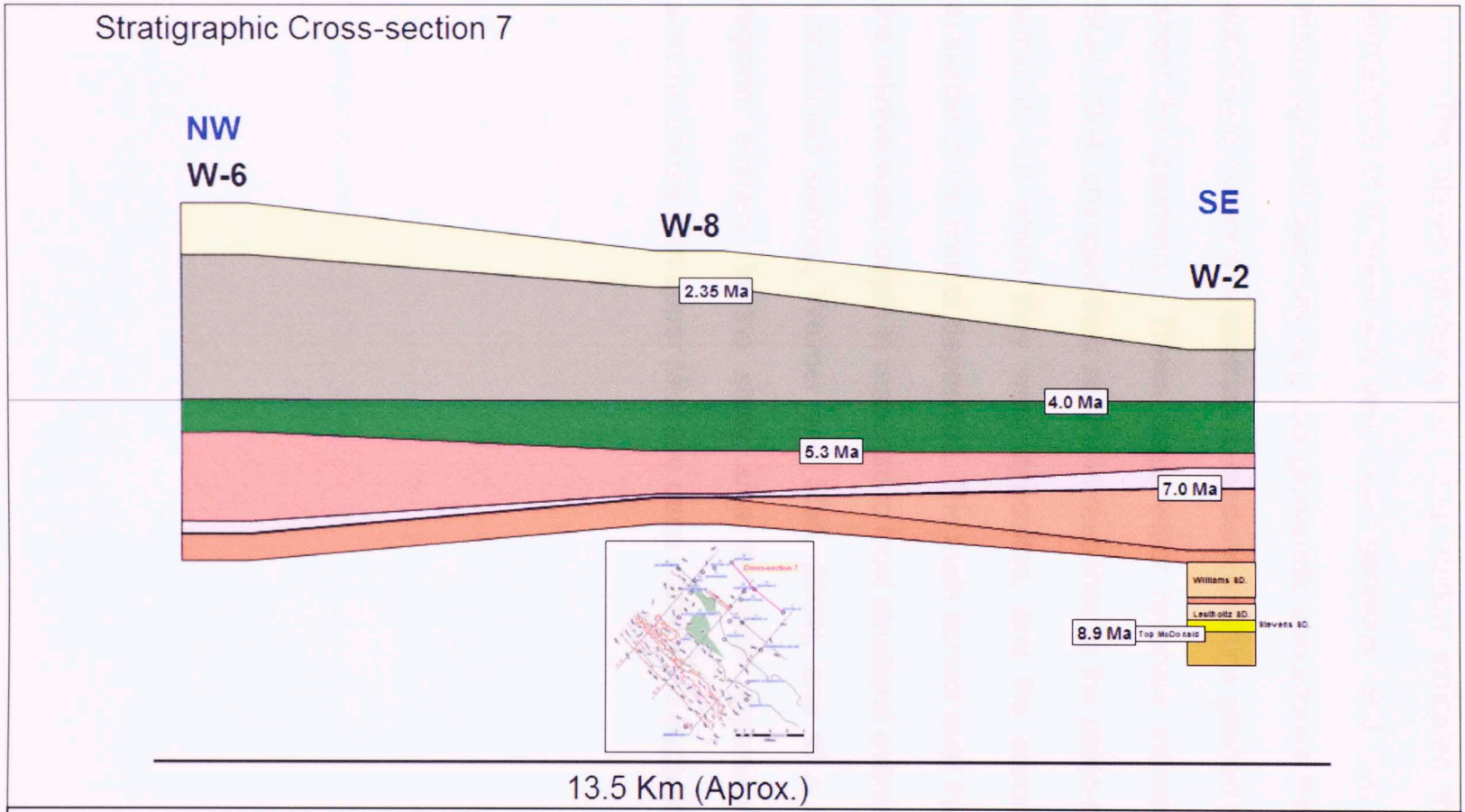


**Figure 81.** Cross-section 7; note the smother correlation of the markers to the northeast of the Midway-Sunset field. This section is located in the Elk-Hills area (see full-scale stratigraphic cross-sections in pocket).

The above stratigraphic interpretation indicates that internally, the formations of interest are very heterogeneous, and that the units include many types of deposits (e.g. conglomeratic sandstones filling deeply incised submarine canyons in contrast to medium and fine grained sandstones with a sheet-like geometry). These deep water reservoir elements (Weimer and Slatt, 2004) changed their nature in response to the paleo-morphology of the substrate on which they were deposited, and the accommodation space available at the time of deposition. The main control over these parameters is the relative water-depth in response to local structural events (e.g. confined or unconfined setting., Weimer and Slatt, 2004), and to a lesser extent the regional eustacy. In the study area the main structural event occurred simultaneously with upper Miocene deep water sand deposition.

# 6. STRUCTURAL FRAMEWORK

The main structures in the study area are a series of anticlines where the Midway-Sunset, the Buena Vista, and the Elk hills oil fields are located (figure 82). The Midway-Sunset and the Buena Vista oil fields are interpreted in this study as a series of parallel, fault-bounded structures, cored by deeper fault-bend folds. The timing, and evolution of the complex structural features observed in the northern part of the Midway-Sunset field (Southern Belgian anticline area) are addressed here. The evolution is examined in relation to the deposition of the upper Miocene turbidite sandstones.

To identify the events, which are directly responsible for the complexities present in the detailed study area, it was necessary to understand the structural evolution from a regional perspective (three regional cross sections) to explain the origin of the Midway-Sunset field and related structures, and then focus in the local area (five detail cross-sections) where the structural geologic model was built (figure 82).

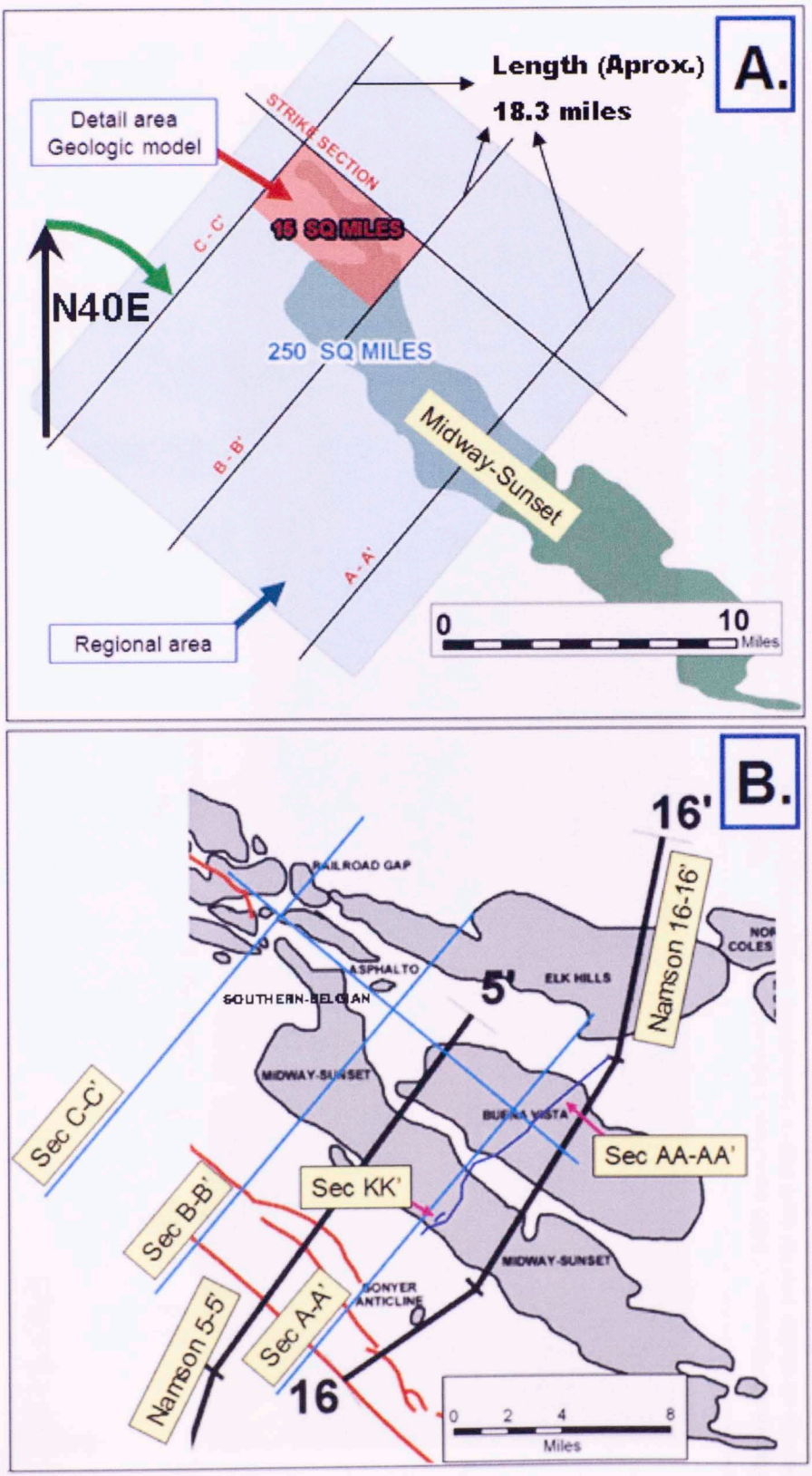


**Figure 82.**
A. Generalized map showing the regional and detail areas of study.

B. Sketch showing the oil fields covered by the regional cross-sections completed in this thesis (light blue), and the location of the main cross sections used from the literature (dark blue). The base map of the oil-fields and the location of cross sections 5-5' and 16-16' are the actual location map from Namson (1998). The length of each of the regional cross-sections is 18.3 miles (aprox).

Notice the orientation of the cross-sections (N40°E) following the average dip direction of the Midway-Sunset main structure.

Upper figure (A); The Midway-Sunset field boundaries were extracted from R. L. Gardiner, A. S. Wylie, Jr., M. J. Gagner., 1996, Pg. 176, Figure 1.)

Lower figure (B); modified from Namson, 2001

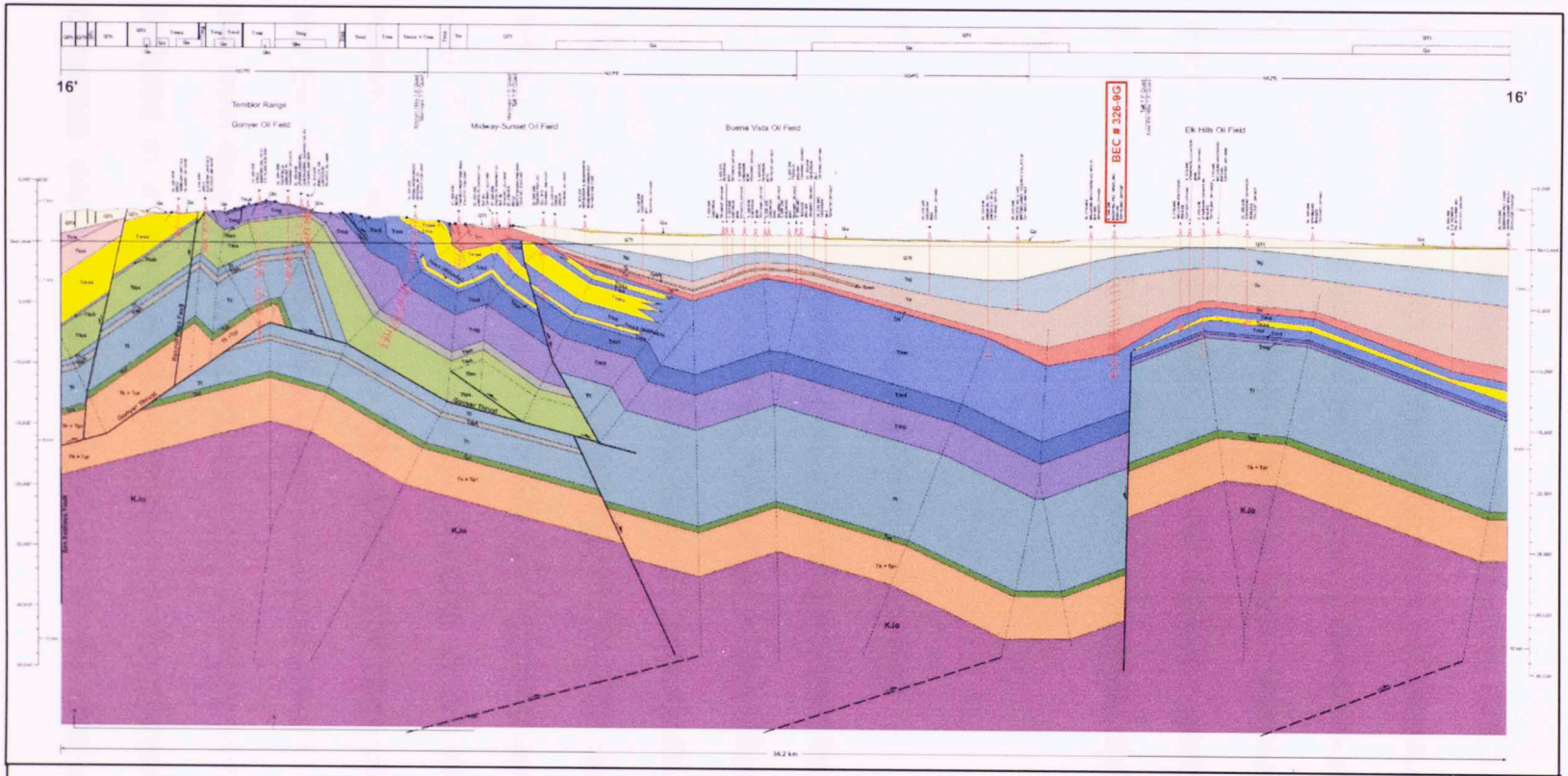


**Figure 83.** Namson (2000) structural cross-section 16-16'. The fault at the detachment of a well developed fault-bend fold to the west cuts across an earlier normal fault that is reversed to accommodate the slip. To the east a normal fault with considerable displacement is shown at the western margin of the Elk Hills oil field. The studies carried in this thesis agree with the fold bend fold presented here to the west and with the normal fault at Elk Hills, but disagrees with the faulted and reversed normal fault to the center of the section and the abrupt termination of the upper detachment in the Temblor formation.

## 6.1 Geologic Background

To evaluate the current understanding of the structural geology of the area, various structural cross-sections in the literature were gathered. These cross sections had to include good ties to the surface geology of the area and to be based on sufficient well-log data. Various structural styles were analyzed and compared with the surface geology, obtaining a good conformity of the interpretation to the mechanical stratigraphy observed in the study area.

### *6.1.1 Structural Cross Sections in the Literature*

A valuable starting point was obtained from Namson (2000). Namson's cross section 16-16', includes the Goyer oil field (Temblor range) to the west, the Midway-Sunset and Buena Vista oil fields to the center and a portion of the Elk Hills oil field to the east (figure 82). The deepest well in this cross section is the BECHTEL PET # 326-9G, reaching approximately -11,500 feet (TD), in the Antelope Shale member of the Monterey Formation. It is located to the northeast in the syncline that separates the Buena Vista and the Elk Hills oil fields. The major structures include a large fault-bend fold to the west displaying normal faults in the back-limb of the fold. The main fault is initiated in a lower detachment level in the Kreyenhagen (Tk) Shale and connects into an upper detachment in the mid section of the Temblor

Formation (Tt). Moving to the east, as the fault slip is transferred along the detachment, Namson presents an ancient normal fault that is cut by the detachment and reversed in response to the compressive stress. It is not clear where the displacement is transferred as the detachment is rapidly truncated and stops beneath the Buena Vista structure. Further west a major normal fault is shown separating two structural realms at the western limit of the Elk Hills oil field (figure 83). The studies conducted in this thesis agree with the fault-bend fold model presented that was responsible for the evolution of the Temblor Range to the west. The present interpretation also suggests that a considerable increase in thickness (growth sediments) is observed for the Monterey Formation to the west of Elk Hills suggesting an agreement with the normal fault interpreted at the eastern margin of the field. The structural interpretation in the present study differs with Namson's idea of the faulting and inversion of a normal fault to the center of the section, and the abrupt termination of the upper detachment in the Temblor Formation. Also, the fault slip carried by this detachment from the compressive stress of the fault-bend fold to the west is not clearly explained by the interpretation presented in cross section 16-16'. Based on the evidence provided in type well # 1 (see figure 54 fault @ 18420 ft), it is recognized in this thesis that this detachment extended further east and was an important factor in the evolution of the series of parallel fault-bounded structures present in the study

area. Type well # 1 was drilled to 19,904 (TVD of – 19,053 ft) feet, reaching total depth in the Kreyenhagen Shale.

A published location map shows cross section 5-5' (Namson 1998) going across the northern part of the Midway-Sunset field (figure 82). Unfortunately, it could not be used in the present study because it actually lacks structural interpretation to the northeast of the San Andreas fault, where the Midway-Sunset structure is located (figure 84).

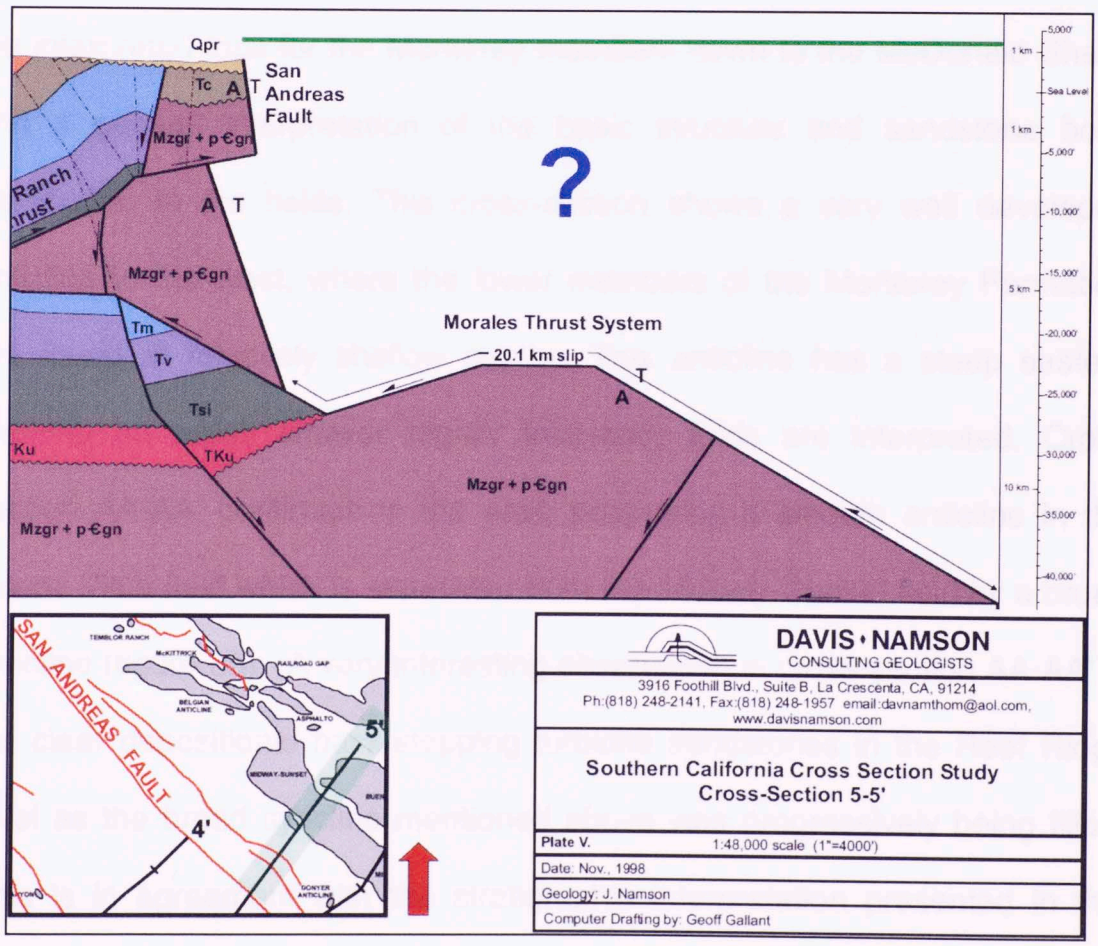


**Figure 84.** Easternmost portion of cross-section 5-5' (modified from Namson, 1998); the blue interrogation sing indicates missing structural interpretation (green line); location of the northern portion of the Midway-Sunset and Buena Vista fields (light green in insert map).

Other geologic information comes from structural cross sections in development geology studies, which are supported by detailed biostratigraphic correlations, and well log interpretations of closely spaced production wells, conducted by other interpreters in the area.

Cross section AA' (Callaway, 1968 in Strum, 1996) cuts across the mid section of the Midway-Sunset and Buena Vista fields (figure 82). It includes the interpreted tops for the Monterey members down to the McDonald Shale, and a general interpretation of the basic structure and sandstone body distribution in the fields. This cross-section shows a very well developed anticline to the west, where the lower members of the Monterey Formation are found at relatively shallow depths. This anticline has a steep eastern forelimb on which smaller higher frequency folds are interpreted. Cross section AA-AA' continues to the east, presenting a smooth anticline in the Buena Vista field which is separated from the Midway-Sunset field by a broad syncline (figure 85). A very interesting observation in cross-section AA-AA' is the clear depositional back-stepping turbidite sandstones in the Reef Ridge level as the broad syncline mentioned above was progressively being filled. This is in agreement with the stratigraphic interpretation presented in this thesis which suggests a continuous sediment deposition in a northeast to southeast direction during the upper-Miocene and into the Pliocene in

response to an active tectonic setting accountable for the evolution of the ancestral Temblor Range (series of fault-bend folds) to the west of the study area. From observations in cross section 16-16' (Namson 2000) and the interpretation conducted in this thesis we believe that a reverse, eastern-dipping fault is present near the steep-dipping forelimb, resulting from the uplift observed to the west. In this thesis, the smooth anticline in the Buena Vista field is interpreted to be associated with a deeper thrust fault originated in a lower detachment.

Cross section K-K' (Strum, 1996) represents the shallow part of the Republic Anticline area in great detail (figure 82). The interpretation by Strum (1996) is tied to 17 wells located in a section less than 1 mile across. This cross section was very useful to understand and validate the terminations of unconformities (e.g. Top Miocene, Etchegoin-San Joaquin) in the western part of cross section A-A'. Near the crest of the anticline, it shows the truncation of the upper-Miocene sandstone bodies of the Monterrey Formation (Spellacy) against the top-Miocene unconformity. (figure 86). The cross sections mentioned above and many others with comparable parameters were used in this thesis to constrain the extension of the interpretation to areas where well data was not available. All comments mentioned above will be explained in the description of the balanced structural cross sections.

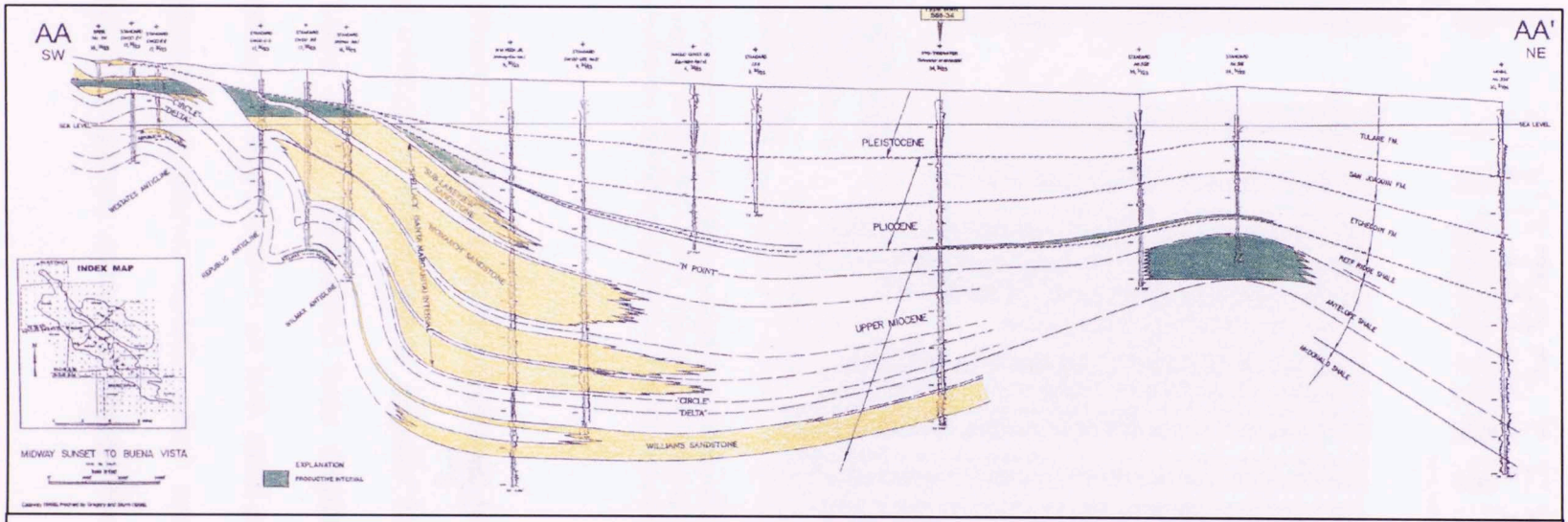


**Figure 85.** Structural cross-section AA-AA' Strum (1996). A well developed anticline displaying a steep eastern forelimb is presented. To the east it continues into the Buena Vista field forming a smooth anticline separated from the midway sunset field by a broad syncline.

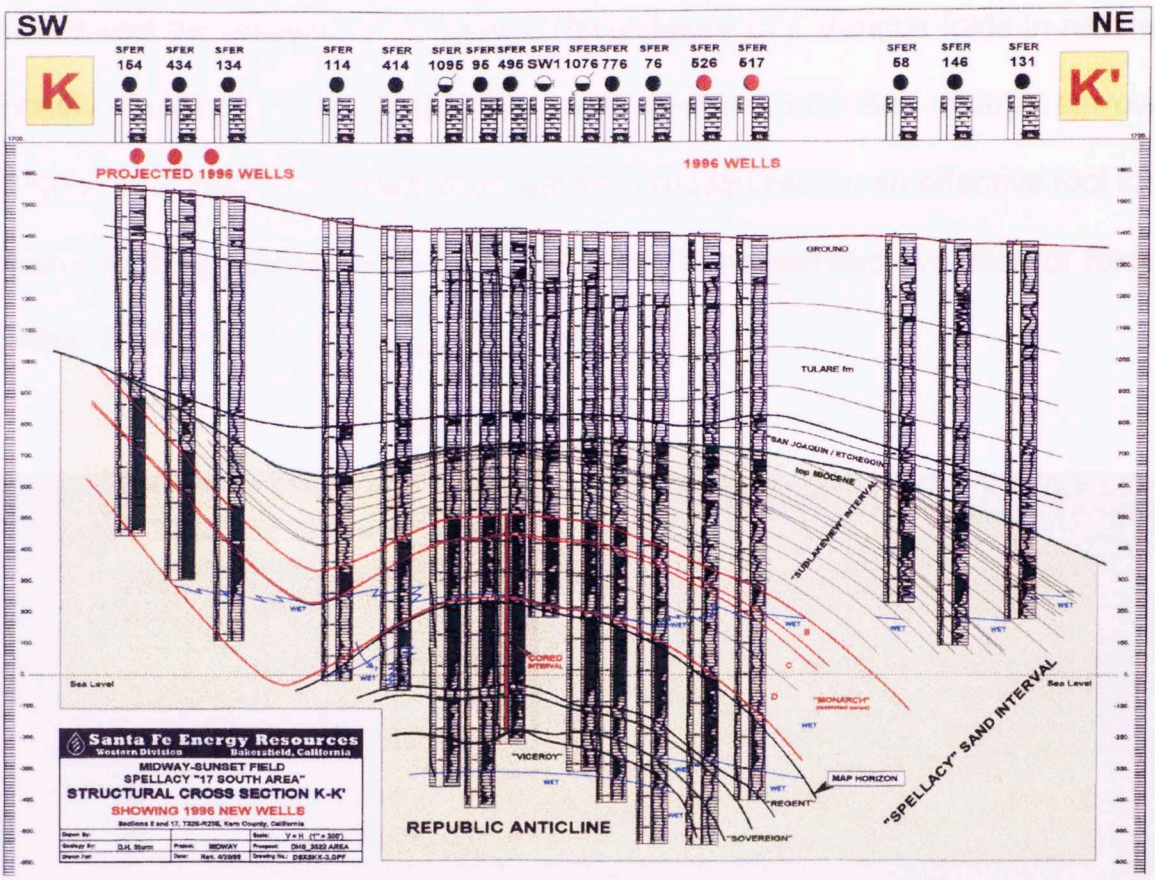


**Figure 86.** Cross section K-K' (Strum, 1996) located near Regional Cross-Section A-A' (Republic Anticline). The cross section is less than 1 mile across and is tied to 17 wells; notice the termination of the upper-Miocene sandstone (Spellacy) against the Top Miocene Unconformity.

For the structural interpretation presented here, the kink-band method was used. This method is applicable to angular folds with planar limbs and sharp hinges (Mitra, 2004). Kink band folds display sharp bends of layered strata across planar surfaces known as kink axial planes (Mitra, 2004); these axial planes separate two planar panels, which are drawn parallel to the dip data (Mitra,2004). Two panels are separated by their bisector angle, which in

turn marks the location of an axial surface (figure 87). Various folds in nature closely display parallel geometries, with planar limbs and sharp, narrow hinges; as a result, the kink band method is recognized as an effective tool for interpreting the geometry and understanding the kinematic evolution of folds (Mitra, 2004).

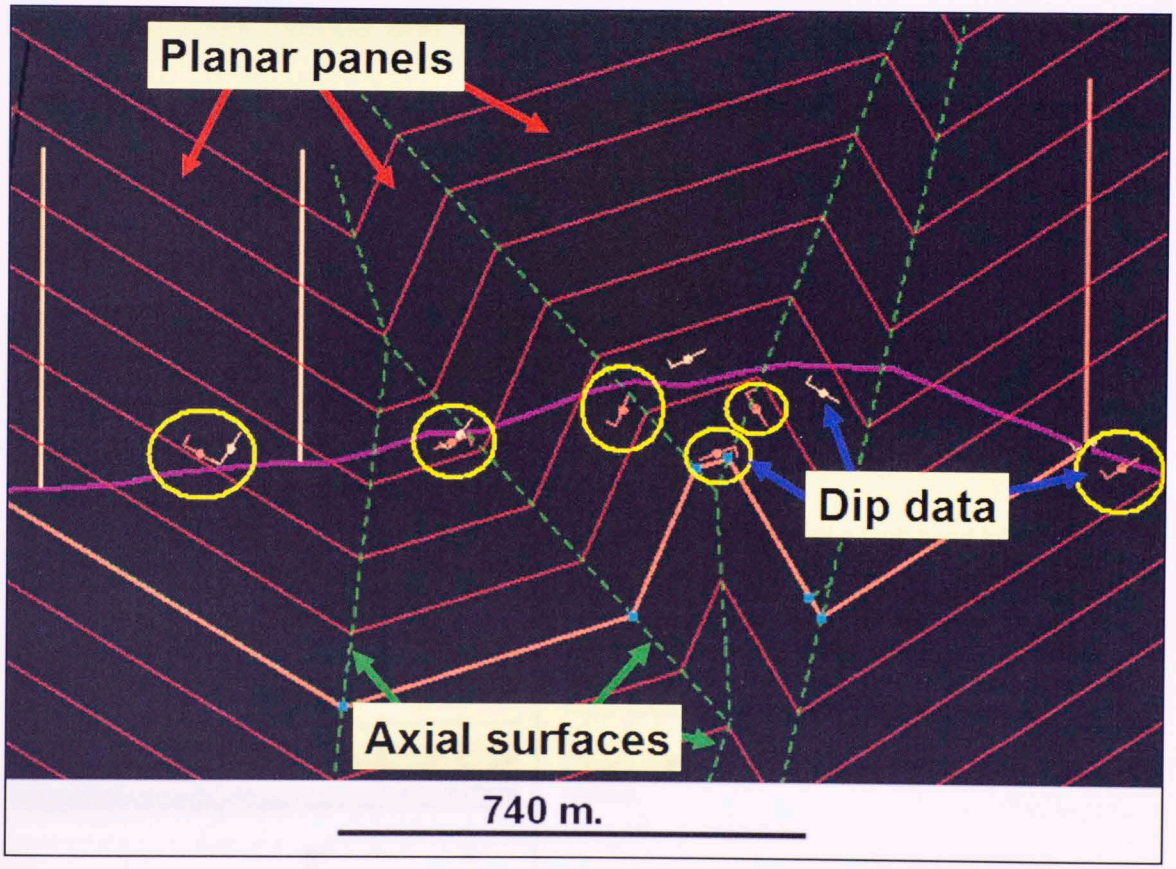


**Figure 87.** The kink band method, used to construct the balanced cross-sections. Dip data points were projected normal to the cross section to construct the planar panels parallel to the dip.

*6.1.2 Fault-bend Folds*

These folds are characterized by a stair-step trajectory where a thrust fault follows a bedding-parallel detachment within incompetent horizons, climbing through competent units along ramps (Suppe, 1983). A quantitative theory that describes the geometry of ramp-related fault-bend-folds was developed by Suppe in 1983 and applied to the interpretation of numerous map-scale folds (Suppe and Namson, 1979; and Suppe, 1983). The theory assumes uniform bed thickness and a parallel fold geometry, where the primary deformation mechanism is flexural slip along bedding planes (Suppe, 1983).

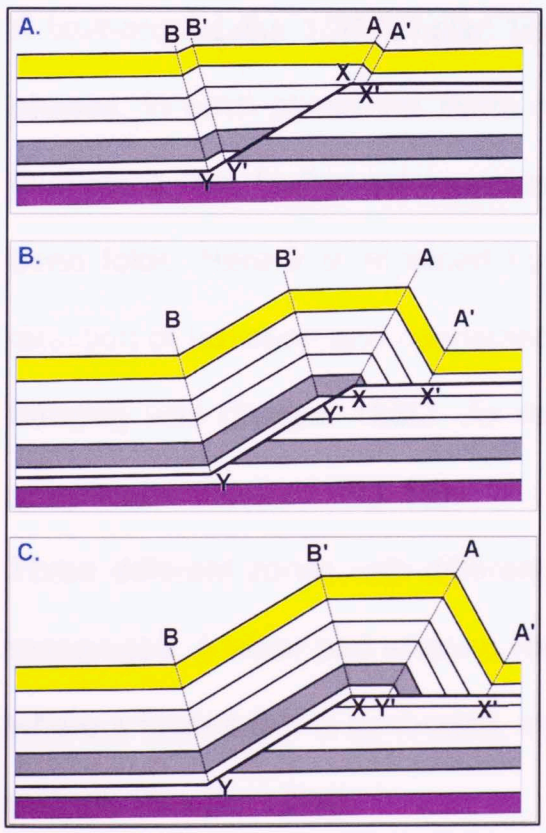


**Figure 88.**
Progressive evolution of a fault-bend fold.

A.) Hanging wall moves over ramp. B.) Structural relief and limb lengths of fold increase, the crest length decrease. C.) Hanging wall cutoff reached upper detachment. No further increase in structural relief occurs, fold crest length increases.

Figure extracted from Suppe (1983, 1985) in Namson (2004).

Figure 88 shows a fold that starts to develop (part A). As the hanging wall moves over the ramp, the structural relief and limb lengths of the fold (AA' and BB') progressively increase, while the crest (A-B') width decreases (part B). Once the entire hanging wall faulted segment is transferred from the lower to the upper detachment, no further increase in structural relief or limb length occurs (part C). This stage is evidenced by the progressive increase in crest width (Suppe, 1983).

*6.1.4 Fault-propagation Folds*

The fold shape is determined by the fault configuration (Suppe, 1985). A fault-propagation fold is better understood if analyzed through deformation phases. In each phase the strata on the hanging wall moves along a lower fault plane. The fault is not connected to a plane at the upper level as in fault-bend folds. Here it is replaced by an asymmetric syncline inverted to the direction of transport and connected to a complementary anticline fold on the hanging wall (Suppe, 1985). As the fault propagates, the folded strata are progressively faulted (Fig. 89).

Three different zones with different prevalence of structural mechanism are recognized. A lower part where a reverse thrust fault dominates, a middle part where a faulted fold is generated, and an upper part where continuous folding prevails (Suppe, 1985).

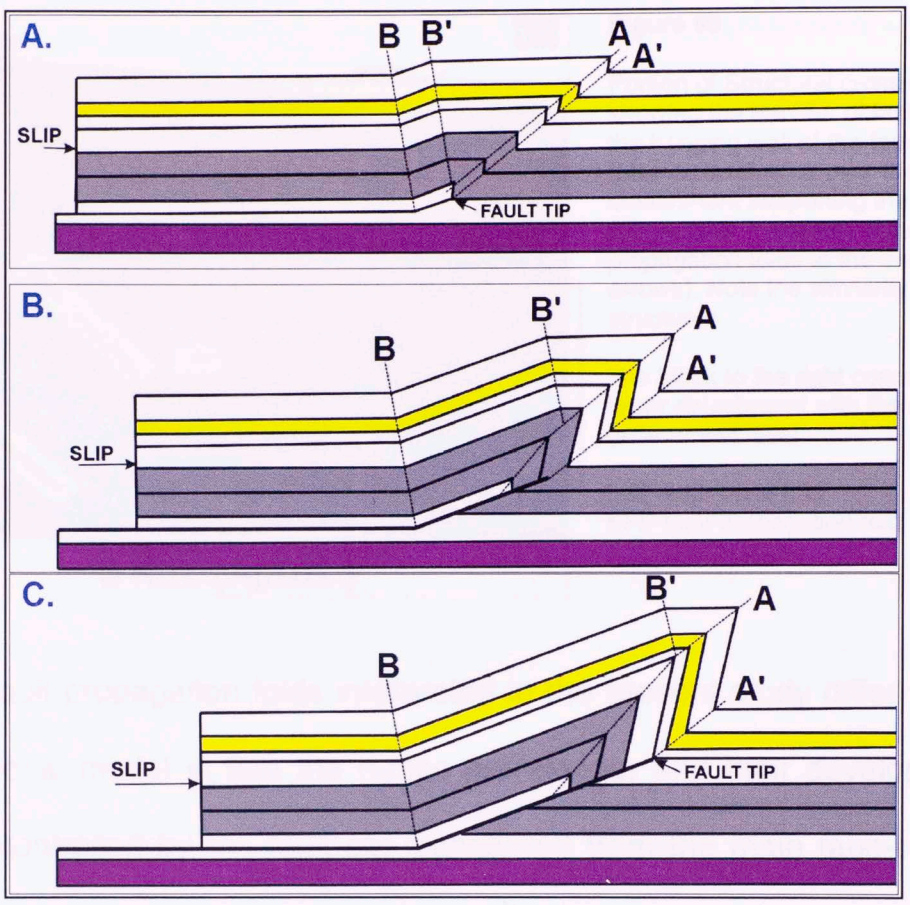


**Figure 89.** Progressive evolution of a fault-propagation fold. A.) As the fault propagates it migrates upward. B, C.) The fault tip is replaced by an inverted syncline wile on the hanging wall a complementary anticline is formed. The axial plane of this anticline is steeper than the principal fault. * Figure extracted from Suppe (1985) in Namson (2004).

Fault-bend folds are interpreted in this thesis to core the structures observed to the west of the study area in the Temblor Range. As the faulted portion of the main fault-bend structure reaches the upper detachment it continues to ride to the east were progressively younger fault-propagation folds are developed to accommodate fault slip (figure 90).

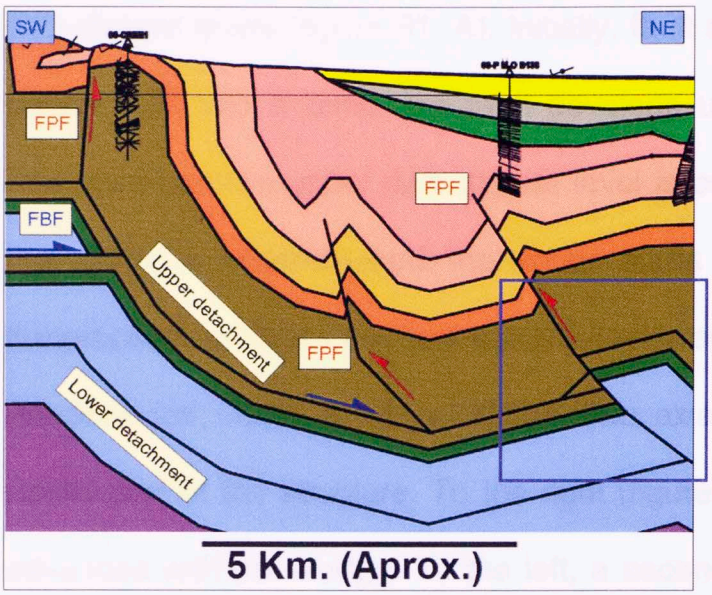


**Figure 90.**

Portion of Structural cross-section BB' showing the transfer of fault slip as the hanging wall of the fault-bend fold (blue arrows) rides over the upper detachment supporting the progressive formation of fault-propagation folds to the east (red arrows). Note the similarity to wedge structures.

The block to the right connects the lower detachment with the upper detachment level

FBF-fault-bend fold
FPF-fault-propagation fold

Fault-propagation folds interpreted in the present study differ from the conventional model in that the ramps are steeper and their development is directly controlled by the fault slip transferred from the main fault-bend fold that developed to the west.

### *6.1.5 Wedge Structures*

Continuous deformation along a detachment that is connected to a ramp produces fault displacement and transfer of slip in the direction of transport. If the slip transfer is restrained and the ramp thrust connects to an existent upper-detachment, a wedge structure can develop. The ideal stratigraphic setting for these type of structures is that of interlayered competent and ductile units; thick Shales favor the development of multiple

detachment levels (figure 91, A). Initially, fault slip is transferred from a lower detachment into a ramp, the fault develops until its ability to propagate is restrained and an upper detachment level is connected (figure 91, B). Once this setting is accomplished, the wedge starts to advance (figure 91, C). As the process continues the fault slip is transferred to an opposite verging thrust (Medewedeff, 1988, in Mitra, 2004). Two axial surfaces are present in the frontal part of the structure. To the right (figure 91 C) an active axial surface advances with the wedge. To the left, a second one that is active within the advancing wedge and inactive in the hanging wall of the opposite verging thrust, is found.

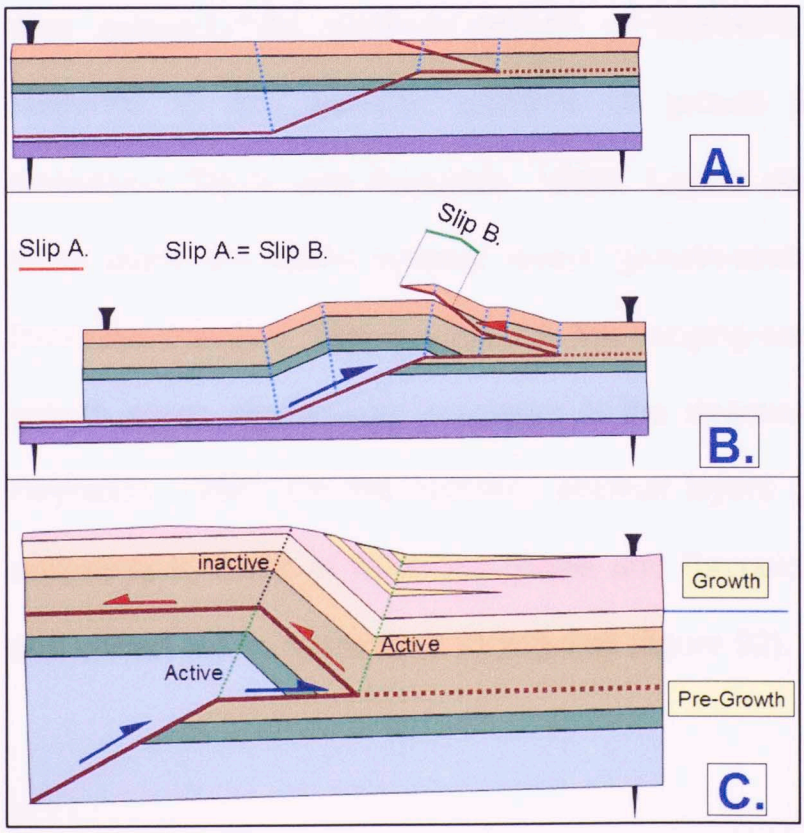


**Figure 91.**
Fundamental geometry of a wedge structure.

A.) Stratigraphic units (colors are for easier comparison to stratigraphic units in this thesis).

B.) Wedge advancement into an upper detachment level. Transfer of fault slip from the lower detachment to the ramp and into an opposite verging trust

C.) Detail of the frontal part of a wedge structure. Note the active and inactive axial surfaces, and the growth strata in response to the wedge advancement into the upper detachment.

* Figure modified from Medwedeff (1988) in Mitra (2004).

Some structures in the study area display a similar mechanism as that of wedge structures. In figure 90, the fault slip from the lower detachment (blue arrows) is transferred to opposite verging thrusts (red arrows). Further east a hanging-wall block is interpreted to connect the lower detachment level in the Kreyenhagen with the upper detachment level in the Temblor Formation enabling fault-slip transfer (figure 90).

*6.1.6 Normal Growth Faults*

In this structural style, sedimentation occurs continuously during the course of faulting. Low topographic areas create more accommodation space, thus receiving the greatest amount of sediment during deformation. In response to this process, patterns of growth fault sedimentation are developed (Davis and Reynolds, 1996). Layers deposited as this process takes place are called synfault layers (growth-strata) and display dramatic thickness changes. This is evident in the hanging-wall where the thickness of growth strata significantly increases in the direction of faulting (Davis and Reynolds, 1996). On the contrary, prefault layers (pre-growth strata) show uniformity in terms of thickness (Davis and Reynolds, 1996) in the foot-wall and across the fault into the hanging-wall (figure 92).

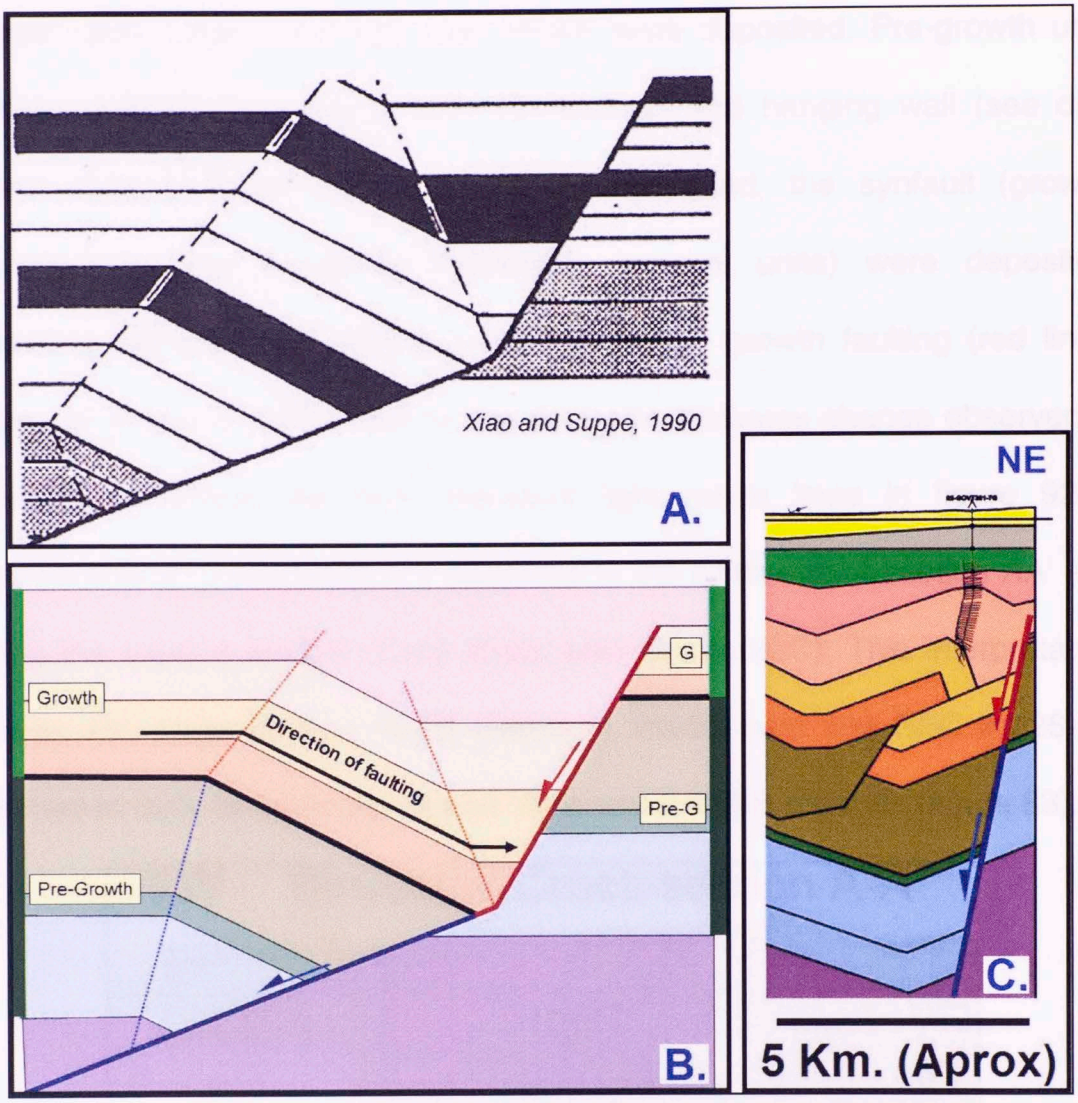


**Figure 92.** A.) Geometry of growth units and growth axial surfaces in listric growth faults (Xiao and Suppe, 1990). B.) Part A modified to better match the interpretation in this thesis. Red lines indicate growth realm, blue lines indicate pre-growth realm. Light green and dark green lines are for thickness comparison on both sides of the fault (Modified from Xiao and Suppe, 1990).
C.) Comparable characteristics of growth fault in structural cross-section AA'.

Figure 92A, extracted from Xiao and Suppe (1990) presents growth faulting as sedimentation and fault slip increase (figure 92A). Figure 92B was modified for better comparison to the structural interpretation in this thesis. The blue lines represent the normal faulting mechanism that started after pre-

growth units (green and light blue strata) were deposited. Pre-growth units display uniform thickness in both the footwall and hanging wall (see dark green lines in figure 92B). As faulting continued, the synfault (growth) members of the Monterrey Formation (orange units) were deposited, switching the structural setting to that of normal growth faulting (red lines, figure 92 B and C) evidenced by the dramatic thickness change observed in these units across the fault (compare light green lines in figure 92B). Comparable characteristics are observed to the northeast of section AA' and along the eastern margin of the study area (figure 92C). This interpretation agrees with cross section 16-16' (Namson, 2000), near well BEC # 326-9G (marked in red), between the Buena Vista and Elk Hills oil fields (figure 83).

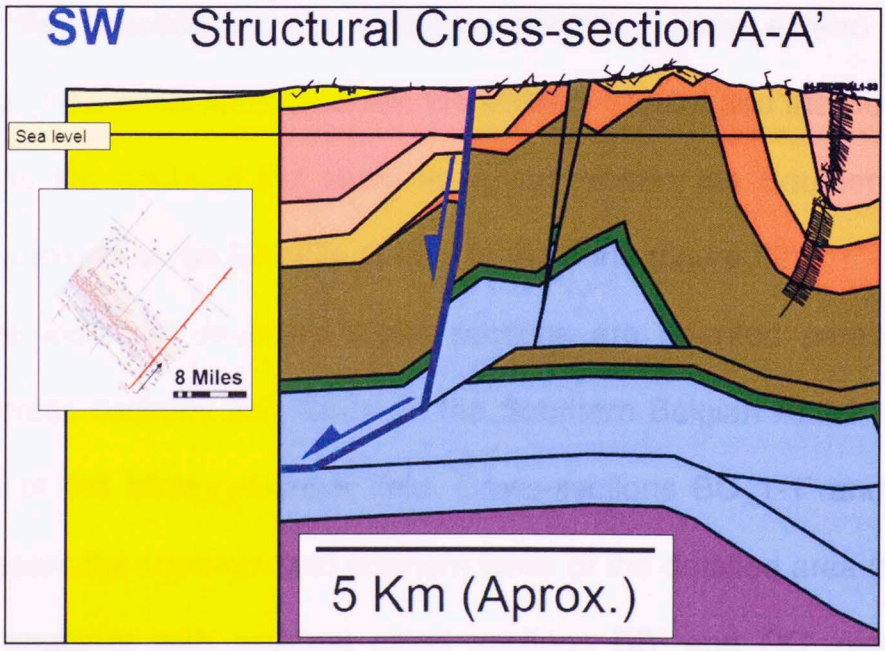


**Figure 93.** Southwest portion of section AA'. Blue lines (pre-growth faulting). Normal listric faulting occurred during a period of extension, after the Monterey formation was deposited.

Episodes of normal faulting also occurred during the later stages of the structural evolution posterior to the deposition of the Monterey Formation. This is evidenced in the western part of the study area where the cross sections show normal listric faults affecting the hanging wall of the major fault-bend fold coring the structural trend of the Midway-Sunset oil field (figure 93).

## 6.2 Balanced Structural Cross-Sections

The regional cross sections are uniformly distributed along the northern part of the Midway-Sunset oil field, and were oriented to the average regional dip direction of the structure (N40°E). They extend for 29.4 kilometers (18.3 miles aprox.) across the Midway-Sunset and the Buena-Vista oil fields to the south of the study area, and across the Southern Belgian Anticline and part of the Elk Hills oil field to the north (figure 82).

The localized structural cross sections are oriented parallel to the regional cross sections and focus on the Southern Belgian Anticline area to the north of the Midway-Sunset field. Cross-sections BC_1-1' and BC_5-5' that represent the southern and northern limits of the detailed area (figure 82) share a segment with regional cross sections BB' and CC' respectively, providing a good tie to the large-scale geology of the area (figure 94).

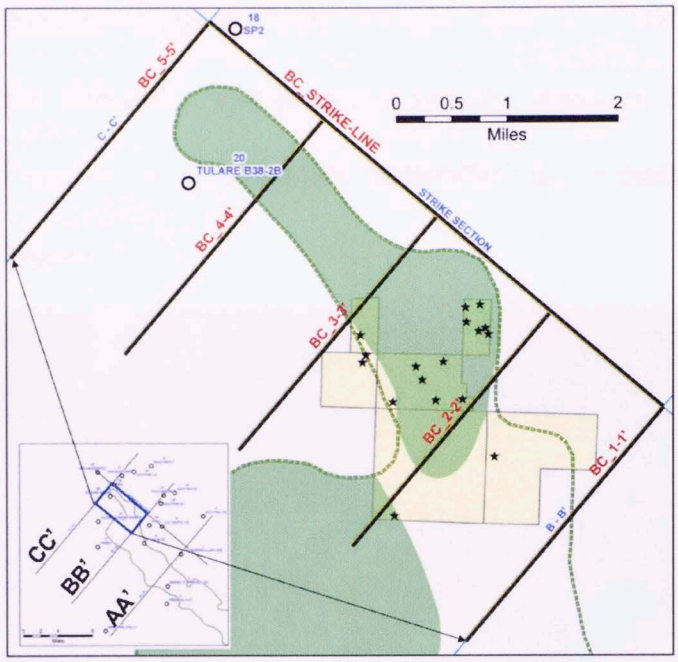


**Figure 94.** Display of the relationship between the regional (insert) and detailed area of study; the tie between localized cross-sections BC_1-1' and BC_5-5' to regional cross sections BB' and CC' respectively provides a good tie to the regional geology.

### *6.2.1 Structural Cross-section A-A'*

*This cross-section is located roughly four miles* northwest of cross-section 16-16', near the southeastern limit of the regional area of study (figure 82). From southwest to northeast, a small portion of the upper Temblor Formation is visible between two outcropping faults. Near these faults, to the southwest, a normal fault outcrops putting the Santa Margarita Formation in contact with the Monterey shale. Structural dip data for the western half of the cross-section are of good quality, exposures of the Monterey Formation down to the Devilwater/Gould member are present. The Upper Monterey is in contact with the Belridge diatomite to the northeast; past the Santa Margarita

outcrop (Tsg) a sharp contact with the Tulare formation is present covering the Pliocene formations from this point to the eastern limit of the section. Patches of Quaternary sediment are present above the Tulare Formation (figure 95).

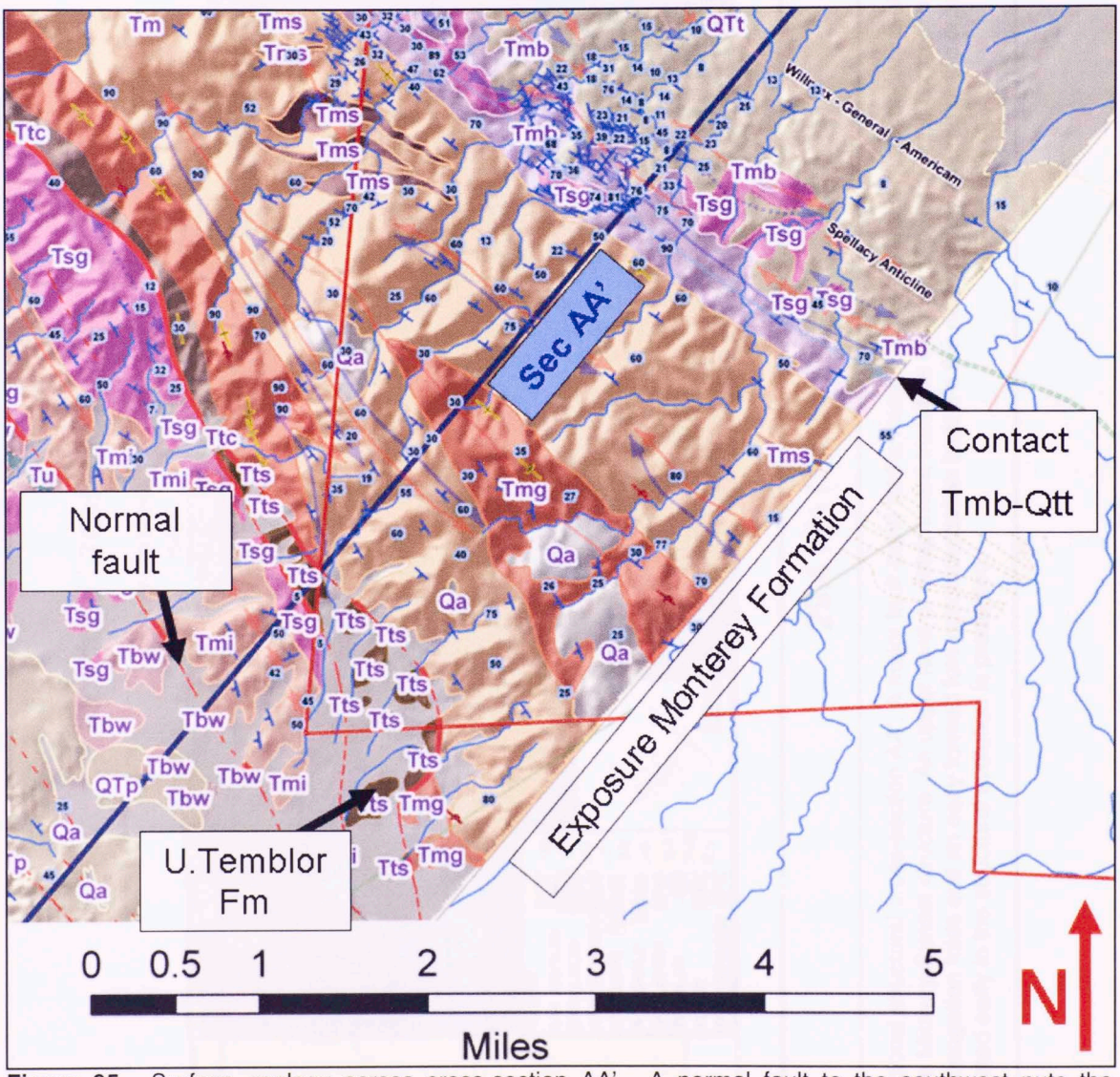


**Figure 95.** Surface geology across cross-section AA'. A normal fault to the southwest puts the Bitterwater shale (younger) in contact with the Monterrey shale (older). There is good exposure of the Monterrey formation and good dip-data for structural control. Past the contact with the Belridge diatomite to the northeast the area is covered by the Tulare Formation.

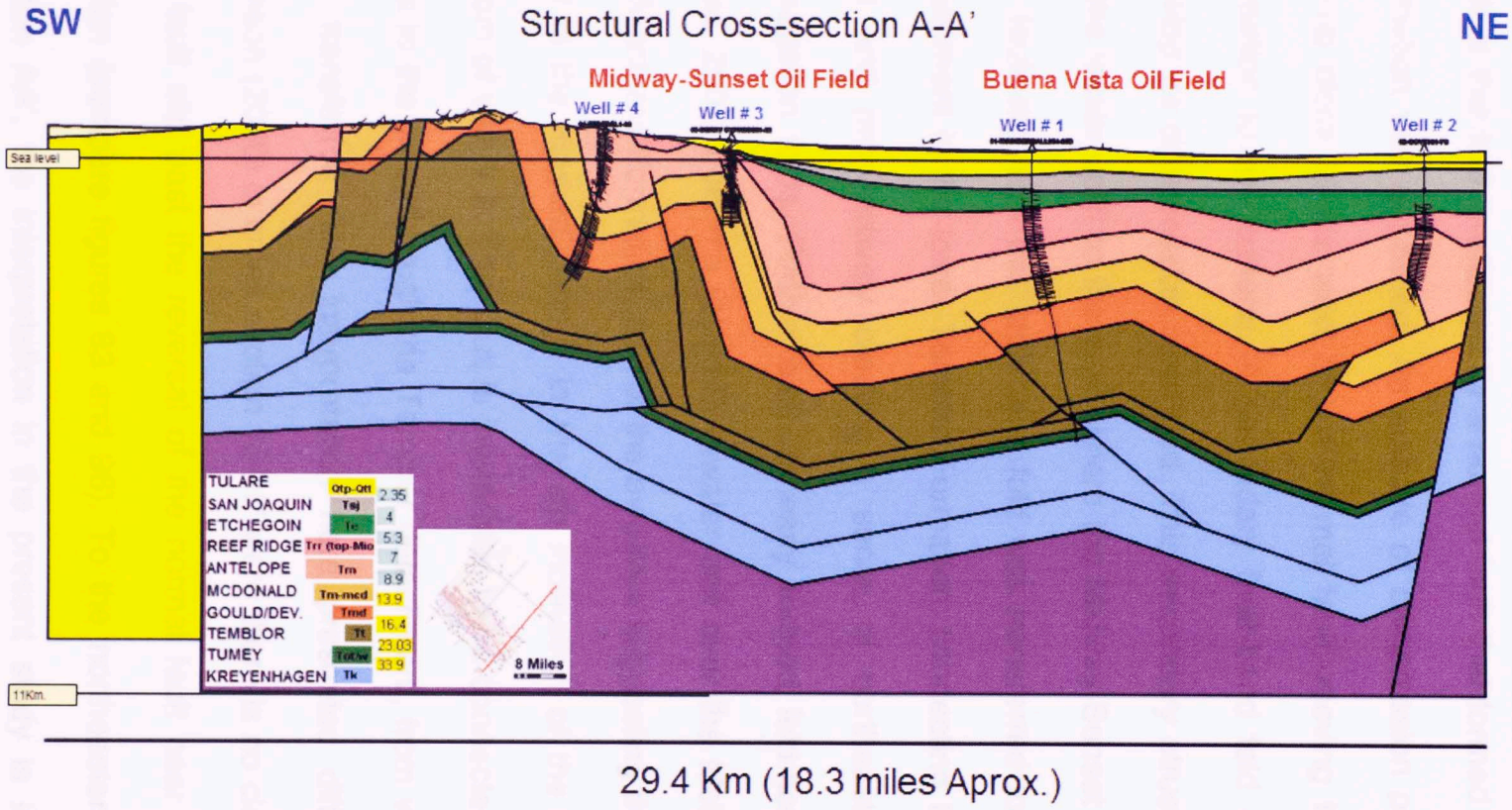


**Figure 96.** Regional structural cross-section AA'. A major fault-bend fold is interpreted to the west. A secondary fault-bend fold is interpreted in relation to the Midway-Sunset structure. An upper level of detachment transfers the fault slip to the east connecting a series of northeastern dipping fault propagation folds and an early formed fold-accommodation fault. To the northeastern margin of the cross section a normal fault that was originated early in the structural evolution is presented.

In the subsurface, a major fault-bend fold is interpreted; the western flank of this fold is affected by a normal fault that formed after the Monterey Formation was deposited. An episode of compression produced the minor pop-up block to the west of the normal fault, moving the upper Temblor Formation to the surface. A secondary fault-bend fold was interpreted to develop as compression continued. This secondary structure is responsible for the lesser uplift to the east, where the Midway-Sunset oil field is located. The fault slip from this fault-bend fold was transferred to an upper level of detachment in the lower Temblor Formation, connecting the fault slip to the east and progressively creating a series of northeastern dipping fault-propagation folds. Further east an early formed fold-accommodation fault (Mitra, 2002) puts the Gould\Devilwater unit over the McDonald member of the Monterey Formation; part of the evidence suggesting the existence of this fault is the marked change in the dip inclination of the tadpoles near the bottom of well # 2. This fault is interpreted to be connected to the fault-bend folds to the west through the Temblor detachment, from where the fault slip was transferred. The interpretation here presented differs from that by Namson (2000) in cross section 16-16' were there is no clear explanation for the fault slip past the reversal of the normal fault near the center of the section (compare figures 83 and 96). To the northeastern margin of cross section AA', the interpretation in the present study is in agreement with

Namson (2000) where a normal fault that was originated early in the structural evolution is present. This fault is interpreted to have started some time after the Temblor Formation was deposited and to continue its activity as a growth normal fault (figure 93) at least until the end of the deposition of the McDonald member of the Monterrey Formation (figure 96). The Antelope member is interpreted to be in unconformable contact with the Reef Ridge unit, based on the variability of its lateral thickness across the structural cross section (thickness revised with the dipmeter and the directional survey), and observation of dipmeter tadpoles near this contact in well #3 (Figures 96 and 97).

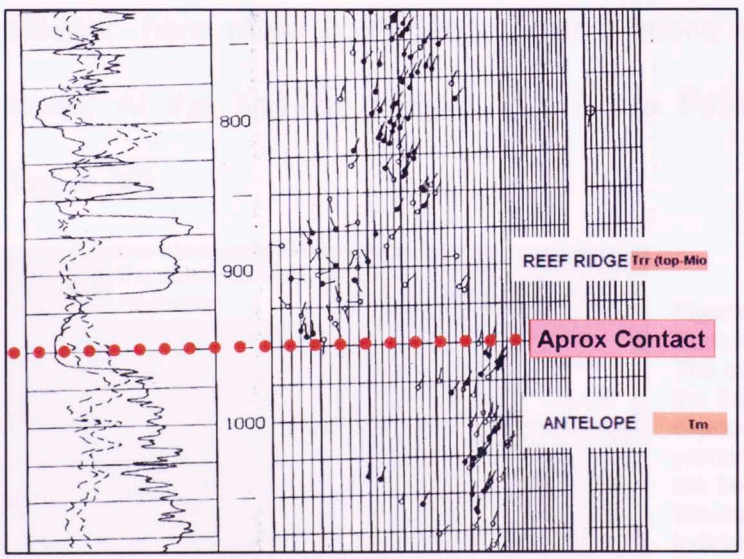


**Figure 97.** Interpreted unconformity at the contact between the Antelope member and the Reef Ridge shale.

The tops for the Reef Ridge shale, the Etchegoin Formation, and the San Joaquin Formation are interpreted to be unconformable. This concurs with the

literature where these units are presented pinching out to the west in the study area (figures 83, 85, and 96).

### *6.2.2 Structural Cross-section B-B'*

The normal fault that puts the Temblor Formation in contact with the Santa Margarita Formation is better exposed here. To the east of this fault, steep dips and overturned layers within the upper-Temblor Formation are exposed, suggesting the presence of an overturned syncline involving the Temblor and the lower members of the Monterrey Formation. Continuing east, the contact between the Antelope member and the Belridge Diatomite is present, here more homogeneous and gentle dips (32° average dip) are found. At the Tsg-Qtt contact, the Tulare Formation covers earlier rocks (figure 98).

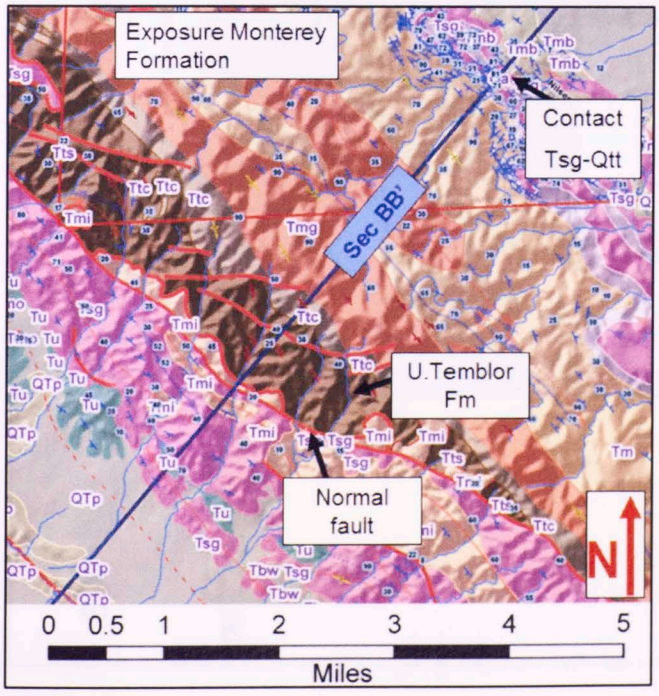


**Figure 98.**
Surface geology across cross-section BB'. The normal fault between the Temblor and the Santa Margarita formations is well exposed. To the east dip data suggests the presence of an overturned fold involving the Temblor and the Monterrey formations. Structural data in the Belridge Diatomite indicates homogeneous and gentler dipping folds.

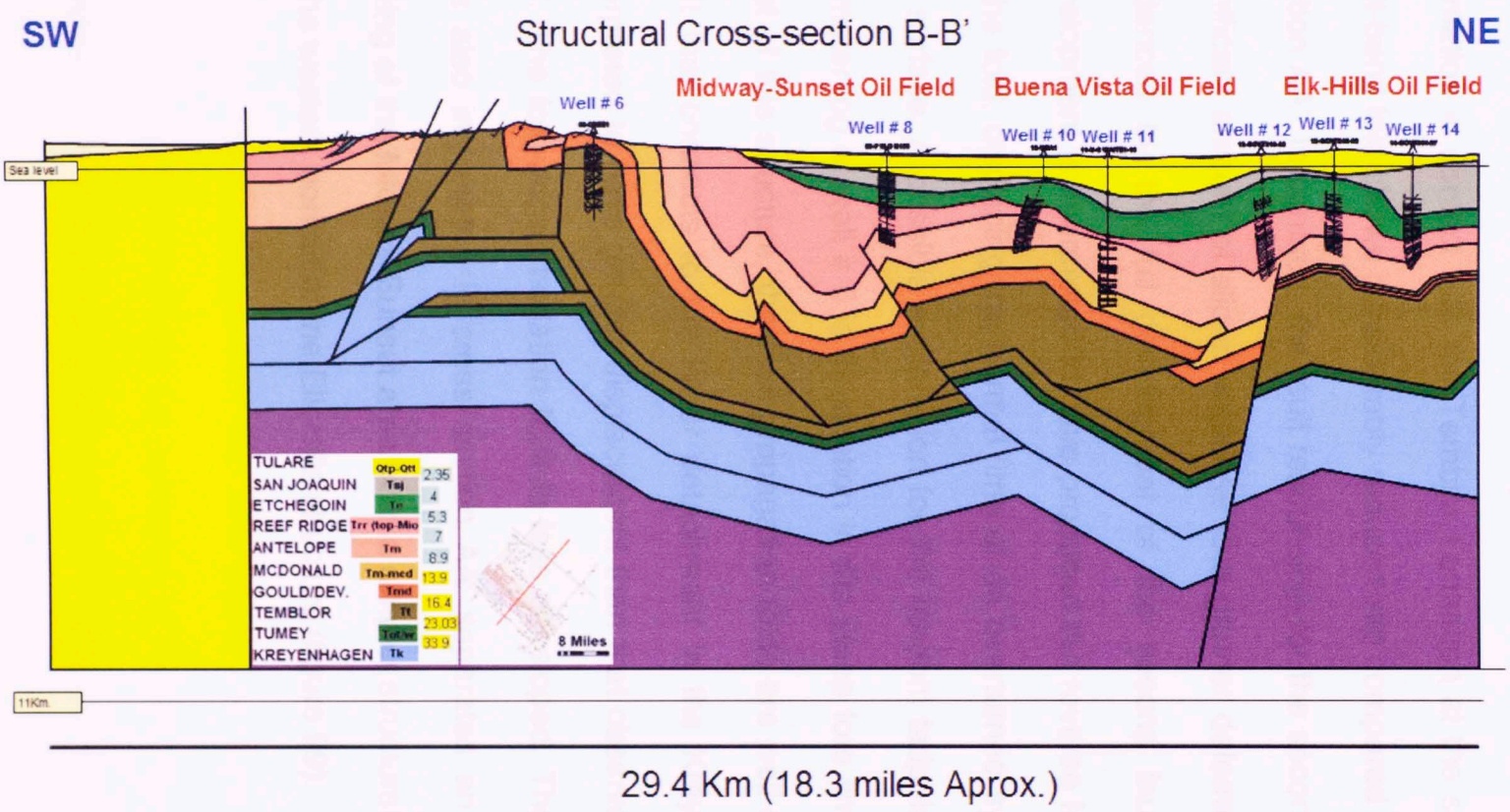


**Figure 99.** Regional structural cross-section BB'. Two normal faults affect the western limb of the fault-bend folds. The secondary fault-bend fold is considerably more developed producing the reverse fault at the forelimb of the structure and the well developed fault propagation folds to the east. A less developed fold-accomodation fault in this section can be attributed to the considerable amount of slip consumed by the reverse fault that is connected to the lower detachment. The large scale normal fault separates an intense structural setting in Midway-Sunset from a moderate setting in the Elk Hills area.

Two normal faults are present in the western limb of the fault-bend folds. The fault to the left displays greater slip, putting the Santa Margarita Formation in contact with the Temblor Formation at the surface. The earlier fault-bend fold shows considerably reduced slip compared to that observed in section AA'. In contrast, the fault responsible for the secondary fold carried a significant amount of slip in response to a greater deformation event that is evidenced by the full development of the second fault-bend fold. This development is interpreted to have produced the reverse fault at the forelimb of the fold, displacing the normal limb of an overturned syncline exposed at the surface. A possible explanation for the random tadpoles observed in the dipmeter-log of well # 6 is its location in the steep fore limb of the structure. East of this structure, the fault-propagation folds are well developed and the fault that connects to the lower detachment in the Kreyenhagen Shale is interpreted to have greater displacement than that observed in cross-section AA'. The fold-accommodation fault is less developed. The normal fault that was also interpreted in cross section AA' separates an intense structural setting of the Midway-Sunset area from a simpler structural geology observed in the western portion of the Elk Hills structure (figure 99).

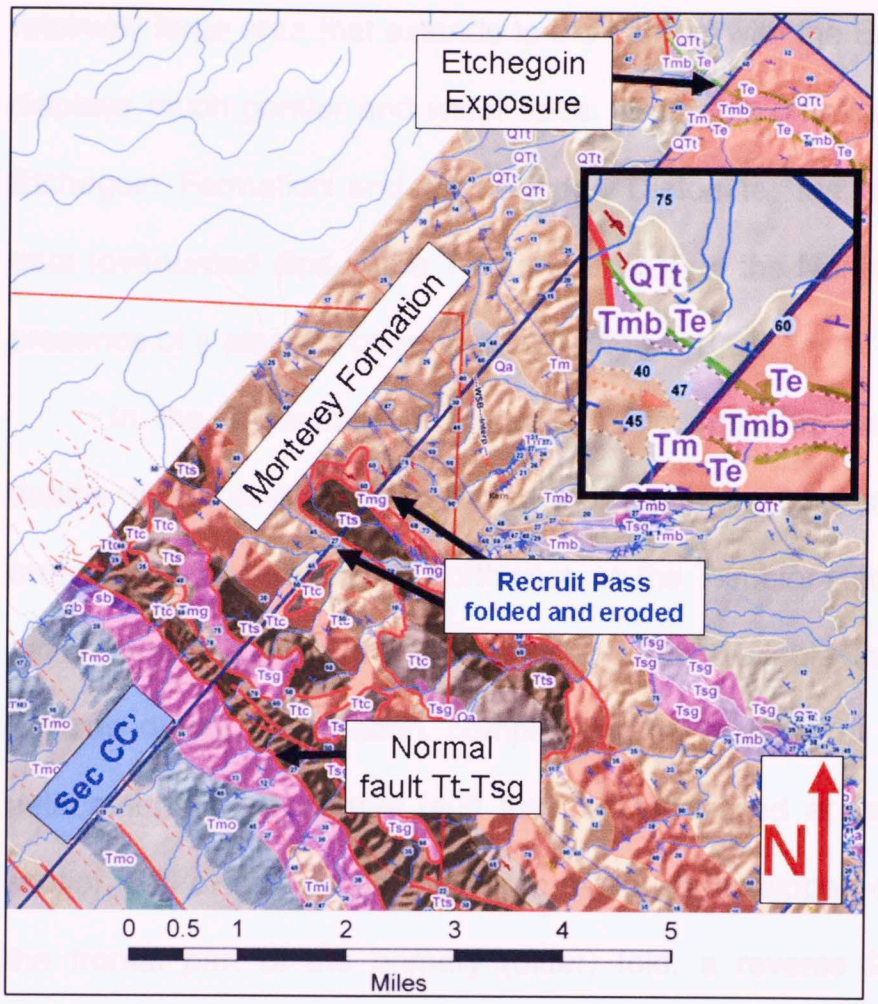


**Figure 100.**

Surface geology of cross-section CC'. The normal fault between the Temblor (Tt) and the Santa margarita (Tsg) formations can be traced to here. The folded and eroded fault plain of the recruit pas fault is present. This area has the best exposure of the Cenozoic formations. To the east the outcrop of the Etchegoin formation and structural dip data indicate the presence of a steep to overturned fold in the subsurface (see insert).

*6.2.3 Structural Cross-section C-C'*

The exposure of pre-Pliocene formations becomes more extensive to the north of the study area. The west dipping normal fault between the Temblor and Santa Margarita Formations continues to be present here. A fault pane (Recruit Pass fault) that was folded and eroded is present. Near this area, dip data indicate the existence of closely spaced anticlines and synclines, presenting steep to moderately dipping flanks. To the east, a

relatively large area that extends to the contact with the Etchegoin Formation, displays much gentler and wider folds. Past this point at the outcrop of the Etchegoin Formation and the Belridge Diatomite, the strongly inclined dip data (overturned dips in the Tulare formation to the Northwest), indicates the presence of a steep to overturned fold (figure 100).

In the subsurface, low stratigraphic units are present at shallower depths than previously observed; indicating that the structural uplift was progressively greater to the northwest, as the Temblor Range was rising. This could be associated with the reduced area available for the structures to develop during deformation, complicating the transfer of fault slip along the detachments. The normal fault that can be traced at the surface to cross section BB' displaces the back-limb of a well developed duplex structure. In the frontal part of the primary (older) fold, a reverse fault displacing the Temblor Formation and part of the Gould/Devilwater member is present. East of this fault, two fault-propagation folds connected to the upper detachment level were formed. At this location, a block detached from the Kreyenhagen Shale overrides an eastern-dipping ramp, creating a wedge-like structure. At the same time, the upper portion of the section was uplifted and a thrust fault was created in response to the relative compression that was formed against the fault-bend folds to the west. Part of the fault slip in this fault was transferred to a secondary frontal thrust that displaces the Reef Ridge unit

and the Etchegoin Formation; these units created a small scale overturned fold to the east. The large scale normal fault, interpreted to have a southeast to northwest strike direction according to its position within the regional cross sections, represents a major boundary that restricted the complex structural setting to the southwest part of the study area, where the Midway-Sunset oil field is located. This allowed for a much gentler structural geology in the vicinity of the Elk Hills oil field. It is important to point out that in order to confirm this last statement it is necessary to perform a detailed structural analysis of the Elk Hills area, which is outside of the scope of this thesis (figure 101).

*6.2.4 Localized Structural Cross-Sections*

Cross sections BC_1-1' and BC_5-5' are located along regional cross-sections BB' and CC'. In Section BC_1-1 a thrust fault that is connected to a lower detachment level in the Kreyenhagen Shale progressively loses fault slip into the Temblor and Monterrey Formations. To the east, a portion of a fold-accommodation fault initiated in an upper detachment is presented. The Belgian anticline, an open-parallel fold, overlies these features. Stratigraphically higher, the unconformable contacts of the Antelope and later formations display moderate erosion (figure 102A).

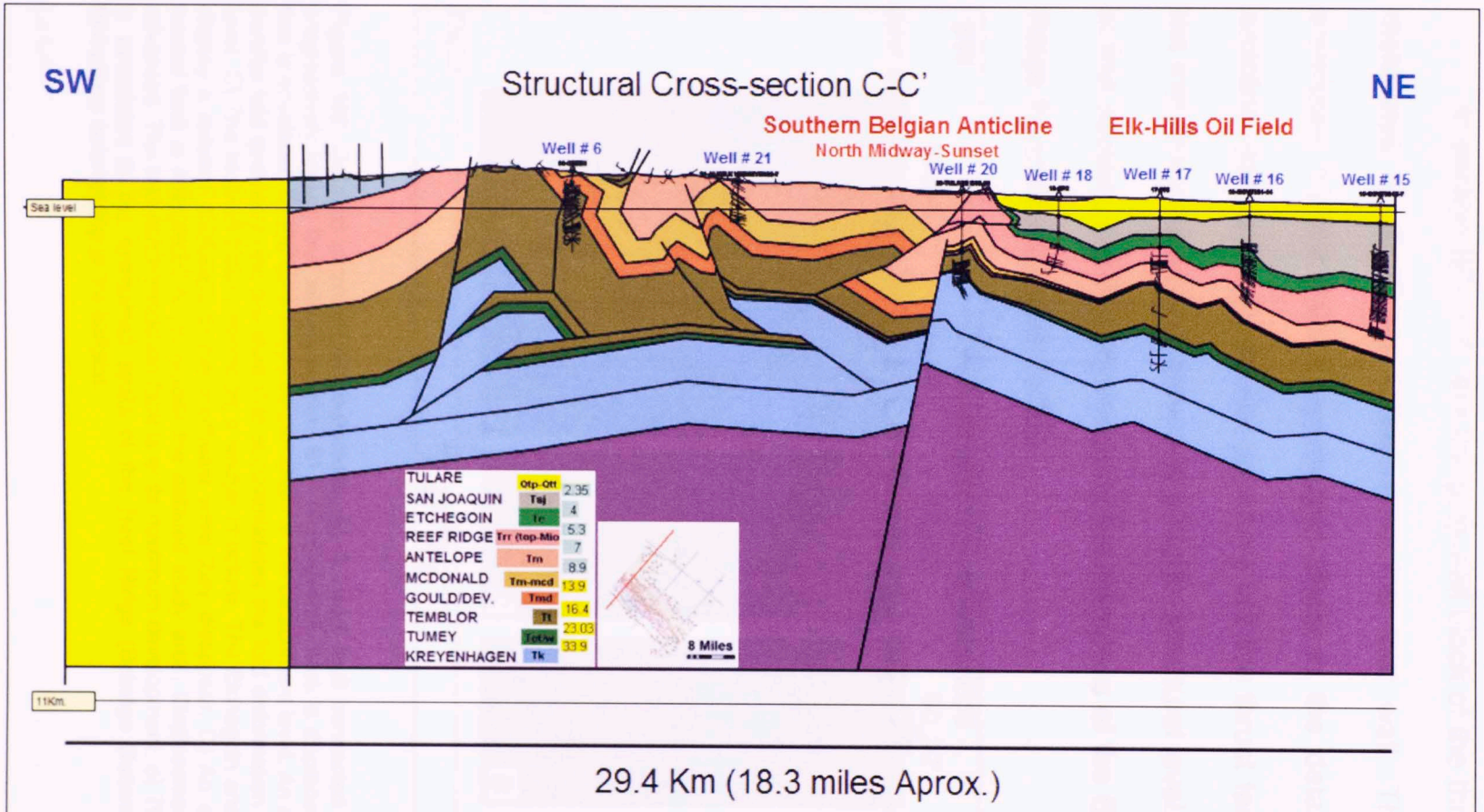


**Figure 101.** Regional structural cross-section CC'. Structural uplift was more intense to the northwest allowing for deep stratigraphic units to be present at shallower depths. To the west a normal fault displaces the back-limb of a duplex structure. In the vicinity of the two fault propagation folds to the east, a block detached from the Kreyenhagen shale overrides an eastern-dipping ramp, creating a wedge-like structure. As it developed a thrust fault was created in response to the relative compression that was formed against the duplex to the west. The large scale normal fault near the middle of the section represents a major boundary that restricted the complex structural setting to southwest part of the study area.

In section BC_2-2', the hanging-wall block of the thrust fault previously mentioned is displaced further over the foot wall. The lower block is enveloped by the thick Kreyenhagen Shale at the detachment level. The anticline retains a very similar geometry but the thrust fault accommodating the fold deformation is observed at a higher structural level. Erosion is greater in this section, significantly reducing the thickness of the Etchegoin and Reef Ridge Formations (figure 102B).

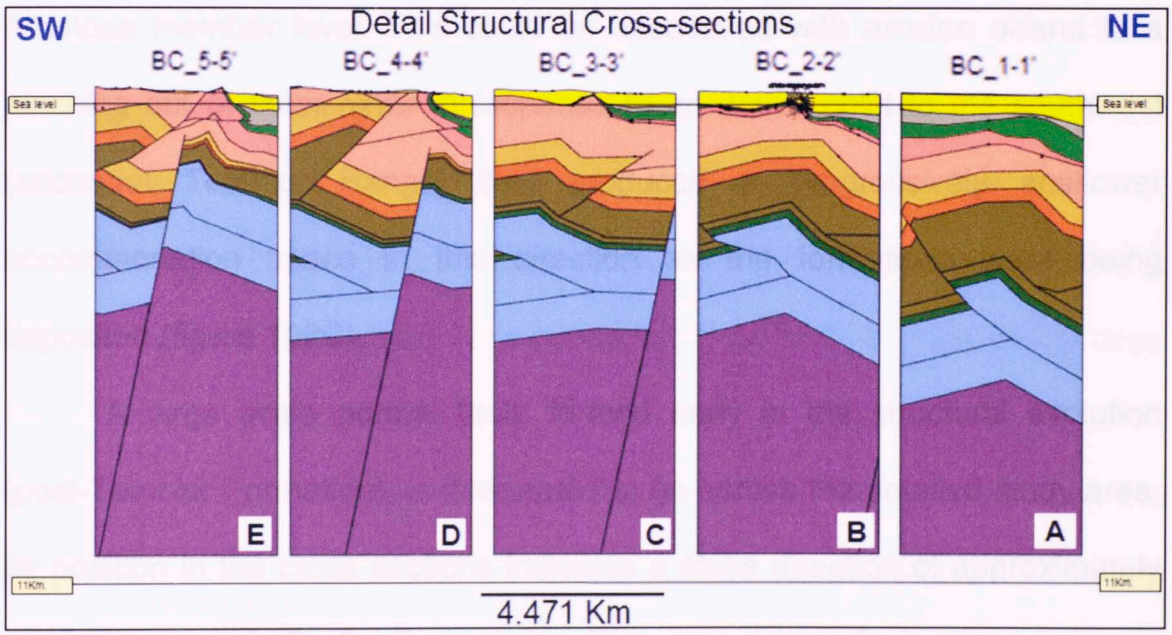


**Figure 102.** Detailed structural cross-sections. A) A thrust fault connected to a lower detachment progressively looses fault slip up section. B) A hanging-wall block is displaced further over a footwall that is enveloped by the thick Kreyenhagen shale at the detachment level. An anticline shows an open-parallel fold geometry and the trust that accommodates the fold deformation is observed at a higher level. C) The footwall block resembles a wedge structure. The Etchegoin and Reef Ridge formations display a reduced thickness to the southeast were they disappear. D) An early formed large scale normal fault is interpreted to go across the detailed study area. Displacement on the ramp is more advanced. The fold accommodation fault is at its maximum development. e) The principal reverse fault is associated to the overturned strata of the Reef Ridge (Belridge Diatomite) and the Etchegoin formations outcropping at the surface.

The hanging wall block previously mentioned is fully developed in cross-section BC_3-3'. Here it goes over the ramp onto a footwall block that now resembles a wedge structure. The fold-accommodation fault located higher in the structure presents a steeper angle (37°) compared to that observed in previous sections (5°), and also presents an increase in displacement. The Etchegoin and Reef Ridge Formations show a reduction in thickness to the southwest were they disappear near a small bulge at the Antelope member level. This could be associated with erosion or/and to a pinching out of these units in response to an active uplift to the southwest (ancestral Temblor Range) that produced a progressively shallower accommodation space in this direction as the formations were being deposited (figure 102C).

A large scale normal fault, formed early in the structural evolution (post-Temblor Formation), is interpreted to go across the detailed study area. Its position in the cross sections indicates a strike direction of approximately 100° (figure 102 B, C, D, and E). This preexistent fault plane extends progressively further west from cross section BC_1-1' to BC_5-5', reducing the space available for structures to develop.

In cross section BC_4-4', the displacement observed on the ramp at the Kreyenhagen level is more advanced, with the first bend of the detachment located very close to the large scale normal fault (figure 102D).

The fold-accommodation fault located now at the crest of the lower hanging wall block, presents the steepest dip angle (45°) observed, reaching the point of maximum development in this section. The hanging wall of the fold accommodation fault that involves the upper–Temblor Formation and the members of the Monterey Formation show the most significant displacement in this cross section (figure 102D). This fault is interpreted to distribute the slip into two faults creating an upper fault-block. As the principal fault (higher level) was developed, the Belridge Diatomite and the Etchegoin Formations that are outcropping in the surface were overturned (figure 100, 102D, and 103). The lower fault is presented in cross sections BC_4-4' and 5-5' displacing the Etchegoin and Reef Ridge units. In cross section 5-5' the secondary fault displaces the crest of a small anticline to the east of the large scale normal fault (figure 102E).

In the small anticline previously mentioned, the thickness of the Gould/Devilwater, the McDonald, and the Antelope members of the Monterrey Formation is considerably reduced compared to the western side of the fault; this indicates that the fault was a normal growth fault in the later stages of evolution (figure 102E).

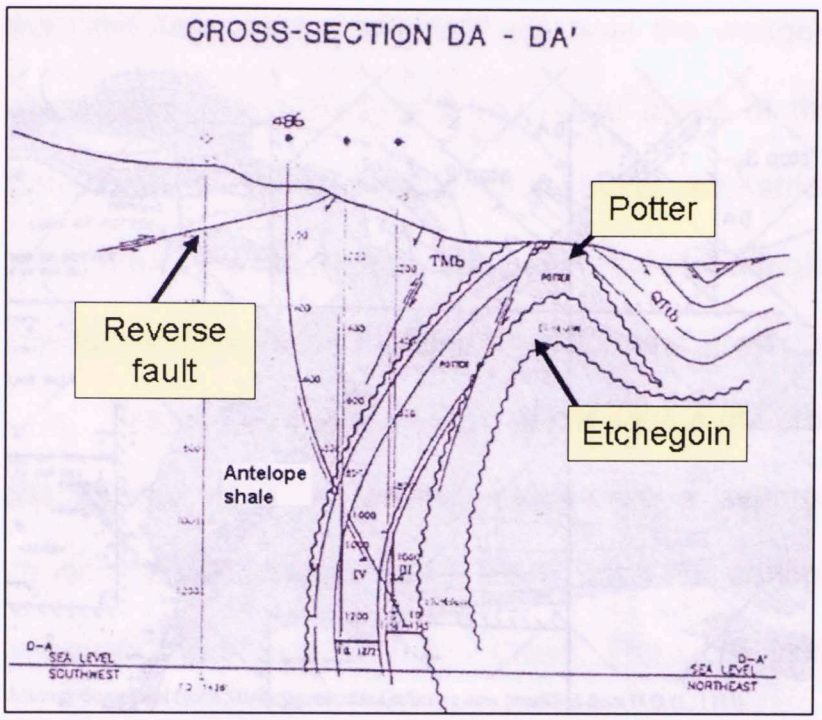


**Figure 103.**

Cross-section showing an overturned fold in the north Midway-Sunset area. Note the reverse fault interpreted to the left.
Notice that the Potter is shown on top of the Etchegoin indicating that the fold is overturned.

Figure extracted from Ponek (1998)

In the regional and detailed cross sections it is possible to observe two gradients of gradual thickness change in the Temblor Formation. From cross-section AA' to CC' the formation becomes thicker in a southeast direction. In the localized cross sections to the north (figure 102 D, E) and in regional cross section CC', the Temblor Formation is observed becoming thicker away from the large scale normal fault towards the northeast and southwest (figure 101). This indicates that the north-central part of the study area was structurally higher when the Temblor Formation was deposited.

The structural deformation observed in the Midway-Sunset area was limited by the large scale normal fault to the northeast of the study area. As deformation continued, the space available became progressively reduced to

the northwest, forcing the fault slip from the wedge-like structure that was developing to be transferred into upper levels of the stratigraphic section, generating southwest-dipping thrust faults (McKittrick) to the north of the study area. The mechanism that generated these faults is accountable for the overturned folds at the Etchegoin stratigraphic level observed in outcrop.

Figure 102 shows various black dots in the cross-sections. These are the location of 400+ well-log picks from a separate interpretation study (Boljen, 2005). These picks were used to perform a blind-test to the interpretation presented in this thesis. The study includes markers down to the McDonald Shale. The match between the two interpretations is very good, enabling the use of the picks to refine the interpretation and populate the surfaces of the structural model in areas located between cross sections.

### 6.3 Kinematic Reconstruction of Regional Cross-Section AA'

To validate the balanced structural cross-sections, a restoration through time was performed. The kinematic reconstruction shows the main events that generated the structures proposed in this thesis. Nine stages are presented, from 16.2-16.5 million years (top Temblor) to the Present (figure 104).

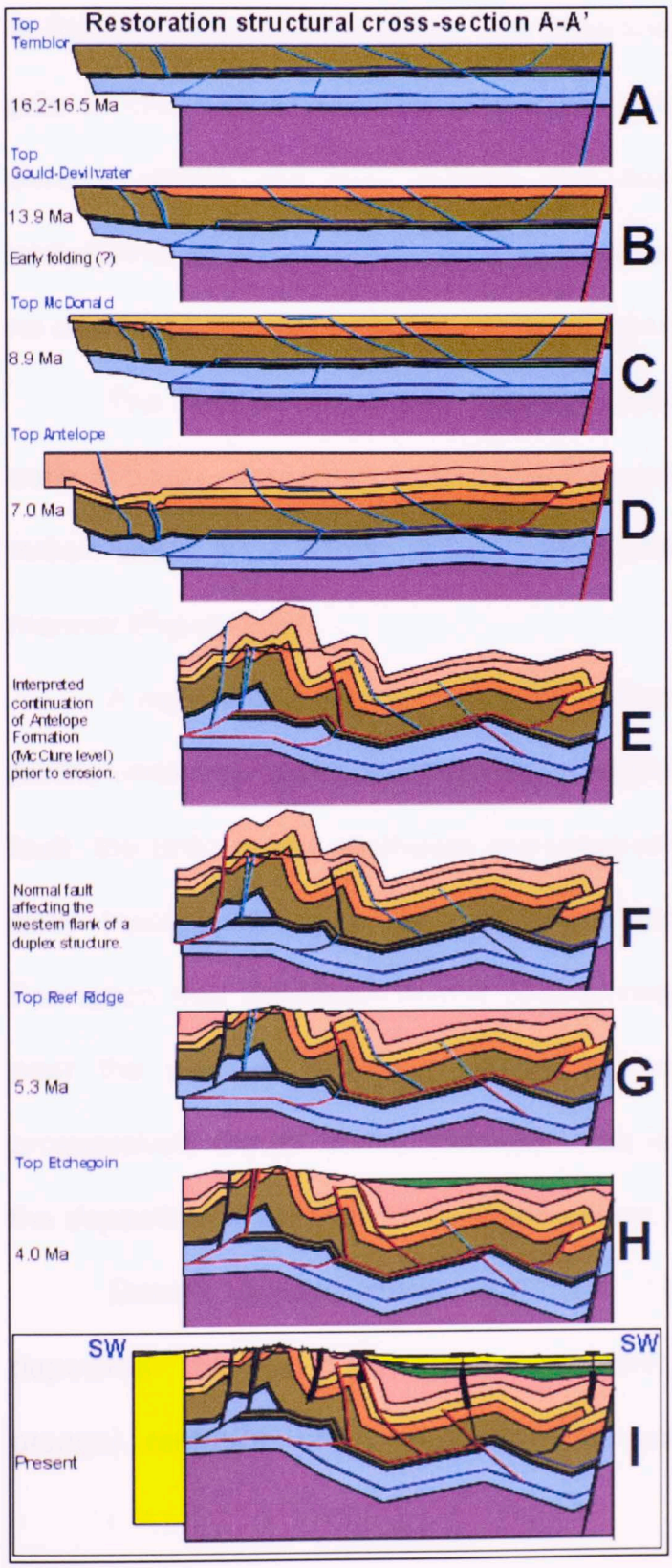


**Figure 104.**

Kinematic reconstruction of structural cross-section A-A'

Light blue lines: future location of faults.
Dark blue lines: detachment locations.
Red lines: active fault or detachment
Grey lines: faults that were active, no current movement.

A-Temblor Formation, tranquil horizontal morphology.

B- A normal fault is formed after the Temblor Formation was deposited. The units gradually subsided to the northeast (growth normal fault).

C-The Gould/Devilwater member becoming thicker to the northeast, was deposited as the growth fault developed.

D-The normal fault came to a stop. The tectonic setting changed from extensive to compressive.

E-The main event of compressive deformation took place. As the hanging wall of the primary fault-bend fold went past the ramp to the northwest, a fault-propagation fold was developed.

F-A short period of extension creates a normal fault that affects the backlimb of the fault-bend fold.

G-Erosion of the Antelope shale. A compressive episode reactivates the secondary fault-bend fold.

H-The event of compression intensified. The lower detachment level breaks-through the ramp, transferring slip into a ramp developing a wedge-like structure that pushed the overlying units up-and-forward.

I- deposition occurred in an active tectonic setting, as the remaining units where deposited.

* See text for full explanation.

In the kinematic reconstruction, light blue lines indicate the location of faults prior to their occurrence, dark blue lines mark detachment levels before they become active, red lines indicate that the fault or detachment level is undergoing movement, and grey lines indicate faults that were active showing no movement at a particular stage (figure 104).

The Temblor Formation deposited late in the Oligocene and into the early Miocene, presented a tranquil horizontal morphology at 16.2 – 16.5 (?) million years. As a matter of fact, earlier units were deposited in this same manner (Figure 104A).

A normal fault was formed after the Temblor Formation was deposited. As the units were gradually subsiding in response to the active growth normal fault, the units to the southwest remained at their original level, creating an early topographic high. The Gould/Devilwater member of the Monterey Formation was deposited in this setting, creating an area of no deposition near the western boundary of the section (paleo-high) and becoming progressively thicker to the northeast. This leveled the phisiography prior to the deposition of the McDonald Shale around 13.9 million years ago (105B)

Growth sedimentation continued as the McDonald Shale was deposited. The rate of subsidence recorded in the growth sediments (light orange) remained comparable to what was observed before, with the

variation that the downward movement of the units was nearly constant for the area to the southwest of the normal fault (figure 104C).

The Antelope Shale began to be deposited around 8.9 million years ago. The normal fault, that was still active, came to a stop in the early stages of Antelope deposition. At this point the tectonic setting changed from extension to compression, giving rise to early folding to the west and the formation of a reverse fault to the northwest that accommodated the deformation (figure 104D).

The deposition of the Antelope Shale concluded 7 million years ago in the late-Miocene (Tortonian). The main compressive deformation then took place. Here, the first fault-bend fold to the southwest was developed. As the hanging wall of this large structure made its way past the ramp to the northwest, a high angle, eastern-dipping fault-propagation fold was developed. During this phase, the early stages of the forward evolution of a second fault-bend fold also took place. Further east the fold-accommodation fault that was formed earlier continued its development. This was enhanced by a reverse fault formed in the Kreyenhagen Shale that connected the upper and lower detachment levels and produced a local uplift of the overlying units (figure 104E).

An episode of relaxation gave rise to a short period of extension that created a normal fault affecting the backlimb of the primary fault-bend fold. All compressive features were "momentarily" inactive (figure 104F).

The Antelope Member of the Monterey Formation underwent significant erosion during the active deformation that took place as the Reef Ridge Shale was deposited. A new compressive episode reactivated the secondary fault-bend fold, displacing the hanging wall over the detachment in the Kreyenhagen Shale. This deformation created displacement on the upper detachment of the Temblor Formation, reactivating the fault-propagation fold and the fold-accommodation fault in the eastern segment of the cross section (figure 104G).

As the Etchegoin formation was deposited the event of compression intensified, reactivating a portion of the ramp of the original fault-bend fold and generating a popup block that exposed the upper-Temblor Formation to the surface. This compression enabled the lower detachment level to breakthrough the ramp of the secondary fault-bend fold where it connected the upper detachment level. This generated displacement that was distributed to the preexistent fault-propagation fold and a newly formed thrust fault. The remaining slip went down into a ramp, developing a wedge-like structure that pushed the overlying units up-and-forward, creating displacement in the fold-accommodation fault (figure 104H).

The deposition of the Reef Ridge Shale and the Etchegoin Formation occurred in an active tectonic setting where erosion from structural highs (Temblor Range) fed sediment into the basin. In a similar way, the San Joaquin and the Tulare formations were deposited in a structurally active environment, with the difference that the depositional environment changed from alternating brackish to fresh-water conditions in the San Joaquin Formation (Walter, 1996) to alluvial and lacustrine environments (Taff, 1933) for the Tulare Formation. In this stage (figure 104l) compression was still active, but less intense. Some time after the Etchegoin Formation was deposited, the upper detachment was disconnected from the fold-accommodation fault to the east. As this occurred, a new fault-propagation fold developed, extending the ramp located to the northeast into the lower members of the Monterrey Formation. This is the last fault that was formed to make up the series of fault bounded structures observed at the surface (figure 104l).

This restoration satisfactorily explains all the events that took place and are responsible for the structures found in the study area. This permitted a complete understanding of the mechanisms accountable for what is observed in the detailed study area, and translates it into a 3D model to assess the structural complexity present.

# 7. STRUCTURAL GEOLOGIC MODEL

The Southern Belgian anticline is a structurally complex area where the Tulare Formation unconformably overlies the pre-Pliocene geologic units. All surface geologic data represent recent structural events, after the San Joaquin Formation was deposited. The structural geologic model in this area was tied to two regional balanced cross-sections (BB' and CC'), and populated with 5 localized cross sections constrained by dipmeter logs and surface structural data (figure 105).

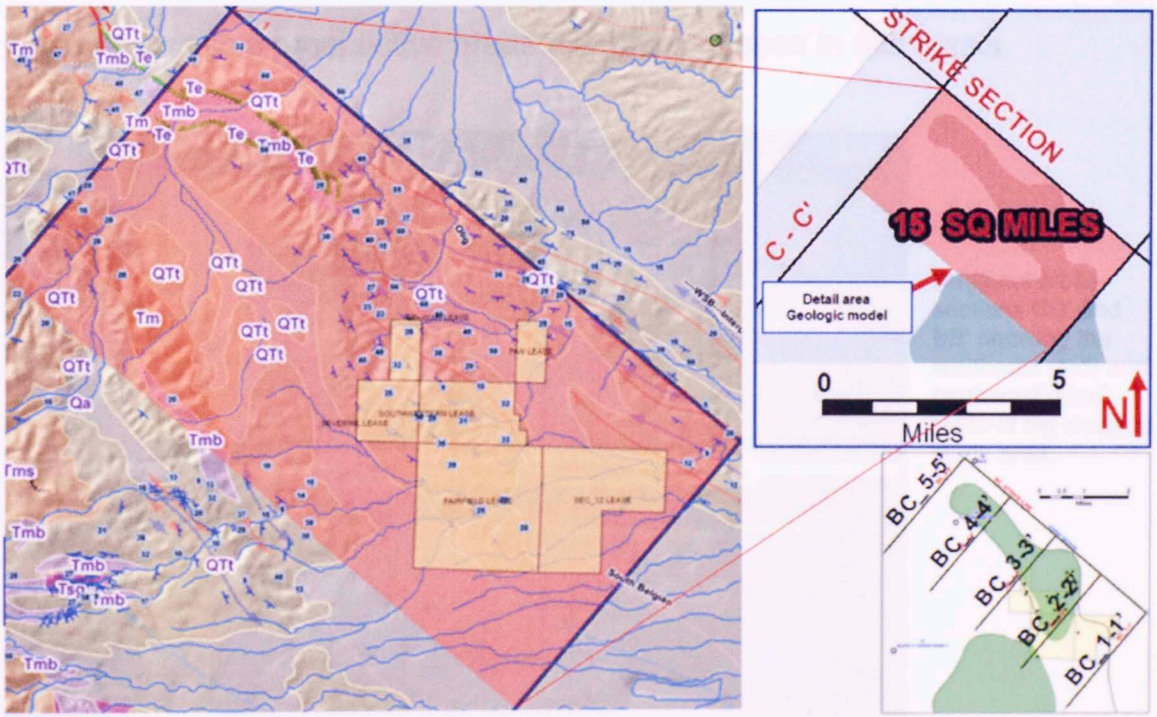


**Figure 105.** Area of the structural model. Most of the surface geology is covered by the Tulare Formation, to the north Tmb and Te are exposed. Notice the distribution of the localized cross sections.

The interpretation of the regional geology in cross sections BB' and CC' (see section 6.2) to the southeast and the northwest, respectively, was used to build the geologic surfaces (faults, unconformities, and time markers) in the detailed area (figure 106). The interpretation between the two cross sections was constructed using 5 localized cross sections and 17 wells, with dipmeter logs to control the slope and the direction of the geologic surfaces (figure 107). To correctly connect faults and detachment levels, a specific nomenclature was given to each interpreted line (figure 108). The deep structure is based on the structural characteristics interpreted from correlation to the regional framework; deeper wells should be drilled in the study area to evaluate possible prospective areas that are proposed in this thesis.

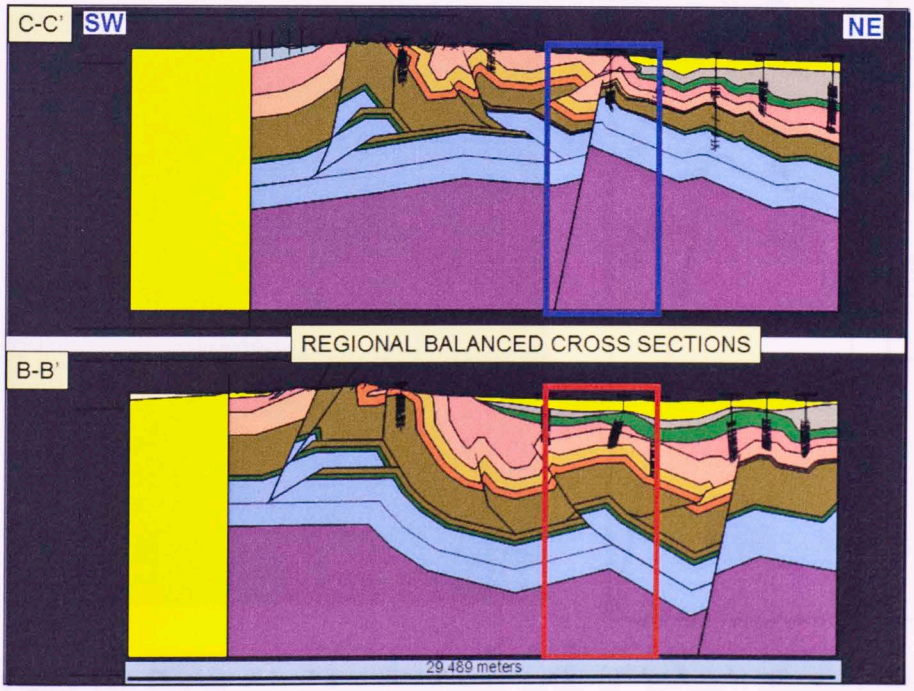


**Figure 106.**

Regional cross-sections CC' and BB' showing the southeast (red) and northwest (blue) limits of the detailed study area.

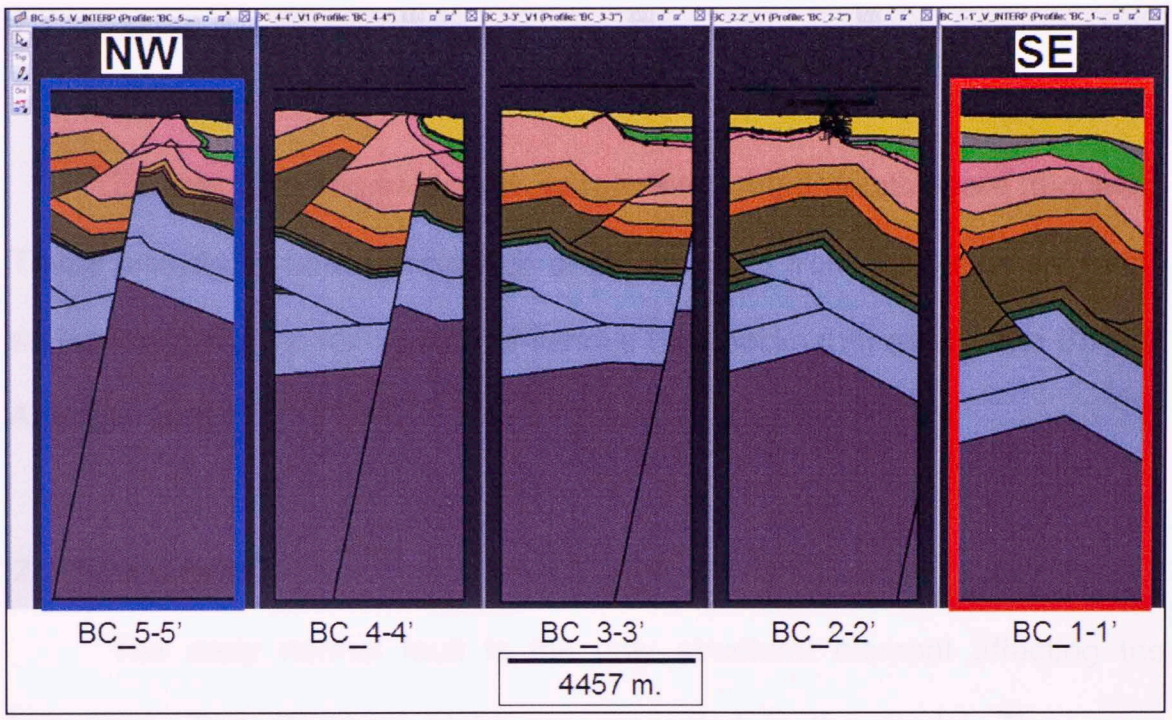


**Figure 107.** Localized cross-sections between regional cross-sections BB' and CC' showing the interpretation of the deep structure ready to be exported for the construction of the model.

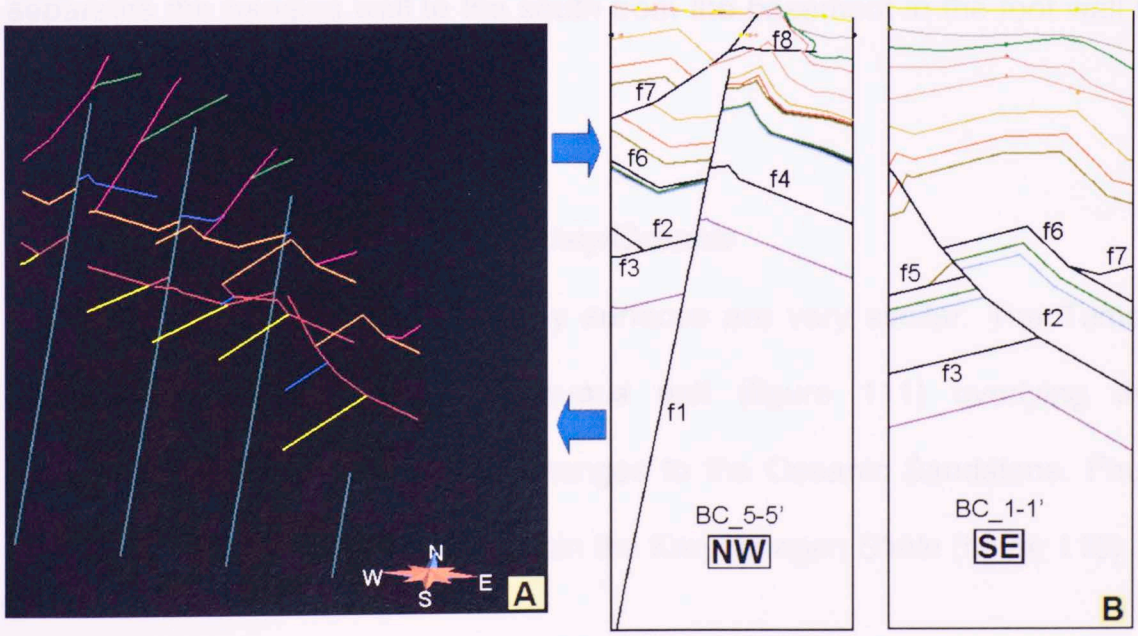


**Figure 108.** Display of fault and detachment levels. A) Position in space. B) Nomenclature to connect the interpretation between sections BC_11' and BC_55'.

## 7.1 Modeled Structural Surfaces

Eleven time markers and seven interpreted faults were modeled. These provided a better perception of the structure from the basement to the surface allowing the recognition of various fault bocks that exist in the Belgian Anticline area.

### *7.1.1 Basement*

The early normal fault is the only structural element affecting the basement. Two structural highs are presented in the model. They were formed during the major compressive deformation event. The normal fault separates the hanging wall to the south from the basement in the foot wall to the north (figure 109)

### *7.1.2 Top Kreyenhagen and Top Tumey/Oceanic*

The Kreyenhagen and Tumey surfaces are very similar. The Tumey Shale is a relatively thin, continuous unit (figure 111) overlying the Kreyenhagen Shale that laterally changes to the Oceanic Sandstone. Fault F2 starts in Detachment level F3 within the Kreyenhagen Shale (figure 110)

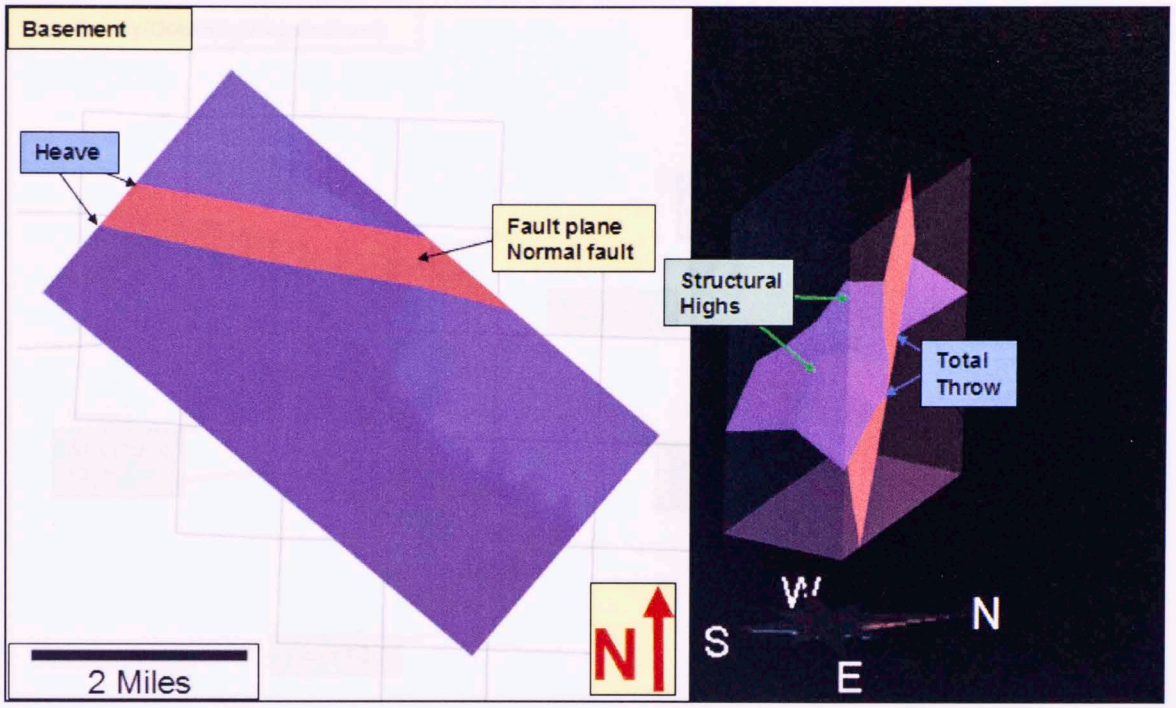


**Figure 109.** Basement surface. Notice the normal fault displacing the surface.

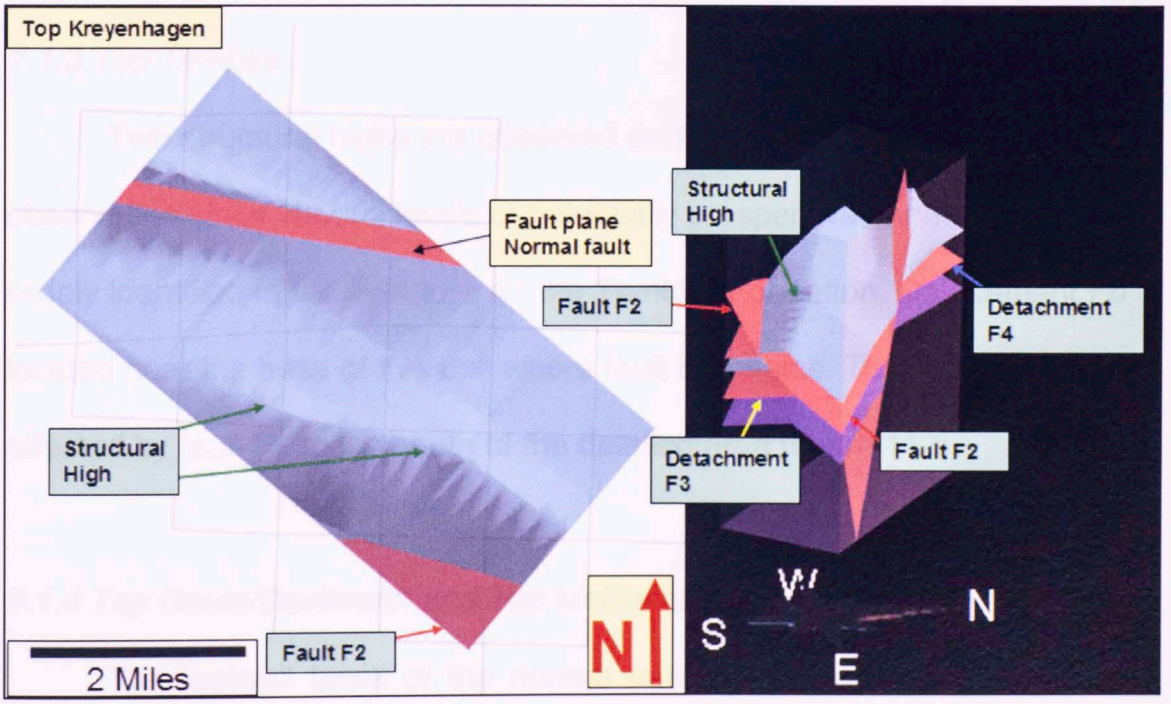


**Figure 110.** Top Kreyenhagen surface. Detachment .F3 is located within this unit.

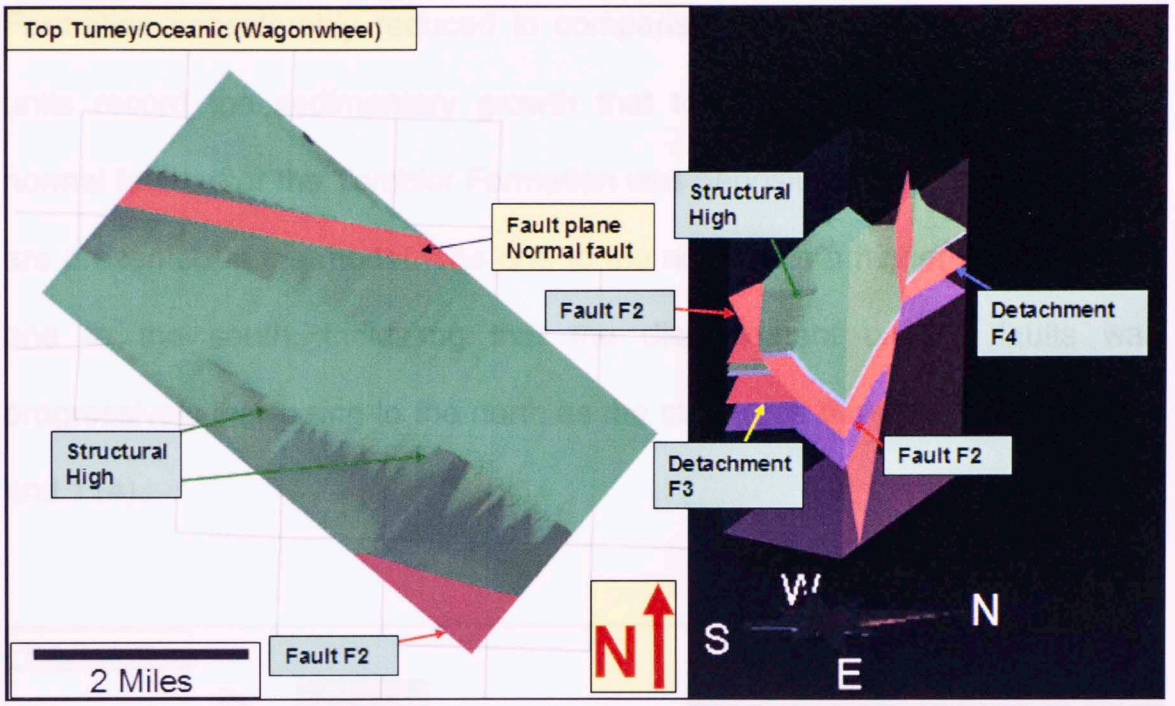


**Figure 111.** Top Tumey/Oceanic surface. Note the morphologic similarity to the Kreyenhagen surface.

### *7.1.3 Top Temblor*

Two structural highs are observed on this surface. This is an important observation since various levels of potentially prospective sandstone units are widely identified in the literature for the Temblor Formation. Detachment F6 is located near the base of this unit where fault F7 begins. This formation is also affected by fault F2 to the south of the detailed area (figure 112).

### *7.1.4 Top Gould/Devilwater and Top McDonald*

The footwall block of the normal fault displays the Gould/Devilwater (figure 113) and the McDonald (figure 114) members of the Monterey

Formation considerably reduced in comparison to the hanging wall. These units record the sedimentary growth that took place at this early-formed normal fault, after the Temblor Formation was deposited. Two structural highs are presented in the model. The one to the north is at a higher level than the one to the south; indicating that the displacement on the faults was progressively increasing to the north as the structures developed (figures 113 and 114).

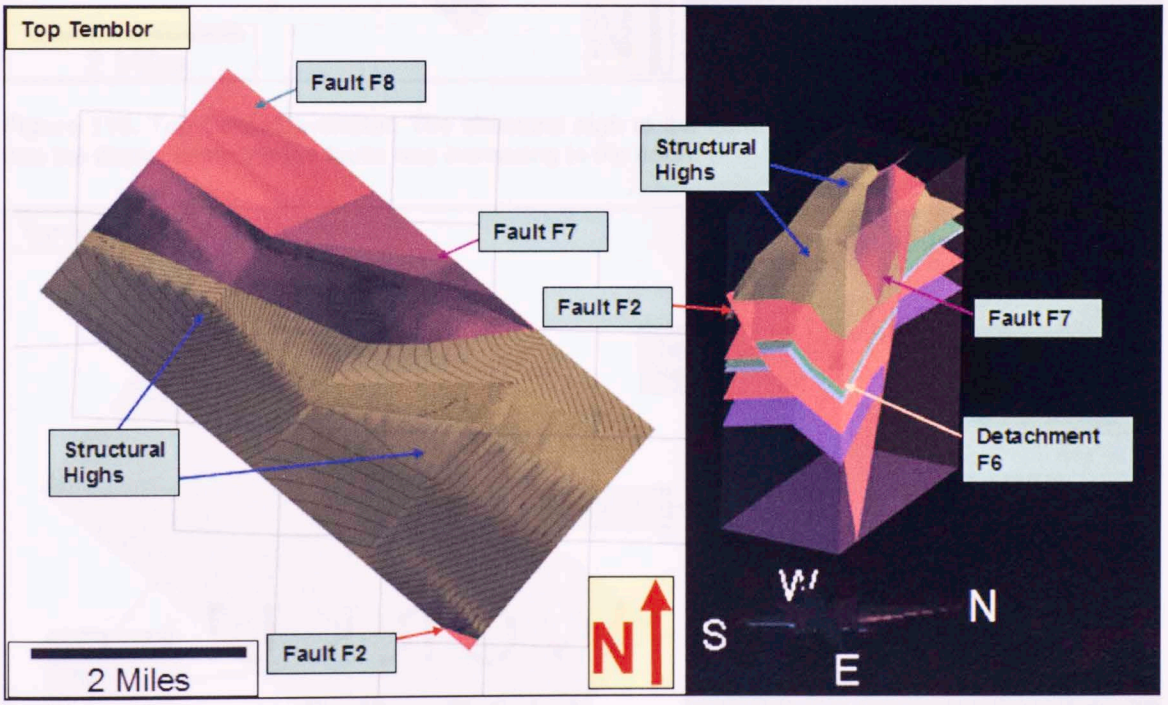


**Figure 112.** Top Temblor. Two structural highs are presented in the model for these level, where various potentially prospective sandstone bodies are identified in the literature. Detachment level F6 is in this unit. Fault F7 starts in this level.

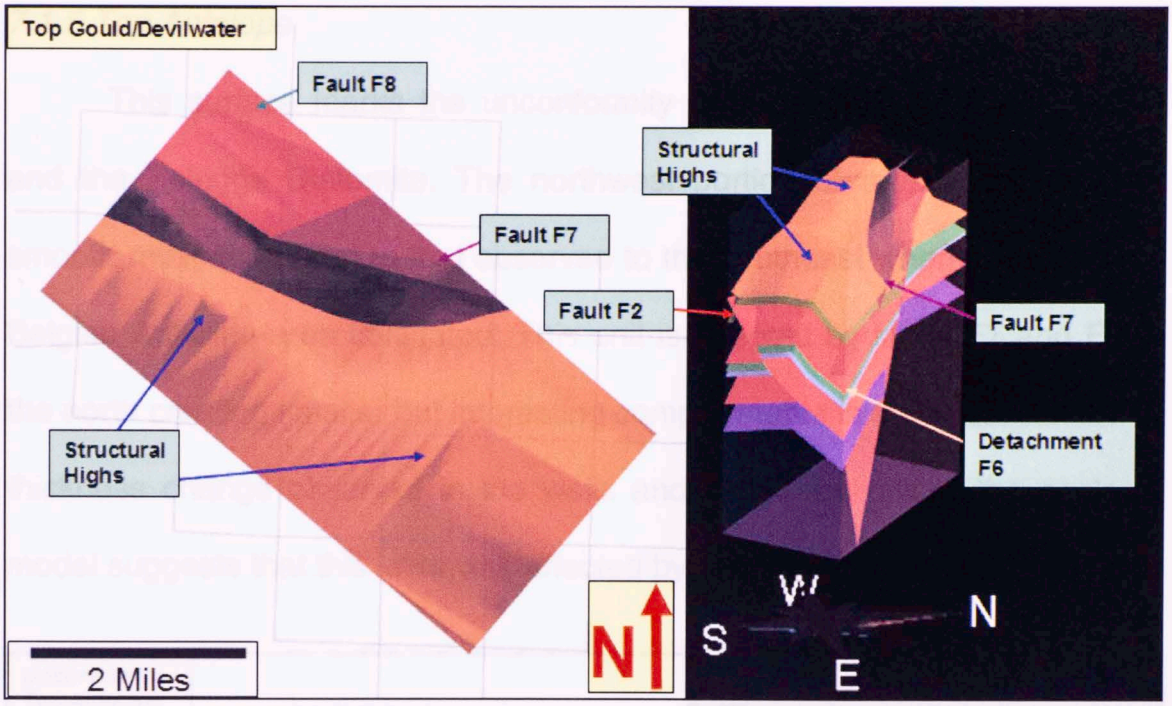


**Figure 113.** Top Gould/Devilwater. The structural high to the north is at a shallower depth, indicating that the displacement on the faults was increasing to the north.

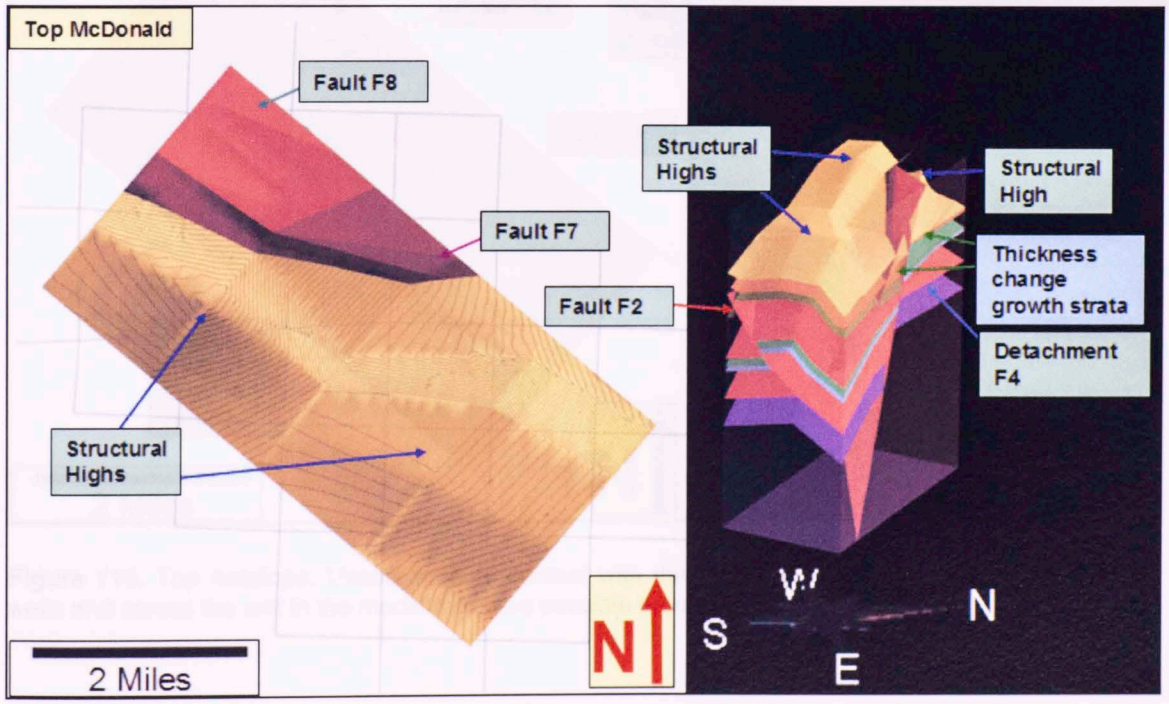


**Figure 114.** Top McDonald. The sedimentary growth that took place at the normal fault after the Temblor formation was deposited is recorded in this unit.

*7.1.5 Top Antelope*

This surface marks the unconformity between the Antelope member and the Belridge Diatomite. The northwest portion of the model shows a smooth relief compared to that observed to the southeast where the southern Belgian Anticline area is located. This unit is affected by faults F7 and F8 to the north creating smaller but interesting compartments in this area. A marked thickness change observed in the wells and within the unit in the geologic model suggests that this level was affected by erosion (figure 115).

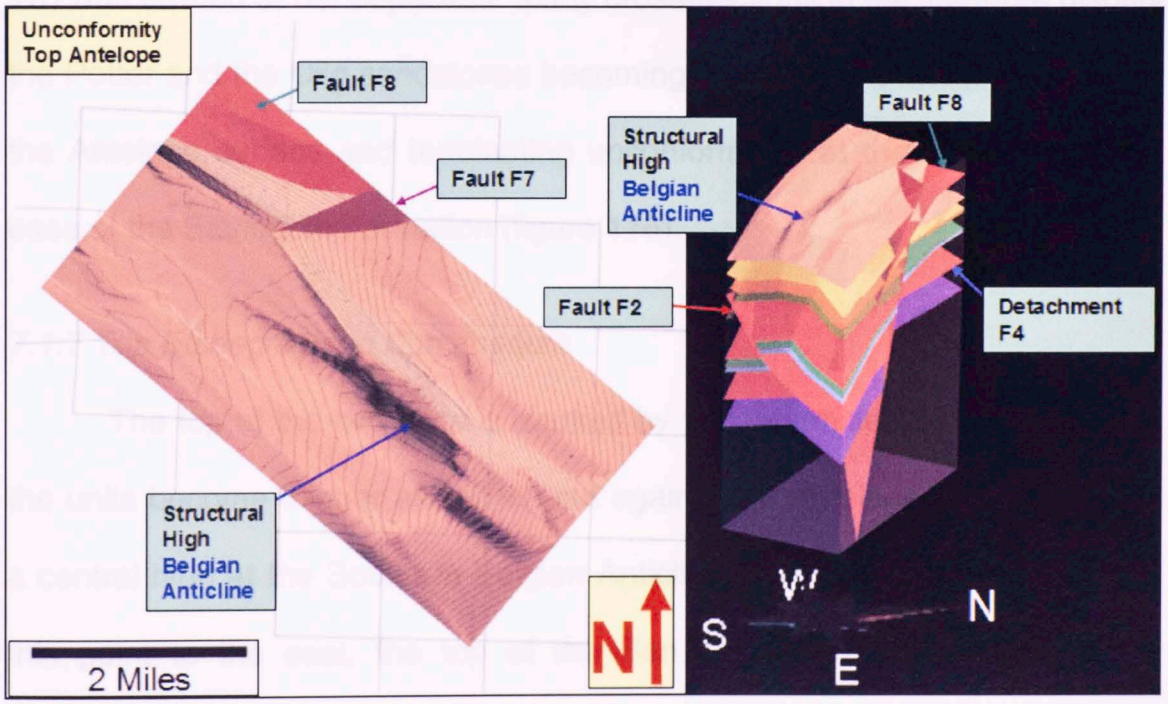


**Figure 115.** Top Antelope. Unconformable contact with the Belridge Diatomite. Thickness change in wells and across the unit in the model indicates possible erosion.

### *7.1.6 Top Reef Ridge*

This surface represents the upper Miocene unconformity; most of the production in the Northern Midway-Sunset field comes from sandstone bodies in the underlying unit. This surface also represents an important factor in the trapping mechanism of the petroleum system, where multiple combination (structural and stratigraphic) traps occur at this level. These traps are formed at the lateral termination of sandstone bodies against this surface that acts like a seal. To the northwest of the model, the unit (includes Tmb, Tbw and Trr) was eroded or not deposited. Many cross-sections in the literature display the Potter and the Oilg sandstones becoming thinner to the northeast against the Antelope surface and terminating unconformably at the contact with the base of the Etchegoin Formation (figure 116).

### *7.1.7 Top Etchegoin and San Joaquin*

The top of the two units is marked by unconformities; to the northwest the units become thinner and pinch out against the Antelope Formation near a central high at the Southern Belgian Anticline (figures 117 and 118). Form this point to the east, the top of the San Joaquin Formation displays a smoother relief and a shallower slope (figure 118) compared to the Etchegoin and the Reef Ridge surfaces. This indicates that the active folding mechanism progressively decreased its intensity as the formations were deposited.

To the northeast corner of the modeled area a smaller overturned fold is located near the outcrop of the McKittrick Fault. The deformation that produced fault F8 is also responsible for the inversion of this fold (figure 119).

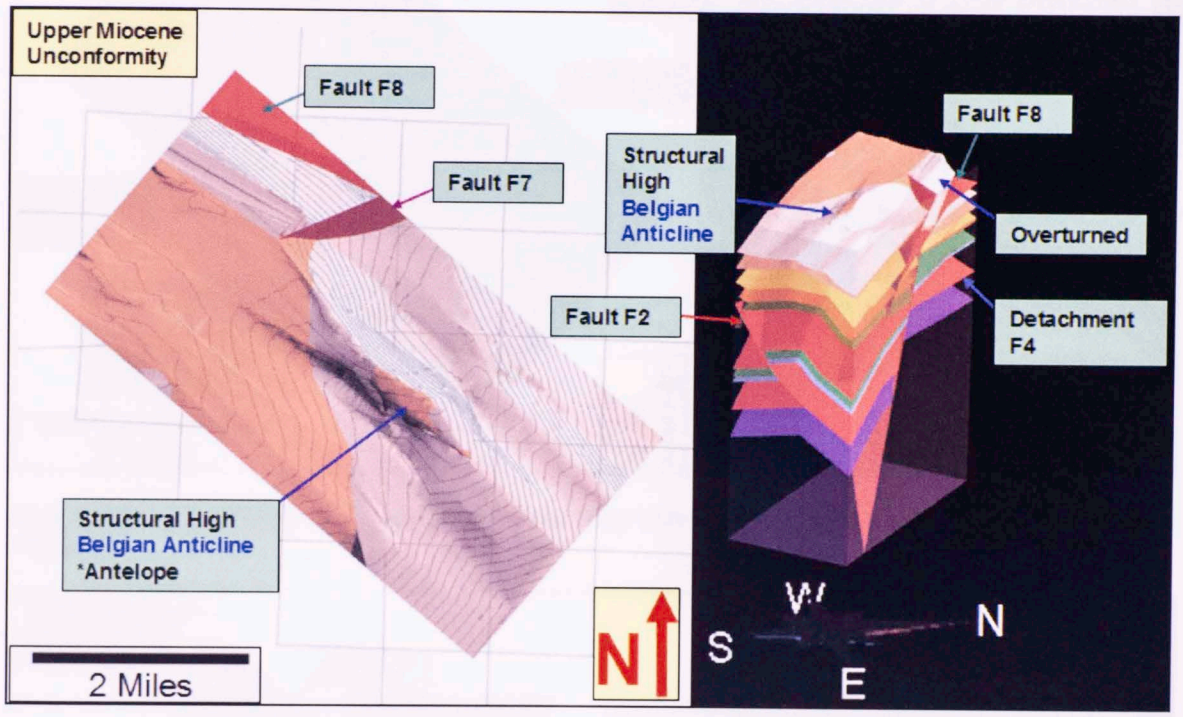


**Figure 116.** Top Reef Ridge. Represents the upper Miocene unconformity. Sandstone bodies terminate laterally against this surface that acts as a seal.

*7.1.8 Ground-Surface (The Tulare Formation)*

Various heavy oil deposits are found in this formation. The upper member is characterized by air sands and hardened-tar caps; this level is also more competent than the adjacent alluvial deposits. This surface was directly extracted from the DEM. Previous modeled surfaces show good correlation to outcrops presented in the literature (figure 119).

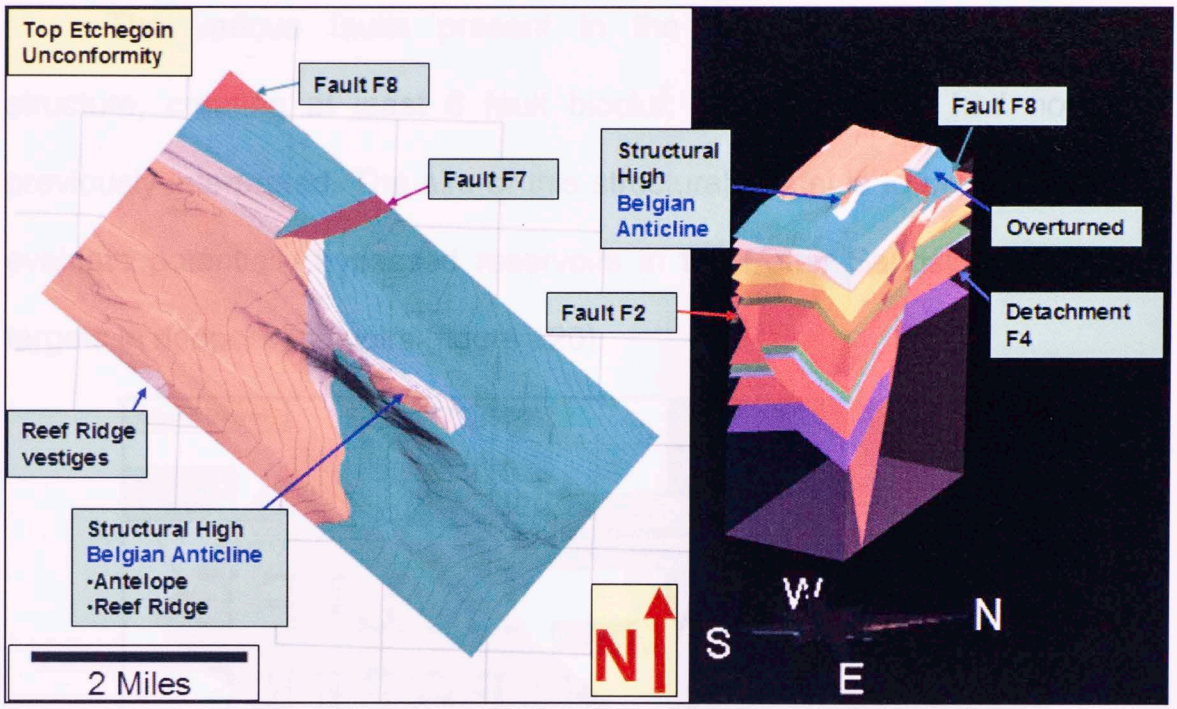


**Figure 117.** Top Etchegoin (unconformity). Becomes thinner to the northwest against the Antelope formation.

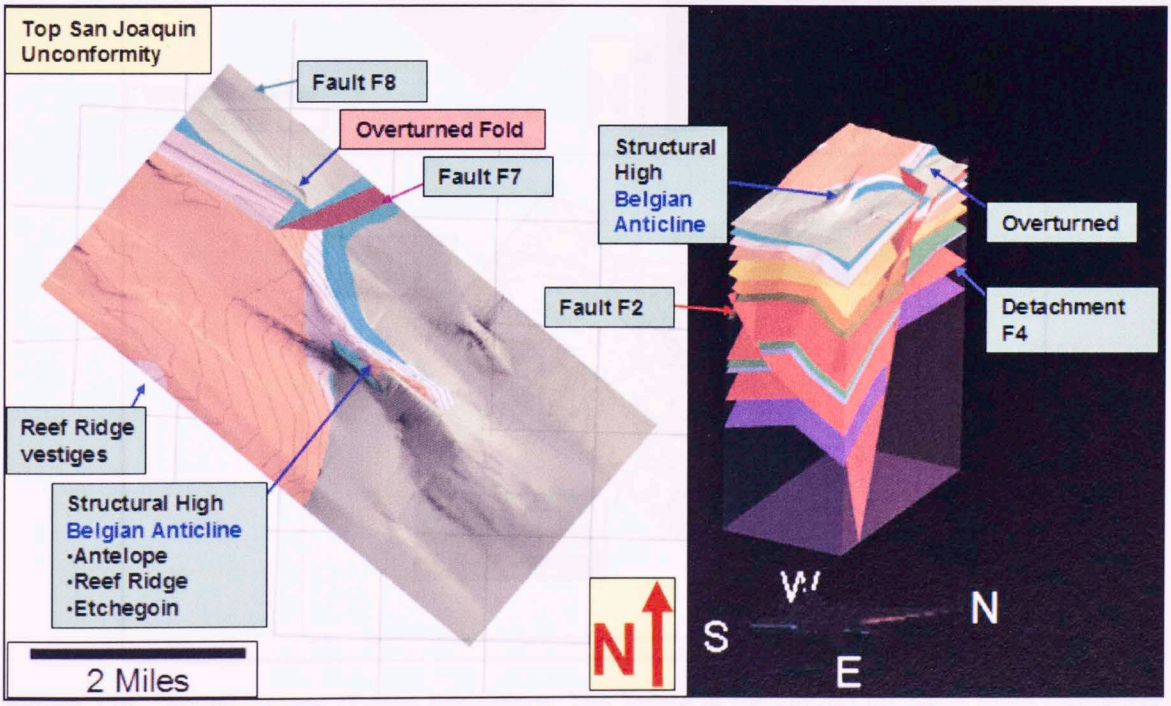


**Figure 118.** Top San Joaquin (unconformity). Fault F8 at the northeastern corner of the model is associated to an overturned fold. To the east of this fold the McKittrick thrust is exposed.

The various faults present in the model compartmentalize the structure, creating at least 6 fault blocks, many of which had not been previously interpreted. The aim of this structural model is to provide a tool to evaluate potentially bypassed reservoirs in the Potter Sandstone, and new targets in deeper reservoirs (figure 120).

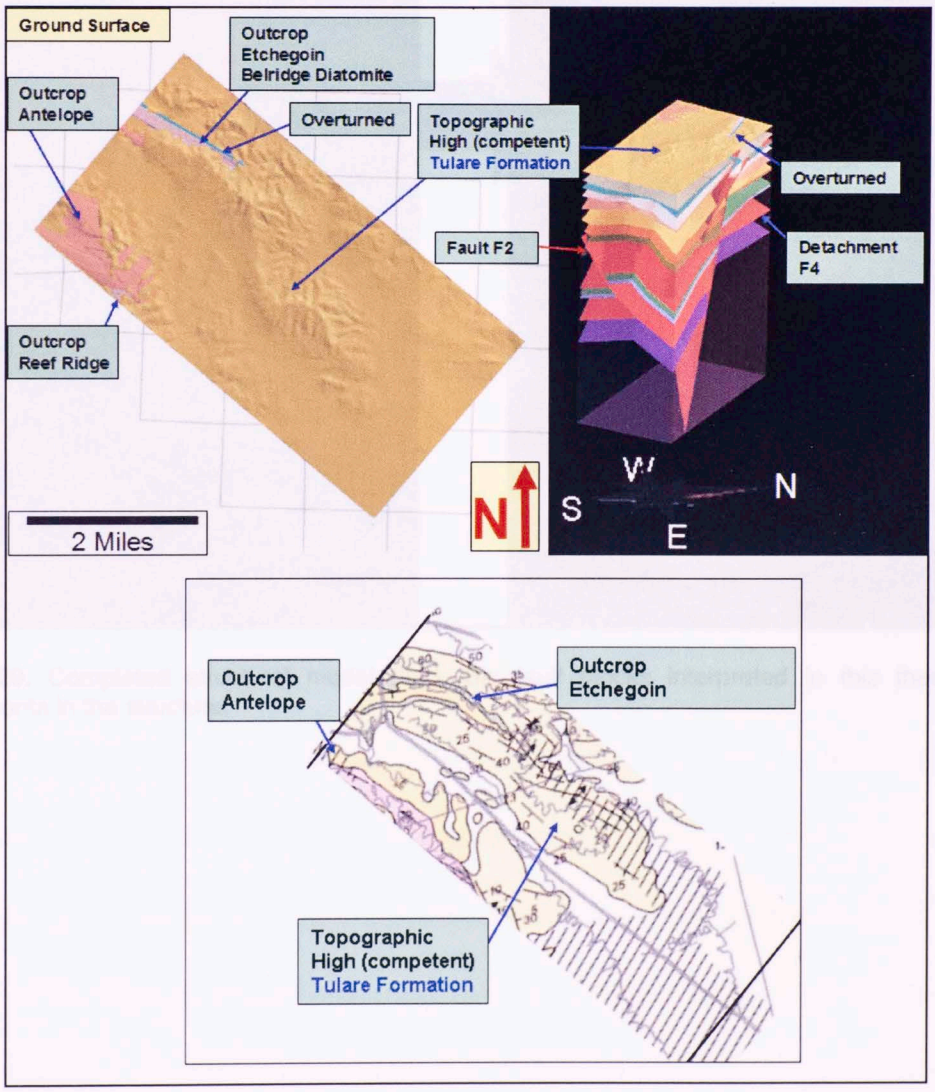


**Figure 119.** Ground-surface (Tulare Formation). The Tulare is recognized for being more competent than the Quaternary alluvial deposits. Notice the agreement between the geologic map of Dibblee (1973) and the intersection of the Ground surface with previous modeled surfaces.

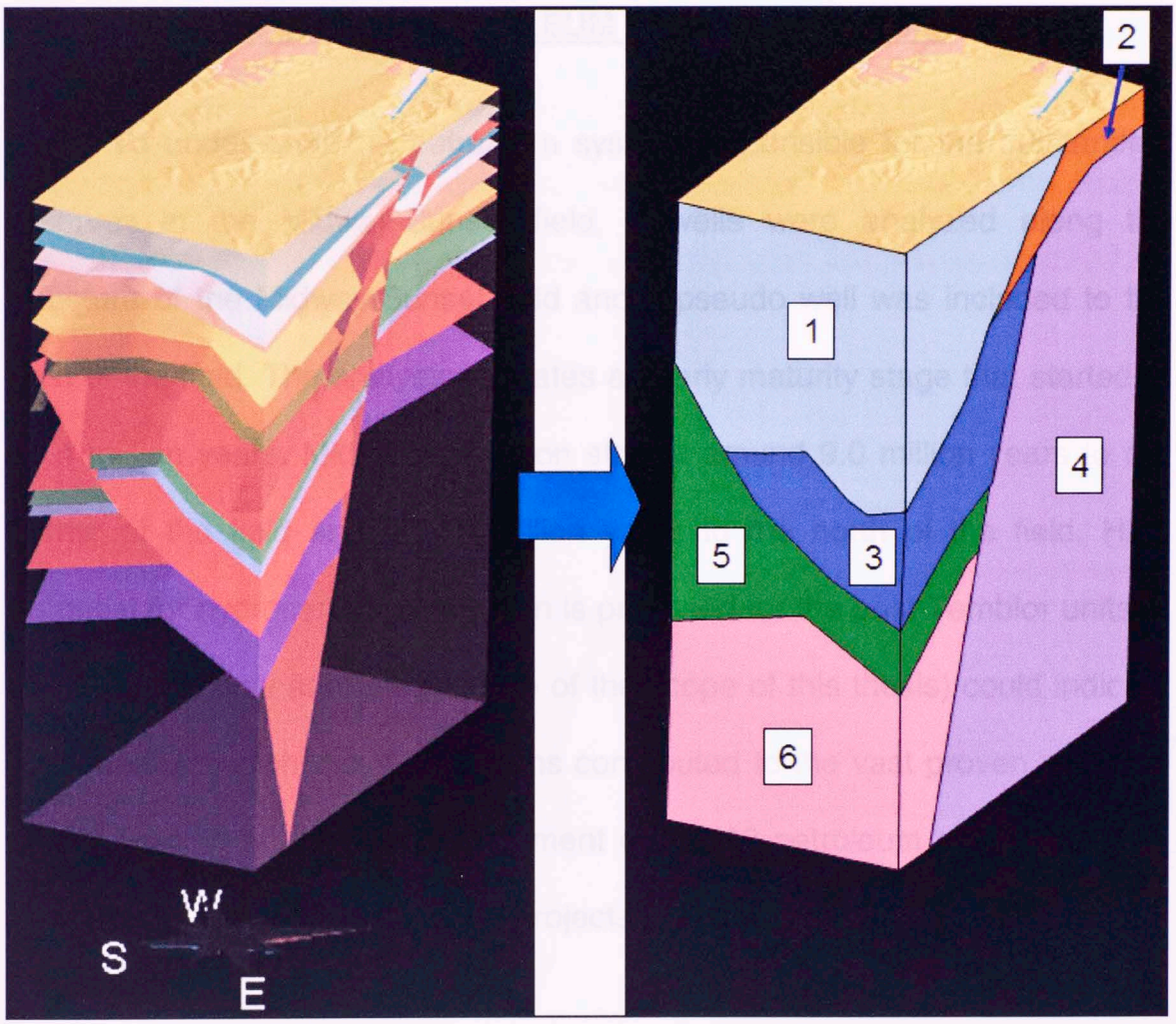


**Figure 120.** Completed structural model (left). Six fault blocks interpreted in this thesis create compartments in the structure.

## ANNEX 1: PETROLEUM SYSTEM ANALYSIS

To understand the petroleum system responsible for the outstanding reserves in the Midway-Sunset field, 3 wells were analyzed along the structure of the Midway-Sunset field and a pseudo well was included to the east of the field. The analysis indicates an early maturity stage that started at 14.4 million years. Mid-oil maturation started around 9.0 million years to the center of the field and at 7.0 million years to the north of the field. High potential for hydrocarbon generation is proposed for the post-Temblor units, a detailed heat flow analysis (outside of the scope of this thesis) could indicate the extent to which these formations contributed to the vast proven reserves of this field. A quantitative assessment of the 10 petroleum system criticals indicates a confidence of 84% for projects in this area.

It is very important to note that this analysis is very general and was only intended to provide a basic understanding of the petroleum system. It is a recommendation in this thesis to perform an in-depth proper basin analysis using the geologic model and the cross-sections here presented. The data used for this brief evaluation comes from published wells from figures in the literature, and in no case from any of the data in the actual wells used in the thesis.

The wells used in the present analysis are located in the central and north part of the structure; the pseudo well is located down-dip to the east of the field (figures 1 and 5). In the following paragraphs the results obtained for these locations are presented.

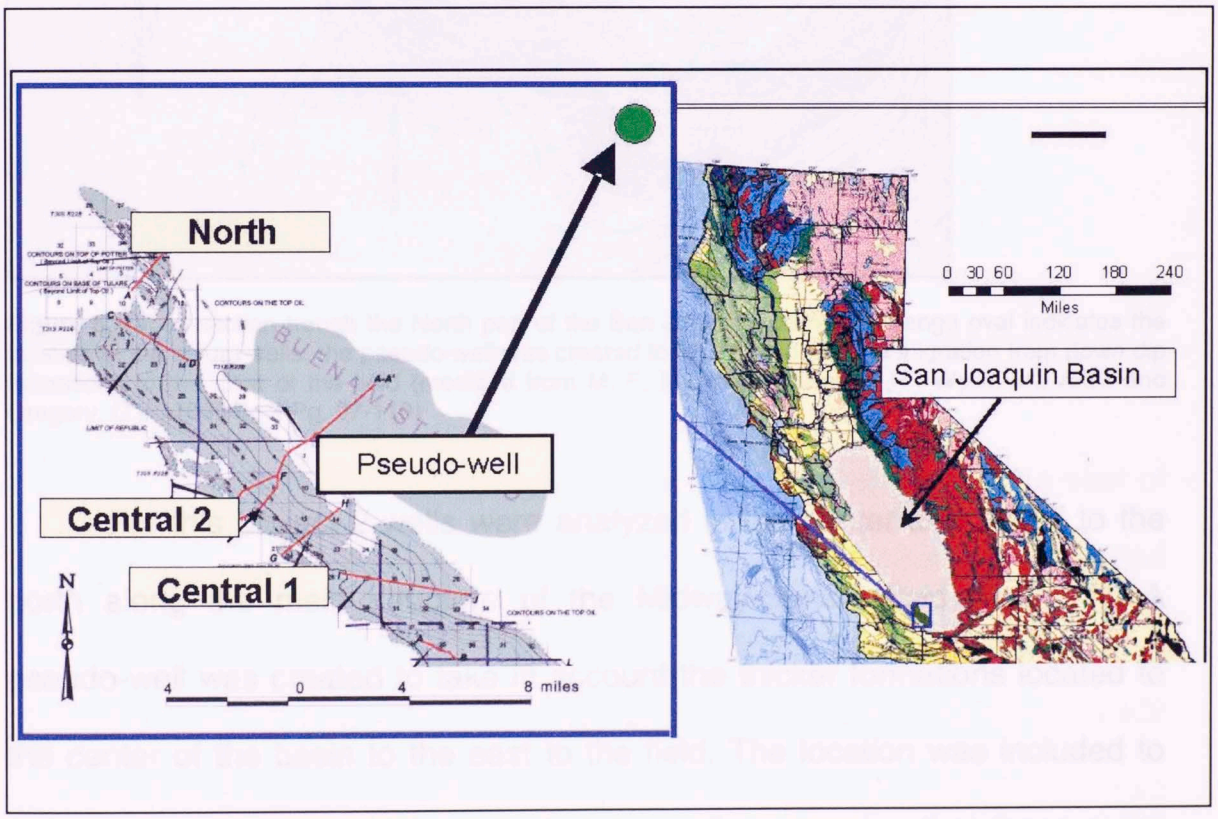


**Figure 1,** Location of the selected places along the structure (wells) and the pseudo-well (Midway sunset field extension from G. J. Gregory p. 67 figure 8., Geologic map from USGS I-512)

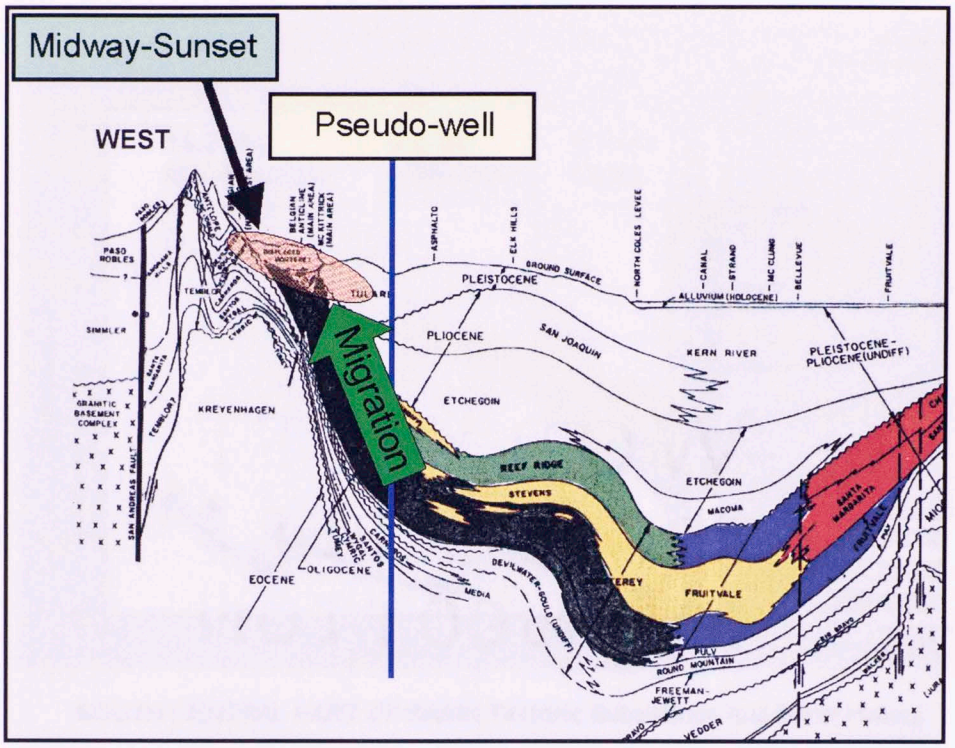


**Figure 5,** Cross-section trough the North part of the San Joaquin basin, the orange oval indicates the location of the actual wells, the pseudo-well was created to take in account the migration from down dip formations to the East of the field (modified from M. F. Mercer in Nilsen, T.H., Wylie, Jr., A.S., and Gregory, G.J., 1996 fig 2 Pg. 97-110)

For this project 2 wells were analyzed in the center and 1 well to the north along the main structure of the Midway-Sunset field (figure 1). A pseudo-well was created to take in account the thicker formations located to the center of the basin to the east to the field. The location was included to account for migration which originated down dip, assuming that these rocks have produced large quantities of oil that migrated up-dip into the Midway-Sunset field (figure 5).

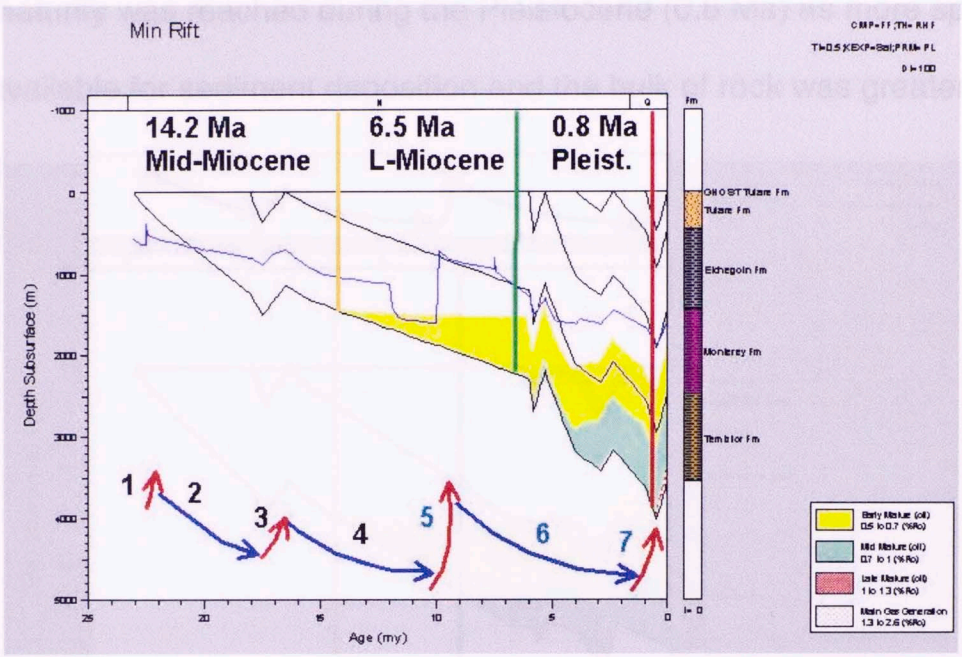


SOUTH CENTRAL PART OF BASIN Tectonic Subsidence And Burial History

**Figure 10.** Pseudo-well, the red arrows indicate compression and the blue arrows extension note the 7 events in relation to the tectonic subsidence.

The pseudo-well represents the thicker section down-dip to the east of the Midway-Sunset field (figure 5). The tectonic subsidence curve presented here for this well is assumed to be representative for the southwestern portion of the San Joaquin Basin (figure 10 and 5). Overall the curve shows a steady slope of subsidence that is interrupted by seven main events of tectonism (figure 10, and table 5 annex). This part of the structure reached early generation at 14.2 Ma in the Middle Miocene and main oil generation was reached at around 6.5 Ma at the closing of the Monterey deposition. Late

maturity was reached during the Pleistocene (0.8 Ma) as more space became available for sediment deposition and the bulk of rock was greater.

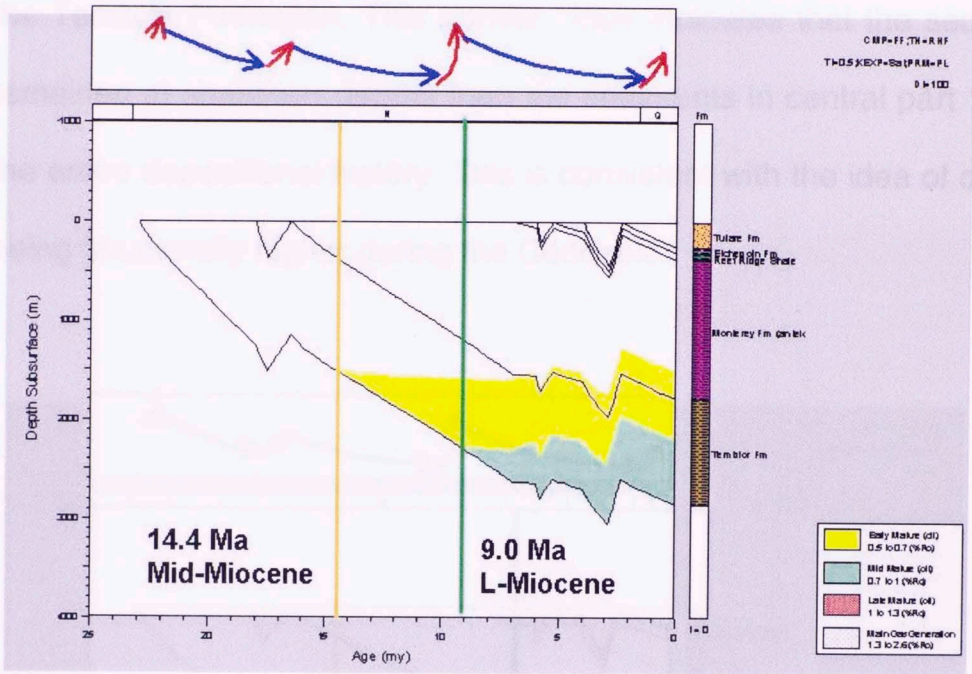


(1) CENTRAL PART OF THE STRUCTURE Burial History

**Figure 12.** Central part of the field (central 1 see figure 1). Tectonic events presented here at the top. The Monterey formation is divided in its members.

The central part of the field shows an interesting change at the start of mid-maturity (figures 12 and 13); central part 1 reaches mid-maturity at 9.0 (my) contrasting with central part 2 which doesn't enter mid-maturity until 6.8 (my). This, coupled with the reduced vertical extent of the oil window that is observed for this well (figure 13), could indicate that there was a structural high in the vicinity of central part 2 at the time of deposition, preventing the same course of burial that is evidenced in central part 1 (figure 12).

Something very interesting that is also observed in the burial history curve of central part 2 is the smoother slope of the lines marking the top and base of the Temblor Formation. This gentler slope indicates that the sediments here remained at shallower depths than the sediments in central part 1 throughout the entire depositional history. This is consistent with the idea of central part 2 being structurally higher during the Cenozoic.

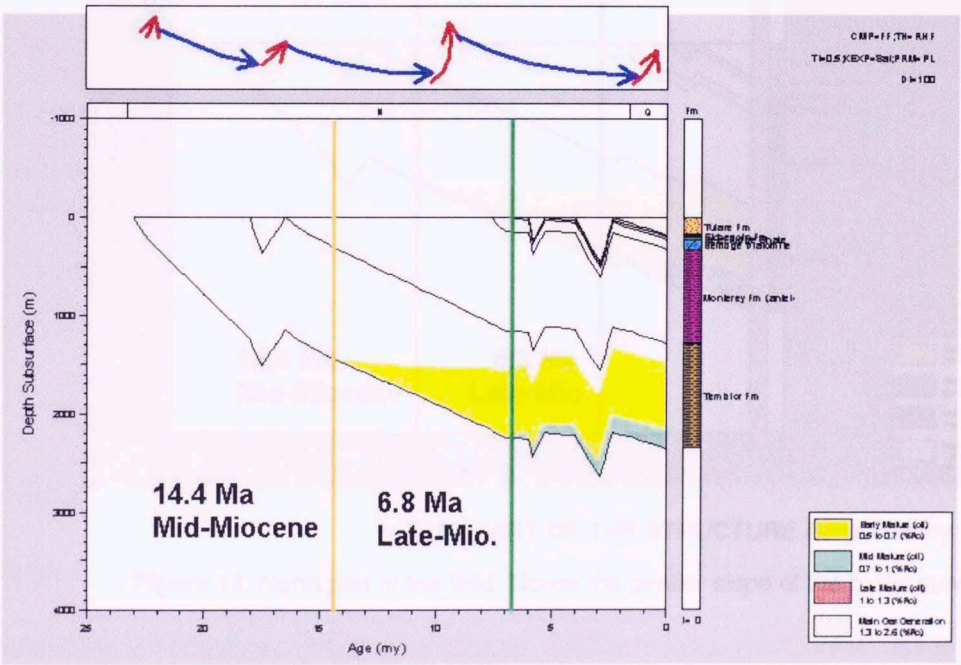


(2) CENTRAL PART OF THE STRUCTURE Burial History

**Figure 13.** Central part of the field (central 2 see figure 1). Notice how reduced the oil window is compared to central part 1.

Comparing the slope of the burial curves along the field reveals how the slope of the burial lines become gentler to the north. A much stronger sediment deposition was occurring to the south compared to the north. This

could be related to the gradual shift of the sediment source further north through time (?). This is also consistent with the gradient observed in balanced cross-section C-C compared to the regional cross sections to the south.

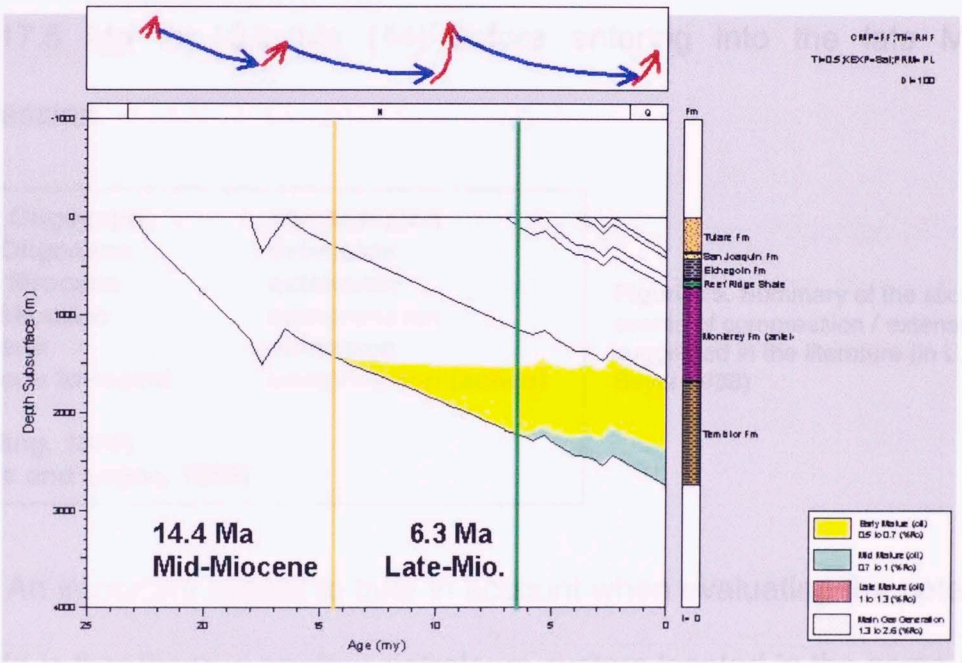


NORTH PART OF THE STRUCTURE Burial History

**Figure 14.** North part of the field. Notice the gentler slope of the burial curves.

The literature indicates six main events of compression or extension (figure 15). The work presented here agrees with a late Miocene compression, an early Pliocene extension and a final Pliocene compression that is still active (see #'s 5, 6, and 7 in figure 10). It is also suggested that

there were four main events prior to the late Miocene. There was a late Oligocene compressional event (see #1 in figure 10) followed by an early Miocene extension (#2 in figure 10). Compression is evident in all the wells by the decrease of burial depth observed from 17.5 Ma to 16.5 Ma at the closing of early Miocene time (#3). And finally a long period of extension took place from 17.5 Ma to 10.5 Ma (#4) before entering into the late Miocene compression.

| | |
|---|---|
| **Early Oligocene** | **compression** |
| **Late Oligocene** | **extension** |
| **Early Miocene** | **extension** |
| **Late Miocene** | **compression** |
| **Pliocene** | **extension** |
| **Pliocene to recent** | **compression (active)** |

**(Harding, 1976)**
**(Davis and Lagoe, 1988)**

**Figure 15.** Summary of the six main events of compression / extension suggested in the literature (in L. A. Beyer 1988)

An important aspect to take in account when evaluating the potential of this field is that there is another petroleum system located in the same area of extent (figure 3) and corresponds to all the formations deposited before the Temblor Formation. This petroleum system has produced large amounts of hydrocarbons and for some plays, the origin of the hydrocarbon is not restricted to a single system. One place that fits this characteristic is the southern Belgian Anticline area located in the north part of Midway-Sunset (figure 1 North); here it is believed that the hydrocarbons come from both levels of the West Side Fold Belt play (L. A. Beyer).

## THE TEN PETROLEUM SYSTEM CRITICALS AND QUALITATIVE "TRAFFIC LIGHT" ASSESSMENT

*1 Srgv (Source Rock Generation Volume)*

The volume of source rock for this petroleum system is outstanding not only because the majority of units are thick organic shales but also because these are enveloped around the reservoirs.

**Quantity rating** **Green**

*2 Srq (Source rock Quality)*

The rocks responsible for the generation are thick units composed primarily of marine organic shale, their TOC values (calculated from the relation to sedimentation rate) range from 2 to 4.8; this classified the quality of the rock in terms of generation as very good to excellent.

**Quality Rating** **LT Green**

The quality was assigned to light green since more data from the actual rocks, like TOC values obtained in the lab, are necessary; this new data would probably push the rating to green.

*3 Srm (Source Rock Maturity)*

Here the Temblor Formation produced the bulk of oil and gas generation, it is important to notice that a better assessment of the heat flow through time would give rise to a more realistic model where post Temblor formations also reached maturity and generated hydrocarbons. In the present work light green was given to the maturity due to the uncertainty of a more reliable heat flow analysis.

**Maturity** **LT Green**

*4 Rrhcv (Reservoir rock-hydrocarbon volume)*

The reservoir rocks here are of various types; one is characterized by extensive sheet sands deposited in unconfined settings (Strum, 1996), a second type includes deep water turbidite channels and incised canyons (Gardiner et al. 1996) that were filled with sand, that were abundant and due to the intense tectonic events and uplifts that were mentioned earlier (erosion in the mountains and intense deposition in the basins See figure 10 numbers 1 to 7). Finally the Tulare Formation, mainly composed by coarse continental sandstones, and deposited as alluvial fans in continental settings (Nilsen, 1996) is a third type of reservoir rock. Note that the Tulare is considered as a good reservoir since in the literature it is mentioned that it is capped by thick layers of tar (Nilsen, 1996) that hardened in the pore space forming a good seal for heavy oils.

**Volume of reservoir** **Green**

*5, 6 Rrsq (reservoir Rock and Seal Quality)*

For the deeper formations like the Potter Sandstone, the porosity and the permeability are good. In terms of seal, most of these sand packets are caped by mudstones. In the case of the Potter Sandstone the cap rock is the Belridge Diatomite, which not only acts as a seal but also as a source. In terms of trapping, there are stratigraphic, structural, and combination traps that formed throughout the history of deposition; this is coupled with intense hydrocarbon generation charging the structures constantly since the middle Miocene.

**Reservoir and seal quality** **Green**

*7 Mpv (Migration pathway)*

This system is located in an elastic, tectonically active basin, where the source rocks have been fractured and compressed creating pathways for hydrocarbons. This basin is overcharged as evidenced by the vast amount of hydrocarbons that have reached the surface through multiple gushers and seeps, with seeps and tar pits still present in the area.

**Pathway Volume** **Green**

*8 Mpq (Migration Pathway Quality)*

The migration here is mainly vertical, with a lateral component for short distances in the case of channels being charged by the mudstones in which they are embedded. A drawback here is the low API gravity of the oil (Campbell, 1996) that has to be moved; which is predominantly heavy oil (11° avg.) for the shallow formations. Higher quality oil (18-30 API) is expected for deeper prospects.

**Pathway quality** **Yellow**

The yellow tag here is for the present projects to be conducted in the shallow formations, and due to the heavy oil secondary methods of recovery that are necessary and active in the area.

*9 Mpr (Migration Pathway Rate flux)*

The rate here is assessed using the modeled fluid velocity. In the graph the first major spike indicates good conditions but not important for this study since oil generation did not start until 14.4 Ma. What is interesting to see is the fluid velocity of 15 to 20 m/my that is maintained from 14 to 7 million years for the Temblor Formation (figure 17). At around 6 Ma the upper units show excellent fluid velocities; this is very important if we keep in mind that these

formations have high potential for hydrocarbon generation (figure 16) and very likely have generated hydrocarbons throughout their history (a better heat flow analysis is necessary for evaluation).

**Rate flux** **Green**

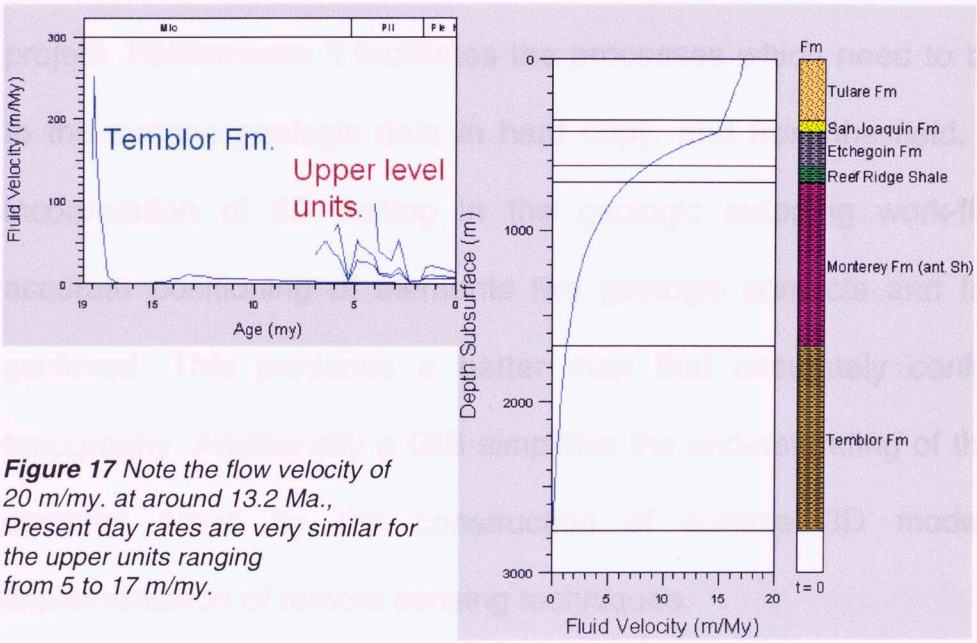


***Figure 17*** *Note the flow velocity of 20 m/my. at around 13.2 Ma., Present day rates are very similar for the upper units ranging from 5 to 17 m/my.*

*10 PStw (Petroleum System Time Window)*

This is a unique petroleum system in terms of timing since oil production was not only vast in terms of volume, but also very constant throughout the history of the basin. This can be attributed to the high quality of source rocks that are predominantly organic (e.g diatomite and foraminiferal-shale) and to the mixed deposition of good reservoirs in contact with high quality source rocks that also serve as seal.

**Petroleum system time window** **Green**

**Petroleum system totals: 84%** **Light Green** **PROCEED!**

# 8. CONCLUSIONS

Geographic information systems provide multiple tools that reduce the time needed to organize and acquire the data needed for any geoscience project. Furthermore it facilitates the processes which need to be performed to the surface geologic data in hard copy, and from the field. Through the incorporation of 3D editing in the geologic mapping work-flow, a more accurate positioning of elements like geologic contacts and faults can be achieved. This produces a better map that accurately conforms to the topography. Additionally a GIS simplifies the understanding of the geology in complex areas by the construction of surface 3D models and the implementation of remote sensing techniques.

The stratigraphic interpretation that was performed revealed that the formations of interest are very heterogeneous, and that the units include various levels and many types of deposits. Based on log character and outcrop observations these deposits range from conglomeratic sandstones filling deeply incised submarine canyons to medium-grained and fine-grained sandstones with a sheet-like geometry. These sandstone reservoirs changed their nature in response to the morphology of the substrate that was present

when they were being deposited, the accommodation space available, and the structural setting.

The structural interpretation presented here differs from other interpretations in the literature, where there is no clear explanation for the fault slip that is transferred to the east in response to the development of two large-scale fault bend folds to the west of the study area. We believe that a detachment in the Basal Temblor Formation extended further east and was an important factor in the evolution of the series of parallel fault-bounded structures present in the study area.

From the northwest margin to the southeast edge of the study area, the Temblor Formation becomes thicker. This is also observed in the detailed area of study from cross-sections BC_4-4' and BC_5-5' near the location of a large scale normal fault, where towards the northeast and southwest the thickness of the Temblor Formation also increases. This indicates that the north-central part of the study area was already a structural high prior to the deposition of the Temblor Formation.

To the northeastern margin of cross section AA', the interpretation is in agreement with the existence of a normal fault that originated early in the

structural evolution after the Temblor Formation was deposited. This large scale fault continued its evolution as a growth normal fault at least until the end of the deposition of the McDonald member of the Monterrey Formation and acted as a structural control in the system reducing the space available for structures to develop. This structural barrier forced the fault slip from the lower levels to be transferred to the east into upper stratigraphic levels, generating southwest-dipping thrust faults (McKittrick) to the north of the study area. This mechanism is accountable for the overturned folds at the Etchegoin stratigraphic level observed in outcrop in the southern Belgian Anticline area.

Normal faulting also took place during the later stages of the structural evolution posterior to the deposition of the Monterey Formation and is evident to the west of the study area where the back limb of a duplex structure is faulted. For this reason and the subsequent reactivation of compressive episodes, we believe that the structural deformation occurred in pulsating events that varied in strength through the structural evolution.

Various cross-sections in the literature present a clear back-stepping of turbidite sandstones in the Reef Ridge level. Even more, the interpretation presented here both in the stratigraphic and structural cross-sections shows a thickening of the Reef Ridge unit towards the broad syncline that separates the Midway-Sunset and Buena Vista field where the cross sections mentioned

above are located. These observations indicate that the structural uplift of the Temblor Range that was produced by the fault bend folds developed to the west, remained active during the deposition of these formations and represented a local source that shed sediment to the northeast and southeast as this sandstones were deposited. Additionally, a decrease in slope of the Etchegoin surface compared to the Reef Ridge surface suggests that the folding mechanism progressively decreased its intensity through time.

Various deepwater sandstone bodies are observed in the stratigraphic section. Sandstones in the Temblor and in the Monterey formations are laterally continuous and fairly homogeneous in thickness. On the other hand, the well-log correlation of sandstone bodies in the Reef Ridge Shale suggests that their thickness is very variable and that they are not as laterally extensive. In the field, the sandstone bodies in the Belridge Diatomite appear to be lenticular in shape and cutting into the diatomite. Laterally continuous and homogeneous sandstones present in the Temblor Formation and the upper members of the Monterey Formation suggest a deposition in an unconfined setting, where no major barriers controlled the sediment distribution. After the Antelope shale was deposited, a major deformation event that took place during the late Miocene created a confined setting, where structural highs controlled the sediment distribution.

The rise of the Temblor Range became a sediment source that locally modified the depositional axes, generating a northeast to southeast area where the Potter and Olig Sandstones where deposited. A combination of depositional and structural events controlled the framework that is present in the study area. Through a careful study of the data these factors were recognized and introduced in the construction of the structural geologic model.

Sedimentary growth is recorded in The Gould/Devilwater and the McDonald members of the Monterey Formation; this is clear near the large scale normal fault that separates the thinner members in the foot wall to the east at Elk Hills, from the enlarged upper Monterrey members present in the Buena Vista oil field.

Important parts of the trapping mechanism in the petroleum system are the unconformities. The most important is the upper-Miocene unconformity since various combination traps are found at the lateral termination of many sandstone bodies against this surface that acted as a seal.

The Belgian Anticline area is structurally complex; here, sandstone bodies are separated by faults that create compartments in the structure. Many of the fault blocks presented in the geologic model had not been previously interpreted. The aim of this thesis is to enhance the steam flooding

project that is active in the area by providing a tool to evaluate potentially bypassed reservoirs in the Potter Sandstone, and propose additional development possibilities represented by new targets in deeper reservoirs.

### 8.1 Petroleum system

From the wells used to analyze the petroleum system, it is suggested that subsidence was greater to the south of the field as is evidenced by steeper burial curves to the south that progressively become gentler to the north. Probably a high was present very early in the system, affecting deposition from the central part all the way to the northern limit of the field. This controlled to some extent the amount of sediment that was deposited.

Development projects to find new pools or bypassed oil have good chances of success based on the qualitative assessment of the 10 petroleum system criticals. It is important to notice that even though the probability of success is 84%, caution has to be taken in the delimitation of sandstone bodies and the reservoirs in general; as their delineation and accurate position in space is the major risk factor in a play like this, where exploration is in the late mature stages.

# 9. RECOMMENDATIONS

It is recommended to Conduct a restoration of the 2 remaining regional cross-sections to model and understand the main hydrocarbon generation and migration events for all the sandstone members in the Tumey (Oceanic), Temblor (Phacoides, Agua, Carneros, and others), Monterrey, and Reef Ridge formations. This will provide a better understanding of the charging mechanism of these sandstone bodies, and the Stevens equivalent (Leutholtz, Williams, Republic, Spellacy, and Potter) deepwater sandstones.

According to thermal history studies, the San Joaquin basin is an overcharged system and plays shallower than 17,000 ft are prospective. This is an incentive to aim for deeper targets where the quality of oil is also better (18-30 API).

New wells drilled to the center of the detailed area could reach lower interpreted blocks of the structure with potential in the Monterey lower members and the Temblor formation.

The structural geologic model presented in this thesis is a tool that should be updated as more data becomes available; this is an iterative process that constantly improves the model. For a structurally complex area as the Belgian Anticline, it is important to tune the model, introducing more wells with dipmeter-logs and, if possible, seismic data. The recommendation here is to use a minimum of 25 wells per cross section, using deeper wells where markers like the Point of Rocks Sandstone, the Kreyenhagen Shale, the Tumey Shale, the Top Temblor and the top of the Devilwater member of the Monterrey Formation are constrained.

## REFERENCES


Atwill, E.R., 1935, Oligocene Tumey formation of California: American Association of Petroleum Geologists Bulletin, v. 19, no. 8, p. 1192-1204.

Beyer, L. A., and Bartow, J. A., 1988, Summary of geology and petroleum plays used to assess undiscovered recoverable petroleum resources, San Joaquin Basin Province, California: U. S. Geological Survey Open-File Report 87-450Z, p. 1-22.

Boljen, S. S., 2005, Well-log picks and stratigraphic interpretation of the Monterey Formation, Berry Petroleum Company internal project.

Callaway, D. C., and Rennie, E. W., Jr., 1991, San Joaquin Basin, California, in Beyer, L. A., and Bartow, J. A., 1988, Summary of geology and petroleum plays used to assess undiscovered recoverable petroleum resources, San Joaquin Basin Province, California: U. S. Geological Survey Open-File Report 87-450Z, 80 p., 4 pls.

Callaway, D. C., 1971, Petroleum potential of San Joaquin Basin, California, in Cram, U. S., ed., Future petroleum provinces of the United States--Their geology and potential: American Association of Petroleum Geologists Memoir 15, p. 239-253.

Campbell M. J., 1996, Tulare Formation in Nilsen, T.H., Wylie, Jr., A.S., and Gregory,G.J., eds. 1996, Geology of the Midway-Sunset Oil Field: AAPG Field Trip Guidebook, p. 213-225

Davis, G. H., and Reynolds, S. J., 1996, Structural Geology of Rocks and Regions: Jhon Wiley & Sons,Inc., Second Edition, United States of America., p. 415-417 and 355-356.

Del Mar D. B., 1996, A Brief Early History of The Midway-Sunset Oil Field in Nilsen, T.H., Wylie, Jr., A.S., and Gregory,G.J., eds. 1996, Geology of the Midway-Sunset Oil Field: AAPG Field Trip Guidebook, p. 39-49

Dibblee, T.W., Jr., 1972, (Digital scale used, 1:25,000) Geologic maps of fourteen 15-minute quadrangles along the San Andreas fault in the vicinity of Paso Robles and Cholame southeastward to Maricopa and Cuyama, California, USGS, Open-File Report 72-89, Geologic Maps; West Elk Hills and Fellows. http://pubs.er.usgs.gov/usgspubs/ofr/ofr7289

Dibblee, T.W., Jr., 1973, Scale 1:125.000 Regional geologic map of San Andreas and related faults in Carrizo Plain, Temblor, Caliente, and La Panza ranges and vicinity, California, USGS, Investigation-757, Geologic Map.

Farley, T., 1990, Heavy oil reserves in the Tulare fold belt, Cymric-McKittrick fields, Kern County, California, in Kuespert, J.G. and Reid, S.A. eds., Structure, Stratigraphy and Hydrocarbon Occurrences of the San Joaquin Basin, California: Pacific Section, American Association of Petroleum Geologists and Society of Economic Paleontologists and Mineralogists, v. 64 and GB65, p. 181-204.

Fortier J. D., 1996, Age of The Main Producing Horizons at The Midway-Sunset Oil Field, California, in Nilsen, T.H., Wylie, Jr., A.S., and Gregory,G.J., eds. 1996, Geology of the Midway-Sunset Oil Field: AAPG Field Trip Guidebook, p. 51-53

Foss, C. D., and Blaisdell, R., 1968, Stratigraphy of the west side southern San Joaquin Valley, in Karp, S. E., ed., Geology and Oil Fields, West Side Southern San Joaquin Valley: Pacific Section, Society of Economic Paleontologists and Mineralogists and Society of Exploration Geophysicists Guidebook, p. 33-43.

Gardiner R. L., Wylie A. S., Jr., and Gagner M. J., 1996, The Potter Sandstone, Midway-Sunset Field, Kern County, California in Nilsen, T.H., Wylie, Jr., A.S., and Gregory, G.J., eds. 1996, Geology of the Midway-Sunset Oil Field: AAPG Field Trip Guidebook, p.175-191

Gregory G. J., 1996, Geology of The Midway-Sunset Oil Field, in Nilsen, T.H., Wylie, A.S., and Gregory, G.J. eds. 1996, Geology of the Midway-Sunset Oil Field: AAPG Field Trip Guidebook, p. 55-88

Gregory G. J., (in press) Sandstones of The Antelope Shale Member, Monterey Formation, Midway-Sunset Oil Field, California in Nilsen, T.H., Wylie, Jr., A.S., and Gregory, G.J., eds. 1996, Geology of the Midway-Sunset Oil Field: AAPG Field Trip Guidebook, p. 115-153

Harding, T.P., 1976, Tectonic significance and hydrocarbon trapping consequences of sequential folding synchronous with San Andreas faulting, California: American Association of Petroleum Geologists Bulletin, v. 60, p. 356-378.

Lennon, R. B., 1990, Midway-Sunset Field-U.S.A. San Joaquin Basin, California: American Association of Petroleum Geologists Special Publications, p. 221-241.

MacPherson, B. A., 1978, Sedimentation and trapping mechanism in upper Miocene Stevens and older turbidite fans of southeastern San Joaquin Valley, California: American Association of Petroleum Geologists Bulletin, v. 62, p. 2243-2274.

Mercer, M, F., 1996, Miocene Monterey Shale Units in Midway-Sunset Field in Nilsen, T.H., Wylie, Jr., A.S., and Gregory, G. J., eds. 1996, Geology of the Midway-Sunset Oil Field: AAPG Field Trip Guidebook, p. 97-114.

Mitra, S., 2002, Fold-accommodation faults: The American Association of Petroleum Geologists Bulletin, V. 86, NO. 4, p. 671-693.

Mitra, S., 2004, Structural Geology of Fold and Thrust Belts: The University of Oklahoma, Class Guidebook and Literature Compilation, Geol 6970.

Nilsen, Parts of Geologic map by Nilsen, 1995., in Nilsen, T.H., Wylie, Jr., A.S., and Gregory,G.J., eds. 1996, Geology of the Midway-Sunset Oil Field: AAPG Field Trip Guidebook, p. 39-49.

Nilsen T. H., and Campbell M. J., 1996, Tulare Formation Core Display Santa Fe Energy Resources, Well 363-25 Midway-Sunset Oil Field, California, in Nilsen, T.H., Wylie, Jr., A.S., and Gregory, G.J., eds. 1996, Geology of the Midway-Sunset Oil Field: AAPG Field Trip Guidebook, p. 303-313

Nilsen T. H., 1996, Regional Geology of The Southwestern San Joaquin Basin, California in Nilsen, T.H., Wylie, Jr., A.S., and Gregory, G.J., eds. 1996, Geology of the Midway-Sunset Oil Field: AAPG Field Trip Guidebook, p. 7-38

**Nilsen, T.H., Wylie, Jr., A.S., and Gregory, G.J., eds. 1996, Geology of the Midway-Sunset Oil Field: AAPG Field Trip Guidebook.**

Ponek, M, 1998., The Potter Sandstone at North Midway-Sunset Field (field trip stops 2&3) in Field Trip sponsored by the San Joaquin Geological Society (SJGS): Classic Outcrops on the West Side of the San Joaquin Valley., p.20.

Quinn, M. J., 1990, Upper Miocene Stevens Sands in the Maricopa depocenter, southern San Joaquin Valley, California, in Kuespert, J. G., and Reid, S. A., eds., Structure, stratigraphy and hydrocarbon occurrences of the San Joaquin Basin, California: Pacific Sections, American Association of Petroleum Geologists, v. GB65, Society of Economic Paleontologists, v. 64, p. 97-113.

Sturm D. H., 1996, Spellacy Reservoir Sandstones, Midway-Sunset Field, in Nilsen, T.H., Wylie, Jr., A.S., and Gregory, G.J., eds. 1996, Geology of the Midway-Sunset Oil Field: AAPG Field Trip Guidebook, p. 155-174.

Taff, J. A., 1933, Geology of McKittrick Oil Field and Vicinity, Kern County, California: American Association of Petroleum Geologists Special Publications, v. 17 p. 1 – 15.

Walter D. R., 1996, The Pliocene San Joaquin Formation Midway - Sunset Field, in Nilsen, T.H., Wylie, Jr., A.S., and Gregory, G.J., eds. 1996, Geology of the Midway-Sunset Oil Field: AAPG Field Trip Guidebook, p. 201-212.

Varnes, K. L., and Dolton, G. L., 1982, Estimated areas and volumes of sedimentary rock in the United States by province--Statistical background data for U. S. Geological Survey Circular 860: U. S. Geological Survey Open-File Report 82-666C, p. 11.

Von Estorff, F. E., 1930, Kreyenhagen Shale at Type Locality, Fresno County, California: American Association of Petroleum Geologists Bulletin, v. 14, p. 1321 – 1336.

Webb, G. W., 1981, Stevens and earlier Miocene turbidite sandstones, southern San Joaquin Valley, California: American Association of Petroleum Geologists Bulletin, v. 65, p. 438-465.

Weimer P. and Slatt R. M., 2004, Petroleum Systems of Deepwater Settings: Society of Exploration Geophysicists and European Association of Geoscientists & Engineers Distinguished Instructor Series, No. 7. p. 2-11 and 4-1 to 4-88.

Wylie A.S., Jr. and Huntoon J.E., 1996, The Etchegoin Formation in The Midway-Sunset Oil Field, California, in Nilsen, T.H., Wylie, Jr., A.S., and Gregory, G.J., eds. 1996, Geology of the Midway-Sunset Oil Field: AAPG Field Trip Guidebook, p.193-199.

*Internet Sources*

A. Namson, J. S., and Davis, T. L., 1998, Southern California Cross Section Study; Cross sections 5-5': Davis and Namson Consulting Geologists webpage http://www.davisnamson.com (internet search date Feb, 2006)

B. Namson, J. S., and Davis, T. L., 2000, Southern California Cross Section Study; Cross sections 16-16: Davis and Namson Consulting Geologists webpage http://www.davisnamson.com (internet search date Feb, 2006)

C. Namson, J. S., and Davis, T. L., 2004, Role of Faults in California Oilfields PTTC Field Trip August 19, 2004: Davis and Namson Consulting Geologists webpage http://www.davisnamson.com (internet search date Feb, 2006)

D. Nigrini, 1996. Thermal History Studies in Visual Display of Reservoir Parameters Affecting EOR, A Proposal Submitted to the U.S. Department of Energy Geoscience/Engineering Reservoir Heterogeneity Program, 1996; The Michigan Technological University, The Institute Of Materials Processing Houghton, Mi., And Digital Petropysics, Inc. Bakersfield, Ca:) http://www.geo.mtu.edu/svl/pioneer/

   - Cooperative Agreement No.: DE-AC22-93BC14892
     Contractor Name and Address: Michigan Technological University, 1400 Townsend Drive, Houghton, MI 49931-1295
     **Date of Report: 31 October 1996.**
     Anticipated Completion Date: 28 September 1996
     Principal Investigator: James R. Wood (906) 487-2894
     Project Manager: Robert E. Lemmon, Bartlesville Project Office (918) 337-4405
     **Reporting Period: 29 September 1993 - 28 September 1996.**
   - Elk Hills 934-29R deep well from this study.

E. Mendocino triple Junction figure 10 sourcs: Department of Geological sciences web page of The University of Colorado at Boulder: http://www.colorado.edu/GeolSci/Resources/WUSTectonics/PacNW/juan_de_Fuca_advanced.html (internet search date Nov, 2005)

F. *The 10 Largest Oil Fields in the U.S.,: http://home.earthlink.net/~loveguru/gasgalore.htm (internet search date Nov, 2005)
G. USGS NOGA (National Oil and Gas Assessment): http://energy.cr.usgs.gov/oilgas/noga/ (internet search date Nov, 2005)

*Other Internet sources*

1. University of Wisconsin , Green Bay webpage ( April 24, 2006): http://www.uwgb.edu/dutchs/FieldMethods/UTMSystem.htm

2. University of Colorado at Boulder webpage (april 24, 2006): http://www.colorado.edu/geography/gcraft/notes/mapproj/gif/utmzones.gif

3. Spatial Analysis Laboratory, School of Forest Resources, Arkansas Forest Resources Center, University of Arkansas, Monticello Webpage (April 24, 2006): http://sal.uamont.edu/pages/nsdd/doq.htm

4. The California spatial information Library (Nov 2005): http://gis.ca.gov/data.epl

5. ESRI Census 2000, TIGER Line Data (Nov 2005): http://arcdata.esri.com/data/tiger2000/tiger_download.cfm

6. USGS, GEODE.,Geo-Data-Explorer (Nov 2005): http://geode.usgs.gov/geode_frame.htm

7. USGS, GIS Data Depot (Nov 2005): http://data.geocomm.com/catalog/index.html

8. USGS, NOGA National Oil and Gas Assessment., 1995, 2005-Update (Nov 2005): http://energy.cr.usgs.gov/oilgas/noga/nogaindex.htm

9. Environmental Modeling Research Laboratory (EMRL) webpage (April, 2006): http://emrl.byu.edu/gsda/data_dem_overview.html

10. U.S. Department of the Interior, USGS, National Mapping Division webpage (April 2006) : http://mapping.usgs.gov/